

INPUT POWER FACTOR PROBLEM AND CORRECTION FOR INDUSTRIAL DRIVES

BY

OSUNDE, DAVIDSON OTENGHABUN

B.Sc (Hons), M.Sc (Electrical Engineering), MBA, M.Sc (Economics), Lagos

MNSE, AMIEE, R. Eng



**UNIVERSITY
OF LAGOS**

**A THESIS SUBMITTED TO THE SCHOOL OF POST GRADUATE
STUDIES, UNIVERSITY OF LAGOS, LAGOS, NIGERIA, FOR THE
AWARD OF THE DEGREE OF DOCTOR OF PHILOSOPHY (Ph.D) IN
ELECTRICAL AND ELECTRONICS ENGINEERING**

MARCH 2010

**SCHOOL OF POSTGRADUATE STUDIES
UNIVERSITY OF LAGOS**

CERTIFICATION

This is to certify that the Thesis

**“INPUT POWER FACTOR PROBLEM AND CORRECTION FOR
INDUSTRIAL DRIVES”**

Submitted to the
School of Postgraduate Studies
University of Lagos

For the award of the Degree of
DOCTOR OF PHILOSOPHY (Ph.D)
is a record of original research carried out

By

OSUNDE, DAVIDSON OTENGHABUN
in the Department of Electrical and Electronics Engineering

_____ AUTHOR’S NAME	_____ SIGNATURE	_____ DATE
_____ 1 ST SUPERVISOR’S NAME	_____ SIGNATURE	_____ DATE
_____ 2 ND SUPERVISOR’S NAME	_____ SIGNATURE	_____ DATE
_____ 1 ST INTERNAL EXAMINER	_____ SIGNATURE	_____ DATE
_____ 2 ND INTERNAL EXAMINER	_____ SIGNATURE	_____ DATE
_____ EXTERNAL EXAMINER	_____ SIGNATURE	_____ DATE
_____ SPGS REPRESENTATIVE	_____ SIGNATURE	_____ DATE

DECLARATION

I declare that this thesis is a record of the research work carried out by me. I also certify that neither this nor the original work contained therein has been accepted in any previous application for a degree.

All sources of information are specifically acknowledged by means of reference.



OSUNDE, O. D

**UNIVERSITY
OF LAGOS**

DATE

DEDICATION

To my entire family and all those who have contributed to my progress in life particularly my wife, Osunde, Isimeme Okaneme and my lovely Children: Osasere Davidson (Jnr), Osayi Stephen and Osarieme Stephanie



UNIVERSITY
OF LAGOS

ACKNOWLEDGEMENTS

It is with great pleasure that I acknowledge the encouragement and guidance of my supervisors: Prof. C.C Okoro and Prof. C.O.A. Awosope for their thorough supervision of this thesis. Particularly, I wish to express my unreserved gratitude to Prof. C.C. Okoro for his confidence in my ability to undertake this research up to doctoral level. I am indeed very grateful for his interest, guidance, and understanding and above all for making his wealth of experience and resources available to me. I hope my emerging career will meet his expectations to justify his huge academic and professional investment on my training. His capacity for hard work, diligence, thoroughness and honesty serve as a source of inspirations for my aspirations. I am also indebted to all lecturers and staff of the department of Electrical/Electronics Engineering of the University Of Lagos: Prof. F.N. Okafor, the acting head of department, Prof. R.I. Salawu (retired), Prof. S.A. Adekola (retired), Prof. O. Adegbenro, Prof. A.I. Mowete, Dr. T.O. Akinbulire, (PG co – ordinator), Dr. P.B Osofisan (retired), Mr. Lawal (retired), former head of Electrical machines laboratory, and others not mentioned for their guidance, advise and useful suggestions. I remain grateful to Prof. V.O. Olunloyo of Systems Engineering, Prof. O. Ogboja (late) of Chemical Engineering, Prof. B.O. Oghojafor of Business Administration, Prof. Fakieyesi of Economics department for their supports and words of encouragements and in particular to the present Dean of Engineering, Prof. M.A Salau

My profound and unreserved gratitude goes to the immediate past Vice – Chancellor, Prof. Oye Ibidapo – Obe for granting me a one year study leave as a visiting research scholar on an exchange programme to the Michigan State University, USA. Most of my modeling analysis and laboratory experiments were carried out at the Michigan State University – Power Electronics Laboratory under the supervision of Prof. P.Z. Peng. I am indeed grateful to him and other staff and Ph.D students of the Power Electronics group. More importantly, I remain grateful to the entire Michigan State University for hosting me and making my stay a worthwhile one.

I would also like to acknowledge the following colleagues who have assisted and contributed in various ways to the completion of this work often with enthusiasm and encouragement: Mr. Peter Otomewo, MD, Perbeto Ventures, Dr. Olumuyiwa Asaolu, and Engr. Chinedu Ucheagbu. My special thanks go to my brother, Patrick Osunde in Atlanta Georgia, USA, for his contributions and to all my friends in America: Barr. Lucky Osagie Enobakhare (NY),

Nosa Aimufua (NY), Francis Omoregbe (Chicago), Late Larry Umumagbe (NY), Engr. Ese Osa (NY), Engr. James Babalola (TX), Engr. Ayo Adedeji (TX), Dr. Emman Ogogo (NY), Dr. Richardson Osazee (GA), Mr. Omoruyi Osakpamwan (MI), Mr. Daniel Osunde (CA), Engr. Chuks Iyasele (TX) and others not mentioned for their moral and financial supports.

It is with all my heart that I acknowledge the moral supports, patience, understanding and encouragement of my beloved wife – Osunde, Isimeme Okaneme and my wonderful children, Osasere Davidson (Jnr), Osayi Stephen and Osarieme Stephanie. You are all more precious than Gold

Finally, I thank the almighty God for his abundant blessings showered on me throughout my course in life. I am indeed grateful to him for his guidance, protection and good health.



UNIVERSITY
OF LAGOS

Osunde, O .D
Lagos, Nigeria

TABLE OF CONTENTS

	<u>Page</u>
Title	i
Certification	ii
Declaration	iii
Dedication	iv
Acknowledgements	v
Table of Contents	vii
List of Figures	xi
List of Tables	xv
List of Abbreviations	xvi
List of Notations	xviii
Abstract	xx

CHAPTER 1:

INTRODUCTION

1.1	Background of Study	1
1.2.	Statement of the problem	3
1.3	Aim	3
1.4	Objectives	4
1.5	Scope of study	4
1.6	Significance of study	5
1.7	Operational Definition of Terms	5
1.8	Presentation of Thesis	8

CHAPTER 2:

LITERATURE AND THEORETICAL FRAMEWORK

2.1	Literature Review	9
-----	-------------------	---

2.2.	The Thyristor	14
2.2.1	I-V Characteristics of a thyristor	15
2.2.2	Dynamic Characteristics of a Thyristor	18
2.3	Circuits and Devices used in power Factor correction Schemes	23
2.3.1	Operational amplifiers and applications	24
2.3.2	Operational amplifier as an Inverting Amplifier	25
2.3.3	Operational amplifier as a non - inverting Amplifier	25
2.3.4	Operational amplifier as an Integrator	26
2.3.5	Operational amplifier as a Differentiator	26
2.3.6	Operational amplifier as a Comparator	27
2.4	The 555 Timer IC	27
2.4;1	Monostable mode	28
2.4.2	Astable mode	29
2.5	The Single – Phase Asymmetrical Bridge Converter	31

CHAPTER THREE:

MODELLING AND ANALYSIS OF THE BRIDGE CONVERTER WITH DC MOTOR LOAD

3.0	Introduction	34
3.1	Modelling the DC Motor	34
3.2	Piece – Wise Linear analysis of the Single – Phase Bridge Converter with DC Motor Load	36
3.3	Modes of Operation	37
3.4	Analysis for AC input current	40
3.5	Harmonics in the AC input Current	50
3.6	Impact of Multiple Drives on Supply Systems	55
3.7	Behaviour Factors of the Drive	59

3.8	The Input Power Factor Problem	62
3.9	Generalised Analysis for the Asymmetrical Bridge	63

CHAPTER 4:

POWER FACTOR CORRECTION (PFC) CONTROL SCHEMES

4.0	Introduction	68
4.1	Passive and Active methods of power factor correction	68
4.1.1	Passive Power Factor Correction Techniques	68
4.1.2	Active Power Factor Correction Techniques	69
4.2	Performance evaluation of the various techniques	69
4.3	Performance Analysis for the methods of control of the Asymmetrical Bridge	79

CHAPTER 5:

PULSE WIDTH MODULATION (PWM) FOR INPUT POWER FACTOR CORRECTION

5.1	Pulse Width Modulation	84
5.2	Types of PWM	86
5.2.1	Equal pulse width modulation (EPWM)	87
5.2.2	Sinusoidal pulse width modulation (SPWM)	87
5.3	Analysis for predicting the Behaviour factors on the AC input current of the Asymmetrical Bridge with pulse width modulation (PWM)	88
5.4	Comparison of Results with the Asymmetrical Bridge without PFC control	96
5.5	AC – DC Boost – Type Asymmetrical Converter for Power Factor Correction	98
5.5.1	The AC – DC Asymmetric Drive with Power Factor Correction Circuit	98
5.5.2	AC – DC Boost - Type Asymmetrical Converter for PFC	98

5.5.3	Control of the Active Boost Switch of the PWM	100
5.6	Waveforms of the PWM control Signals of the Drive	104
5.7	A Simplified PWM AC – DC Asymmetrical Bridge with PFC control	107
5.7.1	Description of the proposed circuit	108
5.7.2	Operation of the Bridgeless Converter	109
5.7.3	Design Considerations of the proposed AC – DC Converter	111

CHAPTER 6:

RESULTS AND DISCUSSION

6.1	Waveforms of the Input Voltage, Current and harmonics with PWM PFC	117
6.1.1	Comparative Results of the PWM and PAC controls	118
6.2	Discussion of Results	119

CHAPTER 7:

CONCLUSIONS AND RECOMMENDATIONS

7.1	Conclusions	121
7.2	Contributions to Knowledge	122
7.3	Recommendations for further work	123

REFERENCES	124
-------------------	-----

APPENDICES	135
-------------------	-----

LIST OF FIGURES

<u>Figure</u>		<u>Page</u>
2.1	Thyristor Structure and symbols	14
2.2	Static I – V characteristics of a thyristor	16
2.3	Junction biased conditions.	17
2.4	Distribution of gate and anode current during delay time	19
2.5	Thyristor voltage and current waveforms during turn-on and turn-off processes	22
2.6	A circuit model of an operational amplifier (op amp) with gain A and input and output resistances R_{in} and R_{out}	24
2.7	Inverting amplifier circuit	25
2.8	Non - inverting amplifier circuit	26
2.9	Integrator circuit	26
2.10	Differentiator circuit	27
2.11	The 741 IC as a Comparator	27
2.12	Schematic of a 555 in monostable mode	29
2.13	Standard 555 Astable Circuit	30
2.14	Single – phase Asymmetrical Bridge Converter	33
3.1	Magnetisation Characteristics of a DC Motor	35
3.2	The asymmetrical single-phase bridge converter with a DC Motor Load	36
3.3	Control Circuit Layout a Single – Phase asymmetric Bridge Drive	38
3.4	Operational intervals and Waveforms of the Bridge Converter	38
3.5	Bridge Converter with half Cycle Equivalent Circuits	40
3.6	Variation of the Forward commutation angle ' μ ' with Firing angle ' α ' of the controller	43

3.7	Variation of the Reverse commutation angle ' β ' with Firing angle ' α ' of the controller	45
3.8	Motor Input current at different Firing angles of the Thyristors: The power factor problem in Graphics	49
3.9	Harmonics Spectrum of the controller at different Firing angles	53
3.10	Variation of Input current harmonic components for different delay angles	54
3.11	Variation of specified Harmonic Currents with Firing Angle	55
3.12	Multiple drives connected to the same source	56
3.13	Input current and waveform for a single drive: $N = 1500$, $PF = 0.628$	57
3.14	Input current and waveform for Two Drives in parallel: $N = 1500$, $PF = 0.166$	57
3.15	Input current and waveform for Three Drives in Parallel $N = 1500$, $PF = 0.106$	58
3.16	Variation of Power Factor with Number of Drives	58
3.17	Behaviour Factors of the Asymmetrical Single – Phase Bridge	66
4.1	Voltage and current waveforms for Phase Angle control – (PAC)	70
4.2	Voltage and current waveforms for Symmetrical Angle control – (SAC)	70
4.3	Voltage and current waveforms for Extinction Angle control – (EAC)	71
4.4	Voltage and current waveforms for Sequence control with forced commutation	71
4.5	Voltage and current waveforms for Pulse Width Modulation control – (PWM)	72
4.6	Relationships between the Input Power Factor and Output Voltage for the various PFC control techniques	82
4.7	Relationships between the Harmonic Factor and Output Voltage for the various PFC control techniques	82
4.8	Relationships between the Displacement Factor and Output Voltage for the various PFC control techniques	82
5.1	Comparator Input and Output waveforms	85
5.2	Practical PWM Circuit	86

5.3	Waveforms of Currents and Voltages for Sinusoidal PWM	87
5.4	Harmonic Currents for specified Harmonic numbers	95
5.5	Variation of Power Factor with Output Voltage of the Bridge	96
5.6	Variation of Harmonic Factor with Output Voltage of the Bridge	97
5.7	Variation of Displacement Factor with Output Voltage of the Bridge	97
5.8	Gate Firing Circuit implementation of the PWM Controlled Asymmetrical Single – Phase Drive	99
5.9	Asymmetrical AC –DC Boost- type Converter with input power factor correction	100
5.10	Schematic circuit layout for the PWM Controlled Asymmetric Single – Phase Bridge (Boost Switch Control)	101
5.11	Gate Firing Circuit Implementation of the PWM Controlled Asymmetric Single – Phase Drive (Thyristor Control)	102
5.12	Test rig with controlled DC machines and the Asymmetrical Bridge with PWM Controllers	103
5.13	A Triangular wave signal at 10 KHz with a DC signal	104
5.14	A Triangular wave signal at 8 KHz with a DC signal	104
5.15	Comparator signal output modulated at 10KHz	105
5.16	Comparator signal output modulated at 8KHz	105
5.17	Comparator signal output modulated at 6KHz	105
5.18	Comparator signal output modulated at 5KHz	105
5.19	Thyristors complimentary gate signals at 10kHz	106
5.20	Thyristors complimentary gate signals at 8kHz	106
5.21	Input Current and Voltage waveforms (PF = 0.9995) at 10KHz	106
5.22	Input Current and Voltage waveforms (PF = 0.9993) at 8KHz	106

5.23	Harmonics of the PWM Controlled Asymmetric Single – Phase Drive	107
5.24	Bridgeless AC – DC PFC Configuration	108
5.25	Current Flow path for the Positive half cycle	109
5.26	Current Flow path for the negative half cycle	110
5.27	Operation of the Bridgeless converter	113
5.28	Triggering Circuit of the Bridgeless Converter (Voltage feedforward approach) the proposed AC – DC Converter: Active Boost Control	116
6.1	Input Current and Voltage waveforms (PF = 0.9998) at 10 KHz	117
6.2	Input Current and Voltage waveforms (PF = 0.9996) at 8KHz	117
6.3	Laboratory Results of the PWM Controlled Asymmetric Single – Phase Drive	117
6.4	Input current waveform of the asymmetrical single phase bridge feeding a DC motor load without PFC control (PF = 0.628)	118
6.5	Input current waveform of the asymmetrical single phase bridge feeding a DC motor load with PFC control (PF = 0.9998)	118
6.6	Input Harmonic Current for the asymmetrical single phase bridge feeding a DC motor load without PFC control	118
6.7	Input Harmonic Current for the asymmetrical single phase bridge feeding a DC motor load with PWM PFC control	118

LIST OF TABLES

<u>Table</u>		<u>Page</u>
4.1	Generalised Equations for Various Converter – Control Techniques using their simplified models	81



UNIVERSITY
OF LAGOS

LIST OF ABBREVIATIONS

AC	Alternating Current
DC	Direct Current
PF	Power Factor
DF	Displacement Factor
HF	Harmonic Factor
RF	Ripple Factor
FF	Form Factor
PFC	Power Factor Correction
THD	Total Harmonic Distortion
PAC	Phase Angle Control
AAC	Asymmetrical Angle Control
EAC	Extinction Angle Control
SAC	Symmetrical Angle Control
SHE	Selective Harmonic Elimination
PWM	Pulse Width Modulation
IEC	International Electrotechnical Commission
EPWM	Equal Pulse Width Modulation
SPWM	Sinusoidal Pulse Width Modulation
CICM	Continuous Inductor Current Mode
DICM	Discontinuous Inductor Current Mode
EI	Electromagnetic Interference

SCR	Silicon Controlled Rectifier
IGBT	Insulated Gate Bipolar Transistor
MOSFET	Metal Oxide Semiconductor Field Effect Transistor
PHCN	Power Holding Company of Nigeria
NNPC	Nigerian National Petroleum Corporation
THR	The threshold at which the interval ends
DIS	Connected to a capacitor whose discharge time will influence the timing interval
GND	Ground



UNIVERSITY
OF LAGOS

LIST OF NOTATIONS

α	Delay or Firing Angle
β	Extinction Angle (Angle after π at which reverse commutation begins)
T	Period
f	Frequency
f_s	Switching Frequency
t	Time
d	Duty Cycle
D	Constant Duty Circle
$i(t)$	Instantaneous Current
I	Constant Current
n	Turns Ratio
N	Number of Turns
P	Active Power
Q	Reactive Power
R	Resistor
S	Apparent Power
S	Active Switch
C	Capacitor
L	Inductor
T_{off}	Off - Time of an Active Switch
T_{ON}	On - Time of an Active Switch
X	Reactance
T_s	Switching Period
ϕ	Displacement Angle
i_f	Forced Current Component
i_n	Natural Current Component
v	Instantaneous Voltage

E	Motor Induced Emf
V_s	RMS Value of Phase Voltage
I_s	RMS Value of Phase Current
I_{s_1}	Fundamental Current of I_s
ϕ_{s_1}	Phase Angle Between V_s and I_{s_1}
PF_{ac}	AC Input Power Factor
ω	Angular Frequency
t_d	Delay time
t_q	Turn – OFF time
t_g	Gate recovery time
t_{rr}	Reverse recovery time
t_{gr}	Gate recovery time
t_c	Circuit turn – off time
R_{in}	Input resistance
R_{out}	Output resistance
V_{cc}	Output voltage
A	Gain of an amplifier
π	Angle representing a half cycle in radians
$E_a(t, i_f)$	The motor back emf,
$L_a(i_f)$	The Armature inductance of a DC motor
$R_a(i_a)$	The Armature resistance of a DC motor
$i_a(t)$	The instantaneous input current to a DC motor

ABSTRACT

The Asymmetrical Single - phase drive has an input power factor problem over its control range. With the race towards industrialisation, power networks in developing economies would face increasing power factor problems with extended application of these drives in industrial and traction systems. This project investigates the assertion that power factor of supply networks with multiple drives deteriorates with increased number of drives. The power factor problem is established analytically following a complete characterization of the AC input current of the drives. The methods of improving the input power factor of industrial drives are studied and the Pulse Width Modulation technique adopted for achieving power factor improvement for such industrial drives. The PWM scheme developed in the laboratory showed improved power factor. Generalised performance equations for the methods and their comparative controls, design and harmonic spectra are developed for application of industrial drives.



UNIVERSITY
OF LAGOS

CHAPTER ONE

INTRODUCTION

1.1 Background of study

In an ideal power system, the voltage supplied to customer equipment and the resulting input currents should be sinusoidal waves. In practice, however, these waveforms can be quite distorted. This deviation from perfect sinusoids is usually expressed in terms of harmonic content of the voltage and current waveforms. Most equipment connected to an electricity distribution network usually may need controlled power conversion equipment which produces a non-sinusoidal line current due to the nonlinear load. With such loads as RLC, the switching action of the devices makes the system non-linear. Also, with the steadily increasing use of such equipment, line current harmonics have become a significant problem. Their adverse effects on the power system are well recognized. Harmonics are unwanted frequency components, which arise from the use of semi-conductor controllers. Modern industries and applications which include the steel plants, traction systems, industrial drives, furnaces etc generate voltage and current harmonics which have adverse effects on the supply lines and equipment connected to such lines. The harmonics generated according to Okoro (1982, 1986) and Redl (1994) result in distortion of line voltages, degradation of power factor of electrical equipment thereby increasing the reactive power consumption and also overall running cost of equipment. The overall effects are reduced efficiency, increased heating effect and lead to Poor Power Factor on the AC inputs of the industrial drives. Also, voltage distortion produces such effects as motor prematurely burning out due to overheating, increased losses and lower efficiency.

There are many problems associated with harmonics within an industrial plant (Agu 1997) and there have been many efforts made without results in the past aimed at collecting data on harmonics from industrial companies operating in Nigeria.(Agu 1997). The up-coming Ajaokuta Steel Company and subsequent industrialization from subsidiary companies are expected to increase the harmonic currents in the National Grid. This study investigates the impact of these harmonics on the AC power supply inputs to these industries. In steel plants, most equipment for moving raw materials and finished products are fed from controlled single-phase AC – DC bridge converters which produce the worst case of harmonic distortion. There is therefore the need to mitigate harmonics at the point where the offending equipment is connected to the power system.

Power system harmonic distortion is not a new phenomenon. Effort to limit it to acceptable proportions has been a concern to power engineers from the early days of utility systems Okoro (1982). At that time, the distortion was typically caused by the magnetic saturation of

transformers by certain industrial loads such as arc furnaces or arc welders. The major concerns were the effects of harmonics on synchronous and induction machines, telephone interference and power capacitor failures (Agu 1997). In the past, harmonic problems could often be tolerated because equipment was of conservative design and grounded WYE- Delta transformer connection was used judiciously. Also, star connections of three – phase windings in rotating machines eliminate the 3rd - order harmonics. S.M. Bashi et. al (2005) proposed a harmonic injection technique, which reduces the line frequency harmonics of the single switch three-phase boost rectifier. In this method, a periodic voltage is injected in the control circuit to vary the duty cycle of the rectifier switch within a line cycle so that the fifth-order harmonic of the input current is reduced to meet the total harmonic distortion (THD) requirement. Ying-Tung Hsiao (2001) presents a method capable of designing power filters to reduce harmonic distortion and correct the power factor in an Industrial distribution network. The proposed method minimizes the designed filters' total investment cost such that the harmonic distortion is within an acceptable range. The optimization process considers the discrete nature of the size of the element of the filter.

It is to be noted that the presence of harmonics in the supply waveforms has other wide-ranging effects on the supply system. These include:

- Communication system interference.
- Degradation of equipment performance and effective life
- Sudden equipment failure
- Protective system mal-operation
- Increased power transmission losses
- Overheating in transformer, shunt capacitor, power cables, AC machines and switchgear leading to pre-mature ageing

Harmonics result in distortion of line voltages and currents, degradation of power factor of electrical equipment thereby increasing the reactive power consumption and also overall running cost of equipment.

The poor Power Factor problems on the AC input of Industrial drives is expected to increase with increased industrialisation where large numbers of such drives are connected to the National Power (PHCN) Network. In order to completely understand the effects of harmonic distortions

and poor input power factor on controlled drives, the single – phase asymmetrical bridge Drive was chosen for the study.

The choice of this Drive is influenced by the fact that

- it presents a high level of harmonic content
- it has a wide range of applications in traction and industrial motor control systems
- it is increasingly being applied to main-line rail propulsion systems
- it is widely used in low power motor control systems
- it is simple and inexpensive

1.2 Statement of the problem

Increasing national interest in the Steel Industries with many auxiliary Industries, the applications of industrial drives are bound to increase geometrically and the Input Power Factor problem due to such drives would also increase. Manufacturing industries may have to pay more for their electricity because of the increased reactive power drawn by industrial drives. These justify the effort to investigate the power factor problem and methods of improving poor power factor in drives.

1.3 Aim

The main aim of this work is to investigate the input power factor problems associated with industrial drives using the Asymmetrical Bridge Converter as a case study and profer solutions with a view to preparing for increased industrialization and a stable and secured power system network in the 21st Century.

1.4 Objectives

The objectives of this study are

1. establishing the Poor Input Power Factor Problem analytically by;
 - developing an understanding of the operation of the asymmetric single - phase bridge with a DC motor load.

- obtaining an explicit expressions of current for each interval of operation of the drive using the piece - wise linear method of analysis and also, a complete characterization of the drive by solution of transcendental equations
 - characterizing the behavior factors of the drive by obtaining the Power Factor (PF), Harmonic Factor (HF) and the Displacement Factor (DF).
 - obtaining harmonics that contribute to the poor input power factor and create malfunctioning of nearby Power and Communication equipment.
2. establishing the Poor Input Factor Problem experimentally in the Laboratory and showing that power factor gets worse with multiple drives connected to the same power supply
 3. critically investigating the various existing power factor correction techniques so as to propose an efficient method of power factor correction and further develop the scheme in the laboratory for application to Industrial Drives.
 4. analytically and experimentally demonstrating how the chosen technique improves the Input Power Factor for Industrial Drives

1.5 Scope of study

To study the Poor Input Power Factor problems of drives, by mathematically modelling the Asymmetrical single – Phase Bridge converter with a DC motor load and to analytically characterise the bridge and subsequently validate the theoretical results using laboratory experimentations on a 5KW, 220V DC motor load.

1.6 Significance of the study

The results of the study would elucidate the performance of industrial drives and provide design and operational data for a growing number of users of industrial drives. In particular, the results would be useful to the steel sectors like the Ajaokuta Steel Company, Ajaokuta, Delta Steel Company at Aladja, Oshogbo Steel rolling mills, the Coal Mining Company at Udi, in Enugu

State, Aluminum smelting Plant at Ikot – Abasi and the manufacturing industries where a large number of drives are used, More importantly, the Power Industry that constantly suffers from the effects of these harmonics would also benefit from the research.

1.7 Operational Definition of Terms

Power Factor(PF): This is defined as:

$$PF = \frac{\text{mean input power}}{\text{rms input volts-ampere}} \quad (1.1)$$

If the supply voltage is an undistorted sinusoid, only then the fundamental component of the current will contribute to the mean input power.

Therefore,

$$PF = \frac{VI_1 \cos \phi_1}{VI} \quad (1.2)$$

Where

V = rms supply phase voltage

I = rms supply phase current

I_1 = rms fundamental component of the supply current

ϕ_1 = angle between supply voltage and fundamental component of
Supply Current

The input power factor is an important parameter because it decides the volt – ampere requirement of the drive system. For the same power demand, if the power factor is poor more volt – amperes (and hence more current) are drawn from the supply current.

Input Displacement Factor(DF): This may be called fundamental power factor and is defined as:

$$DF = \cos \phi_1 \quad (1.3)$$

Where ϕ_1 is known as the input displacement angle. Thus, for the same power demand, if the displacement factor is low, more fundamental current is drawn from the supply.

Harmonic Factor(HF): The input current, being non – sinusoidal, contains currents of harmonic frequencies. The harmonic factor is defined as:

$$\begin{aligned} HF &= \frac{(I^2 - I_1^2)^{1/2}}{I_1} \\ &= \frac{(\sum_{n=2}^{\infty} I_n^2)^{1/2}}{I_1} \\ &= \frac{I_n}{I_1} \end{aligned} \quad (1.4)$$

Where, I_n = rms value of the n^{th} harmonic current

I_1 = rms value of the fundamental harmonic current

The harmonic factor indicates the harmonic content in the input supply current and thus measures the distortion of the input current.

Form Factor (FF): This is a measure of the slope of the output current defined as:

$$FF = \frac{I_{rms}}{I_{dc}} = \frac{I_{rms}}{I_{av}} \quad (1.5)$$

Ripple Factor (RF): This is a measure of the ripple content of the ac input Current defined as:

$$RF = \frac{I_{ac}}{I_{dc}} = \frac{I_{ac}}{I_{av}} \quad (1.6)$$

But the *effective* (rms) value of the ac component of the output current is:

$$I_{ac} = \sqrt{I_{rms}^2 - I_{dc}^2} \quad (1.7)$$

$$\begin{aligned} RF &= \sqrt{\left(\frac{I_{rms}}{I_{dc}}\right)^2 - 1} \\ &= \sqrt{FF^2 - 1} \end{aligned} \quad (1.8)$$

Total Harmonic Distortions (THD): This is called a distortion index of fundamental and distortion component in the supply current $i_s(t)$. It is expressed in percentage as:

$$\begin{aligned} \%THD &= 100 \times \frac{I_{distortion}}{I_{s_1}} = 100 \times \frac{\sqrt{I_s^2 - I_{s_1}^2}}{I_{s_1}} \\ &= 100 \times \sqrt{\left(\frac{I_s}{I_{s_1}}\right)^2 - 1} \end{aligned} \quad (1.9)$$

Asymmetrical Bridge: This is a half – controlled single – phase AC – DC converter comprising of two thyristors and two diodes.

The motivation for this research work is the anticipated rapid industrial development in the steel sector where a large number of drives will be in use thus increasing the harmonic content of power supplies available and thereby bringing the associated poor power factor problems to the fore. The choice of the asymmetrical single – phase drive is because of the worst harmonics it presents to AC supply. Previous work by Kataoka et.al (1977) and (1979) on a three – phase AC – DC converter and single – phase AC – DC converters demonstrate recent interest in the power factor problem. Kataoka et.al (1979) employs the PWM power factor correction technique to achieve a high power factor. The limitations of Kataoka’s work are: high switching frequencies resulting in an increased switching loss, lower efficiency, voltage losses, reduced reliability and the use of many semi – conductor devices thus, leading to high cost of implementation. The asymmetrical bridge is half controlled incorporating two thyristors and two diodes compared to Kataoka’s fully controlled single – phase AC – DC converter that presents low harmonics to AC supply. The high harmonics presented to AC supply by the asymmetrical bridge leads to a low power factor which is the basis of this study. This research will investigate the methods for power factor correction with a view to recommending the most viable method for adoption.

1.8 Presentation of Thesis

This thesis is arranged in the following order: Chapter two contains the literature review, where previous studies relating to the present research are discussed. Also presented in this chapter, is a theoretical framework on circuits and devices used in the implementation of the research. The

methodology for this study is discussed in chapters three, four and five; In particular, chapter three derives the input power factor problem in industrial drives analytically by obtaining the input current during the four intervals of operation and simulating the current flow on a digital computer. Also in this chapter, the harmonics spectrum of the input current was obtained and the results of the laboratory experiments involving the parallel connection of a number of drives to the same AC supply are also discussed. In chapter four, the various methods of power factor improvement techniques are evaluated. A detailed discussion and an analysis of the PWM scheme are presented in chapter five. Also, results of laboratory test and measurement of the PFC circuit design and implementation is presented. The results, though show a great improvement in power factor, an alternative circuit using fewer semi – conductor devices with a lower switching frequency and increased efficiency at a low cost is also discussed in chapter five. Test and discussions of the results of the research work are presented in chapter six. Also, a comparison of results is made with the results obtained without power factor control. Finally, the conclusion, Contributions to Knowledge and the recommendations for further work are presented in chapter seven.

CHAPTER TWO

LITERATURE AND THEORETICAL FRAMEWORK

2.1 Literature Review

Most of the researches on PFC for non-linear loads are related to the reduction of the harmonic content of the line current. Earlier attempts were made by Fujita and Akagi (1998) at reducing harmonics using harmonic filters in situations where harmonics present a problem on the AC system. The filter was placed at the input to the converter to control their level by providing a shunt path of low impedance at the harmonic frequency. However, problems in such filter design include:

- Fluctuations in supply (fundamental) frequency from its nominal value
- Effects of ageing causing changes in filter component values and hence variation in the tuned frequency
- Initial off-tuning as a result of manufacturing tolerances and the size of the tuning steps used.

The cost of providing filters is generally high in relation to the cost of the converter and their application tends to be confined to large converters or for the control of specified problems. Another method was to increase the load inductance to reduce the ripple current; it was found out that the AC system current contains a significant amount of ripples. At high power rating, the required inductance is bulky and heavy. In traction system for instance a 0.3mH choke weighs about three tons. Hence, as an alternative, a capacitive smoothing was introduced at the output of the converter. Again, the current drawn from the AC supply over a relatively short part of each – cycle results in high levels of harmonics being introduced into the supply.

In general, three methods have been used for power factor correction. Agu (1997) suggested the modulation of the rate of switching of the devices as a means of reducing the generation of harmonics and the use of multiple single – phase converters with forced commutation circuits. Pitel and Sarosh (1997) and Zander (1973) proposed the use of filters incorporating inductive and capacitive elements. The contribution made by Pitel and Sarosh of the possible thermal overloading due to harmonics, transmission losses, equipment failure due to harmonics and sub-harmonic resonance (sub-harmonic torques) and transformer insulation failure as well as relay mal-operation for some class of relays calls attention to industry problem due to harmonic currents. Redl (1996) has discussed several solutions to achieve PFC depending on whether active switches (controllable by an external control input) are used or not. PFC solutions can be categorized as passive or active. S.-K. Kil (2008) employs both active and passive PFC techniques at different time slots to achieve high power conversion efficiency and a high power

factor. The general configuration of active PFC converter is by connecting a PF corrector in series with a DC–DC converter. This configuration is commonly used in high power application. The passive approach employs inductors and capacitors to filter and eliminate harmonic currents and can improve PF substantially. The advantage of passive PFC over the active PFC is high efficiency and low electromagnetic interference problem because of the absence of high switching frequency devices. Unfortunately, the usage of this approach is limited due to unattractive physical size and weight of magnetic components

In passive PFC, only passive elements are used in addition to the converter or rectifier to improve the shape of the line current. Obviously, the output voltage is not controllable. For active PFC, active switches are used in conjunction with reactive elements in order to increase the effectiveness of the current shaping and to obtain controllable output voltage. The switching frequency further divides the active PFC solutions into two classes: low and high frequency. In low-frequency active PFC, switching takes place at low – order harmonics of the line – frequency and it is synchronized with the line voltage. In high- frequency active PFC, the switching frequency is much higher than the line – frequency.

Passive PFC methods use passive components in conjunction with the bridge converter. One of the simplest ways as Mohan, *et al* (1995) suggested is to add an inductor at the AC – side of the diode in series with the line voltage. The maximum PF obtained is 0.76. According to Dewan (1981) and Kelly (1992), the inductor can also be placed at the dc – side of the converter. This results in a PF of 0.9 but with a square shape input current. Kelly (1989) placed a capacitor across the supply to the converter (to achieve a PF of 0.905), but with a non-sinusoidal input current. The shape of the line current was further improved by Redl (1994), by using a combination of low pass input and output filters. Passive resonant circuits have been used to attenuate harmonics, Vorperian (1990), by placing large reactive elements (for example a series resonance band – pass filter) at the AC source and tuned to the line frequency to achieve a high PF. However, this is practical for higher frequencies. Hence, the parallel (Band Stop) resonant filter was used to replace the series –filter (Band pass filter). This was then tuned at the third harmonic. It allows for lower values of reactive elements when compared to the series resonant and band pass filter. Another possibility by Erickson (1997) is to use harmonic traps. This is a series of resonance network connected in parallel to an AC source and tuned at a harmonic frequency that must be attenuated. It results in a good line current improvement but at the

expense of an increased circuit complexity. Harmonic traps can also be used in conjunction with other reactive networks such as the band- stop filter, (Redl 1991 and Sokai et al 1998), by placing a capacitor at the input of the converter to reduce harmonics but at the expense of a lower PF. The low PF is not due to the harmonic currents but due to the series connected capacitors.

Passive power factor corrections have certain advantages such as simplicity, reliability and ruggedness, insensitivity to noise and surges, no generation of high frequency electromagnetic interference (EMI) and no high frequency switching loss. However, they also have several drawbacks. They are bulky and heavy because line – frequency reactive components are used. They also have poor dynamic response, they lack voltage regulation and the shape of their input current depends on the load. Even though line current harmonics are reduced, the fundamental component may show an excessive phase shift that reduces the power factor. Moreover, circuits based on resonant networks are sensitive to the line frequency. In harmonic trap filters, series resonance is used to attenuate a specific harmonic. However, parallel- resonance at different frequency occurs too, which can amplify other harmonics (Erickson 1997). The contribution made by the various authors on the use of passive PFC was adopted and modified in the design of the bridgeless AC-DC converter for PFC using active power switching device by having the inductor placed in series at the input to the converter, together with a filtering capacitor placed in parallel across the load to form a boost converter

Active power PFC involves the use of power switching devices such as the thyristor (SCR), metal oxide semi-conductor field effect transistor MOSFET or the insulated gate bipolar transistors IGBT Kelly (1991). The Pulse Width Modulation (PWM) technique involves the switching of power devices with pulses obtained by modulating a ramp with DC reference signal in an equal pulse width or sinusoidal pulse width and producing in – phase voltage and current at the AC input of the converter, thus improving the power factor.

According to Dong Dui et.al (2007) power factor correction (PFC) has become an important design consideration for switching power supplies. For low power applications (below 200W), the single – phase isolated PFC power supply (SSIPP) proposed by Redl et.al (1994) is a cost effective design solution to provide PFC. Basically, the current of SSIPP employs a cascade structure consisting of a boost PFC converter and a forward converter for output regulation.

Mohan et.al (1995) listed the following five different active control measures used in improving the input power factor.

- I. Extinction angle control - (EAC)
- II. Symmetrical angle control - (SAC)
- III. Selective harmonic elimination - (SHE)
- IV. Sequential control with forced commutation
- V. Pulse Width Modulation - (PWM)

This project will evaluate the performance of the above methods of power factor correction as presented in section 4.1 of this report and results showed that the PWM control scheme has the advantage of eliminating lower order harmonics by the proper choice of appropriate number of pulses per half cycle. Hence, it has become increasingly applied in PFC designs. For higher order harmonics according to Sen (1993) and Paul et.al (2006), an input filter can eliminate most of the harmonic currents from the line, thereby making the line current essentially sinusoidal. According to Jianhui (2006), Mohammed (2008) and Mohan et.al (1995), there are two basic types of Pulse Width Modulation (PWM)

- Equal pulse width modulation (EPWM)
- Sinusoidal pulse width modulation (SPWM)

The Equal Pulse Width Modulation involves comparing a triangular voltage with a DC signal in comparator to produce pulses at the output of the comparator that are used to trigger the switching device. While, in the Sinusoidal PWM control, the pulse widths are generated by comparing a triangular reference voltage V_r of amplitude A_r and a frequency f_r with a carrier half sinusoid voltage V_c of variable amplitude A_c and frequency $2f_s$ (Rashid M.H 1993, Bingsen Wang et.al 2007 and Jianhui Zhang 2006). The sinusoidal voltage is in phase with the input voltage V_s and has twice the supply frequency f_s . The widths of the pulses (and the output voltage) are varied by changing the amplitude A_c or the modulating index M from 0 to 1.

Researches on PFC carried out by Kataoka et.al (1977) and (1979), Omar et.al (2004), Malinowski et.al (2004) and Helonde et.al (2008) on three – phase AC – DC converter and on single – phase AC – DC converters by Patil (2002), Lu DDC et.al (2003), Kil (2008) and Dylan

et.al (2008) employs the PWM scheme to achieve a high Power Factor. In particular, Kataoka et.al (1977), (1979) used the single – phase and three – phase AC to DC converters that has associated commutation resonant LC circuits and current path diodes. The limitations of Kataoka’s work are:

- The required switching frequency of the boost switch is usually high. This in turn increases the switching losses and lowers the efficiency.
- Special design of the dc – side inductor is necessary to carry dc current as well as high frequency ripple current.
- The series diode in the path of power flow contributes to voltage losses and reduced reliability.
- At any given point, three semi – conductor devices exist in the power flow path
- The resonant LC commutation circuits increases the number of components and losses in the system.

In this research, various methods for power factor improvement will be investigated and the most effective and efficient method adopted for the control of the Asymmetrical Single – Phase Bridge *with two thyristors and two diodes and having the worst form of harmonics on the AC input of the converter* in other to overcome the limitations of Kataoka’s. The Asymmetrical Single – Phase Bridge converter was chosen for this study because

- ❖ It is *half controlled* and presents the worst form of harmonics to AC line current compared to Kataoka’s (1977), (1979) *fully controlled single and three – phase converters that presents low harmonics to AC supply*. The effect of high harmonics on AC supply is a low power factor which is the focus of this research.
- ❖ The asymmetrical single – phase bridge circuit is also easier to construct

The benchmark for this research work and the choice of the Asymmetrical AC – DC Single – Phase Converter in addition to the above is influenced by the worst form of harmonics it presents to a.c line current compared to three – phase AC – DC converter of Kataoka

2.2 The Thyristor

A thyristor is a four layer, three-junction, four layer p-n-p-n semiconductor switching device. It has three terminals; anode, cathode and gate. Fig. 2.1 (a) gives wafer structure of a typical

thyristor. Basically, a thyristor consists of four layers of alternate p-type and n-type silicon semiconductors with three junctions J_1 , J_2 and J_3 as shown in Fig. 2.1 (a). The Gate terminal is usually kept near the cathode terminal as shown Fig. 2.1 (a). The circuit symbols for a thyristor are shown respectively in Figs. 2.1 (b). The terminal connected to outer 'p' region is called anode (A), the terminal connected to outer 'n' region is called cathode (C) and that connected to inner 'p' region is called the gate (G). For large current applications, thyristors need better cooling; this is achieved to a great extent by mounting them onto heat sinks.

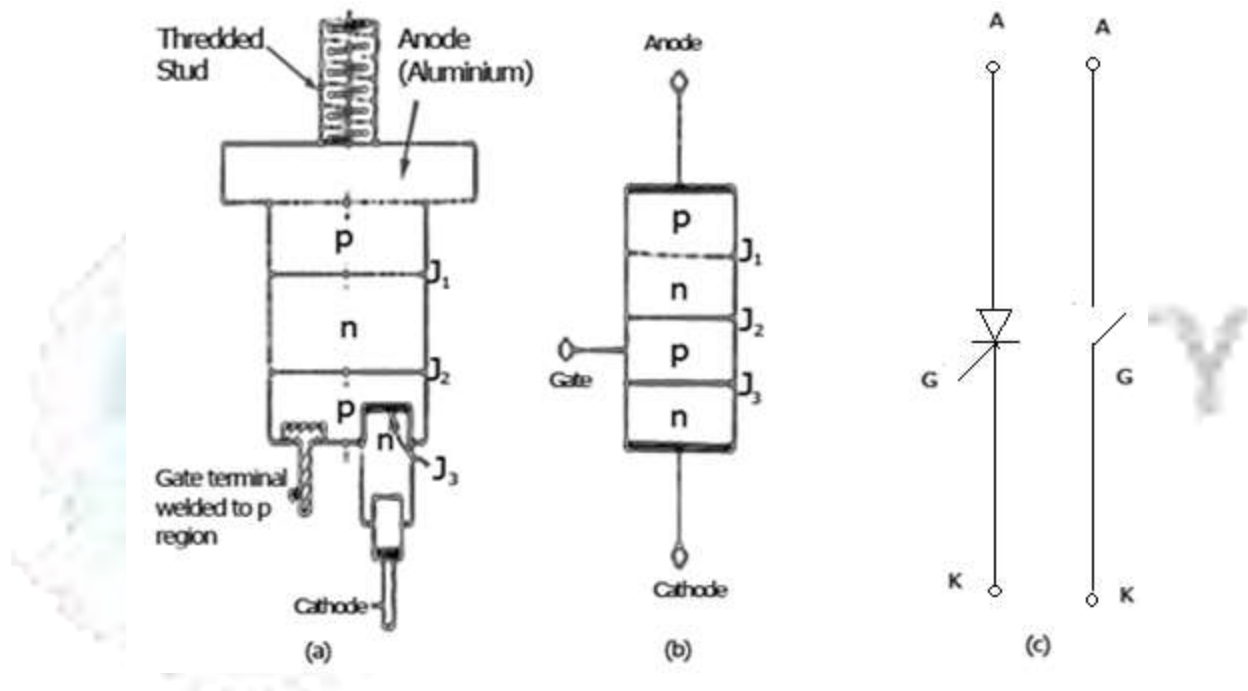


Fig. 2.1: Thyristor Structure and symbols

(a): Structure

(b): Symbols

SCR rating has improved considerably since its introduction in 1957. Now SCRs of voltage rating up to 10 kV and an rms current rating of 3000 A with corresponding power-handling capacity of 30 MW are available. As SCRs are solid state devices, they are compact, possess high reliability and have low loss. Because of these useful features, SCR is almost universally employed these days for all high power-controlled devices.

An SCR is so called because silicon is used for its construction and its operation as a rectifier (very low resistance in the forward conduction and very high resistance in the reverse direction)

can be controlled. Like the diode, an SCR is a unidirectional device that blocks the current flow from cathode to anode. Unlike the diode, a thyristor also blocks the current flow from anode to cathode until it is triggered into conduction by a proper gate signal between gate and cathode terminals.

2.2.1 I – V Characteristics of the thyristor

The static V-I characteristics of a thyristor is shown in Fig. 2.2. Here V_a is the anode voltage across thyristor terminals A, K and I_a is the anode current. The V-I characteristic shown in Fig. 2.2 reveals that a thyristor has three basic modes of operation

Modes of operation of a Thyristors:

Reverse blocking mode — Voltage is applied in the direction that would be blocked by a diode

Forward blocking mode — Voltage is applied in the direction that would cause a diode to conduct, but the thyristor has not yet been triggered into conduction

Forward conducting mode — The thyristor has been triggered into conduction and will remain conducting until the forward current drops below a threshold value known as the "holding current"

Reverse Blocking Mode: When cathode is made positive with respect to anode the thyristor is reverse biased as shown in Fig. 2.3 (a). Junctions J_1 J_3 are seen to be reverse biased whereas junction J_2 is forward biased. The device behaves as if two diodes are connected in series with reverse voltage applied across them. A small leakage current of the order of a few milliamperes (or a few microamperes depending upon the SCR rating) flows. This is reverse blocking mode, called the off-state, of the thyristor. If the reverse voltage is increased, then at a critical breakdown level, called reverse breakdown voltage V_{BR} , an avalanche occurs at J_1 and J_3 and the reverse current increases rapidly. A large current associated with V_{BR} gives rise to more losses in the SCR. This may lead to thyristor damage as the junction temperature may exceed its permissible temperature rise. It should, therefore, be ensured that maximum working reverse voltage across a thyristor does not exceed V_{BR} . When reverse voltage applied across a thyristor is less than V_{BR} , the device offers high impedance in the reverse direction. The SCR in the reverse blocking mode may therefore be treated as an open switch.

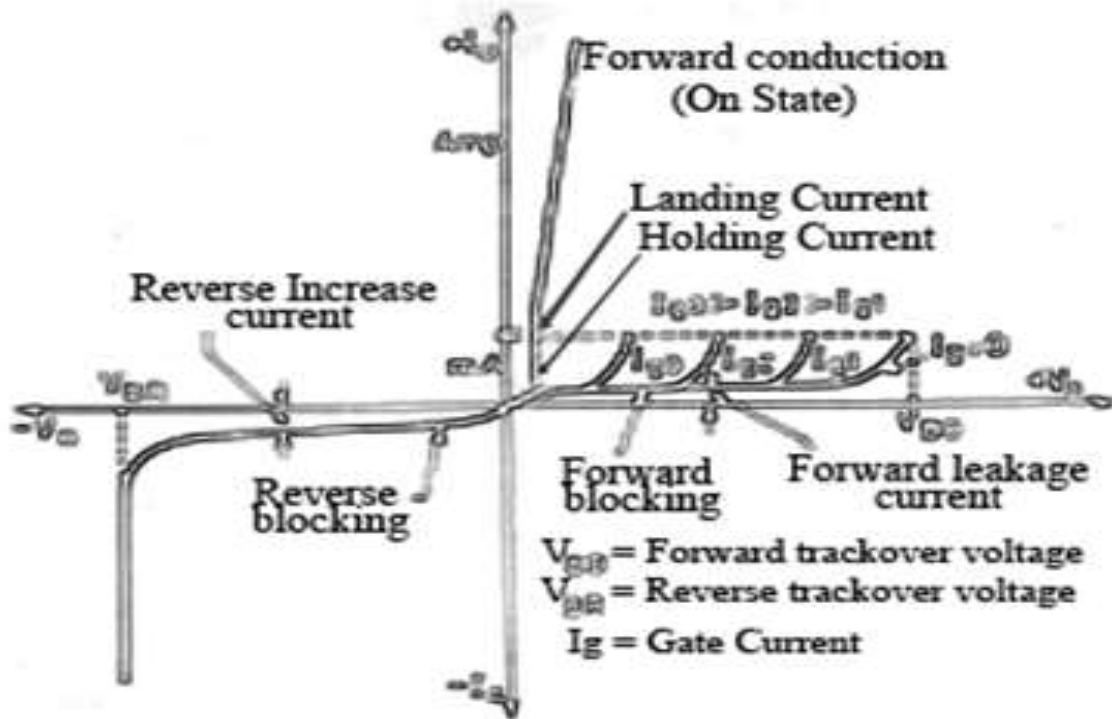


Fig. 2.2: Static I – V Characteristics of a thyristor

Note that V-I characteristic after avalanche breakdown during reverse blocking mode is applicable only when load resistance is zero. In case load resistance is present, a large anode current associated with avalanche breakdown at V_{BR} would cause substantial voltage drop across load and as a result, V-I characteristic in third quadrant would bend to the right of vertical line drawn at V_{BR} .

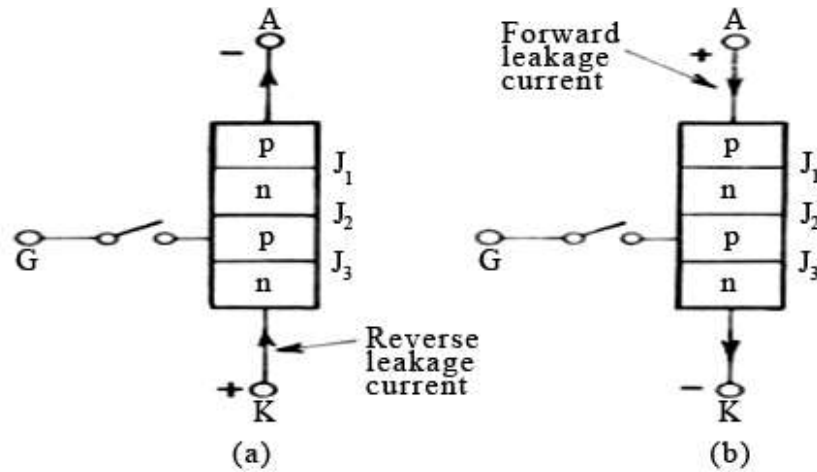


Fig. 2.3: Junction biased conditions

- (a) J_2 forward biased and J_1, J_3 reverse biased,
- (b) J_2 reverse biased and J_1, J_3 forward biased.

Forward Blocking Mode: When anode is positive with respect to the cathode, with gate circuit open, thyristor is said to be forward biased as shown in Fig. 2.3 (b). It is seen from this figure that junctions J_1, J_3 are forward biased but junction J_2 is reverse biased. In this mode, a small current, called forward leakage current, flows as shown in Figs. 2.2 and 2.3 (b). In case the forward voltage is increased, then the reverse biased junction J_2 will have an avalanche breakdown at a voltage called forward breakover voltage V_{BO} . When forward voltage is less than V_{BO} , SCR offers high impedance. Therefore, a thyristor can be treated as an open switch even in the forward blocking mode.

Forward Conduction Mode: In this mode, thyristor conducts currents from anode to cathode with a very small voltage drop across it. A thyristor is brought from forward blocking mode to forward conduction mode by turning it on, by exceeding the forward breakover voltage or by applying a gate pulse between gate and cathode. In this mode, thyristor is in on-state and behaves like a closed switch. Voltage drop across thyristor in the on state is of the order of 1 to 2 V depending on the rating of SCR. It may be seen from Fig. 2.2 that this voltage drop increases slightly with an increase in anode current. In conduction mode, anode current is limited by load impedance alone as voltage drop across SCR is quite small. This small voltage drop V_T across the device is due to ohmic drop in the four layers

2.2.2 Dynamic Characteristics of a Thyristor

Static and switching characteristics of thyristors are always taken into consideration for economical and reliable design of converter equipment. Static characteristics of a thyristor have already been examined. In this section; switching, dynamic or transient, characteristics of thyristors are discussed.

During turn-on and turn-off processes, a thyristor is subjected to different voltages across it and different currents through it. The time variations of the voltage across a thyristor and the current through it during turn-on and turn-off processes give the dynamic or switching characteristics of a thyristor. The switching characteristics during turn-on are described and then the switching characteristics during turn-off

Switching Characteristics during Turn-on

Before a thyristor is turned on, it is forward-biased and a positive gate voltage between gate and cathode. There is, however, a transition time from forward off-state to forward on state. This transition time called thyristor turn-on time is defined as the time during which it changes from forward blocking state to final on-state. Total turn-on time can be divided into three intervals; (i) delay time t_d , (ii) rise time t_r and (iii) spread time t_p , Fig. 2.5.

(i) Delay time t_d : The delay time t_d is measured from the instant at which gate current reaches $0.9 I_g$ to the instant at which anode current reaches $0.1 I_a$. Here I_g and I_a are respectively the final values of gate and anode currents. The delay time may also be defined as the time during which anode voltage falls from V_a to $0.9 V_a$ where V_a = initial value of anode voltage. Another way of defining delay time is the time during which anode current rises from forward leakage current to $0.1 I_a$ where I_a = final value of anode current. With the thyristor initially in the forward blocking state, the anode voltage is OA and anode current is small leakage current as shown in Fig. 2.6. Initiation of turn-on process is indicated by a rise in anode current from small forward leakage current and a fall in anode-cathode voltage from forward blocking voltage OA. As gate current begins to flow from gate to cathode with the application of gate signal, the gate current has non-uniform distribution of current density over the cathode surface due to the p layer. Its value is much higher near the gate but decreases rapidly as the distance from the gate increases, see

Fig. 2.4(a). This shows that during delay time t_d , anode current flows in a narrow region near the gate where gate current density is the highest.

The delay time can be decreased by applying high gate current and more forward voltage between anode and cathode. The delay time is fraction of a microsecond.

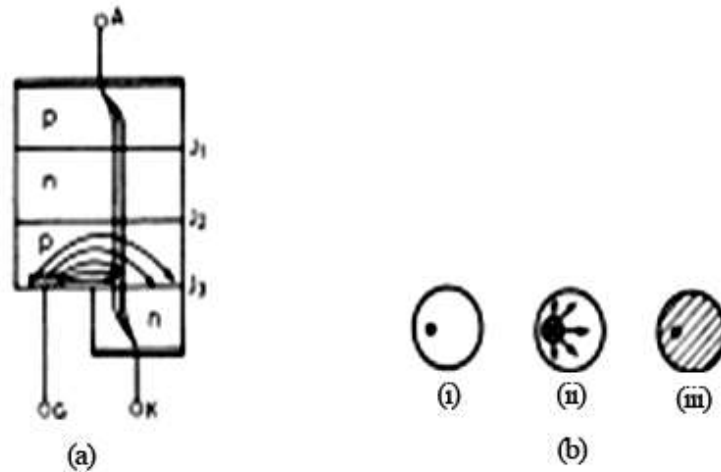


Fig. 2.4: Distribution of gate and anode current during delay time

(ii) Rise time t_r : The rise time t_r is the time taken by the anode current to rise from $0.1 I_a$ to $0.9 I_a$. The rise time is also defined as the time required for the forward blocking off-state voltage to fall from 0.9 to 0.1 of its initial value OA. The rise time is inversely proportional to the magnitude of gate current and its build up rate. Thus t_r can be reduced if high and steep current pulses are applied to the gate. However, the main factor determining t_r is the nature of anode circuit. For example, for series RL circuit, the rate of rise of anode current is slow, therefore, t_r is more. For RC series circuit, di/dt is high, t_r is therefore, less.

From the beginning of rise time t_r anode current starts spreading from the narrow conducting region near the gate. The anode current spreads at a rate of about 0.1 mm per microsecond. As the rise time is small, the anode current is not able to spread over the entire cross-section of cathode. Fig. 2.4(b) illustrates how anode current expands over cathode surface area during turn-on process of a thyristor. Here the thyristor is taken to have single gate electrode away from the

centre of p-layer. It is seen that anode current conducts over a small conducting channel even after t_r -this conducting channel area is however, greater than that during t_d . During rise time, turn-on losses in the thyristor are the highest due to high anode voltage (V_a) and large anode current (I_a) occurring together in the thyristor as shown in Fig. 2.5. As these losses occur only over a small conducting region, local hot spots may be formed and the device may be damaged.

(iii) Spread time t_p : The spread time is the time taken by the anode current to rise from $0.9 I_a$ to I_a . It is also defined as the time for the forward blocking voltage to fall from 0.1 of its value to the on-state voltage drop (1 to 1.5 V). During this time, conduction spreads over the entire cross-section of the cathode of SCR. The spreading interval depends on the area of cathode and on gate structure of the SCR. After the spread time, anode current attains steady state value and the voltage drop across SCR is equal to the on-state voltage drop of the order of 1 to 1.5 V, Fig. 2.5.

Total turn-on time of an SCR is equal to the sum of delay time, rise time and spread time. Thyristor manufacturers usually specify the rise time which is typically of the order of 1 to 4 μ -sec. Total turn-on time depends upon the anode circuit parameters and the gate signal wave shapes.

During turn-on, SCR may be considered to be a charge controlled device. A certain amount of charge must be injected into the gate region for the thyristor conduction to begin. This charge is directly proportional to the value of gate current. Therefore, the higher the magnitude of gate current, the lesser time it takes to inject this charge. The turn-on time can therefore be reduced by using higher values of gate currents. The magnitude of gate current is usually 3 to 5 times the minimum gate current required to trigger an SCR.

When gate current is several times higher than the minimum gate current required, a thyristor is said to be hard-fired or overdriven. Hard-firing or overdriving of a thyristor reduces its turn-on time and enhances its di/dt capability.

Switching Characteristics during Turn-off

Thyristor turn-off means that it has changed from on to off state and is capable of blocking the forward voltage. This dynamic process of the SCR from conduction state to forward blocking state is called commutation process or turn-off process.

Once the thyristor is on, gate loses control. The SCR can be turned off by reducing the anode current below holding current. If forward voltage is applied to the SCR at the moment its anode current falls to zero, the device will not be able to block this forward voltage as the carriers (holes and electrons) in the four layers are still favourable for conduction. The device will therefore go into conduction immediately even though gate signal is not applied. In order to obviate such an occurrence, it is essential that the thyristor is reverse biased for a finite period after the anode current has reached zero.

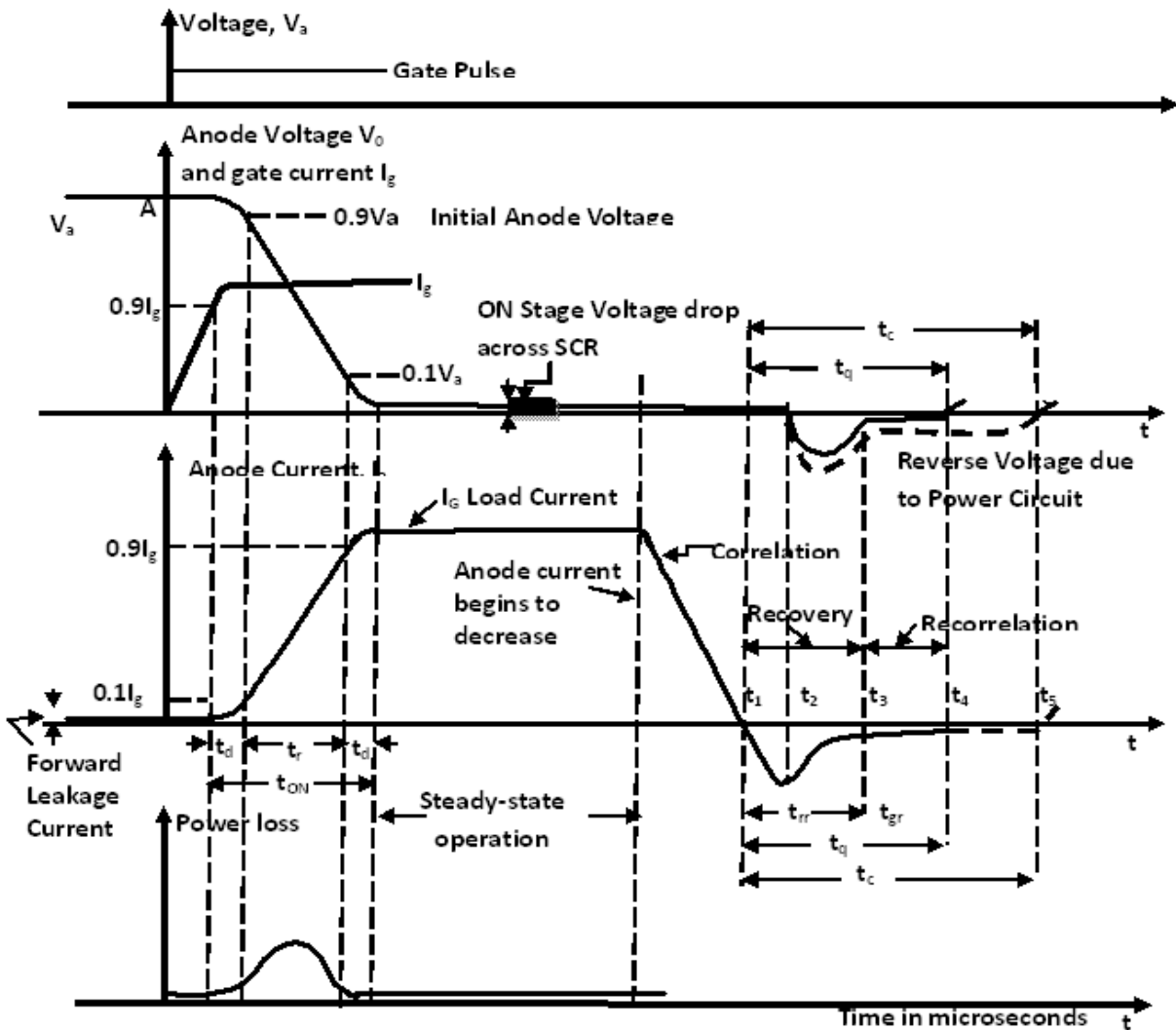


Fig.2.5: Thyristor voltage and current waveforms during turn-on and turn-off processes

The turn-off time t_q of a thyristor is defined as the time between the instant anode current becomes zero and the instant SCR regains forward blocking capability. During time t_q all the excess carriers from the four layers of SCR must be removed. This removal of excess carriers consists of sweeping out of holes from outer p-layer and electrons from outer n-layer. The carriers around junction J_2 can be removed only by recombination. The turn-off time is divided into two intervals; reverse recovery time t_{rr} and the gate recovery time t_{gr} ; i.e. $t_q = t_{rr} + t_{gr}$.

The thyristor characteristics during turn-on and turn-off processes are shown in one Fig. 2.5 so as to gain insight into these processes.

At instant t_1 anode current becomes zero. After t_1 anode current builds up in the reverse direction with the same di/dt slope as before t_1 . The reason for the reversal of anode current after t_1 is due to the presence of carriers stored in the four layers. The reverse recovery current removes excess carriers from the end junctions J_1 and J_3 between the instants t_1 and t_3 . In other words, reverse recovery current flows due to the sweeping out of holes from top p-layer and electrons from bottom n-layer. At instant t_2 , when about 60% of the stored charges are removed from the outer two layers, carrier density across J_1 and J_3 begins to decrease and with this reverse recovery current also starts decaying. The reverse current decay is fast in the beginning but gradual thereafter. The fast decay of recovery current causes a reverse voltage across the device due to the circuit inductance. This reverse voltage surge appears across the thyristor terminals and may therefore damage it. In practice, this is avoided by using protective RC elements across SCR. At instant t_3 , when reverse recovery current has fallen to nearly zero value, end junctions J_1 and J_3 recover and SCR is able to block the reverse voltage. For a thyristor, reverse recovery phenomenon between t_1 and t_3 is similar to that of a rectifier diode.

At the end of reverse recovery period (t_3 -the middle junction J_2 still has trapped charges, therefore, the thyristor is not able to block the forward voltage at t_3 . The trapped charges around J_2 , i.e. in the inner two layers, cannot flow to the external circuit, therefore, these trapped charges must decay only by recombination. This recombination is possible if a reverse voltage is maintained across SCR, though the magnitude of this voltage is not important. The rate of recombination of charges is independent of the external circuit parameters. The time for the recombination of charges between t_3 and t_4 is called gate recovery time t_{gr} . At instant t_4 , junction

J_2 recovers and the forward voltage can be reapplied between anode and cathode. The thyristor turn-off time t_q is in the range of 3 to 100 μsec . The turn-off time is influenced by the magnitude of forward current, di/dt at the time of commutation and junction temperature. An increase in the magnitude of these factors increases the thyristor turn-off time. If the value of forward current before commutation is high, trapped charges around junction J_2 are more. The time required for their recombination is more and therefore turn-off time is increased. But turn-off time decreases with an increase in the magnitude of reverse voltage, particularly in the range of 0 to - 50 V. This is because high reverse voltage sucks out the carriers out of the junctions J_1 , J_3 and the adjacent transition regions at a faster rate. It is evident from above that turn-off time t_q is not a constant parameter of a thyristor.

The thyristor turn-off time t_q is applicable to an individual SCR. In actual practice, thyristor (or thyristors) form a part of the power circuit. The turn-off time provided to the thyristor by the practical circuit is called circuit turn-off time t_c . It is defined as the time between the instant anode current becomes zero and the instant reverse voltage due to practical circuit reaches zero, see Fig. 2.5. Time t_c must be greater than t_q for reliable turn-off, otherwise the device may turn-on at an undesired instant, a process called commutation failure.

Thyristors with slow turn-off time (50 - 100 μsec) are called converter grade SCRs and those with fast turn-off time (3 - 50 μsec) are called inverter-grade SCRs. Converter-grade SCRs are cheaper and are used where slow turn-off is possible as in phase-controlled rectifiers, ac voltage controllers, cycloconverters etc. Inverter-grade SCRs are costlier and are used in inverters, choppers and force-commutated converters.

2.3 Circuits and Devices used in power Factor correction Schemes

A number of the devices discussed in this section were used in the implementation of this research work. The operational amplifier for instance was used as an integrator to obtain the required saw tooth signals that was compared with a dc signal to obtain the desired pulses needed to turn – on the gates of the thyristors. The 555 timer was used either in the astable or monostable mode to generate pulses. The applications of an operational amplifier and the 555 timer are presented below.

2.3.1 Operational amplifiers and applications

The op-amp is basically a differential amplifier having a large voltage gain, very high input impedance and low output impedance. The op-amp has a "inverting" or (-) input and "non-inverting" or (+) input and a single output. The op-amp is usually powered by a dual polarity power supply in the range of +/- 5 volts to +/- 15 volts. A simple dual polarity power supply is shown in the figure below which can be assembled with two 9 volt batteries.

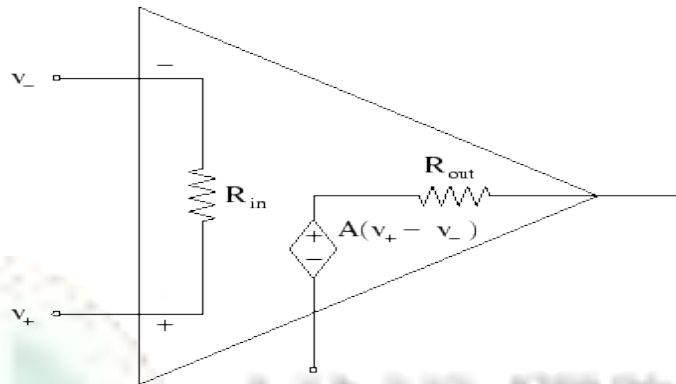


Figure 2.6: A circuit model of an operational amplifier (op amp) with gain A and input and output resistances R_{in} and R_{out} .

A circuit model of an operational amplifier is shown in Figure 2.6. The output voltage of the op amp is linearly proportional to the voltage difference between the input terminals $v_+ - v_-$ by a

factor of the gain, 'A'. However, the output voltage is limited to the range $-V_{cc} \leq v \leq V_{cc}$, where V_{cc} is the supply voltage specified by the designer of the op amp. The range $-V_{cc} \leq v \leq V_{cc}$, is often called the linear region of the amplifier, and when the output swings to V_{cc} or $-V_{cc}$, the op amp is said to be saturated.

An ideal op amp has infinite gain ($A = \infty$), infinite input resistance ($R_{in} = \infty$), and zero output resistance ($R_{out} = 0$). A consequence of the assumption of infinite gain is that, if the output voltage is within the finite linear region, then $v_+ = v_-$. A real op amp has a gain on the range $10^3 - 10^5$ (depending on the type), and hence actually maintains a very small difference in input terminal voltages when operating in its linear region. The operational amplifier can be used as an inverter amplifier, non – inverting amplifier, integrator, differentiator, comparator etc.

2.3.2 Operational amplifier as an Inverting Amplifier

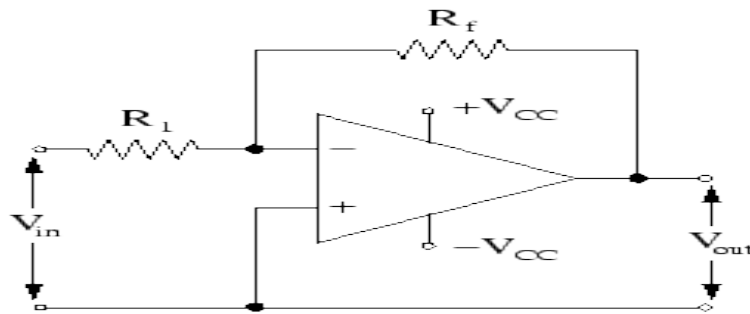


Figure 2.7: Inverting amplifier circuit.

Where the gain of the amplifier is

$$A = -\frac{R_f}{R_1}. \quad (2.1)$$

2.3.3 Operational amplifier as a non - inverting Amplifier

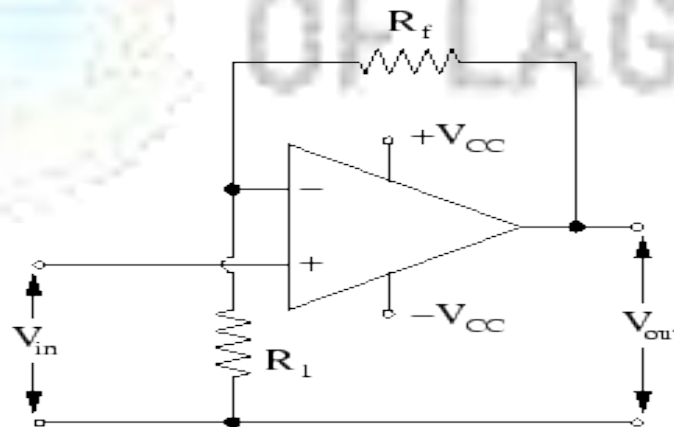


Figure 2.8: Non - inverting amplifier circuit.

Here the gain of the amplifier is

$$A = \frac{R_1 + R_f}{R_1}.$$

2.3.4 Operational amplifier as an Integrator

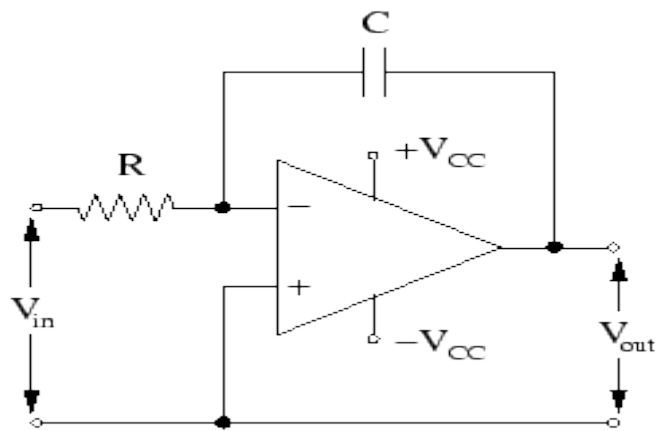


Figure 2.9: Integrator circuit.

The output signal of the amplifier is

$$V_{out} = -\frac{1}{RC} \int V_{in} dt. \quad (2.2)$$

2.3.5 Operational amplifier as a Differentiator

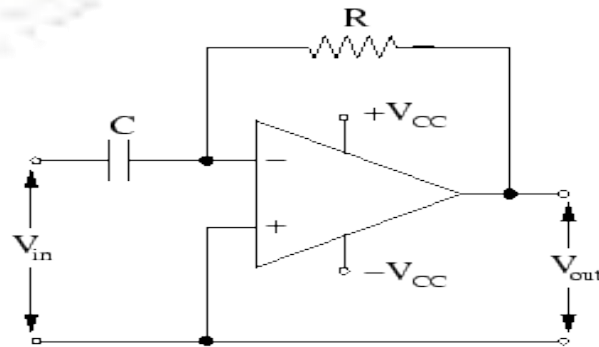


Figure 2.10: Differentiator circuit.

The output signal of the amplifier is

$$V_{out} = -RC \frac{dV_{in}}{dt}. \quad (2.3)$$

2.3.6 Operational amplifier as a Comparator

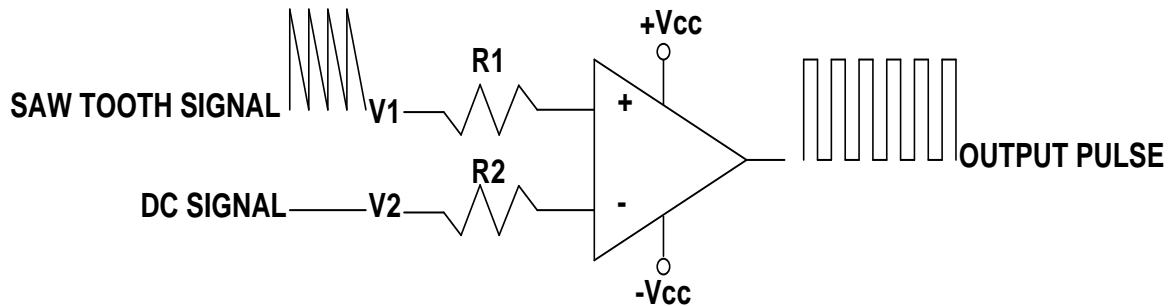


Figure 2.11: The 741 IC as a Comparator

Here, the operational amplifier compares two analog signals to produce a digital output. With this approach, the gate signals required to trigger the thyristors of the AC – DC converter supplying a DC motor load are generated by comparing a triangular wave with a DC signal as shown in Fig. 5.1.

An oscillator can be used to generate the triangular or sawtooth waveform and a potentiometer, to set a steady reference DC voltage. The comparator compares the sawtooth voltage with the reference voltage. When the sawtooth voltage rises above the reference voltage, a pulse appears at the output of the operational amplifier. As it falls below the reference, the lagging edge of the pulse appears. The pulse shown in Fig.5.1 is then used to trigger the thyristor. The time at which the rising edge of the pulse occurs defines the firing angle “ α ”.

2.4 The 555 Timer IC

The 555 Timer IC is an integrated circuit (chip) implementing a variety of timer and multivibrator applications. The 555 gets its name from the three 5-kohm resistors used in typical early implementations. It is easy to use and has a low price and good stability. Depending on the manufacturer, it includes over 20 transistors, 2 diodes and 15 resistors on a silicon chip installed in an 8-pin mini dual-in-line package (DIP – 8). The 556 is a 14-pin DIP that combines two 555s on a single chip. The 558 is a 16-pin DIP that combines four slightly modified 555s on a single chip (DIS & THR are connected internally, TR is falling edge sensitive instead of level

sensitive). Also available are ultra-low power versions of the 555 such as the 7555 and TLC555. The 7555 requires slightly different wiring using fewer external components and less power.

The 555 has three operating modes:

- Monostable mode: in this mode, the 555 functions as a "one-shot". Applications include timers, missing pulse detection, bounce free switches, touch switches, Frequency Divider, Capacitance Measurement, Pulse Width Modulation (PWM) etc
- Astable - Free Running mode: the 555 can operate as an oscillator. Uses include LED and lamp flashers, pulse generation, logic clocks, tone generation, security alarms, pulse position modulation, etc.
- Bistable mode or Schmitt trigger: the 555 can operate as a flip - flop, if the DIS pin is not connected and no capacitor is used. Uses include bounce free latched switches, etc.

2.4.1 Monostable mode

In the monostable mode, the 555 timer acts as a "one-shot" pulse generator. The pulse begins when the 555 timer receives a trigger signal. The width of the pulse is determined by the time constant of an RC network, which consists of a capacitor (C) and a resistor (R). The pulse ends when the charge on the C equals 2/3 of the supply voltage. The pulse width can be lengthened or shortened to the need of the specific application by adjusting the values of R and C. The pulse width of time t is given by

$$t = RC \ln(3) \approx 1.1RC \quad (2.4)$$

which is the time it takes to charge C to 2/3 of the supply voltage. See RC circuit for an explanation of this effect.

The relationships of the trigger signal, the voltage on the C and the pulse width are shown below

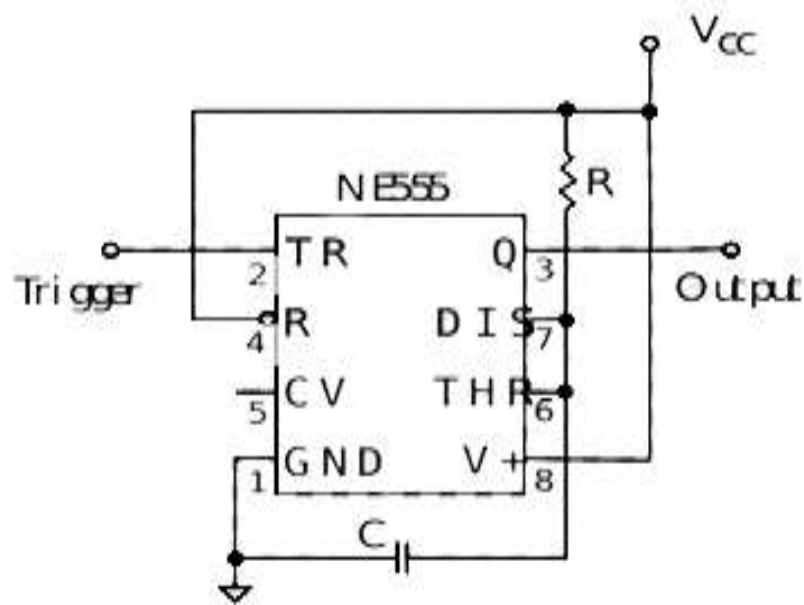


Fig. 2.12: Schematic of a 555 in monostable mode

2.4.2 Astable mode

In astable mode, the 555 timer outputs a continuous stream of rectangular pulses having a specified frequency. A resistor (call it R_1) is connected between V_{cc} and the discharge pin (pin 7) and another (R_2) is connected between the discharge pin (pin 7) and the trigger (pin 2) and threshold (pin 6) pins that share a common node. Hence the capacitor is charged through R_1 and R_2 , and discharged only through R_2 , since pin 7 has low impedance to ground during output low intervals of the cycle, therefore discharging the capacitor. The use of R_2 is mandatory, since without it the high current spikes from the capacitor may damage the internal discharge transistor.

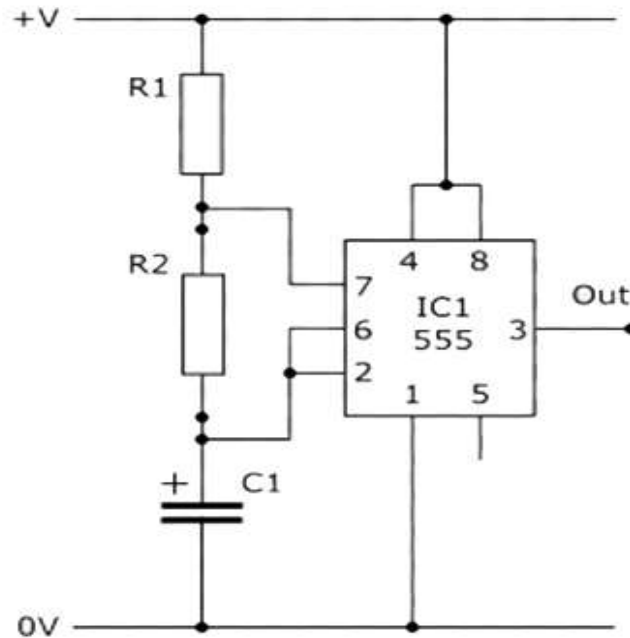


Fig.2.13: Standard 555 Astable Circuit

In the astable mode, the frequency of the pulse stream depends on the values of R_1 , R_2 and C :

$$f = 1/(0.693 \cdot C \cdot (R_1 + 2 \cdot R_2)) \quad (2.5)$$

The high time from each pulse is given by

$$high = 0.693 \cdot (R_1 + R_2) \cdot C \quad (2.6)$$

and the low time from each pulse is given by

$$low = 0.693 \cdot R_2 \cdot C \quad (2.7)$$

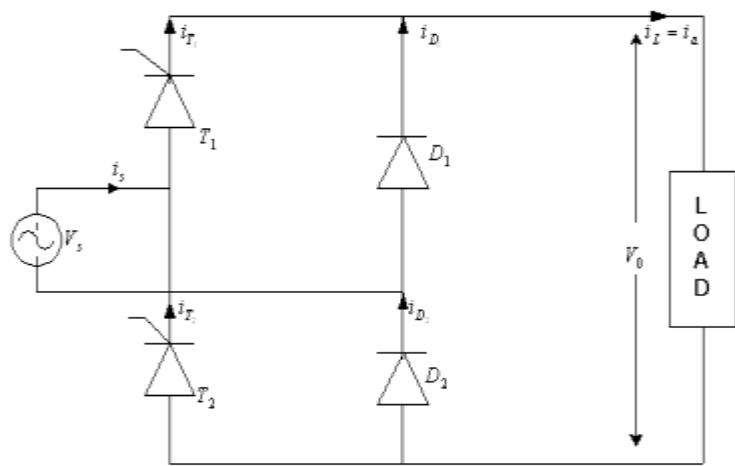
where R_1 and R_2 are the values of the resistors in ohms and C is the value of the capacitor in farad.

2.5 The Single – Phase Asymmetrical Bridge Converter.

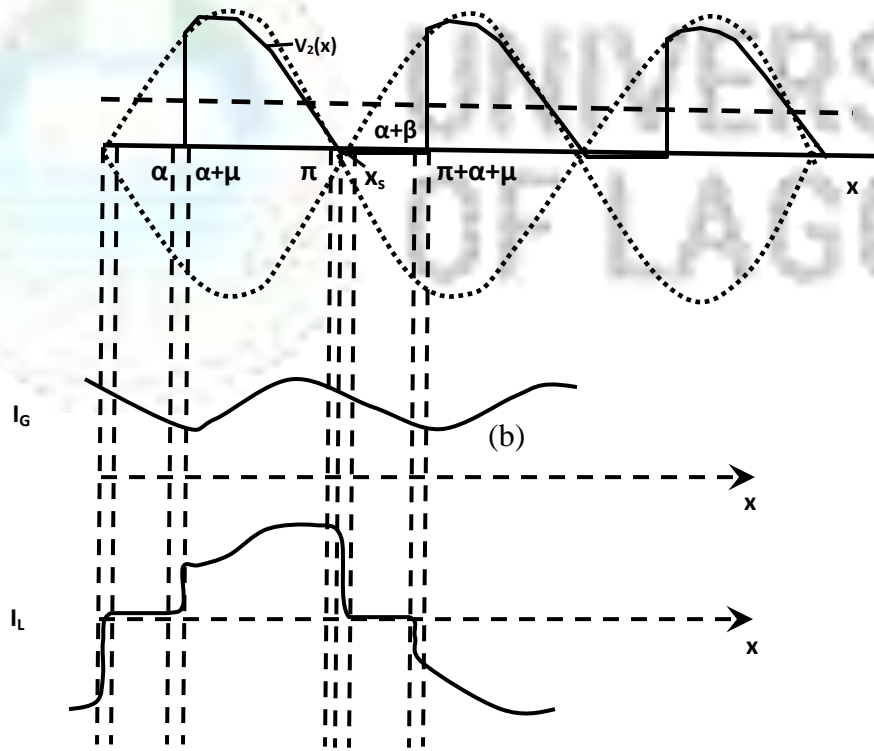
The circuit arrangement of an asymmetrical single – phase bridge converter used for AC - DC conversion is shown in Fig. 2.14. The choice of this controller for this study is influenced by the fact that:

- It presents the worst form of harmonics to its loads which distorts the AC input voltage and current
- It has a wide range of applications
- It is increasingly being applied to main line rail propulsion system
- It is used in low power motor control system
- It is simple to construct

In Fig.2.14, during the positive half – cycle, thyristor T_1 is forward biased. When T_1 is fired at $\omega t = \alpha$ the load is connected to the input supply through T_1 and D_2 in the interval $\alpha \leq \omega t \leq \pi$. During the interval $\pi \leq \omega t \leq (\pi+\alpha)$, the input voltage is negative and the freewheeling diode D_1 is now forward biased and conducts to provide the continuity of current in the inductive load. The load current is transferred from T_1 and D_2 and thyristor T_1 and diode D_2 are turned – off. During the negative half – cycle of the input voltage, thyristor T_2 is forward biased and the firing of thyristor T_2 at $\omega t \leq (\pi+\alpha)$ will reverse biased D_2 . The diode D_2 is turned – off and the load is connected to the supply through T_2 and D_1 .



(a)



(b)

Fig. 2.14: Single – phase Asymmetrical Bridge Converter

(a) Power Circuit Configuration

(b) Waveform of Input Current and Voltage

The input current i_L is clearly non - sinusoidal with the input voltage, this is as a result of the harmonics introduced into the supply due to the switching action of semi – conductor devices

Now that the basic concept of the of the devices used for this research has been described, the subsequent chapters will discuss the establishment of the input power factor problem, the various methods of power factor correction improvement schemes and the most efficient and effective method for the solution to the poor input power factor in drives.



UNIVERSITY
OF LAGOS

CHAPTER THREE

MODELLING AND ANALYSIS OF THE BRIDGE CONVERTER WITH DC MOTOR LOAD

3.0 Introduction

To investigate the problem of harmonics in the AC line current and analytically predict its waveshape, the single – Phase Bridge will be considered to have four intervals of operations (Metha et.al 1974) – Forward Commutation Interval, Conduction Interval, Free-wheeling Interval and Reverse Commutation Interval. This is because, as a result of the finite source inductance, current in a thyristor fired at an instant ‘ α ’ does not rise instantaneously. Explicit expressions are to be developed in each of these intervals using the piecewise linear (PWL) method, with the simplifying assumptions that the terminal conditions of one interval are the initial conditions for the next interval. The waveform of the AC input current is obtained by using the equations determined for the intervals in a half cycle.

The waveform of the input current degenerates as the firing angle of the drive increases. Fourier integral method was applied to the explicit expressions for the motor input current to derive equations for the harmonic currents. It has equally been shown by experiments that where a number of drives are connected to the same AC source, the power factor worsens.

3.1 Modelling the DC Motor

The prediction of supply input current in a DC Drive is influenced by the motor parameters when the motor is fed from the Bridge. The subsequent electrical loop equation is of the form:

$$v_a(t) = E_a(\omega, i_f) + R_a(i_a)i_a(t) + L_a(i_f)\frac{di_a(t)}{dt} \quad (3.1)$$

Where,

$v_a(t)$ is the output voltage of the Bridge

$E_a(\omega, i_f)$ is the motor back emf,

$L_a(i_f)$ is the Armature inductance,

$R_a(i_a)$ is the Armature resistance,

$i_a(t)$ is the instantaneous input current

Saturation is one of the main sources of non – linearity in a DC machine. Flux dependent parameters such as armature inductance and back emf have to be evaluated for a definite operating point or the values modified as the operating point varies. Fig. (3.1) show the magnetization characteristics of the laboratory machine obtained at specific speeds. According to Mukher (1961), the non – linearity associated with magnetic saturation is included in equations describing the machine operation by the use of slopes obtained at the operating points on the magnetization curve. The concept of constant inductance for D.C machines is therefore an aberration (Sinha et.al 1974, Szabados et.l 1972, Damle et.al 1976) and many methods are available in literature according to Agarwal (1959) for modelling D.C machine inductance. In subsequent analysis, the parameters are assumed to be determined at specific operating points.

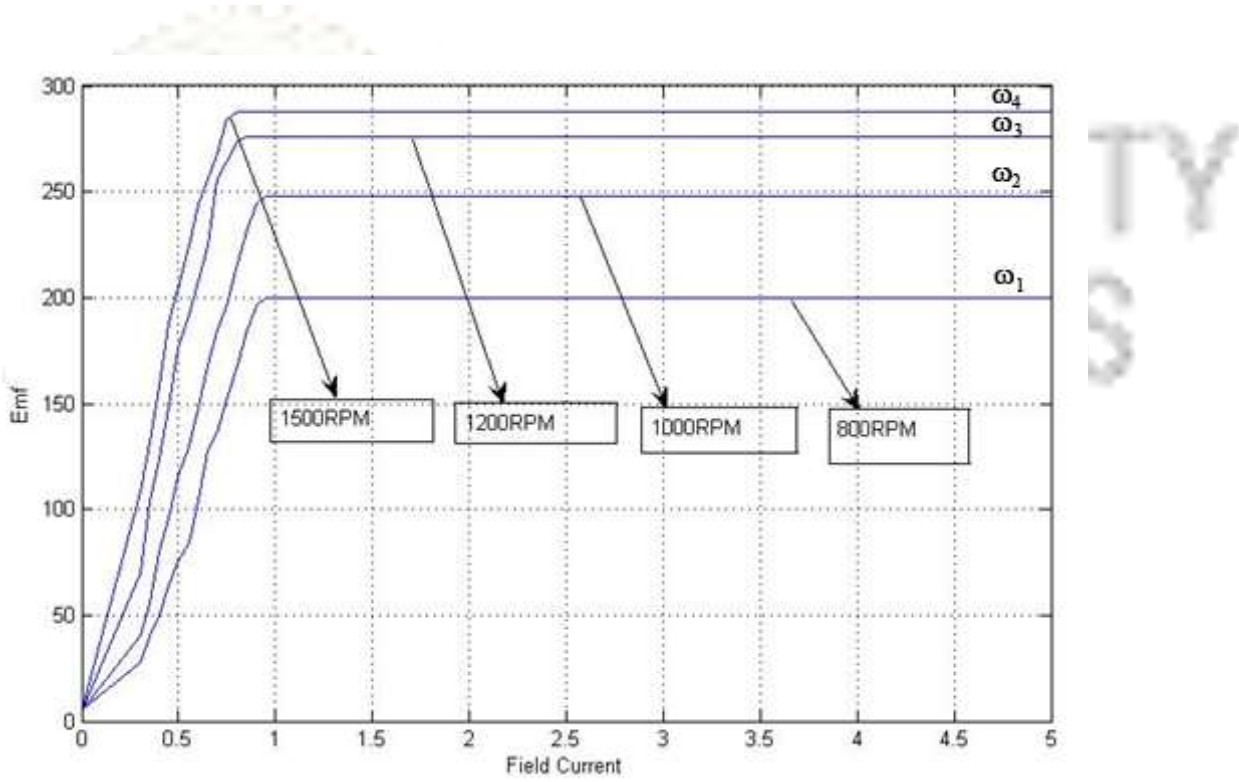


Fig.3.1: Magnetisation Characteristics of a DC Motor

3.2 Piece – Wise Linear analysis of the Single – Phase Bridge Converter with DC Motor Load

The circuit configuration of the asymmetrical single-phase bridge converter with a half-cycle equivalent supplying a separately excited dc motor operating in a discontinuous armature conduction current mode is shown in Fig.3.2. The control circuit layout of the drive is presented in Figure (3.3). The main difficulty in predicting the input ac current of the controller and in analysing the converter circuits is that the switching action of the devices makes the circuits non – linear (Okoro C.C 1987 and Ira Pitel et.al 1977). This difficulty is overcome by using linear equivalent circuits which represent the system in particular time domains of operation according to Mellit et.al (1974) and Nisit et.al (1978).

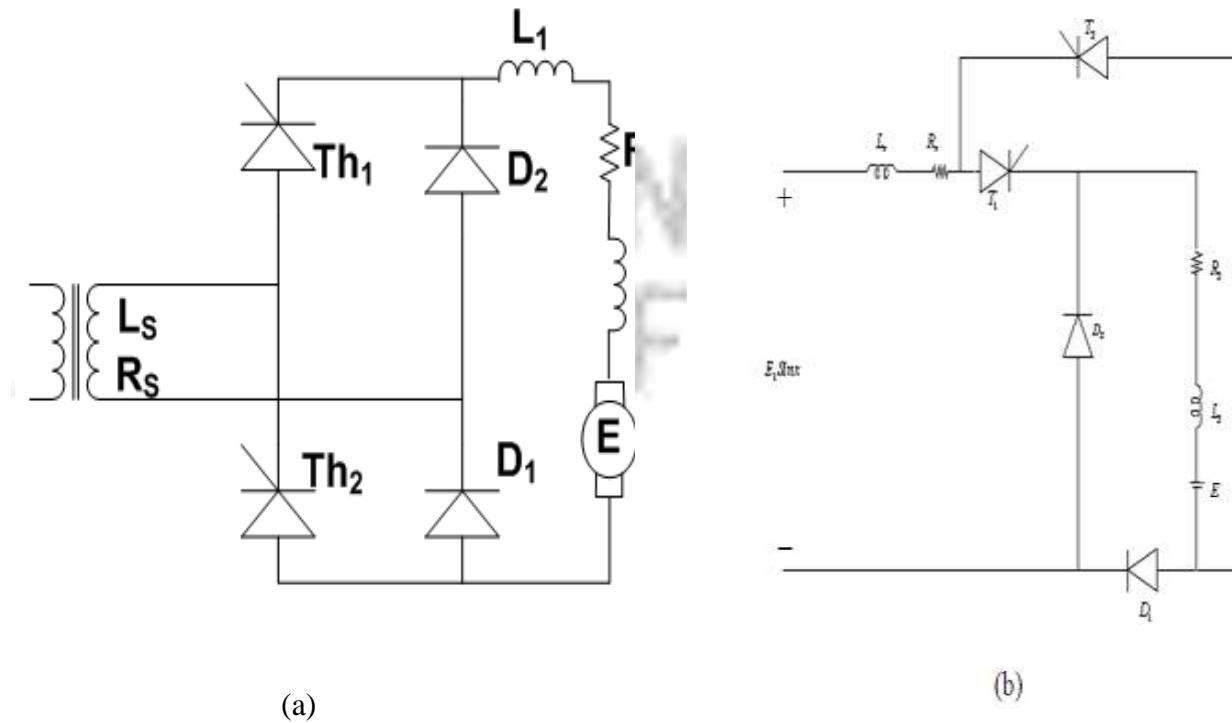


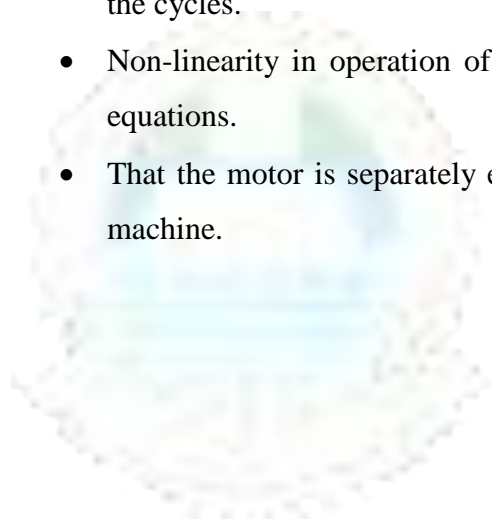
Fig.3.2: The asymmetrical single-phase bridge converter with a DC Motor Load
 (a): Main circuit (b): Half cycle equivalent

The waveform of the currents and voltages of the controller presented in Figure 3.4 show the various intervals of operation

3.3 Modes of Operation

The operation of the Asymmetrical Bridge may be described by the equivalent circuits representing each interval of operation as presented in Fig.3.5. In analyzing the circuits for the different intervals, the terminal conditions of one interval are the initial conditions for the next interval and the simplifying equations are based on the following assumptions (Metha et.al 1974 and Okoro 1980)

- That the thyristor are ideal switches.
- That a steady- state condition has been established to justify repetitive representation of the cycles.
- Non-linearity in operation of the machine is included in the parameters of the system equations.
- That the motor is separately excited and the operating point fixes the parameters of the machine.



UNIVERSITY
OF LAGOS

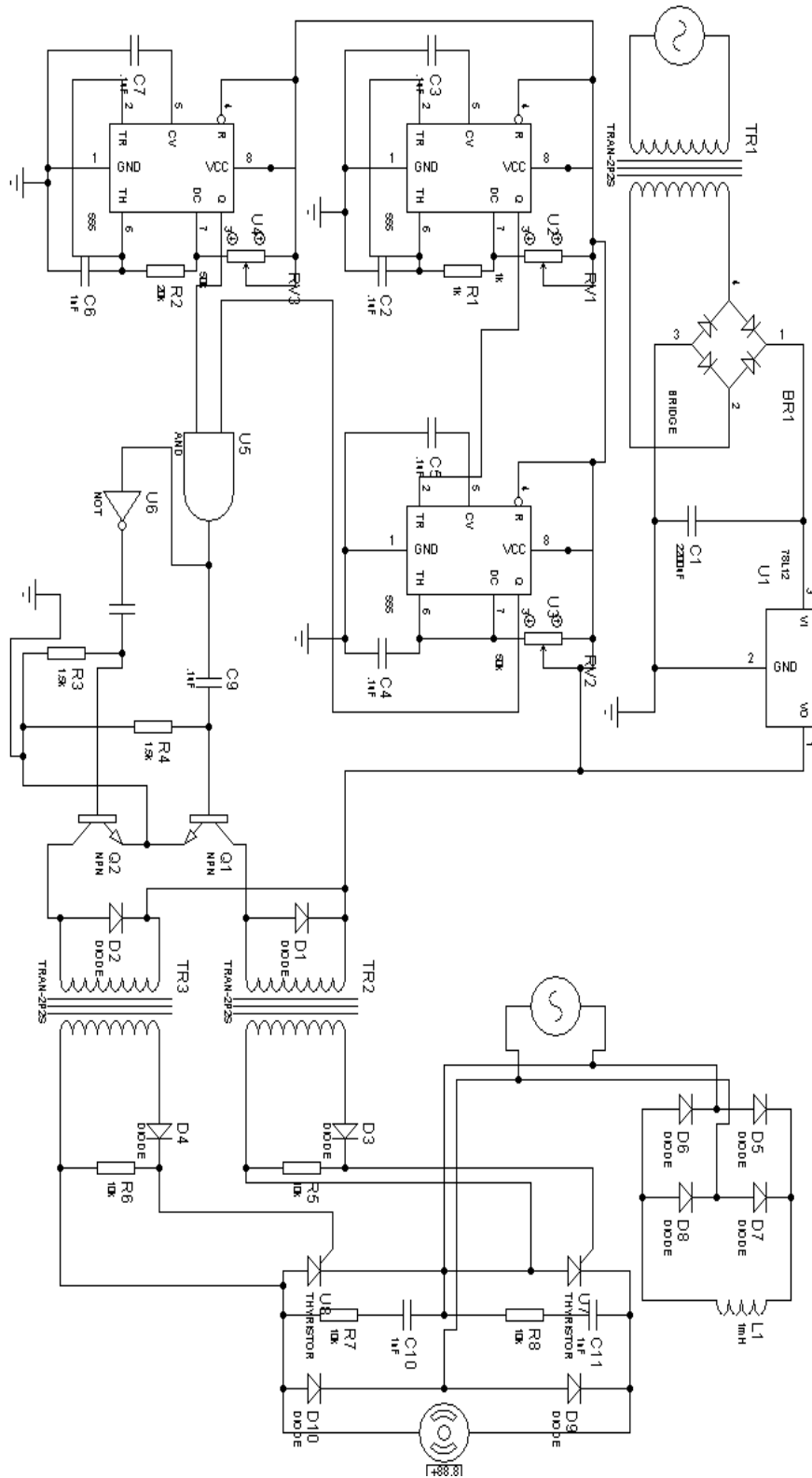


Fig.3.3: Control Circuit Layout for a Single – Phase asymmetric Bridge Drive

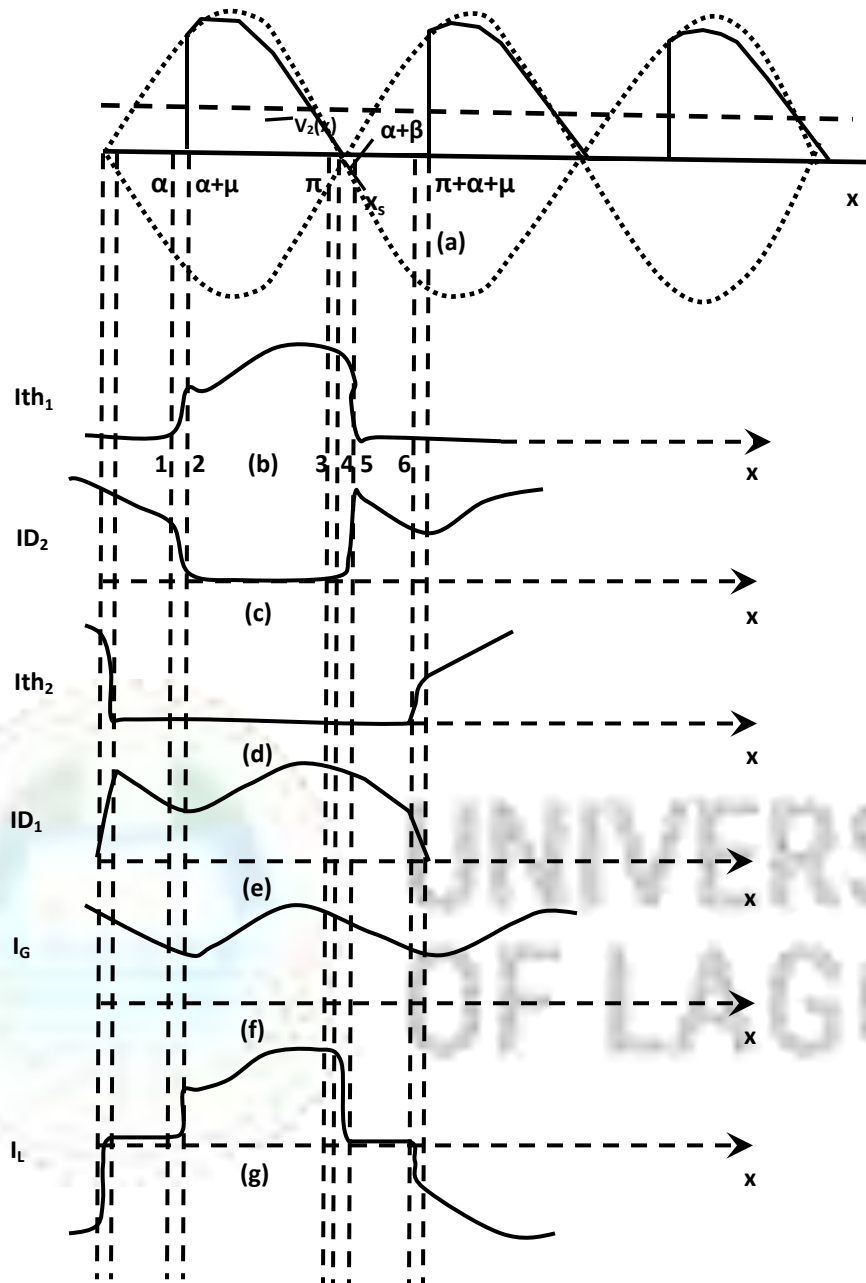


Fig.3.4: Operational intervals and Waveforms of the Bridge Converter

(a) Voltage waveforms

(b-g) Current waveforms

1-2 Forward commutation of Th_1

2-3 Conduction of Th_1

3-4 Angle ' β ' after ' π ' for D_2 to become forward biased

4-5 Extinction Interval

5-6 Freewheeling Interval

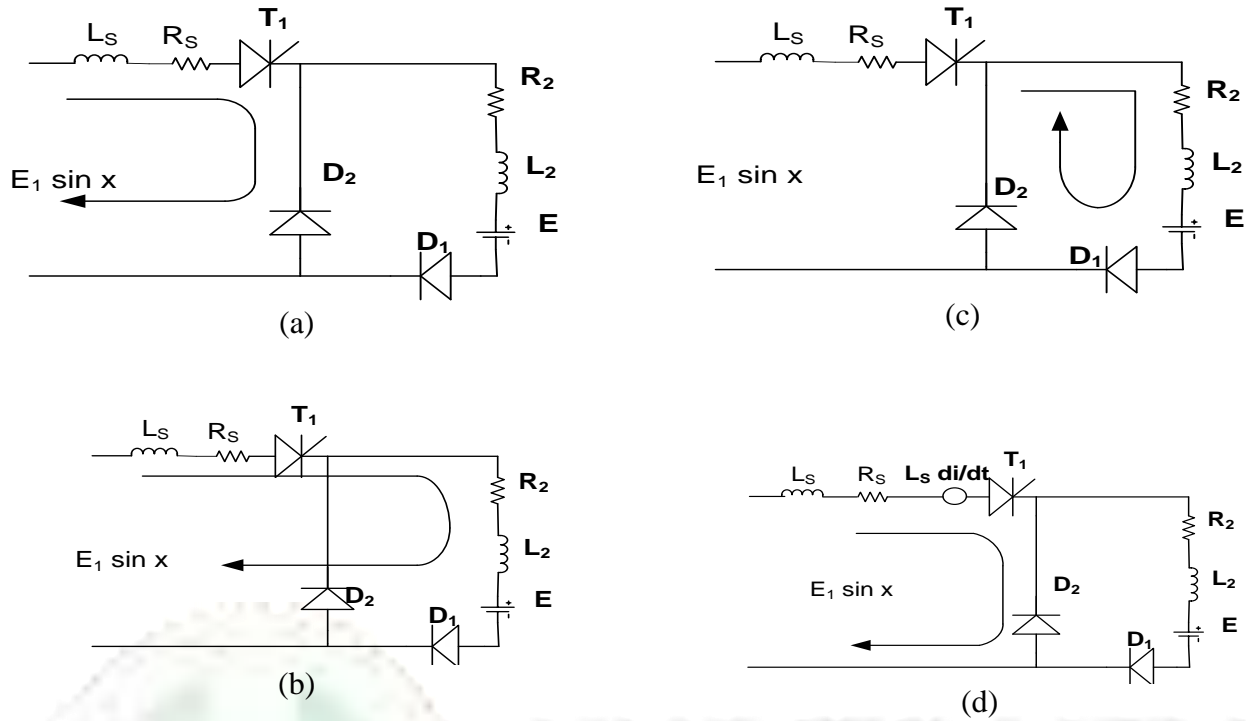


Fig. 3.5: Bridge Converter with half - Cycle Equivalent Circuits

- (a) Forward Commutation Interval, $\alpha < x < \alpha + \mu$
- (b) Thyristor Conduction Interval $\alpha + \mu < x < \pi$
- (c) Freewheeling Interval $0 < x < \alpha$
- (d) Reverse Commutation Interval or Extinction Interval $\pi + \beta < x < \pi + \beta + x_s$

3.4 Analysis for AC input current

Explicit equations for the motor input current of the converter – fed dc motor are derived for the different intervals below. In applying the piece – wise linear method of analysis, the shift in voltage source along the time axis for the different intervals is to enable the prediction of currents at the various intervals of operation. As a result of the finite source inductance, current in the thyristor fired at an instant ' α ' does not rise instantaneously. In the interval $\alpha < \omega t < \alpha + \mu$ shown in Fig.3.4, the thyristor T_1 forward commutates and its current rises to the value of the motor current.

(A) Forward commutation interval

This is defined by interval $\alpha < \omega t < \alpha + \mu$

And having initial condition $i = 0$ at $\omega t = 0$

Equation for current during this interval is obtained from the equivalent circuit of Fig.3.5 (a) as;

$$L_s \frac{di}{dt} + R_s i = E_1 \sin(\omega t + \alpha) \quad (3.2)$$

Where R_s and L_s are the source supply resistance and inductance respectively.

Equation (3.2) can be solved by either Laplace function method or integrating factor method

Using integrating factor method of solving differential equations, the current at the end of the interval is obtained as;

$$i(t) = K_1 \left[\sin(\omega t + \alpha - \theta_1) + \sin(\theta_1 - \alpha) e^{-\frac{t}{\tau_1}} \right]$$

The current at the end of the interval when $\omega t = \mu$, $i(t) = I_{ao}$, is then,

$$I_{ao} = K_1 \left[\sin(\mu + \alpha - \theta_1) + \sin(\theta_1 - \alpha) e^{-\left(\frac{\mu}{\omega \tau_1}\right)} \right] \quad (3.3)$$

Where $\tau_1 = \frac{L_s}{R_s}$, $|z| = \sqrt{(\omega L_s)^2 + R_s^2}$, $\tan^{-1}\left(\frac{\omega L_s}{R_s}\right) = \theta_1$, $K_1 = \frac{E_1}{|z|}$,

A complete analysis is given in APPENDIX I

(B) Conduction interval ($\alpha + \mu < \omega t < \pi$)

In this interval $\alpha + \mu < \omega t < \pi$, the current flows in the path shown in Fig. 3.5(b) and the equation governing this interval with respect to the equivalent circuit is defined by equation (3.4).

$$L \frac{di}{dt} + Ri + E = E_1 \sin(\omega t + \alpha + \mu) \quad (3.4)$$

Where $L = L_s + L_1 + L_a$ and $R = R_s + R_a$

Initial conditions $i(t) = I_{ao}$ when $\omega t = 0$

Using integrating factor method of solving differential equations, the current in this interval is;

$$i(t) = k_2 [\cos \theta_2 \sin(\omega t + \alpha + \mu - \theta_2) - P] + [k_2 (\cos \theta_2 \sin(\theta_2 - \alpha - \mu) + P) + I_{ao}] e^{-\frac{t}{\tau}} \quad (3.5)$$

Where,

$$k_2 = \frac{E_1}{|z|}, P = \frac{E}{E_1}, \tau = \frac{L}{R}, \text{ and } \theta_2 = \tan^{-1} \left(\frac{\omega L}{R} \right)$$

(C) Freewheeling interval $0 < \omega t < \alpha$

In this interval, the load is not connected to the supply, current flows in the path shown in Fig.3.5(c).

This interval is define by the equation

$$L_2 \frac{di}{dt} + R_a i = -E \quad (3.6)$$

Whose initial condition is $i(t) = I_1$ at $\omega t = 0$

The current in this interval derived from equation (3 - 6) is;

$$i(t) = I_1 e^{-\frac{t}{\tau_2}} - \frac{E}{R_a} [1 - e^{-\frac{t}{\tau_2}}] \quad (3.7)$$

At $\omega t = x$, then $t = \frac{x}{\omega}$

$$i(x) = I_1 e^{-\frac{x}{\omega \tau_2}} - \frac{E}{R_a} [1 - e^{-\frac{x}{\omega \tau_2}}]$$

When $\omega t = \alpha$, $i(t) = 0$, then, $t = \frac{\alpha}{\omega}$

Substituting the value of 't'

$$0 = I_1 e^{-\frac{\alpha}{\omega \tau_2}} - \frac{E}{R_a} [1 - e^{-\frac{\alpha}{\omega \tau_2}}] \quad (3.8)$$

Therefore,

$$I_1 = \frac{\frac{E}{R_a} [1 - e^{-\frac{\alpha}{\omega \tau_2}}]}{e^{-\frac{\alpha}{\omega \tau_2}}} \quad (3.9)$$

Also, the current at $x = \pi$ during the conduction interval is equally ' I_1 '.

$$\therefore x = \omega t + \alpha + \mu = \pi, \text{ then, } t = \frac{(x - \alpha - \mu)}{\omega}$$

Hence from equation (3.9);

$$I_1 = k_2[\cos\theta_2 \sin\theta_2 - p] + [k_2(\cos\theta_2 \sin(\theta_2 - \alpha) + p) + I_{a0}]e^{-\frac{(\pi - \alpha - \mu)}{\omega\tau}} \quad (3.10)$$

Equation (3.3) can be substituted into equation (3.10) to give a transcendental equation $f(\mu)$ emanating from a combination of equation (3.9) and (3.10) which is solved to obtain the commutation angle, ' μ ' for any gating angle ' α '

Fig. (3.6) Shows the variation of the commutation angle ' μ ' as the firing angle ' α ' is altered.

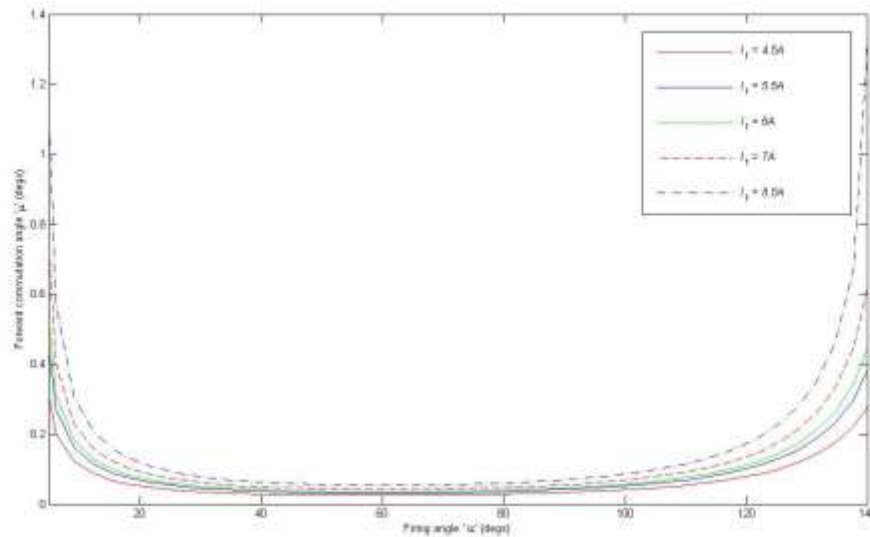


Fig.3.6: Variation of the Forward commutation angle ' μ ' with Firing angle ' α ' of the controller

Angle ' β ' after ' π '

The freewheeling diode ' D_2 ' in Fig.3.5(c) becomes forward biased when the instantaneous supply voltage equals the induced voltage in the source inductance. The induced voltage in the source inductance reverses biases ' D_2 ', until the angle ' β ' after ' π ' when this voltage is neutralized by the instantaneous supply voltage. The current in the conducting thyristor begins to decay to zero and in attempt to oppose this, the voltage in the armature circuit inductance forward biases ' D_2 to begin the freewheeling mode Mellitt (1974)

If the angle ' β ' is defined as $\beta = x - \pi$ then the equation for current in the conduction interval-as shown in equation (3.5) becomes;

$$i(\beta) = k_2[\cos\theta_2\sin(\beta - \theta_2) - P] + [k_2(\cos\theta_2\sin(\theta_2 - \alpha - \mu) + P) + I_{ao}]e^{-\frac{(\pi+\beta-\alpha-\mu)}{\omega\tau}} \quad (3.11)$$

The freewheeling interval begins when;

$$E_1\sin\beta + L_s\frac{di(\beta)}{d\beta} = 0 \quad (3.12)$$

From equation (3.11),

$$\frac{di(\beta)}{d\beta} = -k_2[\cos\theta_2\cos(\beta - \theta_2)] - \frac{1}{\omega\tau_2}[k_2(\cos\theta_2\sin(\theta_2 - \alpha - \mu) + P) + I_{ao}]e^{-\frac{(\pi+\beta-\alpha-\mu)}{\omega\tau}} \quad (3.13)$$

Now, using equation (3.13) in (3.12),

$$E_1\sin\beta - L_s[\cos\theta_2\cos(\beta - \theta_2)] - \frac{1}{\omega\tau_2}[k_2(\cos\theta_2\sin(\theta_2 - \alpha - \mu) + P) + I_{ao}]e^{-\frac{(\pi+\beta-\alpha-\mu)}{\omega\tau}} = 0 \quad (3.14)$$

If $k = k_2(\cos\theta_2\sin(\theta_2 - \alpha - \mu) + p)$,

$$\text{Then, } E_1\sin\beta - L_s[\cos\theta_2\cos(\beta - \theta_2)] + \frac{(k+I_{ao})}{\omega\tau_2}e^{-\frac{(\pi-\beta-\mu)}{\omega\tau}} = 0 \quad (3.15)$$

The value of the motor input current at the beginning of the freewheeling is obtained from equation (3.11) but the value of the angle ' β ' after π corresponding to this current is obtained by solving the transcendental equation (3.15).

The relationship between ' α ' and ' β ' is shown in Fig. (3.7).

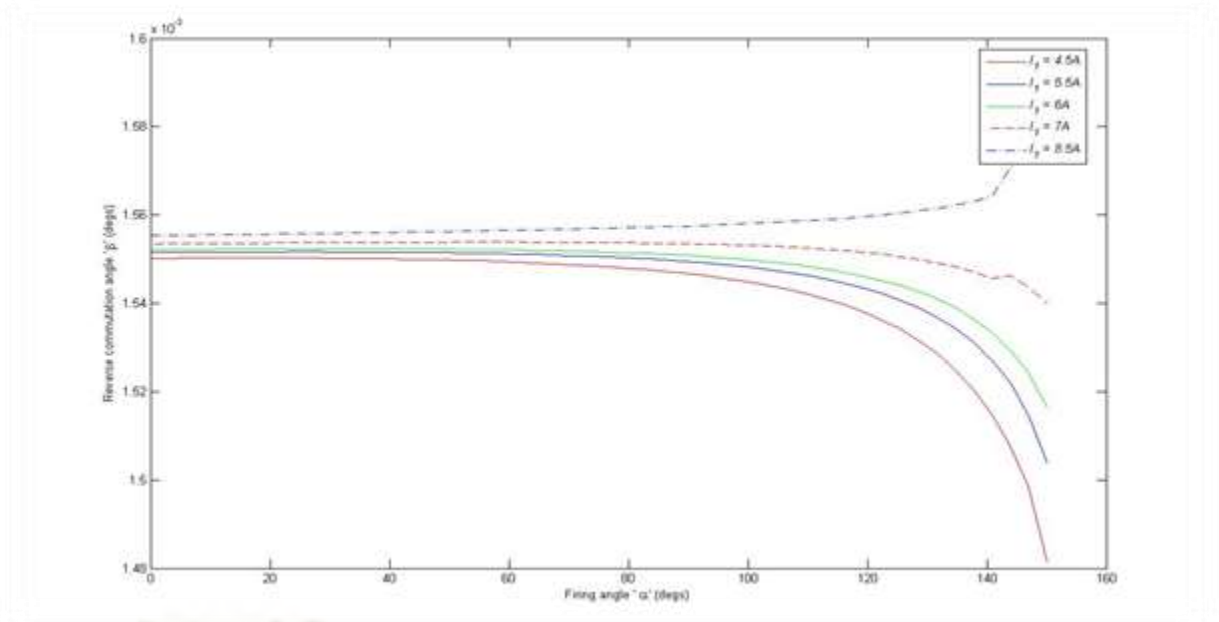


Fig. 3.7: Variation of the Reverse commutation angle 'β' with Firing angle 'α' of the controller

(D) Reverse Commutation or Extinction Interval $\pi + \beta < x < \pi + \beta + x_s$

The reverse commutation of current from a conducting thyristor is opposed by the voltage induced in the source inductance. Defining ωt from $x = \pi$, the current in the reverse commutating thyristor falls to zero from the value at $x = \pi + \beta$, i.e I_β .

The equation of current obtained from the equivalent circuit of Fig. 3.5(d) is

$$L_s \frac{di}{dt} + R_s = -E_1 \sin(\omega t + \beta) \quad (3.16)$$

Re-arranging,

$$\frac{di}{dt} + \frac{R_s}{L_s} = \frac{-E_1 \sin(\omega t + \beta)}{L_s}$$

Natural Component = $Ae^{\frac{-t}{\tau_1}}$

Where, $\tau_1 = \frac{L_s}{R_s}$

Forced Response = $i_f(t) = \frac{-E_1}{Z} \sin(\omega t + \beta - \theta_1)$

Where, $\theta_1 = \tan^{-1} \left(\frac{\omega L_s}{R_s} \right)$, and $Z = \sqrt{R^2 + (\omega L)^2}$

$$\therefore i(t) = Ae^{\frac{-t}{\tau_1}} - \frac{E_1}{Z} \sin(\omega t + \beta - \theta_1) \quad (3.17)$$

Initial condition, $\omega t = 0$, $i(t) = I_\beta$

Hence,

$$A = I_\beta - \frac{E_1}{Z} \sin(\theta_1 - \beta) \quad (3.18)$$

Substituting equation (3.18) in (3.17);

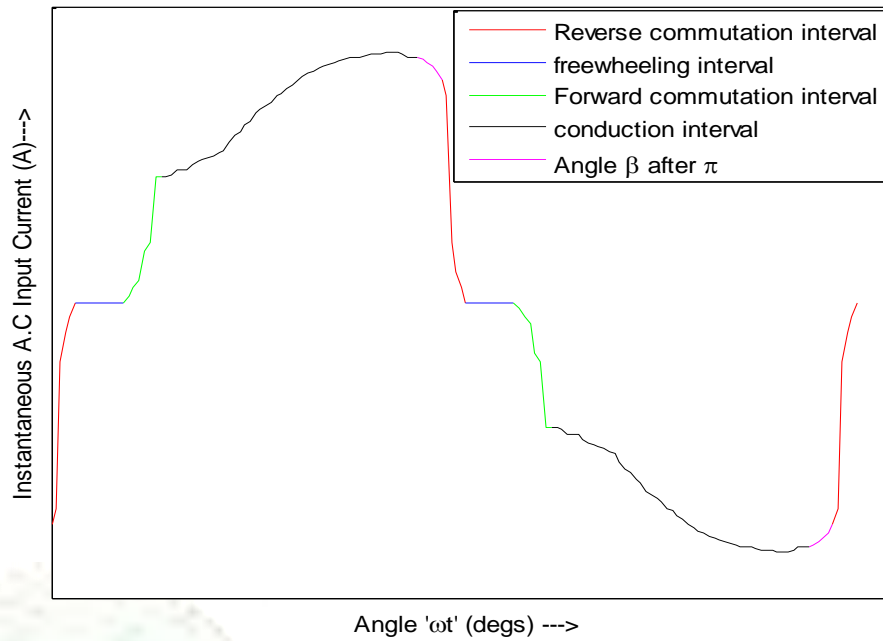
$$i(t) = -\frac{E_1}{Z} \sin(\omega t + \beta - \theta_1) - \left[\frac{E_1}{Z} \sin(\theta_1 - \beta) - I_\beta \right] e^{\frac{-t}{\tau_1}} \quad (3.19)$$

$$= -K_1 \sin(\omega t + \beta - \theta_1) - \left[K_1 \sin(\theta_1 - \beta) - I_\beta \right] e^{\frac{-t}{\tau_1}} \quad (3.20)$$

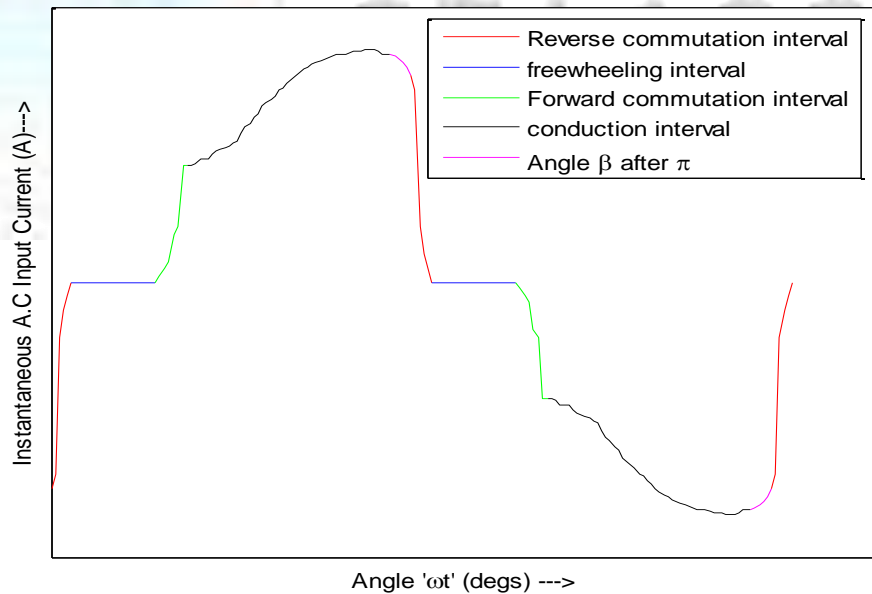
Where, $K_1 = \frac{E_1}{Z}$

The equations of currents for the different intervals put together and plotted for different firing angles are displayed in Fig. 3.8 Also, Figs.3.6 and 3.7 provide a complete characterization of the waveforms of the Asymmetrical Single – Phase Bridge that enables one to obtain the waveform of Fig.3.8 which present the input power factor problem obtained using explicit analytical equations for current derived during the intervals of operation of the Asymmetrical Single – Phase Bridge.

The results of Fig. 3.8 clearly show that as the firing angle of the thyristors of the drive are increased; the instantaneous input current deteriorates which is an indication of an increased harmonic current present in the supply leading to a low input power factor

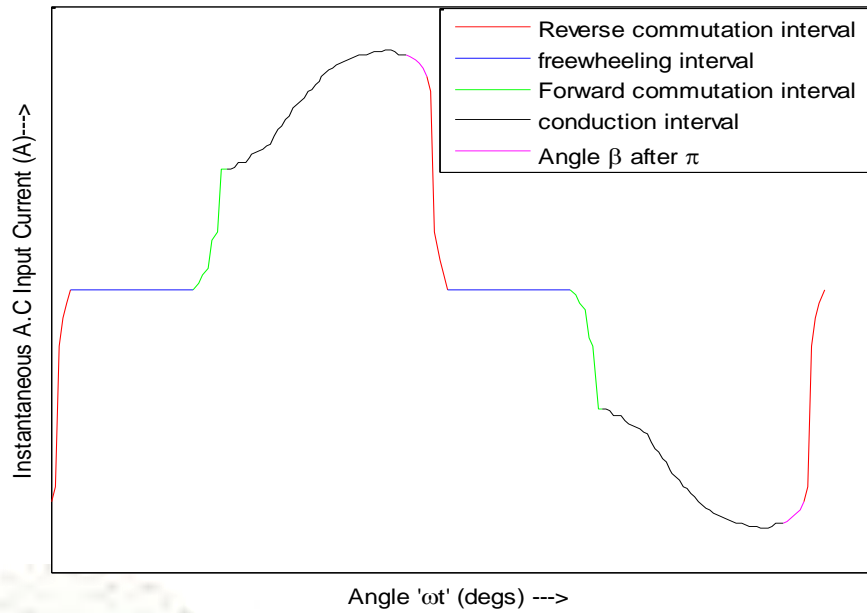


(a): Motor input current for a '20°' Firing angle

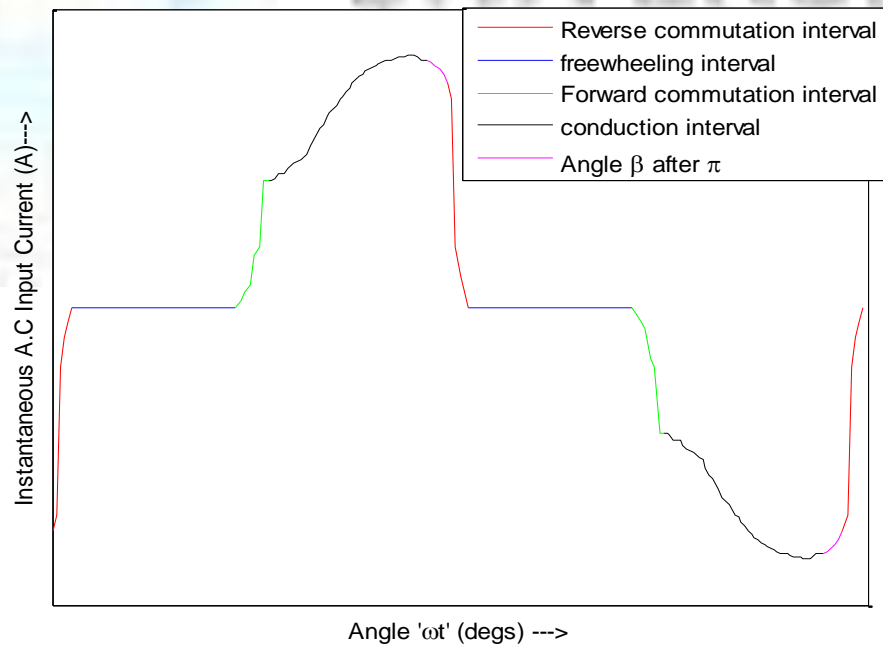


(b): Motor input current for a '40°' Firing angle

Fig.3.8: (a – b): Motor Input current at different Firing angles of the Thyristors: The power factor problem in Graphics

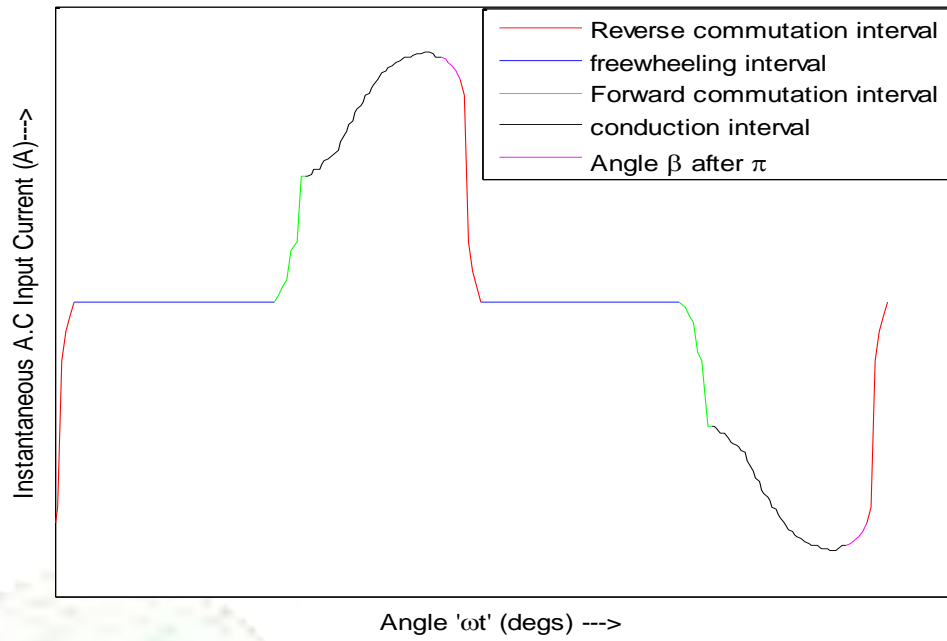


(c): Motor input current for a 60° Firing angle

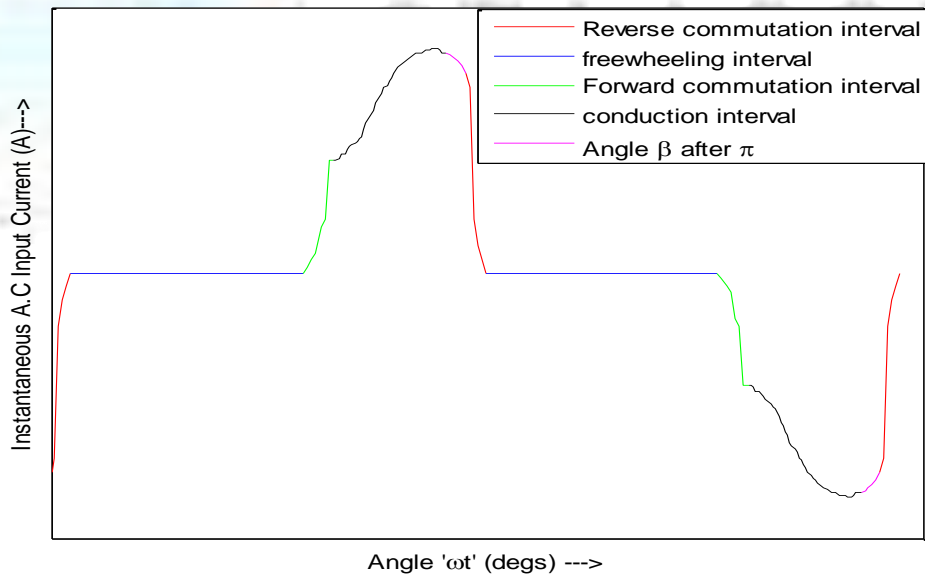


(d): Motor input current for a 80° Firing angle

Fig.3.8: (c – d): Motor Input current at different Firing angles of the Thyristors: The power factor problem in Graphics



(e): Motor input current for a ' 100° ' Firing angle



(f): Motor input current for a ' 160° ' Firing angle

Fig.3.8: (e – f): Motor Input current at different Firing angles of the Thyristors: The power factor problem in Graphics

3.5 Harmonics in the AC input Current

The harmonic spectrum of the motor input current is obtained from Fourier analysis of the explicit expressions for the armature current over a period of the waveform such that;

$$i(x) = \sum_{n=1}^{\infty} (A_n \cos nx + B_n \sin nx) \quad (3.21)$$

The coefficients A_n and B_n are obtained as

$$A_n = \frac{1}{T} \int_0^T i(x) \cos nx \, dx \quad (3.22)$$

$$B_n = \frac{1}{T} \int_0^T i(x) \sin nx \, dx \quad (3.23)$$

T is the period.

The coefficients are obtained as presented in Appendix II

For A_n ($n = 1, 3, 5, \dots, \infty$)

$$\begin{aligned} A_n = & \frac{2}{\pi} \left(I_1 + \frac{E}{R_a} \right) \frac{n(\omega\tau_2)^2 e^{-x/\omega\tau_2} \sin n\alpha - \omega\tau_2 e^{-x/\omega\tau_2} \cos n\alpha + \omega\tau_2}{1+(n\omega\tau_2)^2} - \frac{E}{R_a} \frac{\sin n\alpha}{n} + \\ & \frac{2}{\pi} K_2 \cos\theta_2 \left[\frac{-\cos\theta_2 \cos n\pi - n \sin(\alpha+\mu-\theta_2) \sin n(\alpha+\mu) - \cos(\alpha+\mu-\theta_2) \cos n(\alpha+\mu)}{n^2-1} \right] - \frac{2}{\pi} K_2 P \left[-\frac{\sin n(\alpha+\mu)}{n} \right] \\ & + \frac{2}{\pi} \{ K_2 (\cos\theta_2 \sin(\theta_2 - x) + P) + I_{a0} \} \left[\frac{-\omega\tau \cos n\pi e^{-(\pi-\alpha-\mu)/\omega\tau} - n(\omega\tau)^2 \sin n(\alpha+\mu) + \omega\tau \cos n(\alpha+\mu)}{1+(n\omega\tau)^2} \right] \\ & + \frac{2}{\pi} K_1 \sin(\theta_1 - \alpha) \left\{ \frac{n(\omega\tau_1)^2 e^{-\mu/\omega\tau_1} \sin n(\alpha+\mu) - \omega\tau_1 e^{-u/\omega\tau_1} \cos n(\alpha+\mu) - n(\omega\tau_1)^2 \sin n\alpha + \omega\tau_1 \cos n\alpha}{1+(n\omega\tau_1)^2} \right\} \\ & + \frac{2}{\pi} K_1 \left\{ \frac{n \sin n(\alpha+\mu) \sin(\alpha+\mu-\theta_1) + \cos n(\alpha+\mu) \cos(\alpha+\mu-\theta_1) - n \sin n\alpha \sin(\alpha-\theta_1) - \cos n\alpha \cos(\alpha-\theta_1)}{n^2-1} \right\} \quad (3.24) \end{aligned}$$

In a compact form A_n can be presented as:

$$A_n = \frac{1}{\pi} \left[\begin{aligned} & \frac{k_3}{n+1} \left[\cos((n+1)(\alpha+u) - \theta_2) - (-1)^{n+1} \cos \theta_2 \right] \\ & - \frac{k_3}{n-1} \left[\cos((n-1)(\alpha+u) + \theta_2) - (-1)^{n-1} \cos \theta_2 \right] \\ & + 2 \left(\frac{A_6 \sin n(\alpha+u) - A_5 \sin n\alpha}{n} \right) \\ & + \frac{2k_6 \omega \tau}{1 + (n\omega\tau)^2} \left[\cos n(\alpha+u) - n\omega\tau \sin n(\alpha+u) - (-1)^n e^{-\left(\frac{\pi-\alpha-u}{\omega\tau}\right)} \right] \\ & + \frac{2(I_1 + A_5) \omega \tau_2}{1 + (n\omega\tau_2)^2} \left(1 + e^{-\frac{\alpha}{\omega\tau_2}} (n\omega\tau_2 \sin n\alpha - \cos n\alpha) \right) \\ & + \frac{k_1}{n+1} (\cos((n+1)\alpha - \theta_1) - \cos((n+1)(\alpha+u) - \theta_1)) \\ & - \frac{k_1}{n-1} (\cos((n-1)\alpha + \theta_1) - \cos((n-1)(\alpha+u) + \theta_1)) \\ & + \frac{2k_1 \sin(\theta_1 - \alpha) \omega \tau_1}{1 + (n\omega\tau_1)^2} \left(e^{-\frac{u}{\omega\tau_1}} (n\omega\tau_1 \sin n(\alpha+u) - \cos n(\alpha+u)) + \cos n\alpha \right. \\ & \quad \left. - n\omega\tau_1 \sin n\alpha \right) \end{aligned} \right] \quad (3.25)$$

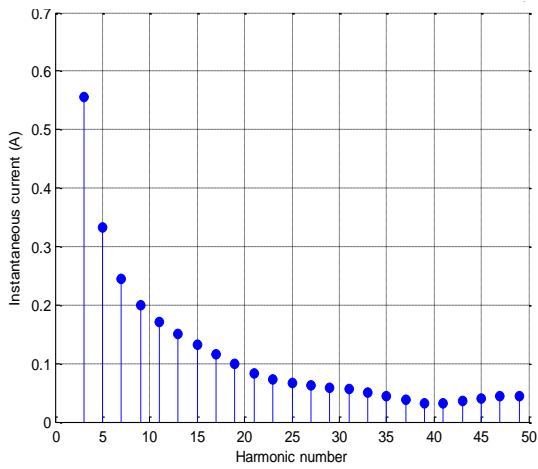
B_n ($n=1, 3, 5, \dots, \infty$)

$$\begin{aligned}
B_n &= \frac{2}{\pi} \left\{ \left(I_1 + \frac{E}{R_a} \right) \left[\frac{-n(\omega\tau_2)^2 e^{-\alpha/\omega\tau_2} \cos n\alpha - \omega\tau_2 e^{-\alpha/\omega\tau_2} \sin n\alpha + n(\omega\tau_2)^2}{1 + (n\omega\tau_2)^2} \right] - \frac{2}{\pi} \frac{E}{R_a} \left(\frac{1 - \cos n\alpha}{n} \right) + \right. \\
& K_2 \cos \theta_2 \left[\frac{n \sin \theta_2 \cos n\pi + n \sin(\alpha + \mu - \theta_2) \cos n(\alpha + \mu) - \cos(\alpha + \mu - \theta_2) \sin n(\alpha + \mu)}{n^2 - 1} \right] \left. \right\} \\
& - \frac{2}{\pi} \left\{ K_2 P \left[\frac{\cos n(\alpha + \mu) - \cos n\pi}{n} \right] \right\} \\
& + \frac{2}{\pi} \{ K_2 (\cos \theta_2 \sin(\theta_2 - x) + P) + \\
I_{a0} \} & \left[\frac{n(\omega\tau_2)^2 e^{-(x-\alpha-\mu)/\omega\tau_2} \cos n\alpha + n(\omega\tau_2)^2 \cos n(\alpha + \mu) - \omega\tau_2 \sin n(\alpha + \mu)}{1 + (n\omega\tau_2)^2} \right] \\
& + K_1 \left\{ \frac{-n \cos n(\alpha + \mu) \sin(\alpha + \mu - \theta_1) + \sin n(\alpha + \mu) \cos(\alpha + \mu - \theta_1) - n \cos n\alpha \sin(\alpha - \theta_1) - \sin n\alpha \cos(\alpha - \theta_1)}{n^2 - 1} \right\} + \\
K_1 \sin(\theta_1 - \alpha) & \left\{ \frac{n(\omega\tau_1)^2 \cos n\alpha + \omega\tau_1 \sin n\alpha - n(\omega\tau_1)^2 e^{-u/\omega\tau_1} \cos n(\alpha + \mu) - \omega\tau_1 e^{-u/\omega\tau_1} \sin n(\alpha + \mu)}{1 + (n\omega\tau_1)^2} \right\} \quad (3.26)
\end{aligned}$$

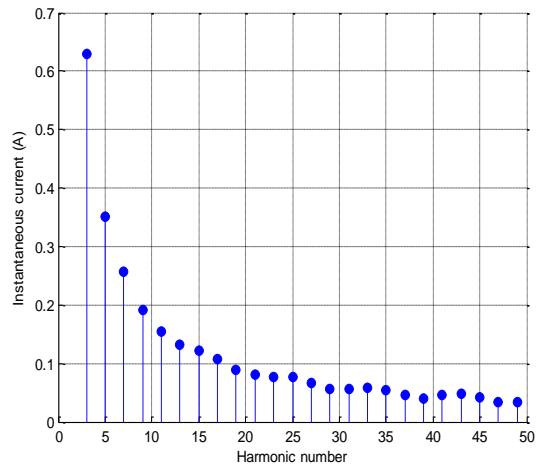
In a compact form B_n can be presented as;

$$\begin{aligned}
 B_n = \frac{1}{\pi} & \left[\begin{aligned}
 & \frac{k_3}{n+1} \left[\sin((n+1)(\alpha+u) - \theta_2) + (-1)^{n+1} \sin \theta_2 \right] \\
 & - \frac{k_3}{n-1} \left[\sin((n-1)(\alpha+u) + \theta_2) - (-1)^{n-1} \sin \theta_2 \right] \\
 & + \frac{2}{n} \left(A_6 \left((-1)^n - \cos n(\alpha+u) \right) - A_5 (1 - \cos n\alpha) \right) \\
 & + \frac{2k_6 \omega \tau}{1 + (n\omega\tau)^2} \left[n\omega\tau \cos n(\alpha+u) - n\omega\tau (-1)^n e^{-\left(\frac{\pi - \alpha - u}{\omega\tau}\right)} + \sin n(\alpha+u) \right] \\
 & + \frac{2(I_1 + A_5) \omega \tau_2}{1 + (n\omega\tau_2)^2} \left(n\omega\tau_2 - e^{-\frac{\alpha}{\omega\tau_2}} (n\omega\tau_2 \cos n\alpha + \sin n\alpha) \right) \\
 & + \frac{k_1}{n-1} \left(\sin((n-1)(\alpha+u) + \theta_1) - \sin((n-1)\alpha + \theta_1) \right) \\
 & - \frac{k_1}{n+1} \left(\sin((n+1)(\alpha+u) - \theta_1) - \sin((n+1)\alpha - \theta_1) \right) \\
 & + \frac{2k_1 \sin(\theta_1 - \alpha) \omega \tau_1}{1 + (n\omega\tau_1)^2} \left(\begin{aligned}
 & n\omega\tau_1 \cos n\alpha + \sin n\alpha \\
 & - e^{-\frac{u}{\omega\tau_1}} (n\omega\tau_1 \cos n(\alpha+u) + \sin n(\alpha+u))
 \end{aligned} \right)
 \end{aligned} \right] \quad (3.27)
 \end{aligned}$$

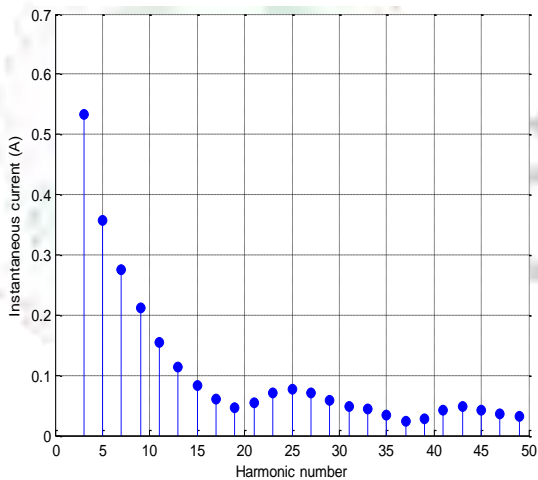
The harmonic spectrum of the input current for varying delay angles are shown in Figs.3.9 (a-d)



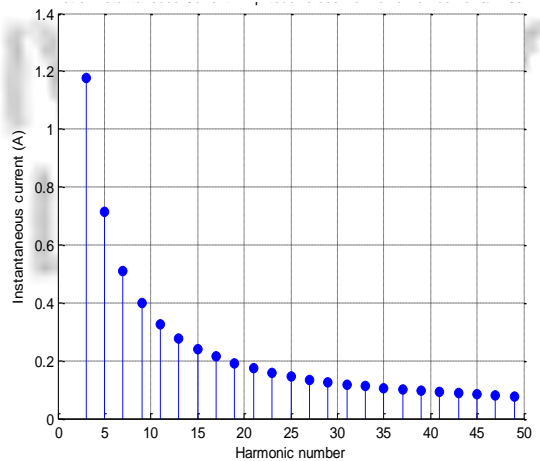
(a): Harmonics Spectrum of the Input Current at a Firing angle ' α ' = 10°



(c): Harmonics Spectrum of the Input Current at a Firing angle ' α ' = 70°



(b): Harmonics Spectrum of the Input Current at a Firing angle ' α ' = 20°



(d): Harmonics Spectrum of the Input Current at a Firing angle ' α ' = 90°

Fig.3.9 (a-d): Harmonics Spectrum of the controller at different Firing angles

Like in figure 3.8, the harmonic spectrum of the controller presented in Fig. 3.9(a-d) reveals that the harmonic current decreases as the harmonic number increases.

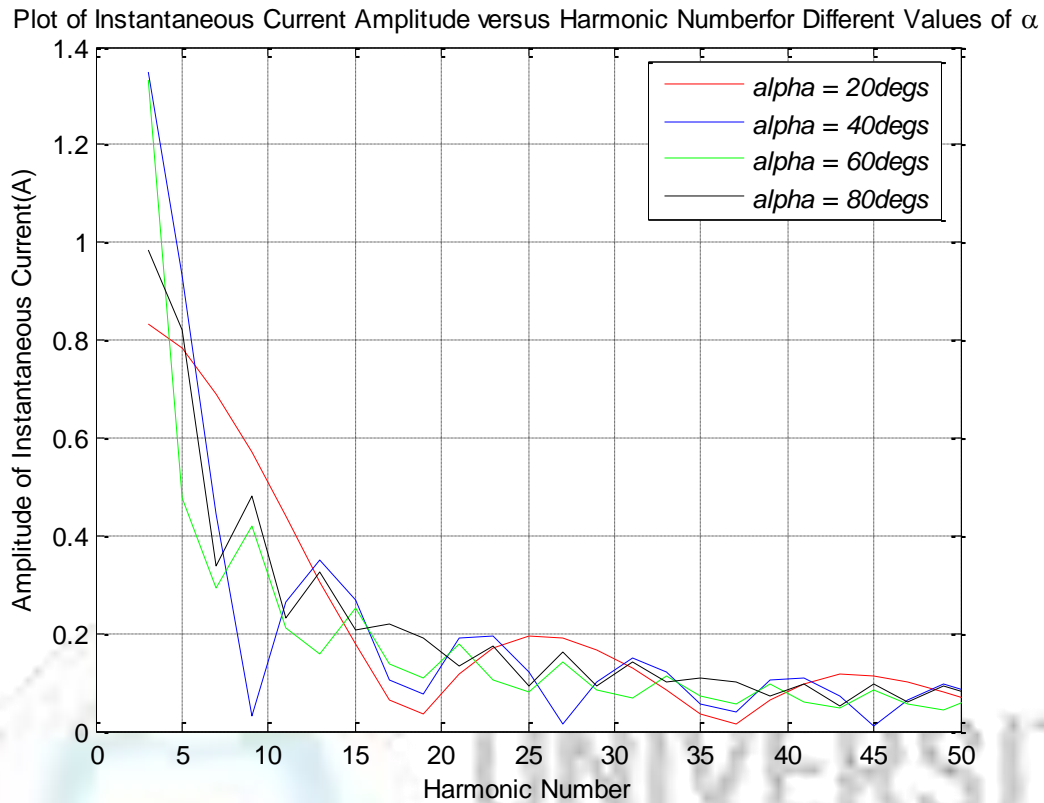


Fig.3.10: Variation of Input current harmonic components for different delay angles

Figure 3.8 showed the distorted waveform of the AC input current due to Phase Angle Control (PAC). It is seen that as the firing angle ' α ' increases, the input current distortion increases. The variation of the harmonic spectrum of the input current with the firing angle is displayed in Fig. 3.9. From fig. 3.9, it is obvious that the 3rd and 5th harmonics contributes significantly to the instantaneous input current; it is considerably reduced at higher harmonic number.

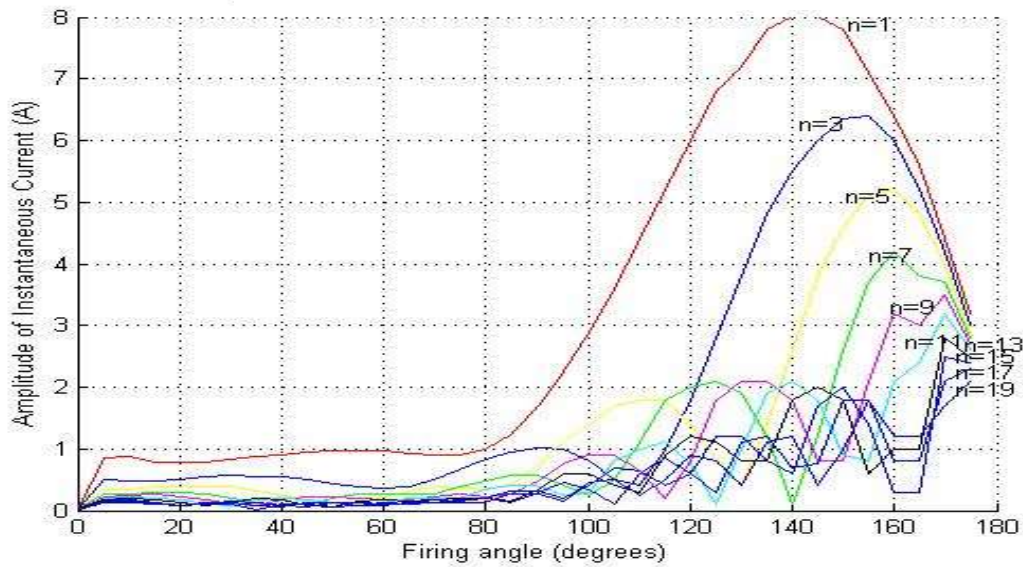


Fig. 3.11: Variation of specified Harmonic Currents with Firing Angle

Fig. 3.11 suggests that a very high harmonic content is present in the input supply current increase when the drive is operated between 120 to 160 degrees at a frequency range of 150 – 750Hz. The implication of this is that communication equipment and circuits operating within this range of frequencies will be adversely affected at such significant harmonic levels. Also, signalling in traction systems can be affected by such a significant level of supply input current harmonics.

3.6 Impact of Multiple Drives on Supply Systems

This research postulates that as a nation like Nigeria industrialises, there will be increased application of industrial drives which impact the power supply system. In this regard, a number of Asymmetrical single – phase converters were connected in parallel to the same source. Experimental results were obtained and analysed for one converter. This was extended to two; three and four of such drives connected in parallel. Measurements show that input power factor deteriorates as the number of drives connected in parallel increases. The thyristors are fired at chosen instant. The thyristors of the multiple drives are fired at the same angle ' α '. Fig.3.12 shows multiple asymmetrical drives connected to the same source.

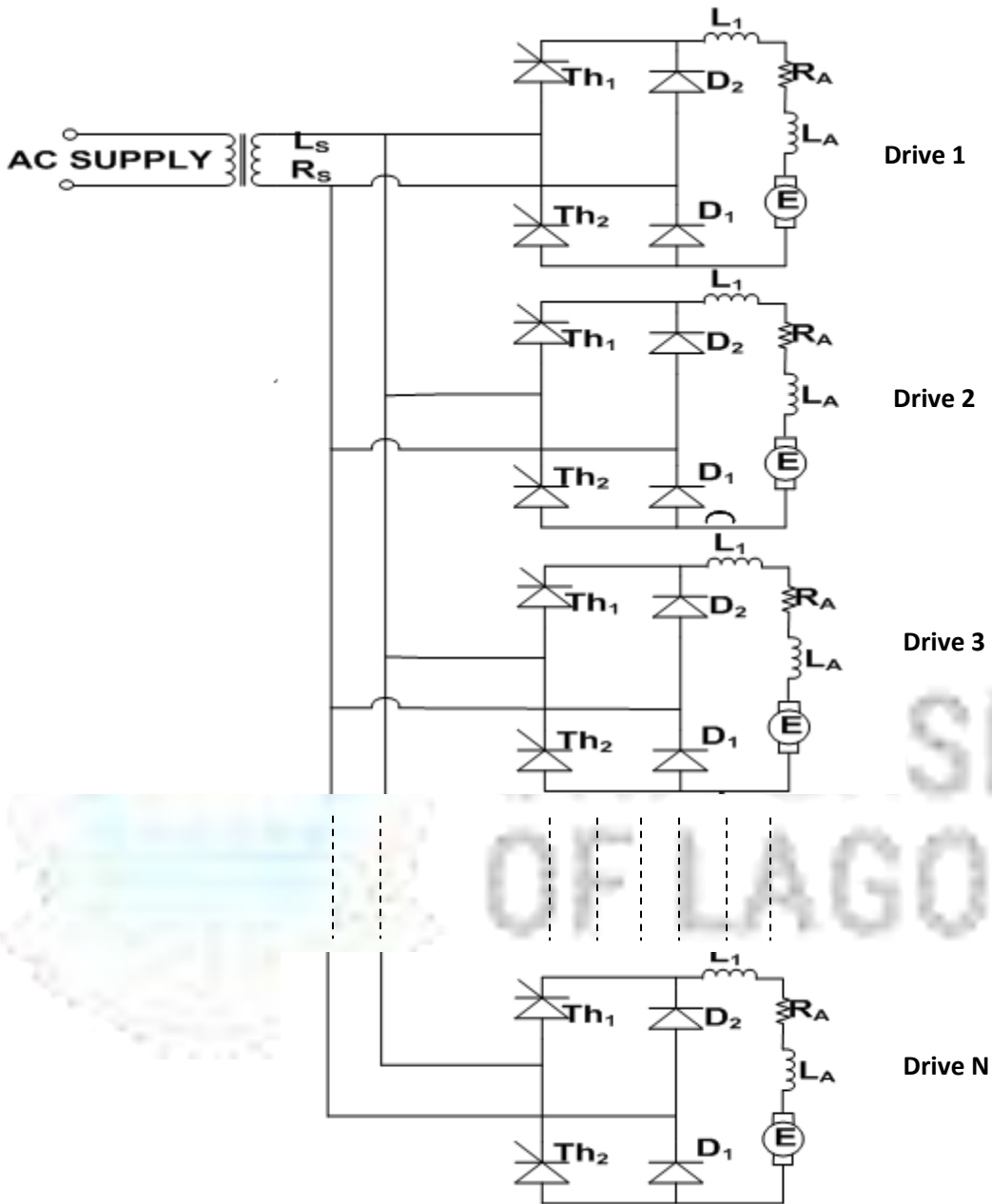


Fig. 3.12: Multiple drives connected to the same AC source

Waveforms of the input current and voltage were obtained from the oscilloscope display while measurements of the corresponding input power factor were recorded. The non – sinusoidal input waveform deteriorates each time the number of drives is increased and the power factor worsens. The waveforms of the supply voltage and current as the number of drives is increased are shown in figs. 3.13, 3.14 and 3.15, thereby establishing experimentally the power factor problem with

increased used of industrial drives. Subsequently, Fig. 3.16 shows the variation of input power factor with the number of drives.

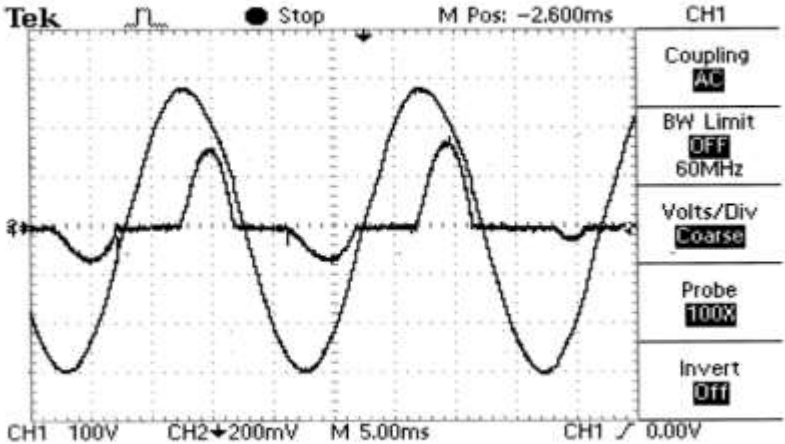


Fig. 3.13: Input current and waveform for a single drive: $N = 1500$, $PF = 0.628$

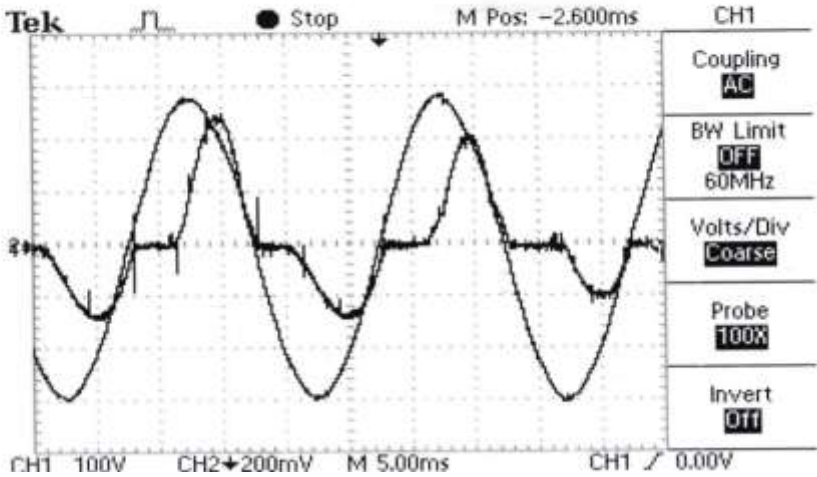


Fig. 3.14: Input current and waveform for Two Drives in parallel: $N = 1500$, $PF = 0.166$

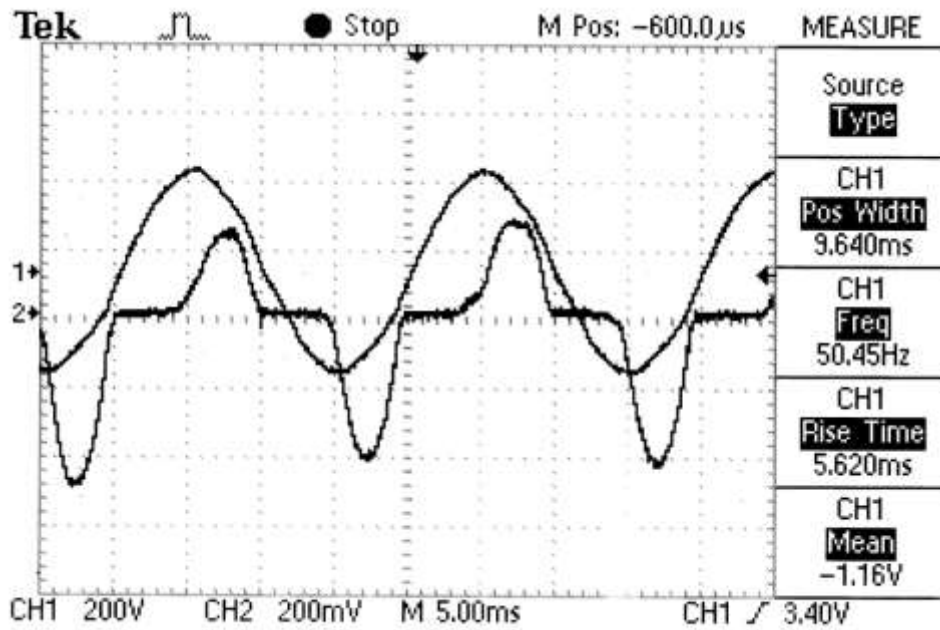


Fig. 3.15: Input current and waveform for Three Drives in Parallel $N = 1500$, $PF = 0.106$

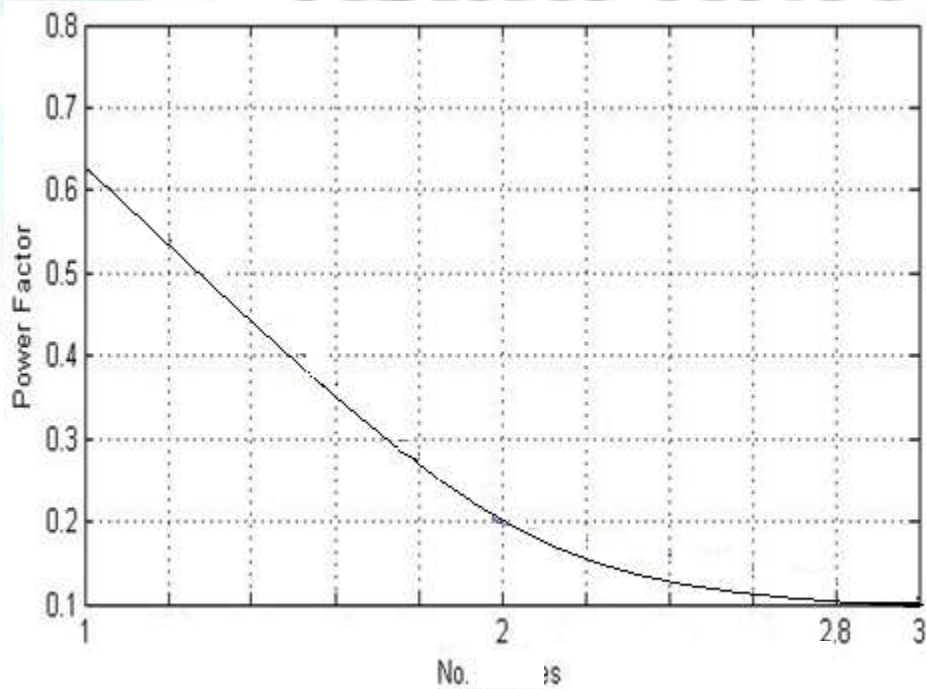


Fig. 3.16: Variation of Power Factor with Number of Drives

3.7 Behaviour Factors of the Drive

The basic concept employed in the study is presented and described below.

A. Input Power Factor (PF)

In an AC to DC converter (asymmetrical single – phase bridge converter), the ac source voltage is usually non sinusoidal and often times contains harmonics. Consequently, only the fundamental component of the converter input current at the source frequency contributes to real converter input power. For an a.c to d.c converter supplied by an m- phase ac source, the converter real power (P) and the apparent power (S) inputs (Rashid 1993, Mohan 1995) are:

$$P = mV_s I_{s_1} \text{Cos} \phi_{s_1} \quad (3.28)$$

$$S = mV_s I_s \quad (3.29)$$

where,

V_s = Rms value of the converter input phase voltage

I_s = Rms value of the converter input current

I_{s_1} = Rms fundamental component of I_s

ϕ_{s_1} = Phase angle between V_s and I_{s_1}

Then,

Input power Factor PF_{ac}

$$PF_{ac} = \frac{P}{S} = \frac{mV_s I_{s_1} \text{Cos} \phi_{s_1}}{mV_s I_s} \quad (3.30)$$

$$= \frac{I_{s_1}}{I_s} \text{Cos} \phi_{s_1} \quad (3.31)$$

= (Distortion Factor). (Displacement Factor)

Ideally, if the input power factor is unity (Rashid 1993), its converter input current is sinusoidal and in phase with the source voltage. But this is not the case because the converter control introduces harmonics and often times phase angle difference in the converter input current.

B. Input Displacement Factor (DF)

This may be referred to as fundamental power factor defined as:

$$DF = \cos \phi_{s_1} \quad (3.32)$$

Where,

ϕ_{s_1} = is the displacement angle.

For the same power demand, if the displacement factor is low, more fundamental current is drawn from the supply.

C. Harmonic Factor. (HF)

The harmonic factor indicates the harmonic content in the input supply current and this measures the distortion of the input current.

$$HF = \frac{I_{distortion}}{I_{s_1}} = \frac{\sqrt{I_s^2 - I_{s_1}^2}}{I_{s_1}} \quad (3.33)$$

$$= \frac{\left[\sum_{n=2}^{\infty} I_{s_n}^2 \right]^{\frac{1}{2}}}{I_{s_1}} = \frac{I_{s_n}}{I_{s_1}} \quad (3.34)$$

Where,

$$I_s = \sqrt{I_{s_1}^2 + I_{distortion}^2} \quad (3.35)$$

I_s = Input supply current

I_{s_1} = Input fundamental current

$I_{distortion}$ = Current distortion component

D. Form Factor (FF)

This is a measure of the shape of the output defined (Rashid 1993) as:

$$FF = \frac{V_{rms}}{V_{dc}} \quad (3.36)$$

E. Ripple Factor (RF)

Ripple factor measures the amount of ripple content and is defined as:

$$RF = \frac{V_{ac}}{V_{dc}} = \frac{V_{ripple}}{V_{dc}} \quad (3.37)$$

Where,

V_{ac} = Effective (rms) value of the ac component of output voltage

$$= \sqrt{V_{rms}^2 - V_{dc}^2} \quad (3.38)$$

Therefore,

$$\begin{aligned} RF &= \frac{\sqrt{V_{rms}^2 - V_{dc}^2}}{V_{dc}} \\ &= \sqrt{\left(\frac{V_{rms}}{V_{dc}}\right)^2 - 1} \\ &= \sqrt{FF^2 - 1} \end{aligned} \quad (3.39)$$

F. Total Harmonic Distortions (THD)

This is called a distortion index of fundamental and distortion component in the supply current $i_s(t)$. It is expressed in percentage as:

$$\begin{aligned} \%THD &= 100 \times \frac{I_{distortion}}{I_{s_1}} = 100 \times \frac{\sqrt{I_s^2 - I_{s_1}^2}}{I_{s_1}} \\ &= 100 \times \sqrt{\left(\frac{I_s}{I_{s_1}}\right)^2 - 1} \end{aligned}$$

$$THD^2 = \left(\frac{I_s}{I_{s_1}}\right)^2 - 1$$

Therefore,

$$\frac{I_s}{I_{s_1}} = \sqrt{1 + THD^2} \quad (3.40)$$

Substituting equation (3.32) in (3.31)

$$PF = \frac{I_{s_1}}{I_s} DF$$

Hence from equation (3.40),

$$PF = \frac{1}{\sqrt{1+THD^2}} \cdot DF \quad (3.41)$$

From equation (3.41), it is clear that if the displacement factor is unity, a total harmonic distortion of 100 percent (Sen 1980), which is possible in drives unless corrective measures are taken, can reduce the power factor to approximately 0.7 (or $\frac{1}{\sqrt{2}} = (0.707)$).

3.8 The Input Power Factor Problem

To establish the input power factor problem of the asymmetrical Single – Phase Bridge, Fourier series analysis will be employed. In an ideal converter, both the AC source voltage and the converter input current are sinusoidal i.e.

$$I_S = I_{S_1}$$

and,

$$\phi_{S_1} = 0 \text{ (i.e. phase angle between } V_S \text{ and } I_{S_1} \text{)}$$

$$PF_{ac} = \text{Cos } \phi_{S_1} = 1$$

Hence in an ideal converter, the AC input power factor is unity.

To establish the power factor problem in an ac to dc converter of an asymmetrical single-phase bridge, the following should be noted:

Where I_S and I_{S_1} obtained from Fourier analysis of the waveform are different, it implies that the converter input current is non – sinusoidal and hence not in phase with the ac source voltage; this brings about the phase difference between V_S and I_{S_1} . And from equation (3.31), the ac input current power factor PF_{ac} deviates from unity. Implying that there is an input power factor problem.

Where the Fourier waveform analysis contains harmonics, it shows that the converter input current is not sinusoidal and is out of phase with the ac source voltage; this is because harmonics bring about a distortion in the waveform of a signal.

Fourier series analysis will be needed in order to determine:

- (a) The Harmonic Factor (HF)
- (b) The Displacement Factor (DF)
- (c) The Input Power Factor (PF_{ac})

From these derivations, the input power factor will become clearer.

3.9 Generalised Analysis for the Asymmetrical Bridge.

The instantaneous input current to an asymmetrical Single – Phase Bridge can be expressed in Fourier series as:

$$i_s(t) = I_{dc} + \sum_{n=1,2,\dots}^{\infty} (a_n \cos n\omega t + b_n \sin n\omega t) \quad (3.42)$$

Solving for components “ I_{dc} ”, “ a_n ” and “ b_n ” we have that;

$$I_{dc} = 0$$

$$a_n = \frac{-2I_a}{n\pi} \sin n\alpha \quad \text{For } n = 1, 3, 5, \dots \text{ odd}$$

$$b_n = \frac{2I_a}{n\pi} (1 + \cos n\alpha) \quad \text{For } n = 1, 3, 5, \dots \text{ odd}$$

Hence equation (3.42) can be written as:

$$\begin{aligned} I_s(t) &= \sum_{n=1,3,5,\dots}^{\infty} \left[\frac{-2I_a}{n\pi} \sin n\alpha \cos n\omega t + \frac{2I_a}{n\pi} (1 + \cos n\alpha) \sin n\omega t \right] \\ &= \sum_{n=1,2,3,\dots}^{\infty} (a_n \cos n\omega t + b_n \sin n\omega t) \end{aligned} \quad (3.43)$$

Equation (3.43) can also be written in the form;

$$i_s(t) = \sum_{n=1,2,3,\dots}^{\infty} \sqrt{2} I_n \sin(n\omega t + \phi_n)$$

where,

$$\phi_n = \tan^{-1} \frac{a_n}{b_n} = \frac{-n\alpha}{2}$$

Thus, the rms value of the nth harmonic current of the input current is derived as:

$$I_{s_n} = \frac{1}{\sqrt{2}} (a_n^2 + b_n^2)^{\frac{1}{2}}$$

$$I_{s_n} = \frac{2\sqrt{2}}{\pi} I_a \cos \frac{\alpha}{2}$$

$$I_{s_1} = \frac{2\sqrt{2}}{\pi} I_a \cos \frac{\alpha}{2} \quad (\text{i.e. } n = 1)$$

Determination of the rms value of the input current supply is derived as I_s :

$$I_s = \left[\frac{2}{2\pi} \int_{\alpha}^{\pi} I_a^2 d(\omega t) \right]^{\frac{1}{2}} = I_a \left[1 - \frac{\alpha}{\pi} \right]^{\frac{1}{2}}$$

Now,

$$\text{PF} = \frac{I_{s_1} \cos \phi_{s_1}}{I_s}$$

Where,

$$\phi_{s_1} = -\frac{\alpha}{2}$$

Hence,

$$\text{PF} = \frac{\sqrt{2}[1 + \cos \alpha]}{[\pi(\pi - \alpha)]^{\frac{1}{2}}}$$

From the expression of equation (3.33);

$$\text{HF} = \left[\frac{I_s^2 - I_{s_1}^2}{I_{s_1}^2} \right]^{\frac{1}{2}} = \left[\left(\frac{I_s}{I_{s_1}} \right)^2 - 1 \right]^{\frac{1}{2}}$$

Substituting for I_s and I_{s_1}

$$\text{HF} = \left[\frac{\pi(\pi - \alpha)}{4(1 + \cos \alpha)} - 1 \right]^{\frac{1}{2}}$$

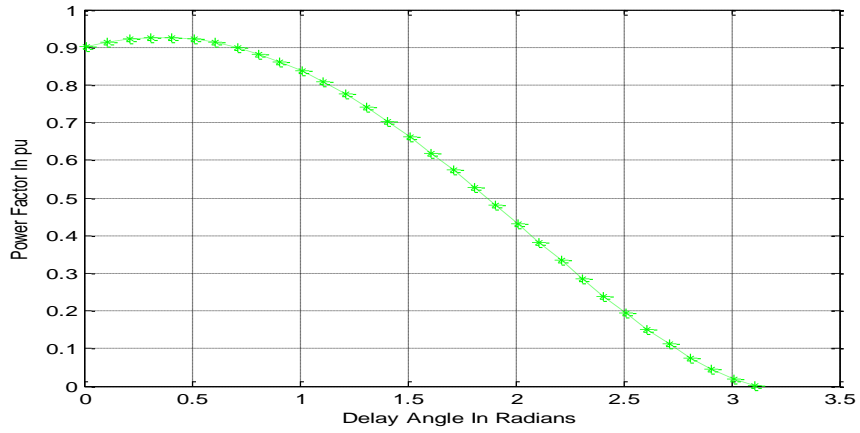
If ϕ_{s_1} is the angle between the fundamental component of the input current and AC input voltage, then the displacement factor DF is:

$$\text{DF} = \cos \phi_{s_1} = \cos \frac{-n\alpha}{2}$$

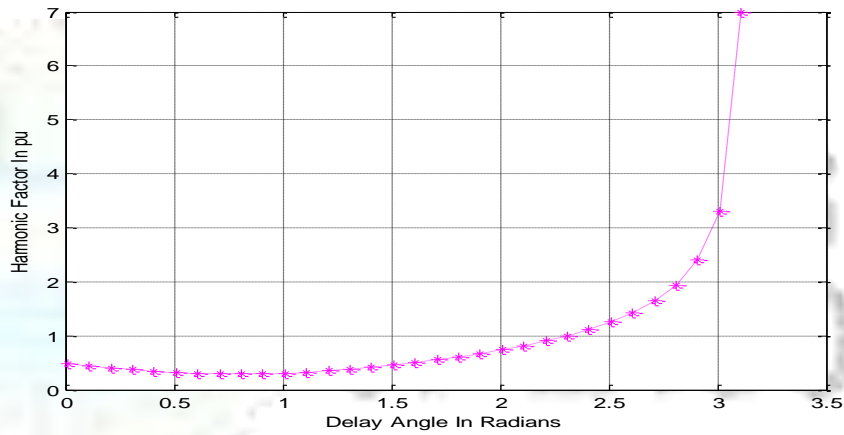
$$\cos \phi_{s_1} = \cos \left(\frac{-\alpha}{2} \right) \quad (3.44)$$

Derivations of the expressions for PF, HF and DF is presented in APPENDIX III

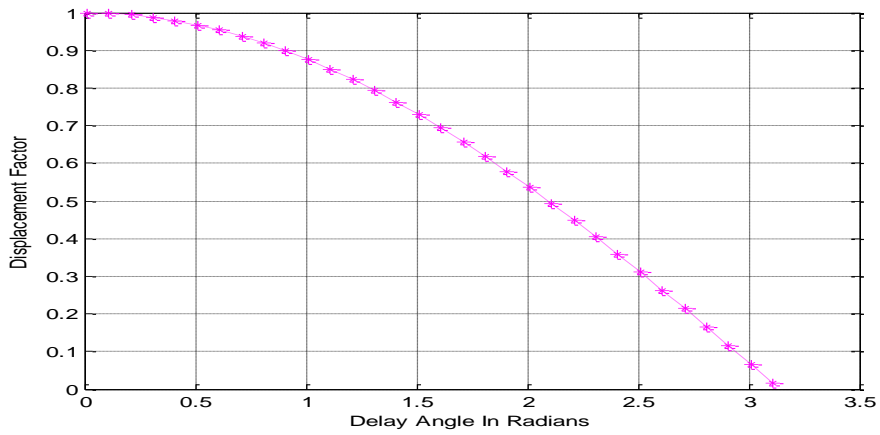
Fig. 3.17: shows the variation of the behaviour factors with the firing angle of the bridge thyristors.



(a) Power Factor



(b) Harmonic Factor

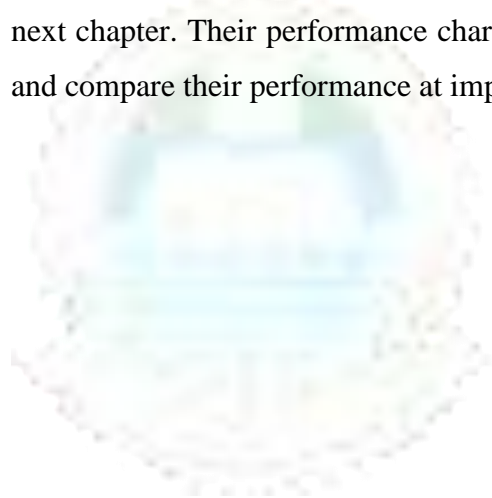


(c) Displacement Factor

Fig.3.17: Behaviour Factors of the Asymmetrical Single – Phase Bridge

From figs. 3.15, 3.16 and 3.17, it is clear that as the firing or the delay angles of the thyristors of the drive is increased, its power factor deteriorates and the harmonic content is increased tremendously. Also, results of the analytical descriptions of the input current model of fig. 3.4 presented in fig. 3.8(a – f) reveals that the supply input current deteriorates as a result of the high harmonic current present in the supply leading to a low input power factor. The poor input power factor problem was further demonstrated experimentally by having a number of Asymmetrical single – phase converters connected in parallel to the same source. Results shown in figs 3.13, 3.14 and 3.15 indicates that the input power factor deteriorates with an increase in the number of such drives connected in parallel, thus establishing the input power factor problem in industrial drives where many drives are constantly in use.

The various existing schemes employed in input power factor improvement are discussed in the next chapter. Their performance characteristics expressions will be obtained in order to evaluate and compare their performance at improving power factor.



UNIVERSITY
OF LAGOS

CHAPTER FOUR

POWER FACTOR CORRECTION (PFC) CONTROL SCHEMES

4.0 Introduction

This chapter presents the various methods of power factor control and improvement techniques. Both passive and active methods of control are discussed. A performance characteristic of the various control schemes has been derived and simulation results of the behaviour factors for the different schemes using MATLAB are also presented for comparison and evaluation.

4.1 Passive and Active methods of power factor correction

There are two approaches to solving the power factor problem. One way is by Passive control method which involves the use of capacitors and inductors and the second is by Active control method which involves the use of active devices like the Silicon Controlled Rectifier (SCR), Metallic Oxide Semi – Conductor Field Effect Transistor (MOSFET) and Insulated Gate Bipolar Transistor (IGBT). Some of these devices can be turned on either naturally or by Forced commutation i.e by means of an external circuit.

4.1.1 Passive Power Factor Correction Techniques

The traditional methods of power factor correction involve the use of capacitive and inductive elements. They are limited to low power applications and may lead to resonance because of RLC components. Besides, the waveform distortion caused by non-linear loads, which distort the current, and voltage waveforms introduce harmonic currents in the supply, which cannot be completely eliminated by the application of the traditional passive power factor correction methods. New methods of power factor improvement techniques have evolved employing Natural and Forced Commutation (Patel et.al 1983). Passive power factor corrections have certain advantage such as simplicity, reliability and ruggedness, insensitivity to noise and surges, no generation of high frequency EMI and no high frequency switching loss. However, they have several drawbacks. They are bulky and heavy because line – frequency reactive components are used. They also have poor dynamic response, lack voltage regulation and the shape of their input current depends on the load.

4.1.2 Active Power Factor Correction Techniques

Better characteristics are obtained with active PFC circuits. Active PFC involves the use of power switching devices such as the thyristor (SCR), metal oxide semi-conductor field effect transistor MOSFET or the insulated gate bipolar transistors IGBT. In all active PFC, active switches are used in conjunction with reactive elements in order to increase the effectiveness of the current shaping. The switching frequency further divides the active PFC solutions into two classes: low and high frequency. In low-frequency active PFC, switching takes place at low – order harmonics of the line – frequency and it is synchronized with the line voltage. In high- frequency active PFC, the switching frequency is much higher than the line – frequency. Advancement of power semi – conductor devices has made the active control method more popular and realizable when implemented in practical systems. It achieves a high power factor and at a reduced harmonic level. The various PFC techniques of interest depend on the type of control scheme implemented.

Active PFC is classed into two categories;

- I. Natural Commutation Control Scheme: This involved the use of controlled flywheeling; Asymmetrical Control and Sequence as well as Simultaneous Control.
- II. Forced Commutation Control Scheme: These may be the Extinction Angle Control (EAC), Symmetrical Angle Control (SAC), Selective Harmonic Elimination (SHE) and Sequence Control with forced Commutation.

The various methods of control of the Asymmetrical Bridge will be evaluated and the results compared so as to adopt one that has a great potential for improved AC input Power Factor for development in the laboratory.

4.2 Performance evaluation of the various techniques

The simplified voltage and current waveforms shown in Figs 4.1 - 4.4, were used to obtain the performance characteristic expressions for evaluation of the various control techniques as presented in table 1. (Dubey et.al 1986)

In deriving the expressions for the behaviour factors of the bridge using the simplified waveforms, it was assumed;

- That the load current is constant
- That the current is ripple free

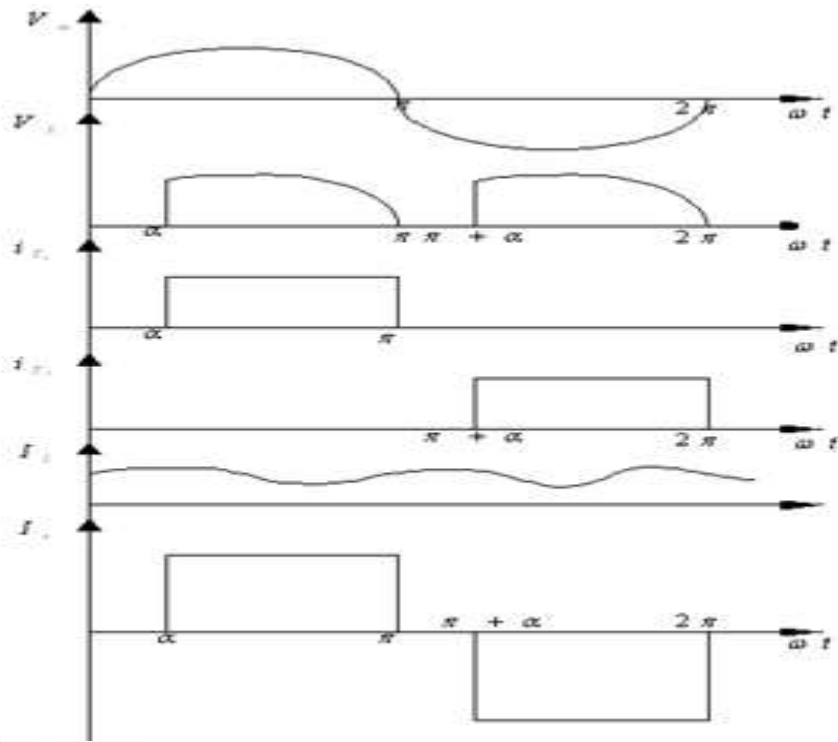


Fig. 4.1: Voltage and current waveforms for Phase Angle control – (PAC)

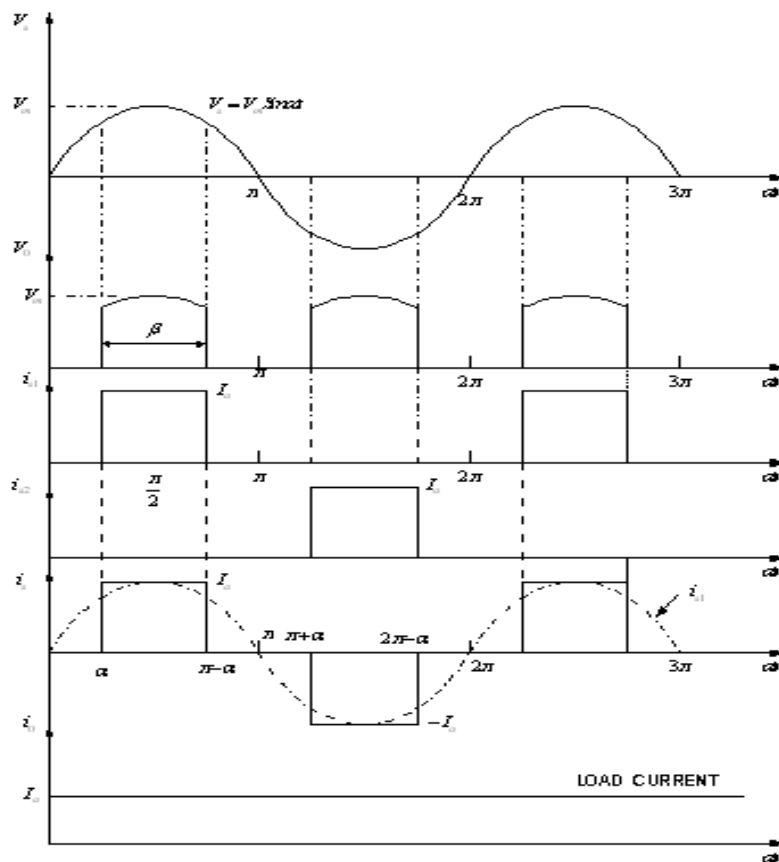


Fig. 4.2: Voltage and current waveforms for Symmetrical Angle control – (SAC)

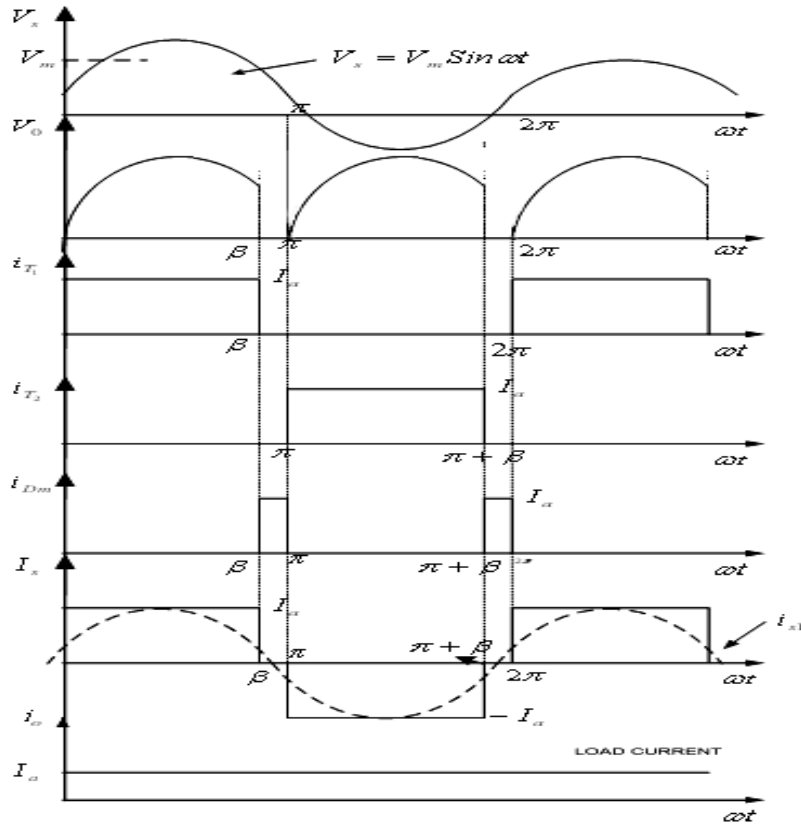


Fig.4.3: Voltage and current waveforms for Extinction Angle control – (EAC)

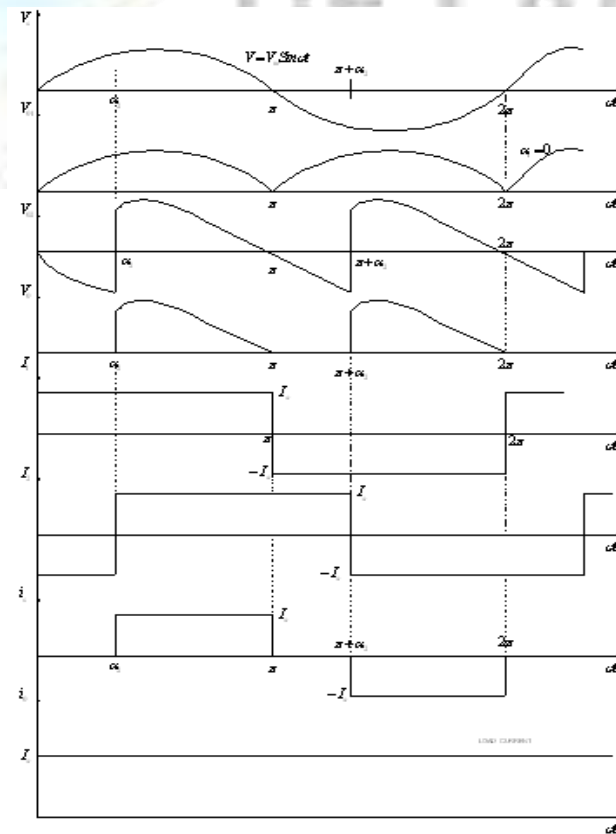


Fig.4.4: Voltage and current waveforms for Sequence control with forced commutation

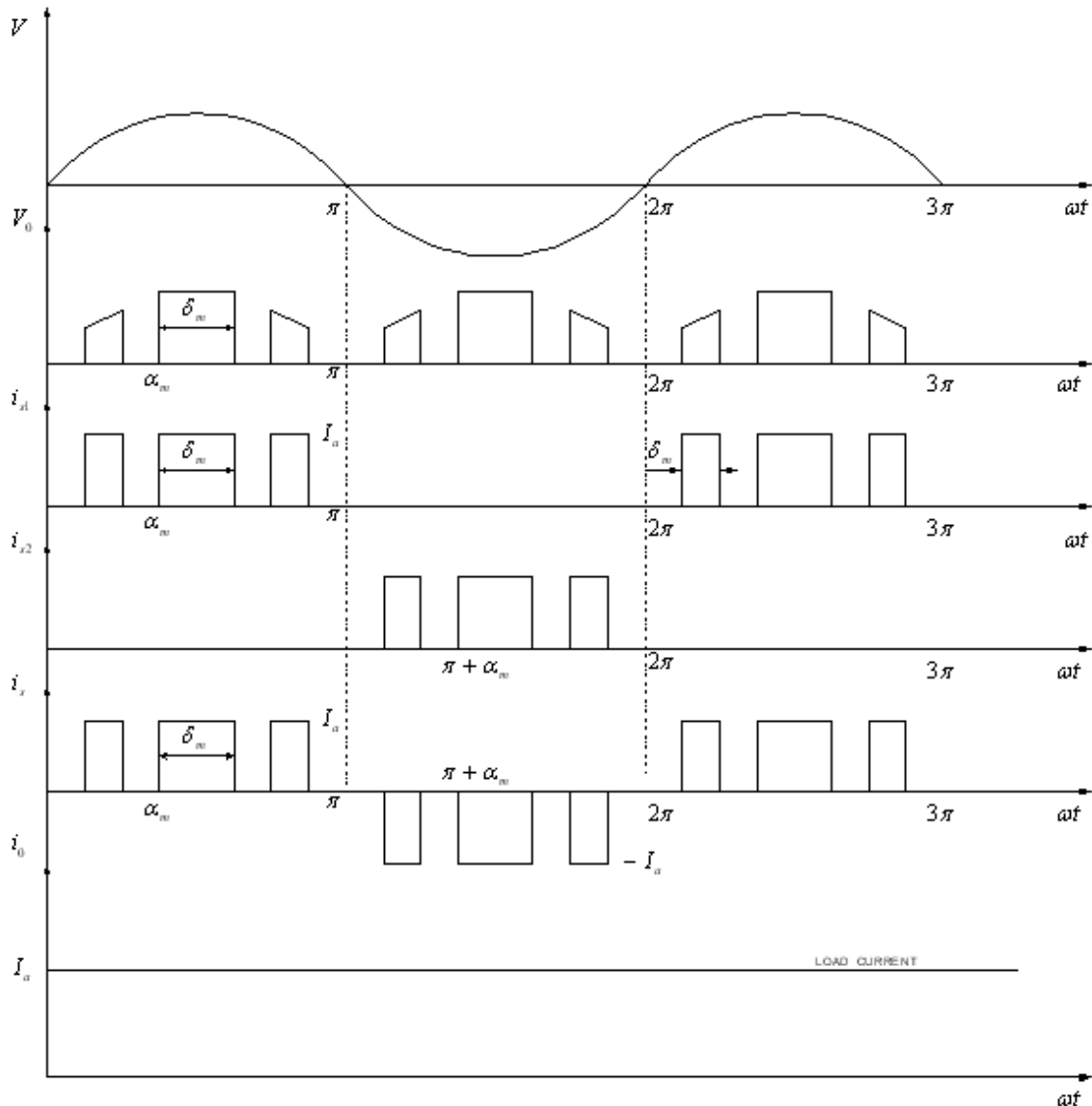


Fig. 4.5: Voltage and current waveforms for Pulse Width Modulation control – (PWM)

Analysis of the various PFC control schemes for improving the input power factor and a comparative evaluation of the techniques was carried out. The performance characteristic expressions of the various control techniques are presented in table 4.1.

In deriving the expressions shown in table 4.1, the waveforms of current and voltage displayed in figs. 4.1 – 4.5 provide information for the analysis. The detail of the Analysis for the extinction angle control is presented here whilst the details for the other methods are included in Appendix III. In the extinction angle control for example, switch S_1 is turned on

at $\omega t = 0$ and turned off by forced commutation at $\omega t = \beta$. Switch S_2 is turned on at $\omega t = \pi$ and is turned off at $\omega t = (\pi + \beta)$. The output voltage is controlled by the extinction angle β . The waveforms for voltage and current through the switches are shown in Fig. 4.3

Consider the waveform of Fig.4.3 for the Extinction Angle Control (EAC),

The average output voltage is:

$$V_{dc} = \frac{1}{\pi} \int_0^{\pi} V_m \sin \omega t d(\omega t) \quad (4.1)$$

$$\begin{aligned} V_{dc} &= \frac{1}{\pi} \int_0^{\beta} V_m \sin \omega t d(\omega t) \\ &= \frac{1}{\pi} V_m [-\cos \omega t]_0^{\beta} \\ &= \frac{V_m}{\pi} [1 - \cos \beta] \end{aligned} \quad (4.2)$$

V_{dc} can be varied from $\frac{2V_m}{\pi}$ to 0 by varying ' β ' from π to 0

$$\therefore \text{The maximum average output voltage is } V_{dm} = \frac{2V_m}{\pi} \quad (4.3)$$

Hence, the normalized average output Voltage V_n is;

$$\begin{aligned} V_n &= \frac{V_{dc}}{V_{dm}} = \frac{\frac{V_m}{\pi} (1 - \cos \beta)}{\frac{2V_m}{\pi}} \\ &= \frac{1}{2} (1 - \cos \beta) \end{aligned} \quad (4.4)$$

The rms output voltage is given by:

$$V_{rms} = \left[\frac{1}{\pi} \int_0^{\beta} V_m^2 \sin^2 d(\omega t) \right]^{\frac{1}{2}} \quad (4.5)$$

$$\begin{aligned}
&= V_m \left[\frac{1}{\pi} \int_0^\beta \frac{1}{2} - \frac{\cos 2\omega t}{2} d(\omega t) \right]^{\frac{1}{2}} \\
&= V_m \left[\frac{1}{\pi} \left| \frac{\omega t}{2} - \frac{\sin 2\omega t}{4} \right|_0^\beta \right]^{\frac{1}{2}} \\
&= V_m \left[\frac{1}{\pi} \left(\frac{\beta}{2} - \frac{\sin 2\beta}{4} \right) \right]^{\frac{1}{2}} \\
&= \frac{V_m}{\sqrt{2}} \left[\frac{1}{\pi} (2\beta - \sin 2\beta) \right]^{\frac{1}{2}} \tag{4.6}
\end{aligned}$$

Similarly, the instantaneous input current can be expressed in Fourier series as:

$$i_s(t) = I_{dc} + \sum_{n=1,2,3,\dots}^{\infty} (a_n \cos n \omega t + b_n \sin n \omega t) \tag{4.7}$$

Where,

$$I_{dc} = \frac{1}{2\pi} \int_0^{2\pi} i_s(t) d(\omega t) \tag{4.8}$$

$$= \frac{1}{2\pi} \int_0^{\pi+\beta} i_s(t) d(\omega t)$$

$$= \frac{1}{2\pi} \left[\int_0^\beta I_a d(\omega t) - \int_\pi^{\pi+\beta} I_a d(\omega t) \right]$$

$$= \frac{I_a}{2\pi} \left[\omega t \Big|_0^\beta - \omega t \Big|_\pi^{\pi+\beta} \right]$$

$$= \frac{I_a}{2\pi} [\beta - 0 - (\pi + \beta) + \pi] = 0$$

∴

$$I_{dc} = 0 \tag{4.9}$$

$$a_n = \frac{1}{\pi} \int_0^{\pi+\beta} i_s(t) \cos n \omega t d(\omega t) \tag{4.10}$$

$$\begin{aligned}
&= \frac{1}{\pi} \left[\int_0^{\beta} I_a \text{Cosn } \omega t d(\omega t) - \int_{\pi}^{\pi+\beta} I_a \text{Cosn } \omega t d(\omega t) \right] \\
&= \frac{I_a}{\pi} \left[\left| \frac{\text{Sinn } \omega t}{n} \right|_0^{\beta} - \left| \frac{\text{Sinn } \omega t}{n} \right|_{\pi}^{\pi+\beta} \right] \\
&= \frac{I_a}{n\pi} [\text{Sinn } \beta - 0 - (\text{Sinn}(\pi + \beta) - \text{Sinn } \pi)] \\
&= \frac{I_a}{n\pi} [\text{Sinn } \beta - (\text{Sin } \pi \text{Cos } \beta \text{n} + \text{Cos } \pi \text{Sinn } \beta - \text{Sin } \pi \text{n})] \\
&= \frac{2I_a}{n\pi} \text{Sinn } \beta \quad \text{For n} = 1, 3, 5, \tag{4.11}
\end{aligned}$$

$$= 0 \quad \text{for n} = 2, 4, 6, \tag{4.12}$$

$$b_n = \frac{1}{\pi} \int_0^{\pi+\beta} i_s(t) \text{Sinn } \omega t d(\omega t) \tag{4.13}$$

$$\begin{aligned}
&= \frac{1}{\pi} \left[\int_0^{\beta} I_a(t) \text{Sinn } \omega t d(\omega t) - \int_{\pi}^{\pi+\beta} I_a(t) \text{Sinn } \omega t d(\omega t) \right] \\
&= \frac{I_a}{\pi} \left[\left| \frac{-\text{Cosn } \omega t}{n} \right|_0^{\beta} - \left| \frac{-\text{Cosn } \omega t}{n} \right|_{\pi}^{\pi+\beta} \right] \\
&= \frac{I_a}{\pi} [\{\text{Cos } 0^0 - \text{Cosn } \beta\} - \{\text{Cos } \pi \text{n} - \text{Cosn}(\pi + \beta)\}] \\
&= \frac{I_a}{n\pi} [\text{Cos } 0^0 - \text{Cosn } \beta + (\text{Cosn } \pi \text{Cosn } \beta - \text{Sinn } \pi \text{Sinn } \beta) - \text{Cosn } \pi] \\
&= \frac{I_a}{n\pi} [1 - \text{Cosn } \beta + \text{Cosn } \pi \text{Cosn } \beta - \text{Sinn } \pi \text{Sinn } \beta - \text{Cosn } \pi]
\end{aligned}$$

$$\therefore b_n = \frac{2I_a}{n\pi} (1 - \text{Cosn } \beta) \quad \text{For n} = 1, 3, 5, \tag{4.14}$$

$$= 0 \quad \text{for n} = 2, 4, 6. \tag{4.15}$$

Since, $I_{dc} = 0,$

The instantaneous input current can now be written as:

$$i_s(t) = \sum_{n=1,3,5,\dots}^{\alpha} \sqrt{2} I_n \text{Sinn}(\omega t + \phi_n) \quad (4.16)$$

Where, $\phi_n = \tan^{-1} \frac{a_n}{b_n}$ (4.17)

$$= \tan^{-1} \left[\frac{\frac{2I_a}{n\pi} \text{Sinn}\beta}{\frac{2I_a}{n\pi} (1 - \text{Cosn}\beta)} \right] = \tan^{-1} \left[\frac{\text{Sinn}\beta}{(1 - \text{Cosn}\beta)} \right]$$

$$= \tan^{-1} \left[\frac{\text{Sin} \left(\frac{n\beta}{2} + \frac{n\beta}{2} \right)}{2 \text{Sin}^2 \frac{n\beta}{2}} \right] = \tan^{-1} \left[\frac{\left(\text{Sin} \frac{n\beta}{2} \text{Cos} \frac{n\beta}{2} + \text{Cos} \frac{n\beta}{2} \text{Sin} \frac{n\beta}{2} \right)}{2 \text{Sin}^2 \frac{n\beta}{2}} \right]$$

$$= \tan^{-1} \left[\frac{2 \text{Sin} \frac{n\beta}{2} \text{Cos} \frac{n\beta}{2}}{2 \text{Sin}^2 \frac{n\beta}{2}} \right] = \tan^{-1} \left[\frac{\text{Cos} \frac{n\beta}{2}}{\text{Sin} \frac{n\beta}{2}} \right]$$

Hence, $\tan \phi_n = \frac{\text{Cos} \frac{n\beta}{2}}{\text{Sin} \frac{n\beta}{2}}$ (4.18)

But, $\text{Cos}^2 \phi_n + \text{Sin}^2 \phi_n = 1$ (4.19)

$$1 + \frac{\text{Sin}^2 \phi_n}{\text{Cos}^2 \phi_n} = \frac{1}{\text{Cos}^2 \phi_n} \quad (4.20)$$

$$1 + \tan^2 \phi_n = \frac{1}{\text{Cos}^2 \phi_n}$$

Substituting equation (4.18) into equation (4.20),

$$1 + \frac{\cos^2 \frac{n\beta}{2}}{\sin^2 \frac{n\beta}{2}} = \frac{1}{\cos^2 \phi_n}$$

simplifying gives; $\cos^2 \phi_n = \sin^2 \frac{n\beta}{2}$ (4.21)

hence, $\cos \phi_n = \sin \frac{n\beta}{2}$

therefore, Displacement factor (DF) becomes,

$$\begin{aligned} DF &= \cos \phi_1 \\ &= \sin \frac{\beta}{2} \text{ leading} \end{aligned} \quad (4.22)$$

Thus, the rms value of the nth harmonic component of the input current is:

$$\begin{aligned} I_{s_n} &= \frac{1}{\sqrt{2}} (a_n^2 + b_n^2)^{\frac{1}{2}} \quad (4.23) \\ &= \frac{1}{\sqrt{2}} \left[\left(\frac{2I_a}{n\pi} \sin n\beta \right)^2 + \left(\frac{2I_a}{n\pi} (1 - \cos n\beta) \right)^2 \right]^{\frac{1}{2}} \\ &= \frac{2I_a}{\sqrt{2n\pi}} \left[\sin^2 n\beta + (1 - 2\cos n\beta + \cos^2 n\beta) \right]^{\frac{1}{2}} \\ &= \frac{2I_a}{\sqrt{2n\pi}} [1 + (1 - 2\cos n\beta)]^{\frac{1}{2}} \\ &= \frac{2I_a}{\sqrt{2n\pi}} [2(1 - \cos n\beta)]^{\frac{1}{2}} \\ &= \frac{2I_a}{\sqrt{2n\pi}} \left[2 * 2 \sin^2 \frac{n\beta}{2} \right]^{\frac{1}{2}} \\ &= \frac{4I_a}{\sqrt{2n\pi}} \left[\sin^2 \frac{n\beta}{2} \right]^{\frac{1}{2}} \quad (4.24) \end{aligned}$$

Hence,
$$I_{s_n} = \frac{2\sqrt{2}}{n\pi} I_a \text{Sin} \frac{n\beta}{2} \quad (4.25)$$

The rms value of the fundamental current (i.e. n=1) is:

$$I_{s_1} = \frac{2\sqrt{2}}{\pi} I_a \text{Sin} \frac{\beta}{2} \quad (4.26)$$

Next, the rms input current is
$$I_s = \left[\frac{1}{\pi} \int i_s^2(t) d(\omega t) \right]^{\frac{1}{2}} \quad (4.27)$$

$$\begin{aligned} &= \left[\frac{1}{\pi} \int_0^\beta I_a^2 d(\omega t) \right]^{\frac{1}{2}} = I_a \left[\frac{1}{\pi} \omega t \Big|_0^\beta \right]^{\frac{1}{2}} \\ &= I_a \sqrt{\frac{\beta}{\pi}} \end{aligned} \quad (4.28)$$

From equation (3.33), the expression for the harmonic current factor is:

$$HF = \left[\left(\frac{I_s}{I_{s_1}} \right)^2 - 1 \right]^{\frac{1}{2}} \quad (4.29)$$

Substituting equations (4.26) and (4.28) in equations (4.29), it becomes:

$$\begin{aligned} &= \left[\frac{\left\{ I_a \sqrt{\frac{\beta}{\pi}} \right\}^2}{\left\{ \frac{2\sqrt{2} I_a \text{Sin} \frac{\beta}{2}}{\pi} \right\}^2} - 1 \right]^{\frac{1}{2}} = \left[\left(\frac{\sqrt{\beta}}{\sqrt{\pi}} * \frac{\pi}{2\sqrt{2} \text{Sin} \frac{\beta}{2}} \right)^2 - 1 \right]^{\frac{1}{2}} \\ &= \left[\frac{\beta * \pi^2}{8\pi \text{Sin}^2 \frac{\beta}{2}} - 1 \right]^{\frac{1}{2}} = \left[\frac{\beta \pi}{8 \text{Sin}^2 \frac{\beta}{2}} - 1 \right]^{\frac{1}{2}} \\ &= \left[\frac{\beta \pi}{4(1 - \text{Cos} \beta)} - 1 \right]^{\frac{1}{2}} \end{aligned} \quad (4.30)$$

From equation (3.31), the expression for the input current power factor is:

$$PF = \frac{I_{s1}}{I_s} \cos \phi_1 \quad (4.31)$$

And from equation (4.22),

$$\cos \phi_1 = \sin \frac{\beta}{2} \quad (4.32)$$

Hence substituting equations (4.26), (4.28) and (4.32) into equation (4.31) and simplifying,

$$\begin{aligned} &= \frac{2\sqrt{2}}{\pi} \frac{\sin \frac{\beta}{2}}{I_a \sqrt{\frac{\beta}{\pi}}} * \sin^2 \frac{\beta}{2} = \frac{2\sqrt{2}}{\pi} * \frac{\sqrt{\pi}}{\sqrt{\beta}} * \sin^2 \frac{\beta}{2} \\ &= \frac{2\sqrt{2}}{\sqrt{\pi\beta}} \sin^2 \frac{\beta}{2} = \frac{2\sqrt{2}(1 - \cos \beta)}{2\sqrt{\pi\beta}} \\ &= \frac{\sqrt{2}(1 - \cos \beta)}{\sqrt{\pi\beta}} \quad (4.33) \end{aligned}$$

The performance expressions in table 4.1 for the output voltage and the behaviour factors of the drive; displacement factor, harmonic factor and input power factor of the extinction angle control scheme are represented by equations (4.4), (4.22), (4.30) and (4.33) respectively. Matlab programming was used to simulate these expressions and their results are presented in Figs. 4.6, 4.7 and 4.8. Similar expressions for the other active control schemes can be derived in a similar way presented above. (See APPENDIX IV)

4.3 Performance Analysis for the methods of control of the Asymmetrical Bridge

The performance expressions for the different methods of controls of the Asymmetrical bridge given in table 4.1 (Dubey et al 1986 and Sen 1991) were simulated to obtain a complete monograph of the behaviour factors of the drive as shown in Figs. 4.5, 4.7 and 4.8.

Control Technique	Output Voltage	Displacement Factor (DF)	Harmonic Current (HF)	Input Current (PF)
Conventional phase Angle Control (PAC)	$\frac{1}{2}(1 + \cos \alpha)$	$\cos \frac{\alpha}{2}$	$\left[\frac{\pi(\pi - \alpha)}{4(1 + \cos \alpha)} - 1 \right]^{\frac{1}{2}}$	$\frac{2\sqrt{2}\cos^2 \frac{\alpha}{2}}{[\pi(\pi - \alpha)]^{\frac{1}{2}}}$
Controlled Flywheeling	$\frac{1}{2}(1 + \cos \alpha)$	$\cos \frac{\alpha}{2}$	$\left[\frac{\pi(\pi - \alpha)}{4(1 + \cos \alpha)} - 1 \right]^{\frac{1}{2}}$	$\frac{2\sqrt{2}\cos^2 \frac{\alpha}{2}}{[\pi(\pi - \alpha)]^{\frac{1}{2}}}$
Sequence Control $0.5 < V_a < 1.0$ pu	$\frac{1}{4}(3 + \cos \alpha)$	$\frac{3 + \cos \alpha}{(10 + 6\cos \alpha)^{\frac{1}{2}}}$	$\left[\frac{\pi \left(1 - \frac{3\alpha}{4\pi} \right)}{(5 + 3\cos \alpha)} - 1 \right]^{\frac{1}{2}}$	$\frac{3 + \cos \alpha}{\left[\pi \left(2\pi - \frac{3\alpha}{2} \right) \right]^{\frac{1}{2}}}$
$0 < V_a < 0.5$ pu	$\frac{1}{4}(1 + \cos \alpha)$	$\cos \frac{\alpha}{2}$	$\left[\frac{\pi(\pi - \alpha)}{4(1 + \cos \alpha)} - 1 \right]^{\frac{1}{2}}$	$\frac{\sqrt{2}(1 + \cos \alpha)}{\pi \left(1 - \frac{\alpha}{\pi} \right)^{\frac{1}{2}}}$
Extinction Angle Control (EAC)	$\frac{1}{2}(1 - \cos \beta)$	$\sin \frac{\beta}{2}$	$\left[\frac{\beta\pi}{4(1 - \cos \beta)} - 1 \right]^{\frac{1}{2}}$	$\frac{\sqrt{2}(1 - \cos \beta)}{\sqrt{\pi\beta}}$
Symmetrical Angle Control (SAC)	$\cos \alpha$	1	$\left[\frac{\pi(\pi - 2\alpha)}{8\cos^2 \alpha} - 1 \right]^{\frac{1}{2}}$	$\frac{2\sqrt{2}\cos \alpha}{[\pi(\pi - 2\alpha)]^{\frac{1}{2}}}$
Sequence Control (with Forced Commutation) $0.5 < V_a < 1.0$ pu	$\frac{1}{2}(1 + \cos \alpha)$	1	$\left[\frac{\pi \left(\pi - \frac{3\alpha}{2} \right)}{2(1 + \cos \alpha)^2} - 1 \right]^{\frac{1}{2}}$	$\frac{\sqrt{2}(1 + \cos \alpha)}{\left[\pi \left(\pi - \frac{3\alpha}{2} \right) \right]^{\frac{1}{2}}}$
$0 < V_a < 0.5$ pu	$\frac{\cos \alpha}{2}$	1	$\left[\frac{\pi(\pi - 2\alpha)}{8\cos^2 \alpha} - 1 \right]^{\frac{1}{2}}$	$\frac{2\sqrt{2}\cos \alpha}{\pi \left(1 - \frac{2\alpha}{\pi} \right)^{\frac{1}{2}}}$
Sinusoidal PWM, "p" Pulses/half cycle with kth pulse from α_k to δ_k	$\frac{1}{2} \sum_{m=1}^p \left[\cos \alpha_m - \cos(\alpha_m + \delta_m) \right]$	1	$\left[\frac{\pi \sum_{m=1}^p [(\alpha_m + \delta_m) - \alpha_m]}{2 \sum_{m=1}^p [\cos \alpha_m - \cos(\alpha_m + \delta_m)]^2} - 1 \right]^{\frac{1}{2}}$	$\frac{\sqrt{2} \sum_{m=1}^p [\cos \alpha_m - \cos(\alpha_m + \delta_m)]}{\pi \sum_{m=1}^p [(\alpha_m + \delta_m) - \alpha_m]^{\frac{1}{2}}}$

(a)

Control Technique	Output Voltage	Harmonic Current/Output Current	Input Current/Output Current
Conventional Phase Angle Control (PAC)	$\frac{1}{2}(1 + \cos \alpha)$	$\frac{2\sqrt{2}}{n\pi} \cos \frac{n\alpha}{2}$	$\left[\pi - \frac{\alpha}{\pi} \right]^{\frac{1}{2}}$
Controlled Flywheeling	$\frac{1}{2}(1 + \cos \alpha)$	$\frac{2\sqrt{2}}{n\pi} \cos \frac{n\alpha}{2}$	$\left[\pi - \frac{\alpha}{\pi} \right]^{\frac{1}{2}}$
Sequence Control $0.5 < V_a < 1.0 \text{ pu}$ $0 < V_a < 0.5 \text{ pu}$	$\frac{1}{4}(3 + \cos \alpha)$ $\frac{1}{4}(1 + \cos \alpha)$	$\frac{1}{n\pi} (5 + 3 \cos n\alpha)^{\frac{1}{2}}$ $\frac{\sqrt{2}}{n\pi} \cos n\alpha$	$\left[1 - \frac{3\alpha}{4} \right]^{\frac{1}{2}}$ $\frac{1}{2} \left(1 - \frac{\alpha}{\pi} \right)^{\frac{1}{2}}$
Extinction Angle Control (EAC)	$\frac{1}{2}(1 - \cos \beta)$	$\frac{2\sqrt{2}}{n\pi} \sin \frac{n\beta}{2}$	$\left[\frac{\beta}{\pi} \right]^{\frac{1}{2}}$
Symmetrical Angle Control (SAC)	$\cos \alpha$	$\frac{2\sqrt{2}}{n\beta} \cos n\alpha$	$\left[1 - \frac{2\alpha}{\pi} \right]^{\frac{1}{2}}$
Sequence Control (with Forced Commutatio) $0.5 < V_a < 1.0 \text{ pu}$ $0 < V_a < 0.5 \text{ pu}$	$\frac{1}{2}(1 + \cos \alpha)$ $\frac{\cos \alpha}{2}$	$\frac{\sqrt{2}}{n\pi} (1 + \cos \alpha)$ $\frac{\sqrt{2}}{n\pi} \cos n\alpha$	$\left[1 - \frac{3\alpha}{2\pi} \right]^{\frac{1}{2}}$ $\frac{1}{2} \left(1 - \frac{2\alpha}{\pi} \right)$
Sinusoidal PWM, "p" pulses/half cycle with k th pulse from α_k to δ_k	$\frac{1}{2} \sum_{m=1}^p [\cos \alpha_m - \cos(\alpha_m + \delta_m)]$	$\frac{\sqrt{2}}{n\pi} \sum_{m=1}^p [\cos n\alpha_m - \cos n(\alpha_m + \delta_m)]$	$\frac{1}{\sqrt{\pi}} \left[\sum_{m=1}^p [(\alpha_m + \delta_m) - \alpha_m] \right]^{\frac{1}{2}}$

(b)

Table 4.1: Generalised Equations for Various Converter – Control Techniques using their simplified models

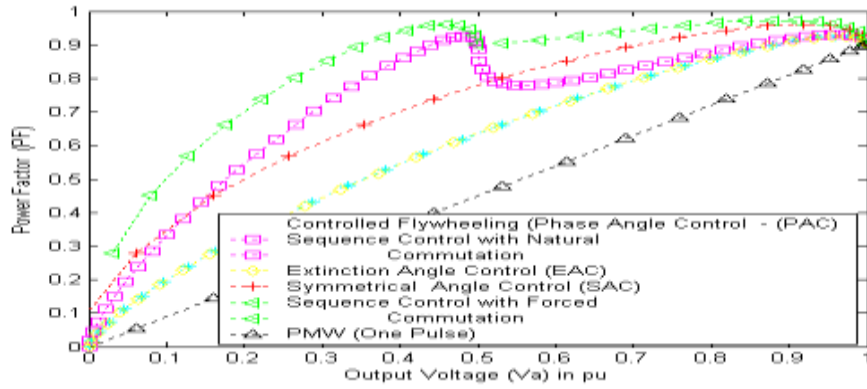


Fig.4.6: Relationships between the Input Power Factor and Output Voltage for the various PFC control techniques

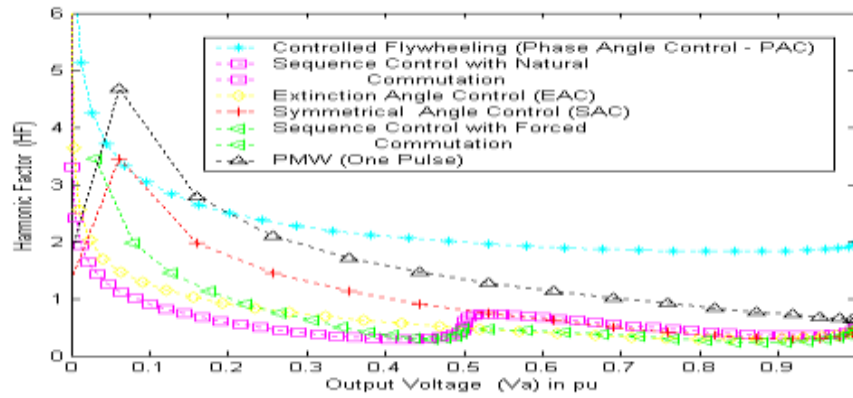


Fig.4.7: Relationships between the Harmonic Factor and Output Voltage for the various PFC control techniques

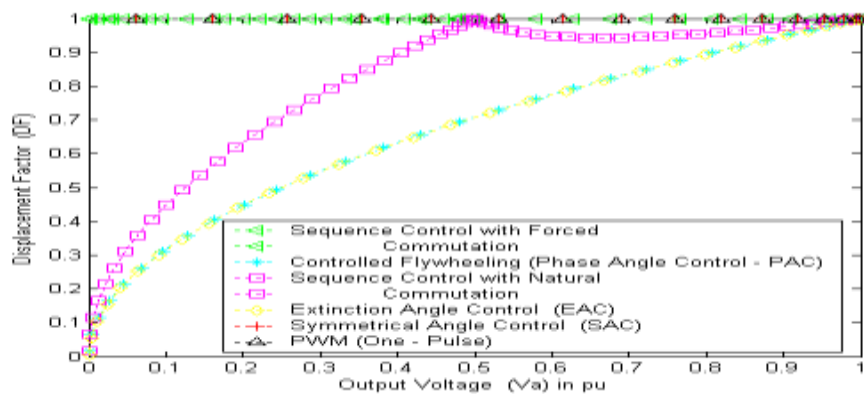


Fig. 4.8: Relationships between the Displacement Factor and Output Voltage for the various PFC control techniques

The various power factor correction (PFC) techniques for improving power factor of the Asymmetrical Single – Phase Drive have been discussed in the preceding section. The performance characteristics simulated from the simplified equations are shown in Figs. 4.6 to 4.8 for convenience of comparison. Information about the total harmonic content (Fig.4.7) is important only if input filters are not used. Currents with high harmonic content distort the supply voltage. In some control schemes, the harmonic factor is high in the low speed region (Fig.4.7). This is due to high contents of higher harmonics, which are easily filtered out if input filters are not used. The important current harmonics that the designer needs to consider are those of the lowest order. In this regard, the PWM control scheme has the advantage because by the proper choice of pulse numbers per half cycle, the lower order harmonics can be eliminated. An input filter can eliminate most of the harmonic current from the line thereby making the line currents essentially sinusoidal. A higher number of pulses per half cycle increase the ripple frequency of the motor current. The armature circuit inductance may be sufficient to smooth out the motor current and additional inductance may not be necessary at the armature circuit.

Also from Fig.4.8, the PWM control scheme gives a unity displacement factor implying that it can be used to achieve a near unity power factor; hence it is adopted for further development and applications in the laboratory for power factor improvement.

CHAPTER FIVE

PULSE WIDTH MODULATION (PWM) FOR INPUT POWER FACTOR CORRECTION

5.1 Pulse Width Modulation

The various methods of improving the poor power factor were evaluated in chapter four and the PWM control scheme for power factor correction was adopted as the most effective because it provides an improved power factor close to unity. Also, by proper choice of the number of pulses per half cycle, the lower-order harmonics can be eliminated. The input supply current is essentially sinusoidal and the need for input filters to reduce harmonic currents is obviated. In Pulse Width Modulation, the converter switches are turned on and off several times during a half cycle and the output voltage is controlled by varying the width of the pulses (Mohan 1995, Tao 2000 and Lazaro 2007). By having many pulses of the output voltage per half cycle of the source voltage, the ripple in the motor current can be substantially reduced and discontinuous conduction can be completely eliminated without using any filter inductance. (Ismail 2006)

The operation of the Pulse Width Modulation control scheme involves an astable multivibrator triggering a monostable to produce pulses of variable width which are then integrated to obtain a triangular signal at a desired frequency. (for example, 20KHz). The triangular signal together with a DC signal are fed into an AND gate. This produces a train of high frequency pulses used to trigger the bridge thyristors. The pulses are processed to a Darlington pair with pulse transformers at the collector of the transistors. The pulse transformers are used to isolate the electronic control circuit from the power circuit of the asymmetrical bridge. Waveforms of the electronic control circuits and the input current and voltage are used to explain the success of the scheme.

The choice of the pulse width modulation technique was based on the comparative analysis of the various methods of power factor correction techniques presented in the preceding section. It gives improved characteristics in terms of higher input power factor and sinusoidal shape of input current (Lu Bing et.al 2005, Srinivasan, R 1999 and Liu Y et.al 2003).

The Comparator input and output waveforms are shown in Fig.5.1

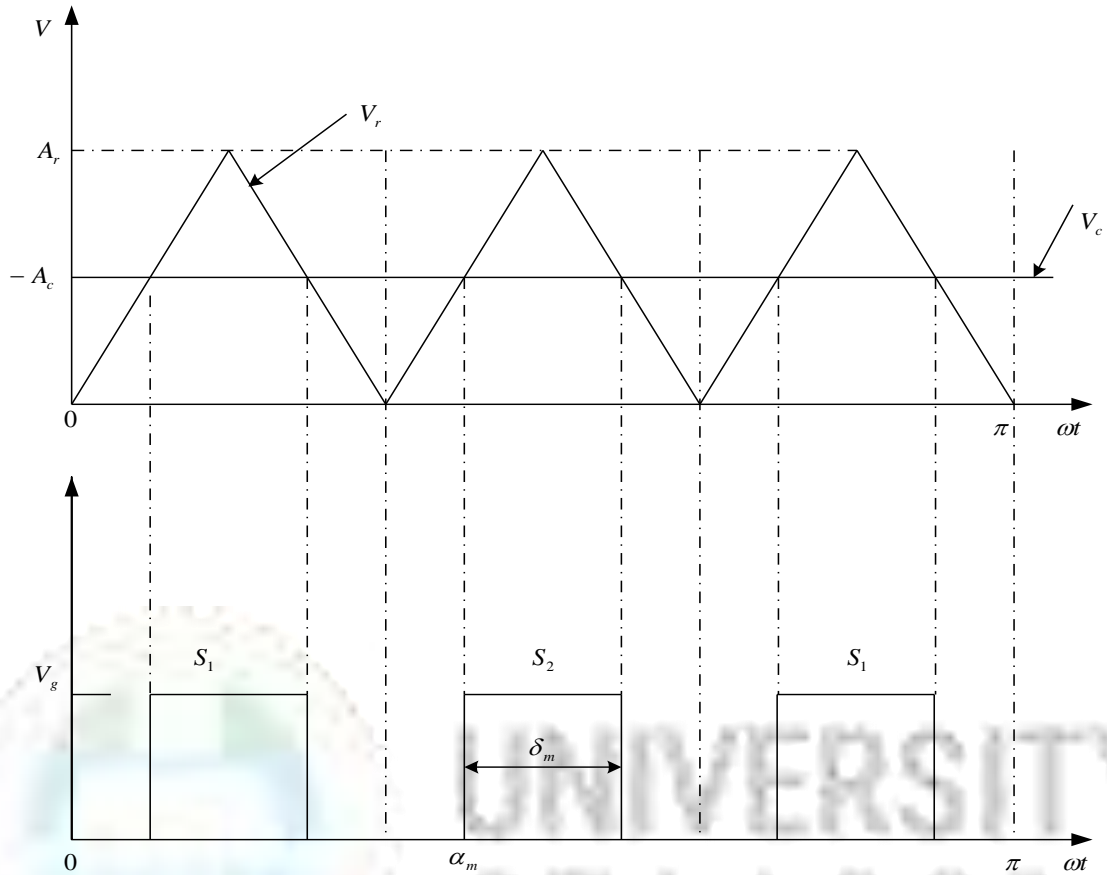


Fig. 5.1: Comparator Input and Output waveforms.

In Fig. 5.1,

A_c represents the amplitude of the carrier signal (sawtooth waveform) and

A_r represents the amplitude of the reference signal (DC voltage)

In the PWM control, the displacement factor is unity and the power factor is improved. The lower-order harmonics are eliminated or reduced. For example, with four pulses per half – cycle, the lowest-order harmonic is the fifth and with six pulses per half – cycle, the lowest harmonic is the seventh. (Grahame et.al 2003 and Rashid et.al 1993)

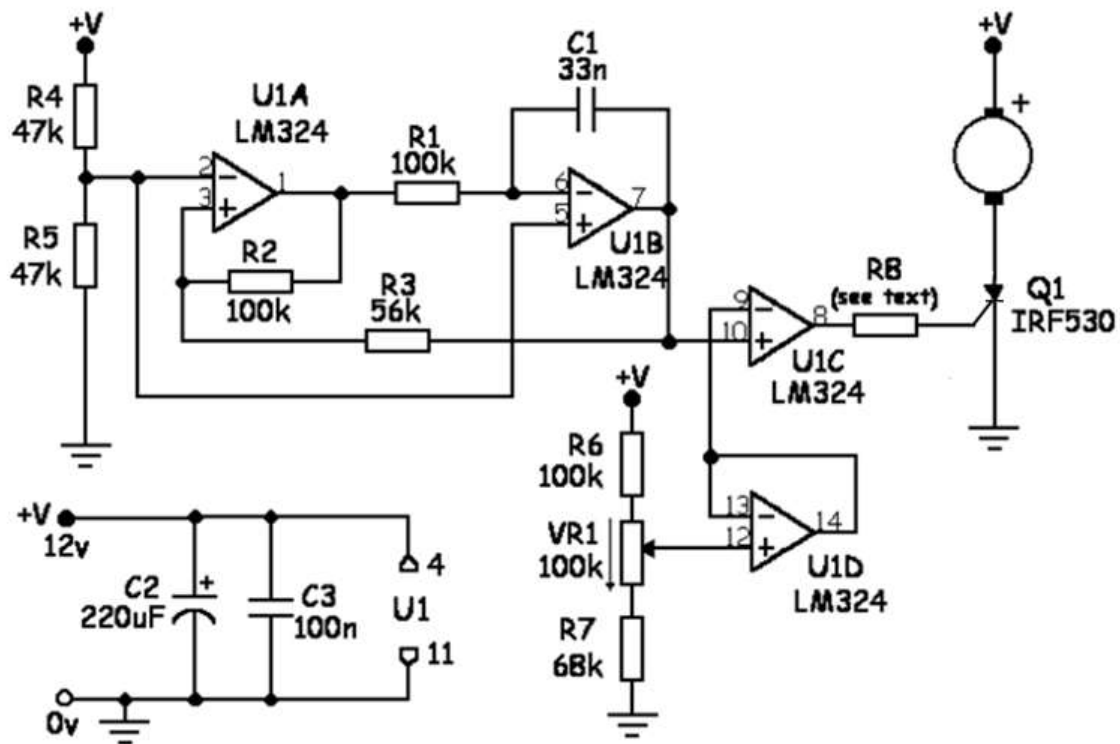


Fig. 5.2: Practical PWM Circuit

Figure 5.2 shows a practical PWM circuit. This circuit uses LM324, a 14 – pin IC containing four individual op – amps and running off a single power supply. The sawtooth is generated with two of them (U1A and U1B) configured as a Schmitt Trigger and Miller Integrator and a third (U1C) is used as a comparator to compare the sawtooth with the reference voltage and switch the power transistor on. The fourth op – amp is used as a voltage follower to buffer the reference potential divider.

5.2 Types of PWM

There are two basic types of pulse width modulation:

- Equal pulse width modulation (EPWM)
- Sinusoidal pulse width modulation (SPWM)

5.2.1 Equal pulse width modulation (EPWM)

This involves comparing a triangular voltage with a DC signal in a comparator to produce pulses at the output of the comparator that are used to trigger the switching device as presented in preceding section.

5.2.2 Sinusoidal pulse width modulation (SPWM)

In the sinusoidal PWM control shown in Fig.5.3, the pulse widths are generated by comparing a triangular reference voltage V_r of amplitude A_r and frequency f_r with a carrier half sinusoidal voltage V_c of variable amplitude A_c and frequency $2f_s$. The sinusoidal voltage is in phase with the input phase voltage V_s and has twice the supply frequency f_s . The widths of the pulses (and the output voltage) are varied by changing the amplitude A_c or the modulation index 'M' from 0 to 1. The modulation index is defined as:

$$M = \frac{A_c}{A_r} \quad (5.1)$$

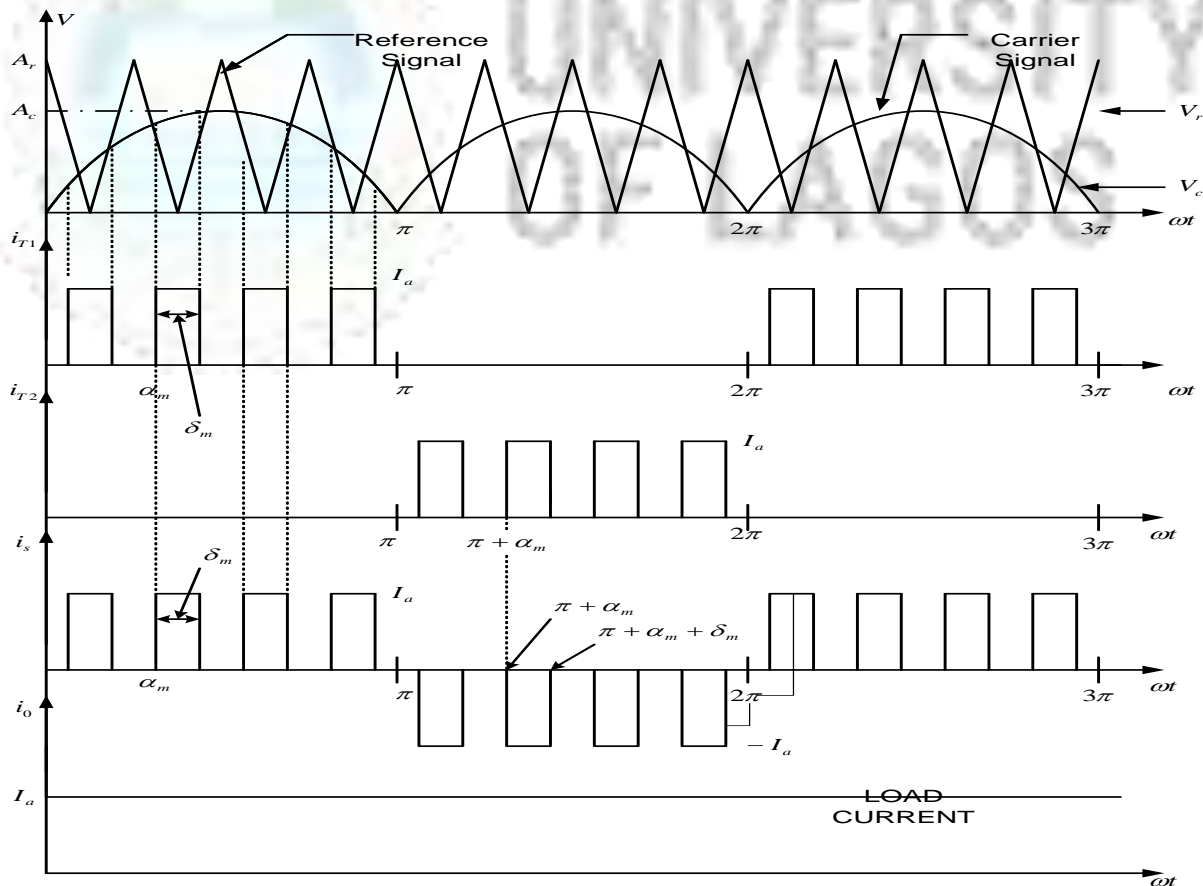


Fig.5.3: Waveforms of Currents and Voltages for Sinusoidal PWM.

5.3 Analysis for predicting the Behaviour factors on the AC input current of the Asymmetrical Bridge with pulse width modulation (PWM)

The performance of the converter can be determined in two steps: (Rashid 1993; Venkatarmmaman and Wang 2004)

- (i) By considering only one pair of pulses such that if one pulse starts at $\omega t = \alpha_1$ and ends at $\omega t = \alpha_1 + \delta_1$, the other pulse starts at $\omega t = \pi + \alpha_1$ and ends at $\omega t = (\pi + \alpha_1 + \delta_1)$ and
- (ii) By combining the effects of all points. If m^{th} pulse starts at $\omega t = \alpha_m$ and its width is δ_m , the input current due to 'p' number of pulse is found from equation (5-2) below.

In an attempt to evaluate the expressions for the behaviour factors of the drive, we consider the Fourier expression of a sine waveform, since with a PWM Power factor controlled drive, a sinusoidal input current waveform results with a near unity power factor fig. 5.20.

The instantaneous input current to the bridge is expressed in Fourier series as:

$$i_s(t) = I_{dc} + \sum_{m=1,2,3,\dots}^{\infty} (a_n \cos n\omega t + b_n \sin n\omega t) \quad (5.2)$$

And due to symmetry of the input current waveform, there will be no even harmonics and I_{dc} will be zero:

$$I_{dc} = \frac{1}{T} \int_0^T i(t) dt = \frac{1}{2\pi} \int_0^{2\pi} i(t) dt \quad (5.3)$$

If δ_m is the width of the pulse, then I_{dc} can be written in the form;

$$\begin{aligned} I_{dc} &= \frac{1}{2\pi} \left[\int_{\alpha_m}^{\alpha_m + \delta_m} i(t) dt - \int_{\pi + \alpha_m}^{\pi + \alpha_m + \delta_m} i(t) dt \right] \\ &= \frac{I_a}{2\pi} \left[|t|_{\alpha_m}^{\alpha_m + \delta_m} - |t|_{\pi + \alpha_m}^{\pi + \alpha_m + \delta_m} \right] \\ &= \frac{I_a}{2\pi} [(\alpha_m + \delta_m) - \alpha_m - \{(\pi + \alpha_m + \delta_m) - (\pi + \alpha_m)\}] \\ &= \frac{I_a}{2\pi} [\alpha_m + \delta_m - \alpha_m - \{\pi + \alpha_m + \delta_m - \pi - \alpha_m\}] \\ &= \frac{I_a}{2\pi} [(\delta_m - \delta_m)] = 0 \end{aligned} \quad (5.4)$$

Therefore, I_{dc} equal zero.

The coefficients of equation (5.2) are:

$$\begin{aligned}
 a_n &= \frac{2}{T} \int_0^T i_s(t) \cos n\omega t d(\omega t) \\
 &= \sum_{m=1}^p \left[\frac{1}{\pi} \int_{\alpha_m}^{\alpha_m + \delta_m} I_a \cos n\omega t d(\omega t) - \int_{\pi + \alpha_m}^{\pi + \alpha_m + \delta_m} I_a \cos n\omega t d(\omega t) \right] \\
 &= \frac{I_a}{n\pi} \sum_{m=1}^p \left[|\sin n\omega t|_{\alpha_m}^{\alpha_m + \delta_m} - |\sin n\omega t|_{\pi + \alpha_m}^{\pi + \alpha_m + \delta_m} \right] \\
 &= \frac{I_a}{n\pi} \sum_{m=1}^p [\sin n(\alpha_m + \delta_m) - \sin n\alpha_m - \sin n(\pi + \alpha_m + \delta_m) - \sin n(\pi + \alpha_m)] \\
 &= \frac{I_a}{n\pi} \sum_{m=1}^p [\sin n(\alpha_m + \delta_m) - \sin n\alpha_m - \{\sin n(\pi + \alpha_m + \delta_m) - \sin n(\pi + \alpha_m)\}] \\
 &= \frac{I_a}{n\pi} \sum_{m=1}^p [\sin n(\alpha_m + \delta_m) - \sin n\alpha_m - \{\sin n(\alpha_m + \delta_m) \cos n\pi + \sin n\pi \cos(\alpha_m + \delta_m)\} \\
 &\quad - \{\sin n\pi \cos \alpha_m + \sin n\alpha_m \cos n\pi\}] \\
 &= \frac{I_a}{n\pi} \sum_{m=1}^p \sin n(\alpha_m + \delta_m) [1 - \cos n\pi] + \sin n\alpha_m (\cos n\pi - 1) + \cos \alpha_m \sin n\pi
 \end{aligned}
 \tag{5.5}$$

For “n” even,

$$a_n = \frac{I_a}{n\pi} \sum_{m=1}^p [\sin(\alpha_m + \delta_m) \{1 - 1\} + \sin \alpha_m \{1 - 1\}] = 0
 \tag{5.6}$$

For “n” odd,

$$\begin{aligned}
 a_n &= \frac{I_a}{n\pi} \sum_{m=1}^p [\sin(\alpha_m + \delta_m)\{1 + 1\} + \sin\alpha_m\{-1 - 1\}] \\
 &= \frac{I_a}{n\pi} \sum_{m=1}^p [2\sin(\alpha_m + \delta_m) - 2\sin\alpha_m] \\
 &= \frac{2I_a}{n\pi} \sum_{m=1}^p [\sin(\alpha_m + \delta_m) - \sin\alpha_m]
 \end{aligned}$$

Provided that $\delta_m \ll \alpha_m$ or that “p” $\gg 1$,

Therefore,

$$a_n = 0 \quad \text{for all “n”} \quad (5.7)$$

Similarly,

$$\begin{aligned}
 b_n &= \frac{2}{T} \int_0^T i_s(t) \sin\omega t d(\omega t) = \frac{1}{\pi} \int_0^{2\pi} i_s(t) \sin\omega t d(\omega t) \\
 &= \frac{1}{\pi} \sum_{m=1}^p \left[\int_{\alpha_m}^{\alpha_m + \delta_m} I_a \sin n\omega t d(\omega t) - \int_{\pi + \alpha_m}^{\pi + \alpha_m + \delta_m} I_a \sin n\omega t d(\omega t) \right] \\
 &= \frac{I_a}{n\pi} \sum_{m=1}^p \left[|-\cos n\omega t|_{\alpha_m}^{\alpha_m + \delta_m} - |-\cos n\omega t|_{\pi + \alpha_m}^{\pi + \alpha_m + \delta_m} \right] \\
 &= \frac{I_a}{n\pi} \sum_{m=1}^p \cos n \alpha_m - \cos n(\alpha_m + \delta_m) + \cos n(\pi + \alpha_m + \delta_m) - \cos n(\pi + \alpha_m) \\
 &= \frac{I_a}{n\pi} \sum_{m=1}^p [\cos n \alpha_m - \cos n(\alpha_m + \delta_m) + \cos n \pi \cos n(\alpha_m + \delta_m) - \sin n \pi \sin n(\alpha_m + \delta_m) \\
 &\quad - \cos n \pi \cos n \alpha_m + \sin n \pi \sin n \alpha_m]
 \end{aligned} \quad (5.8)$$

For “n” even,

$$\begin{aligned}
 &= \frac{I_a}{n\pi} \sum_{m=1}^p [\cos n\alpha_m - \cos n(\alpha_m + \delta_m) + \cos n(\alpha_m + \delta_m) - \cos n\alpha_m] \\
 &= 0
 \end{aligned} \tag{5.9}$$

For “n” odd,

$$\begin{aligned}
 b_n &= \frac{I_a}{n\pi} \sum_{m=1}^p [\cos n\alpha_m - \cos n(\alpha_m + \delta_m) - \cos n(\alpha_m + \delta_m) + \cos n\alpha_m] \\
 &= \frac{2I_a}{n\pi} \sum_{m=1}^p [\cos n\alpha_m - \cos n(\alpha_m + \delta_m)]
 \end{aligned} \tag{5.10}$$

Hence,

$$\begin{aligned}
 i_s(t) &= I_{dc} + \sum_{m=1,2,3,\dots}^{\infty} (a_n \cos n\omega t + b_n \sin n\omega t) \\
 &= \sum_{m=1,2,3,\dots}^{\infty} b_n \sin n\omega t
 \end{aligned} \tag{5.11}$$

Since $I_{dc} = 0$, and $a_n = 0$ for $\delta_m \ll \alpha_m$, then.

$$\phi_c = \tan^{-1} \frac{a_n}{b_n} = 0 \tag{5.12}$$

Determination of rms value of the nth harmonic current:

$$I_{sn} = \sqrt{\frac{a_n^2 + b_n^2}{2}} = \sqrt{\frac{b_n^2}{2}} = \frac{b_n}{\sqrt{2}} \tag{5.13}$$

Substituting for b_n ,

$$I_{s_n} = \frac{\frac{2I_a}{n\pi} \sum_{m=1}^p [\cos n\alpha_m - \cos n(\alpha_m + \delta_m)]}{\sqrt{2}}$$

Therefore,

$$I_{s_1} = \frac{\sqrt{2}I_a}{\pi} \sum_{m=1}^p [\cos n\alpha_m - \cos n(\alpha_m + \delta_m)] \quad (5.14)$$

Determination of rms value of the input current “ I_s ”.

$$I_s = \left[\frac{1}{T} \int_0^T i_s^2(t) dt \right]^{\frac{1}{2}} = \left[\frac{1}{\pi} \int_0^{\pi} i_s^2(t) dt \right]^{\frac{1}{2}} \quad (5.15)$$

$$\begin{aligned} &= \left[\frac{1}{\pi} \int_{\alpha_m}^{\alpha_m + \delta_m} I_a^2 dt \right]^{\frac{1}{2}} \\ &= \frac{1}{\sqrt{\pi}} \left[\int_{\alpha_m}^{\alpha_m + \delta_m} I_a^2 dt \right]^{\frac{1}{2}} \\ &= \frac{I_a}{\sqrt{\pi}} [(\alpha_m + \delta_m) - \alpha_m]^{\frac{1}{2}} \end{aligned} \quad (5.16)$$

For “p” pulses,

$$I_s = \frac{I_a}{\sqrt{\pi}} \sum_{m=1}^p [(\alpha_m + \delta_m) - \alpha_m]^{\frac{1}{2}} \quad (5.17)$$

Displacement Factor (DF);

$$DF = \cos\phi_1$$

But

$$\phi_1 = 0$$

Therefore,

$$DF = \cos\phi_1 = \cos 0 = 1 \quad (5.18)$$

Harmonic Factor (HF):

Previously, (HF) was defined in section 3.7 as;

$$HF = \left[\left(\frac{I_s}{I_{s_1}} \right)^2 - 1 \right]^{\frac{1}{2}}$$

Substituting for “ I_s ” and “ I_{s_1} ” gives,

$$\begin{aligned} HF &= \left[\left(\frac{\frac{I_a}{\sqrt{\pi}} \sum_{m=1}^p [(\alpha_m + \delta_m) - \alpha_m]^{\frac{1}{2}}}{\frac{\sqrt{2}I_a}{\pi} \sum_{m=1}^p [\cos\alpha_m - \cos(\alpha_m + \delta_m)]} \right)^2 - 1 \right]^{\frac{1}{2}} \\ &= \left[\frac{\frac{I_a^2}{\pi} \sum_{m=1}^p [(\alpha_m + \delta_m) - \alpha_m]}{\frac{2I_a^2}{\pi^2} [\sum_{m=1}^p [\cos\alpha_m - \cos(\alpha_m + \delta_m)]]^2} - 1 \right]^{\frac{1}{2}} \\ &= \left[\frac{\pi \sum_{m=1}^p [(\alpha_m + \delta_m) - \alpha_m]}{2 [\sum_{m=1}^p [\cos\alpha_m - \cos(\alpha_m + \delta_m)]]^2} - 1 \right]^{\frac{1}{2}} \end{aligned} \quad (5.19)$$

Input Power Factor (PF).

Input power factor as defined in equation (3.31) is;

$$PF = \frac{I_{s_1}}{I_s} \cos\phi_1$$

Again substituting for “ I_{s_1} ” and “ I_s ”,

$$\begin{aligned}
 PF &= \frac{\frac{\sqrt{2}I_a}{\pi} \sum_{m=1}^p [\cos n\alpha_m - \cos n(\alpha_m + \delta_m)]}{\frac{I_a}{\sqrt{\pi}} \sum_{m=1}^p [(\alpha_m + \delta_m) - \alpha_m]^{\frac{1}{2}}} * 1 = \frac{\sqrt{2} \sum_{m=1}^p [\cos n\alpha_m - \cos n(\alpha_m + \delta_m)]}{\sqrt{\pi} \sum_{m=1}^p [(\alpha_m + \delta_m) - \alpha_m]^{\frac{1}{2}}} \\
 &= \sqrt{\frac{2}{\pi}} \frac{\sum_{m=1}^p [\cos n\alpha_m - \cos n(\alpha_m + \delta_m)]}{\sum_{m=1}^p [(\alpha_m + \delta_m) - \alpha_m]^{\frac{1}{2}}} \quad (5.20)
 \end{aligned}$$

In an effort to compare the behaviour factors obtained with the PWM scheme and those obtained by Phase Angle Control scheme, there is the need to evaluate the output voltage with the PWM control scheme so as to have a comparison on the same basis.

Now, the average output voltage due to “p” number of pulses is:

$$\begin{aligned}
 V_{dc} &= \frac{1}{\pi} \left[\sum_{m=1}^p \int_{\alpha_m}^{\alpha_m + \delta_m} V_m \sin \omega t d(\omega t) \right] \\
 &= \frac{V_m}{\pi} \left[\sum_{m=1}^p \left. -\cos \omega t \right|_{\alpha_m}^{\alpha_m + \delta_m} \right] \\
 &= \frac{V_m}{\pi} \sum_{m=1}^p [\cos \alpha_m - \cos(\alpha_m + \delta_m)] \quad (5.21)
 \end{aligned}$$

If we let $\beta_m = (\alpha_m + \delta_m)$,

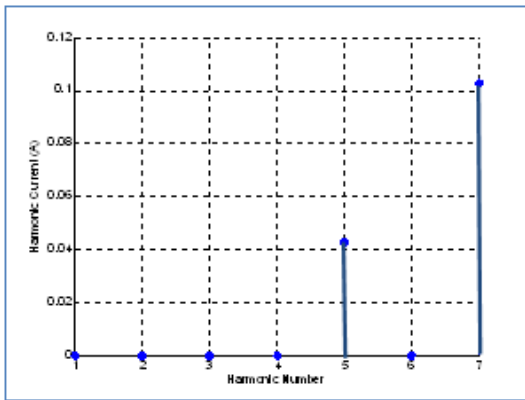
Then the maximum dc voltage is $\frac{2V_m}{\pi}$, which is obtained by varying “ α_m ” and “ β_m ” from 0 to π

The normalized dc output voltage V_n is;

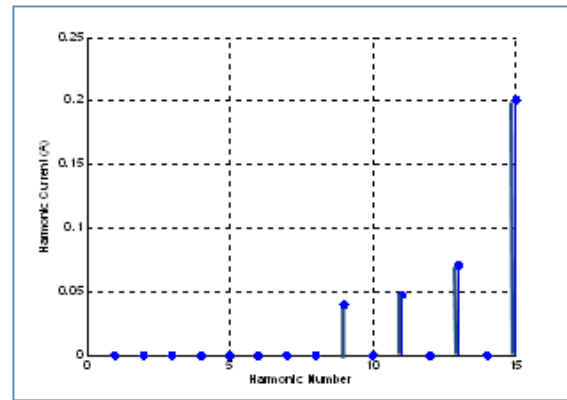
$$\begin{aligned}
 V_n &= \frac{V_{dc}}{V_{dcmax}} \\
 &= \frac{\frac{V_m}{\pi} \sum_{m=1}^p [\cos \alpha_m - \cos \beta_m]}{\frac{2V_m}{\pi}}
 \end{aligned}$$

$$= \frac{1}{2} \sum_{m=1}^p [\cos\alpha_m - \cos\beta_m] \quad (5.22)$$

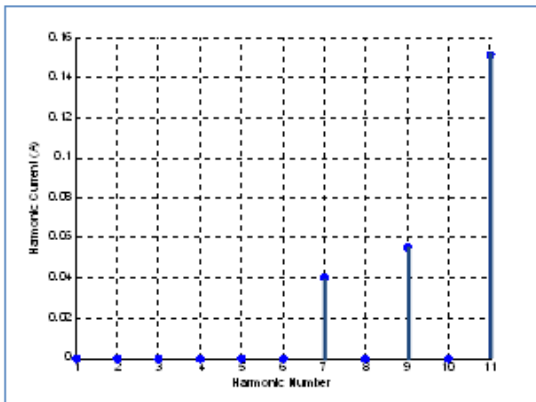
The equation of the rms value of the n^{th} harmonic current was plotted against harmonic numbers for various pulses “m”; for $m = 4, 6, 8, 10$. The results are displayed in Fig. 5.4(a-d). Also, results of computer simulations of the expressions for Power Factor, Harmonic Factor and the Displacement factor compared with those obtained for the Phase Angle Control are displayed in Figs. 5.5, 5.6 and 5.7 respectively.



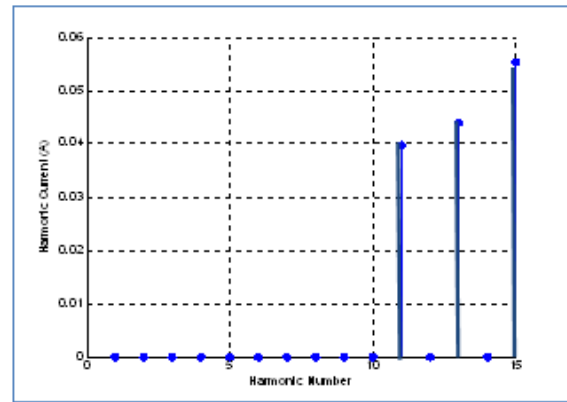
(a) Pulse Number “m” = 4



(c) Pulse Number “m” = 8



(b) Pulse Number “m” = 6



(d) Pulse Number “m” = 10

Fig. 5.4(a-d): Harmonic Currents for specified Harmonic numbers

Evidently, Fig. 5.4 reveals that with four pulses per half – cycle, the lowest-order harmonic is the fifth and with six pulses per half – cycle, the lowest harmonic is the seventh. In general, for an ‘m’ number of pulses per half cycle, the lowest – order harmonic is the ‘m+1’ harmonic. This is in agreement with Sen P.C (1991) and Rashid M.H (1993)

5.4 Comparison of Results with the Asymmetrical Bridge without PFC control

A comparison of the behaviour factors with the output voltage for the PAC and the PWM control of the asymmetric bridge shows the improvement of the factors when it is adopted. These factors are presented in Figs, 5.5, 5.6 and 5.7.

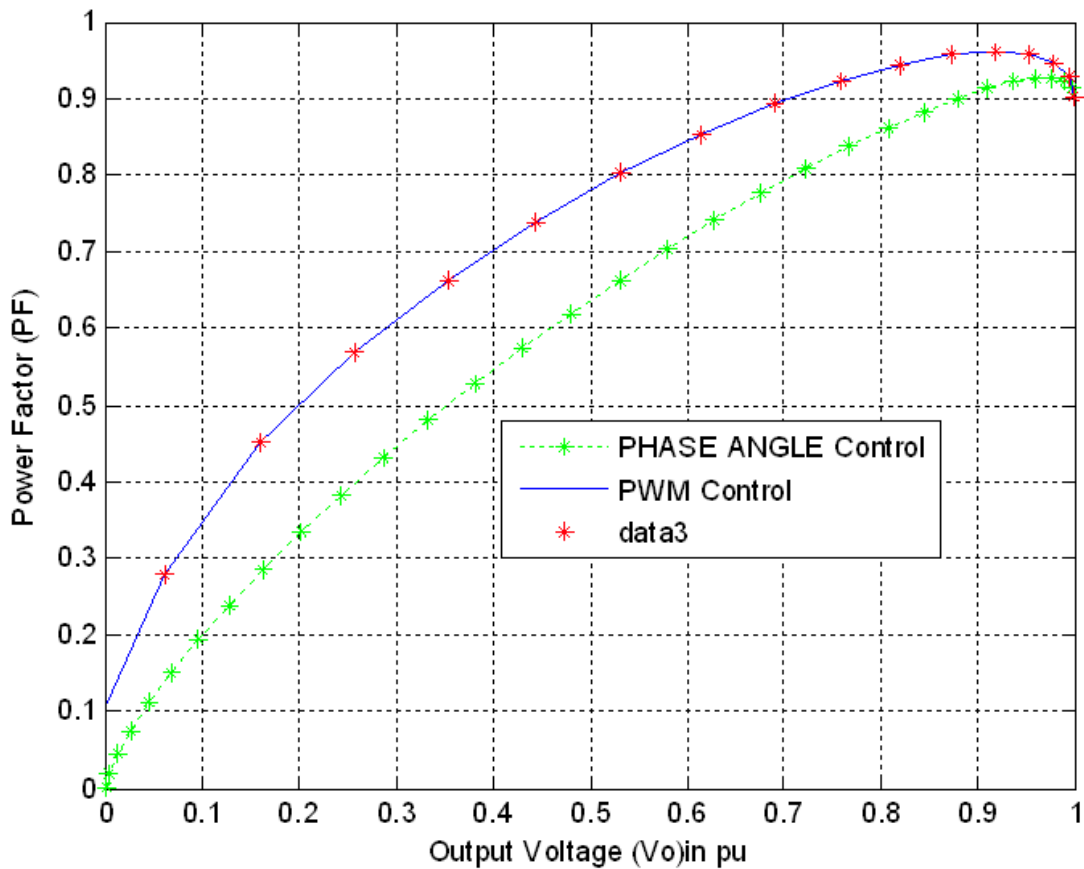


Fig. 5.5: Variation of Power Factor with Output Voltage of the Bridge

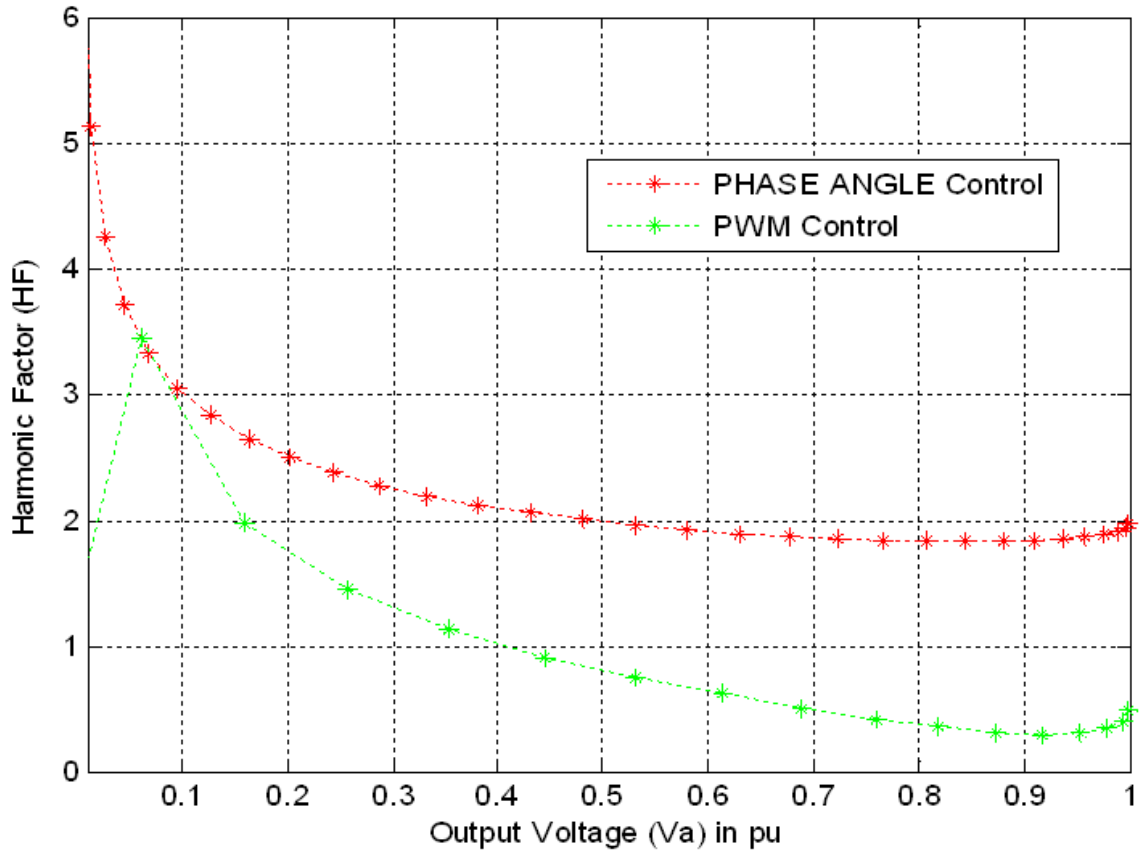


Fig.5.6: Variation of Harmonic Factor with Output Voltage of the Bridge

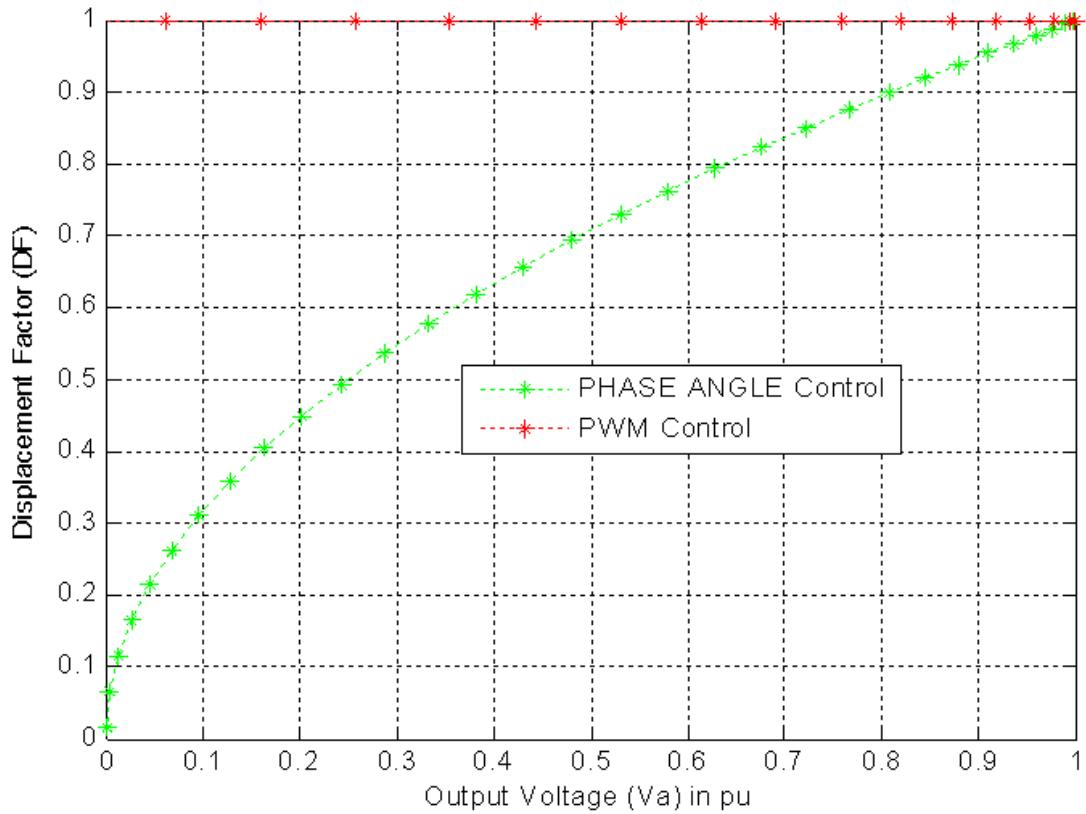


Fig. 5.7: Variation of Displacement Factor with Output Voltage of the Bridge

5.5 AC – DC Boost – Type Asymmetrical Converter for Power Factor Correction

5.5.1 The AC – DC Asymmetric Drive with Power Factor Correction Circuit

Power Factor correction of the Asymmetric Single – Phase Drive can be achieved by the PWM scheme by generating thyristor gate signals as described in section 2.35 and 5.1. The circuit implementation is presented in Fig. 5.8.

There are numerous variations of the firing circuits and the control logic circuits that can be used to control the firing of the thyristors. One of such ways has been discussed earlier. The principle of operation of the thyristor firing circuit designed and built for controlling the thyristors of the Asymmetrical Single – Phase Bridge shown in Fig.5.8 is hereby described.

The 50-Hz astable signal clocks the monostable through pin 2 known as the trigger input. The monostable triggers at one period of the astable signal fed into it. The monostable period of oscillation can be varied to adjust the pulse width. The output of the monostable is logically added with another 20KHz astable signal which is used in the modulation. The output of the AND gate (acting as a Comparator) is a modulated pulse signal with a positive going transition. The period before the first rising edge defines the firing angle of the thyristors. A path of this signal is fed through an inverter to invert the signal. This produces a complimentary signal that is used to fire the other thyristor. The output of the inverted signal is processed through a high pass filter to filter off signals below 50Hz thus turning the signal to leading spikes which go to the pulse transformer and then to a clipping diode to clip all the negative signals. The signals from the pulse transformers are complimentary and are used to fire the gate of the thyristors. The test rig made up of the controlled DC motor with a load DC generator and the Asymmetrical bridge system are shown in Fig.5.12.

5.5.2 AC – DC Boost - Type Asymmetrical Converter for PFC

The conventional active boost arrangement of an AC – DC Single – Phase Converter feeding a DC load is shown in Fig.5.9. Like every other boost regulator configurations used in power factor correction except the fly back converter (Dubey *et al* 1986), it share a common input-output power line, hence the output is not isolated and is electrically linked to the ac line supply. The controls for this system are for;

- I. The active boost switch “S” of the PWM scheme and
- II. The thyristors of the bridge

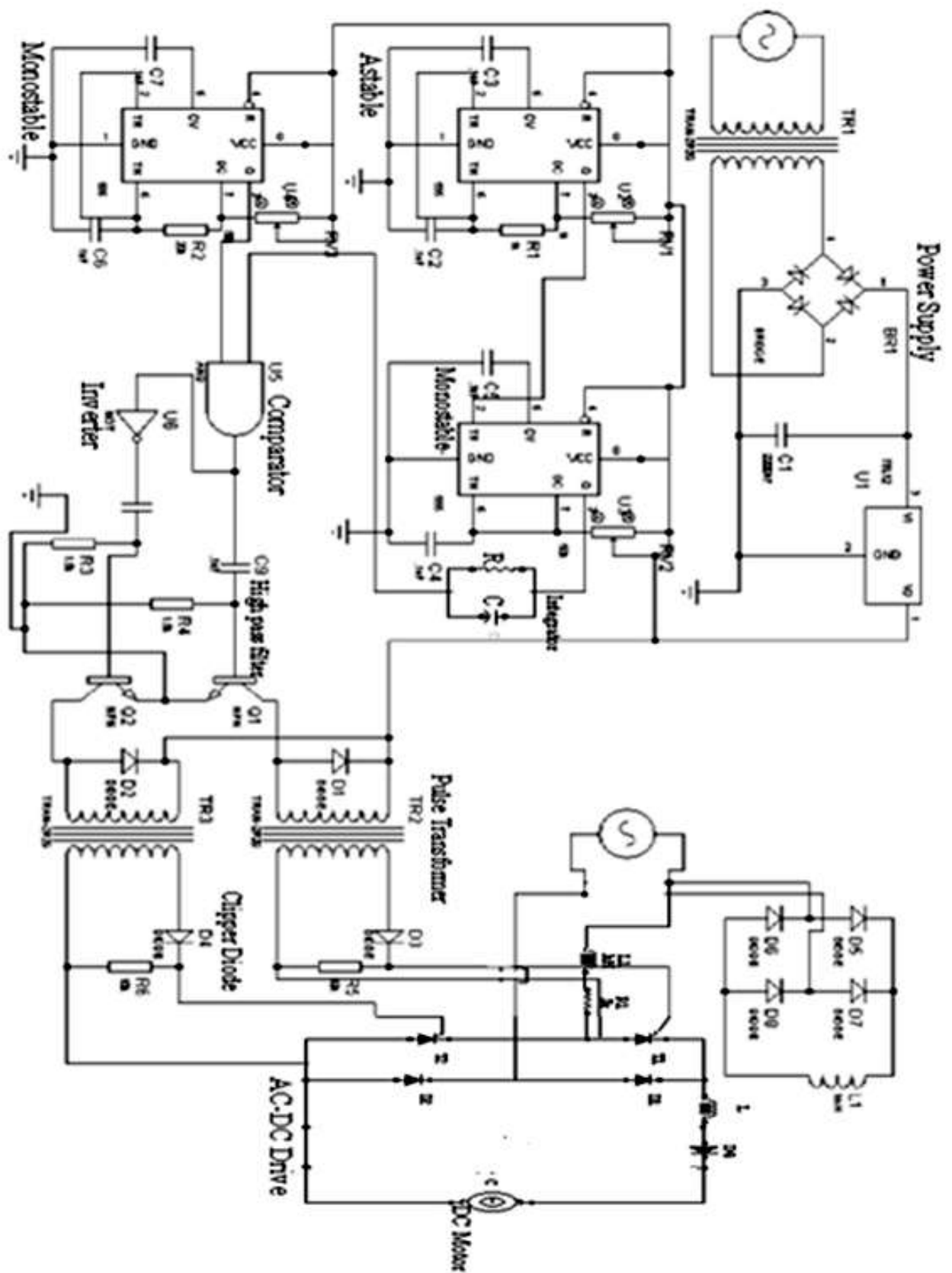


Fig.5.8: Gate Firing Circuit Implementation of the PWM Controlled Asymmetric Single – Phase Drive.

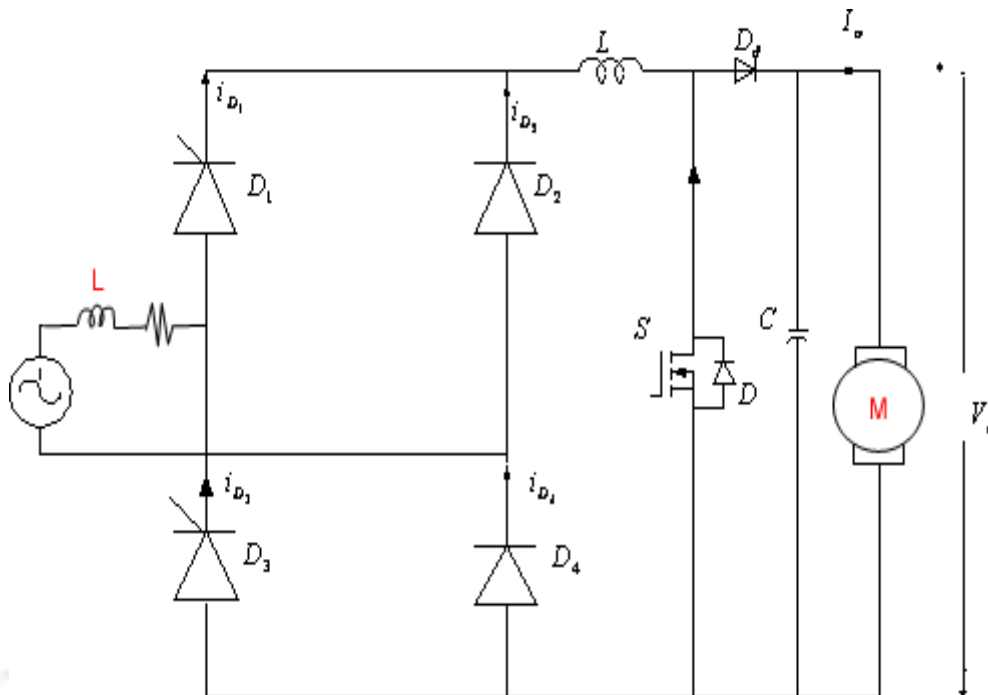


Fig. 5.9: Asymmetrical AC –DC Boost- type Converter with input power factor correction

5.5.3 Control of the Active Boost Switch of the PWM

The schematic circuit layout for the control of the boost switch in the PWM Controlled Asymmetric Single – Phase AC – DC Boost Converter is presented in Fig.5.10. The current sensor is in series with the source of the switching device which could be a power MOSFET or a THYRISTOR. A MOSFET is preferred because of it is a fast switching device. Transistor current is initiated by the PWM clock and terminates when it reaches a peak level proportional to the instantaneous value of the input voltage. The output voltage is sensed with a voltage divider string and compared to a reference voltage in the error amplifier. The triangular wave is fed to one input of the multiplier and the voltage error amplifier output is fed to the other input so that the multiplier output is again triangular scaled in amplitude by the output of the voltage error amplifier.(Pandey.et.al 2006 and Rossetto L et.al 2004). The current in the MOSFET is compared with the half-sine-wave reference signal and when it equals this signal, the power MOSFET is turned off. The MOSFET remains off until it is turned on again by the fixed – frequency clock.

The thyristors of the bridge are controlled in the same way as described in section 5.5.1

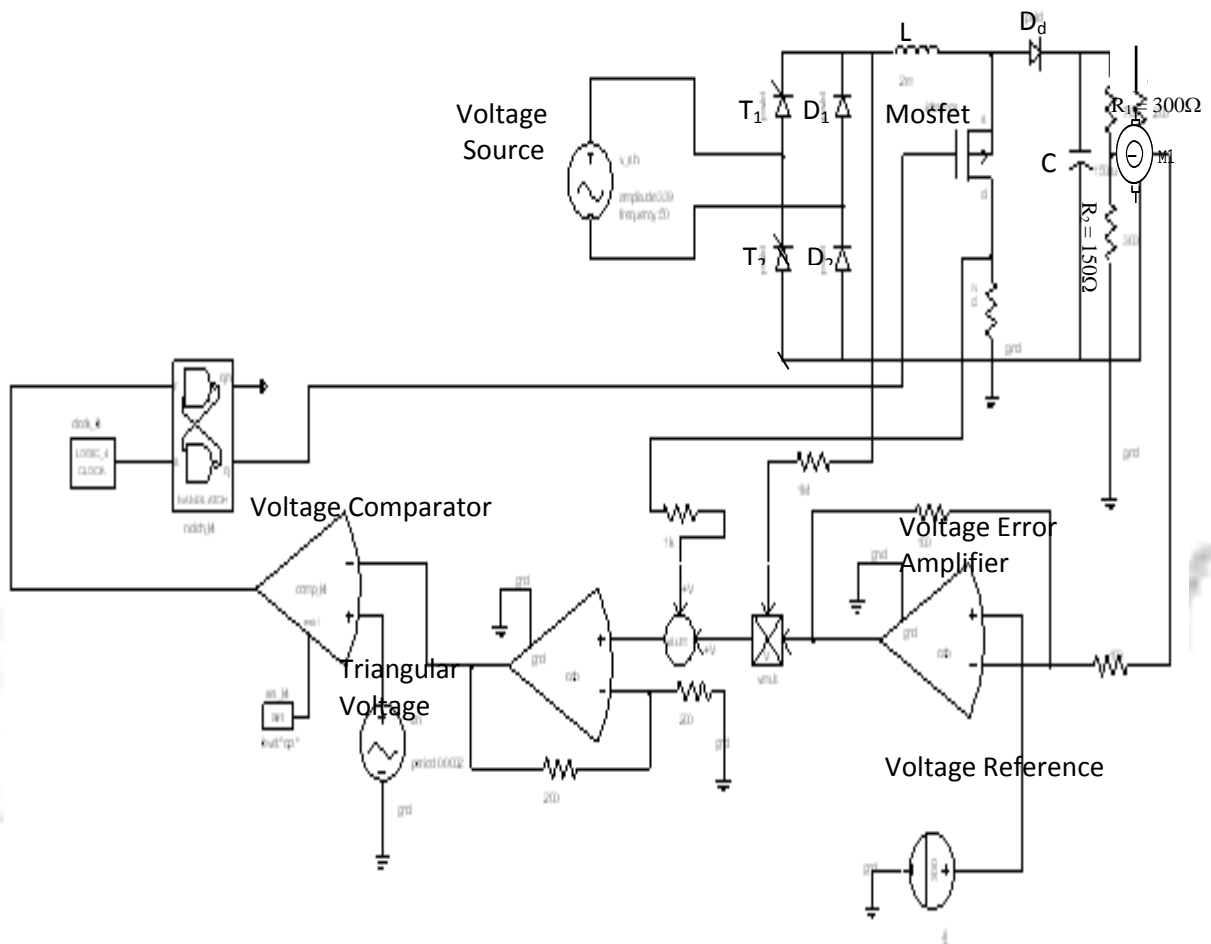


Fig.5.10: Schematic circuit layout for the PWM Controlled Asymmetric Single – Phase Bridge (Boost Switch Control)

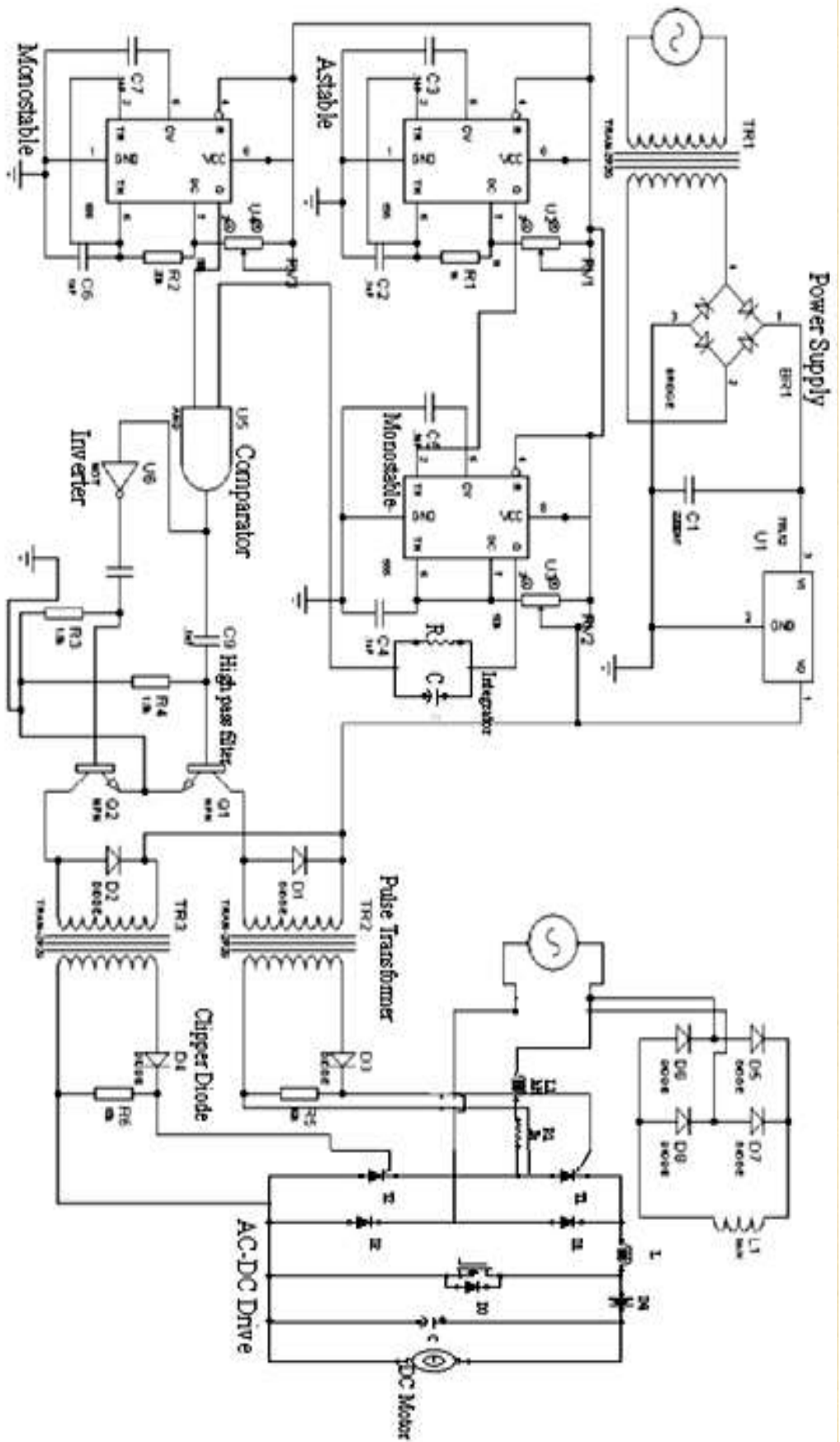


Fig.5.11 : Gate Firing Circuit Implementation of the PWM Controlled Asymmetric Single – Phase Drive (Thyristor Control)

circuits of Fig.5.10 and Fig 5.11 was designed and constructed in the laboratory for experimentation.

The AC – DC Asymmetrical Drive with PWM controls for PFC gives the same results as the AC - DC Boost Type Asymmetrical converter except that the latter has a greater efficiency as a result of the higher switching capacity of the Mosfet compared to the Thyristors. PWM signals, the waveforms of the input current, voltage and the harmonic spectrum are presented in the next section.



Fig.5.12: Test rig with controlled DC machines and the Asymmetrical Bridge with PWM Controllers

5.6 Waveforms of the PWM control Signals of the Drive.

Figures 5.13 and 5.14 shows the modulation of a triangular wave at a frequency of 10KHz and 8KHz respectively with a DC signal in a comparator to generate output pulses. The width of the pulses is dependent on the level of the DC signal and the modulating frequency of the triangular wave. Figs.5.15 – 5.18 show the output pulses of the comparator for different modulating frequencies. These pulses are further processed to obtain the complementary gate signals required to turn on the thyristors of the drive. These signals are shown in Figs. 5.19 and 5.20 for modulating frequencies of 10KHz and 8KHz. Correspondingly, waveforms of input current and voltage are displayed in Figs.5.21 and 5.22. A near unity power factor was obtained in both cases. The level of harmonics obtained from laboratory measurements is presented in Fig.5.23

(A) Waveforms of the Modulation of the Triangular wave signals with a DC signal



Fig.5.13: A Triangular wave signal at 10 KHz with a DC signal

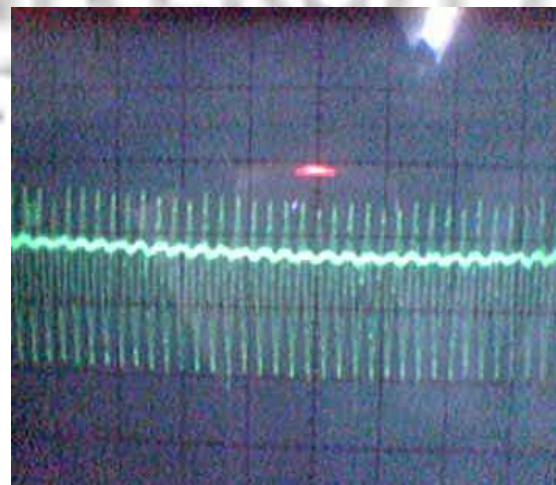


Fig.5.14: A Triangular wave signal at 8 KHz with a DC signal

(B) Output signals of the Comparator

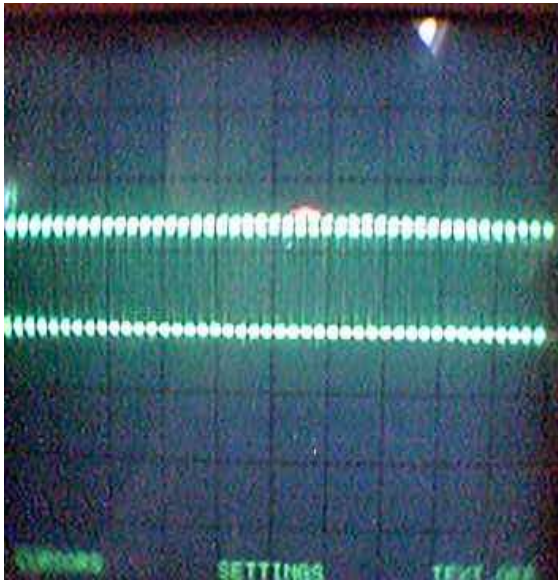


Fig.5.15: Comparator signal output modulated at 10 KHz



Fig.5.16: Comparator signal output modulated at 8KHz

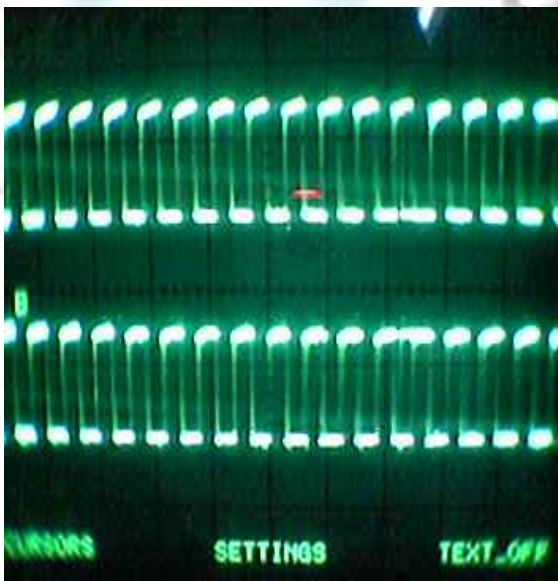


Fig.5.17: Comparator signal output modulated at 6KHz

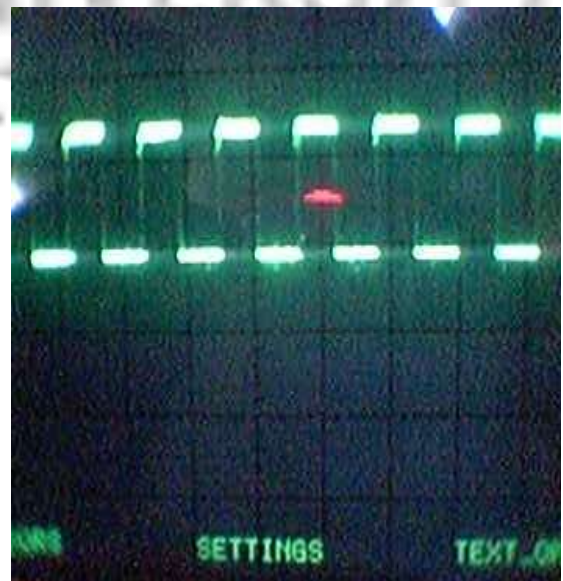


Fig.5.18: Comparator signal output modulated at 5KHz

(C) Thyristors gate signals

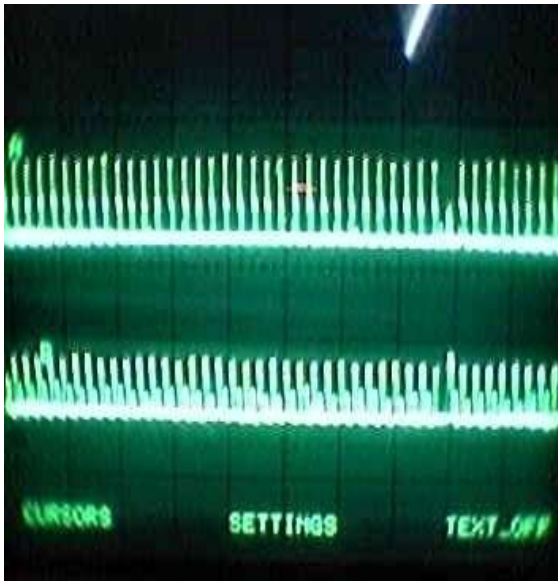


Fig.5.19: Thyristors complimentary gate signals at 10kHz

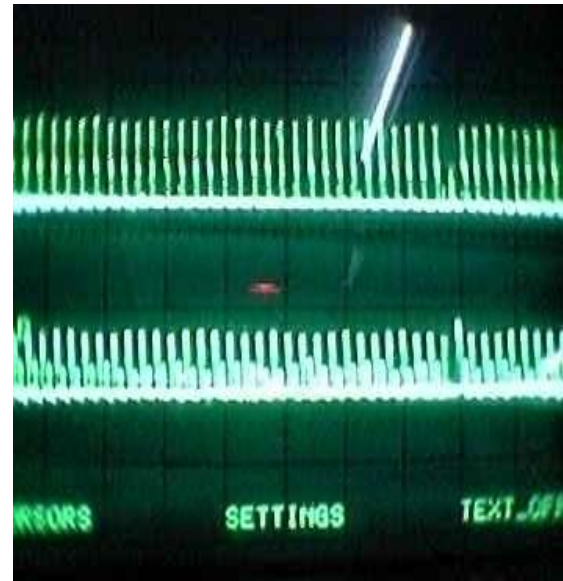


Fig.5.20: Thyristors complimentary gate signals at 8kHz

(D) Waveforms of Input Voltage and Current



Fig.5.21: Input Current and Voltage waveforms (PF = 0.9995) at 10KHz

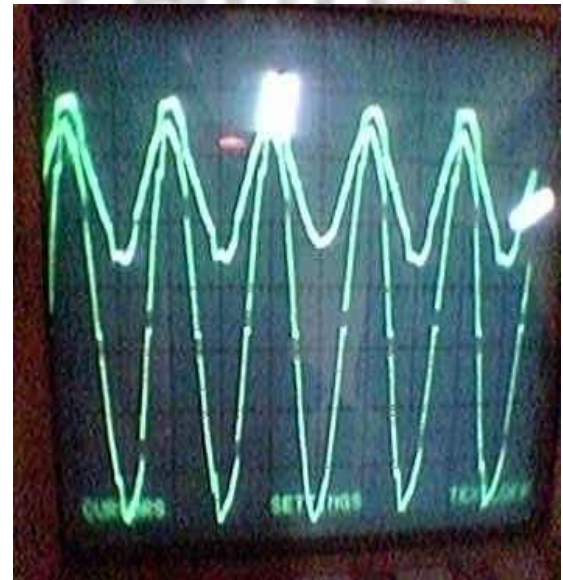


Fig.5.22: Input Current and Voltage waveforms (PF = 0.9993) at 8KHz

Input Current and Voltages (Upper Curve is CURRENT & lower Curve is VOLTAGE)

(E)

Harmonics

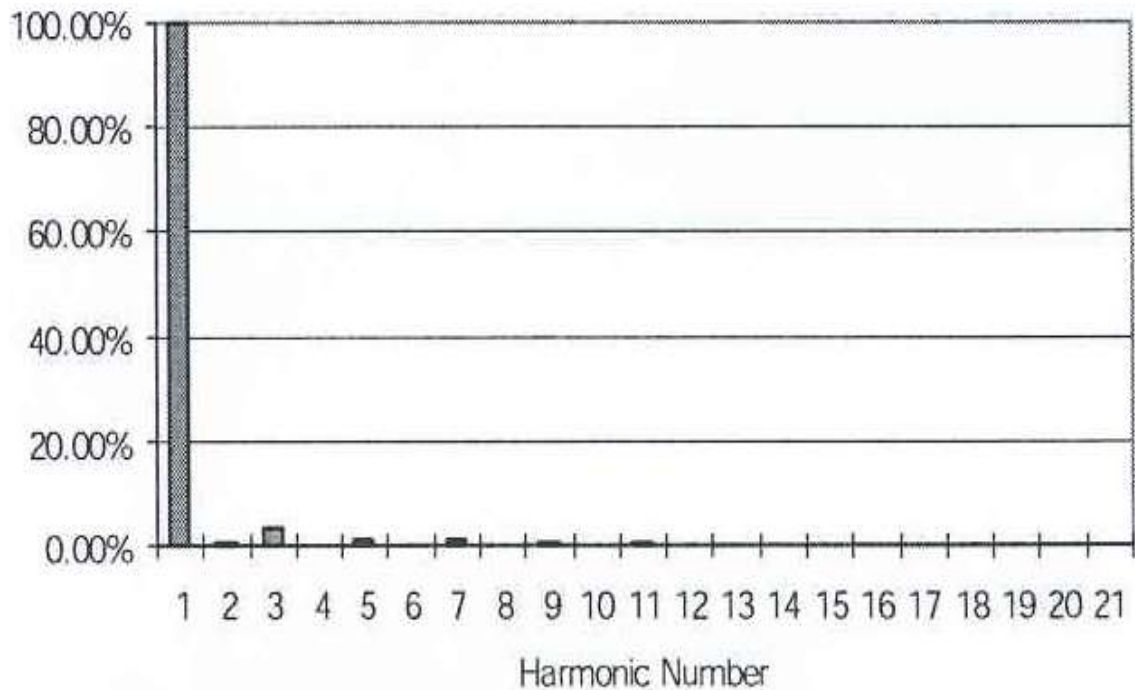


Fig. 5.23: Harmonics of the PWM Controlled Asymmetric Single – Phase Drive

5.7 A Simplified PWM AC – DC Asymmetrical Bridge with PFC control

The active boost PFC circuit for the Single – Phase drives of Fig.5.9 and the asymmetrical Single – Phase Bridge of Fig.5.8 are both efficient in power factor control. However, the conventional active boost PFC has the following limitations according to Martinez R, and Enjeti P.N. (1996):

- The required switching frequency of the boost switch is usually high. This in turn increases the switching losses and lowers the efficiency.
- Special design of the dc – side inductor is necessary to carry dc current as well as high frequency ripple current.
- The diode D_d in the series path of power flow contributes to voltage losses and reduced reliability.

At any given point, three semi – conductor devices exist in the power flow path

An alternative circuit that gives similar results but overcomes the limitations of the conventional PWM (Sanzaeihi et.al 2006) circuits is proposed in Fig.5.24. It has a reduced harmonic current content for switching power converters and motor drive systems fed from a modified asymmetrical single – Phase Bridge acting as a boost converter. Analysis and

design approach of the proposed circuit along with experimental results are presented in the next section.

5.7.1 Description of the proposed circuit

The laboratory model presented in Fig.5.9 though effective for PFC applications uses asymmetrical bridge to rectify the AC input voltage to DC, which is then followed by the boost section. This approach is good for a low to medium power range. As the power level increases, the diodes of the drive begin to become an important consideration to deal with the problem of heat dissipation in a limited surface area from the efficiency point of view. The proposed Bridgeless AC – DC asymmetric single – phase drive with PWM power factor correction (Lu Bing et.al 2005, Laszlo H et.al 2007 and P kong et.al (2006) scheme is presented in Fig. 5.24.

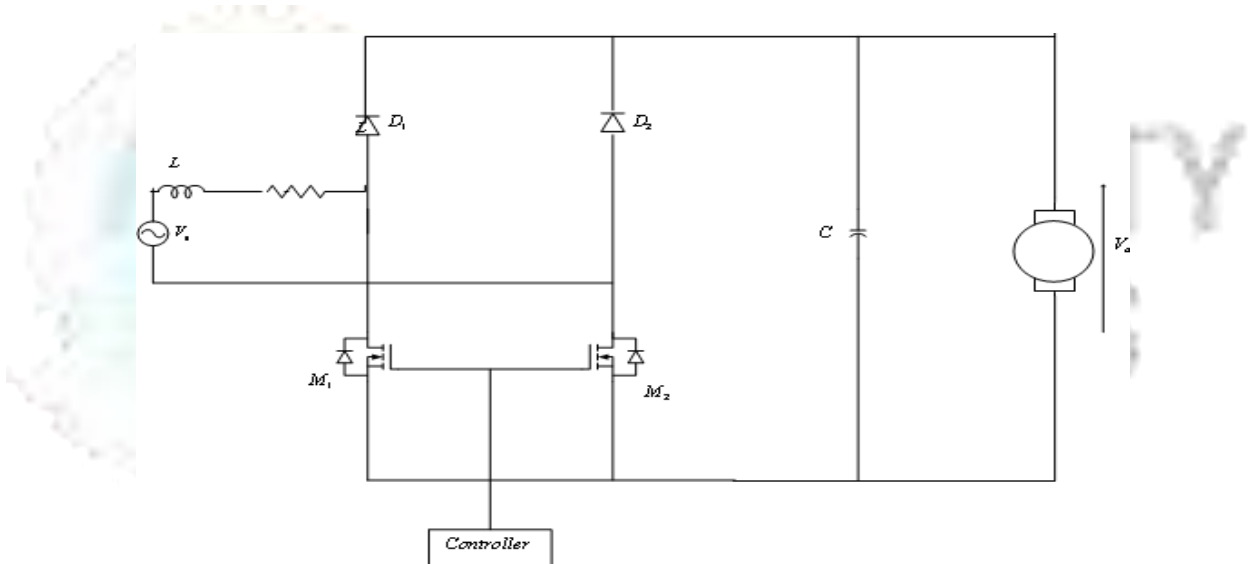


Fig. 5.24: Bridgeless AC – DC PFC Configuration

The bridgeless configuration applied in this research, avoids the need for the conventional input bridge, and yet maintains the classic boost arrangement. This is easily done by replacing the thyristors of the asymmetrical single - phase bridge converter in fig.5.9 by a power MOSFET with a diode connected between the drain and the source of the MOS switch as shown in Fig.5.24. A thyristor could be used as the switching device too.

In this approach, the series diode D_d in the conventional boost circuitry of Fig.5.9 has been eliminated. Also, the dc – side inductor is no longer necessary and instead an ac – side inductor is required.

The advantages of the proposed approach are (Eric Ho Y.K et.al 2000):

- Improved characteristics in terms of input power factor and sinusoidal shape of the input current.
- Only two semi-conductor device drops exist in the power flow path at any given instant.
- The boost inductor 'L' on the ac side contributes to the reduction in Electromagnetic (EMI) interference.
- The gates of the MOS switches are referenced to the same ground.

5.7.2 Operation of the Bridgeless Converter

The analysis shall be discussed in two ways according to Martinez R and Enjeti P.N. (1996). To understand the operation, the proposed circuit of figure 5.24 can be viewed as two sections: section one operates as the boost stage (positive half cycle) and the second operates as the return path for AC signal during the negative half cycle. (Martinez R. et.al 1996 and Laszlo H et.al 2007)

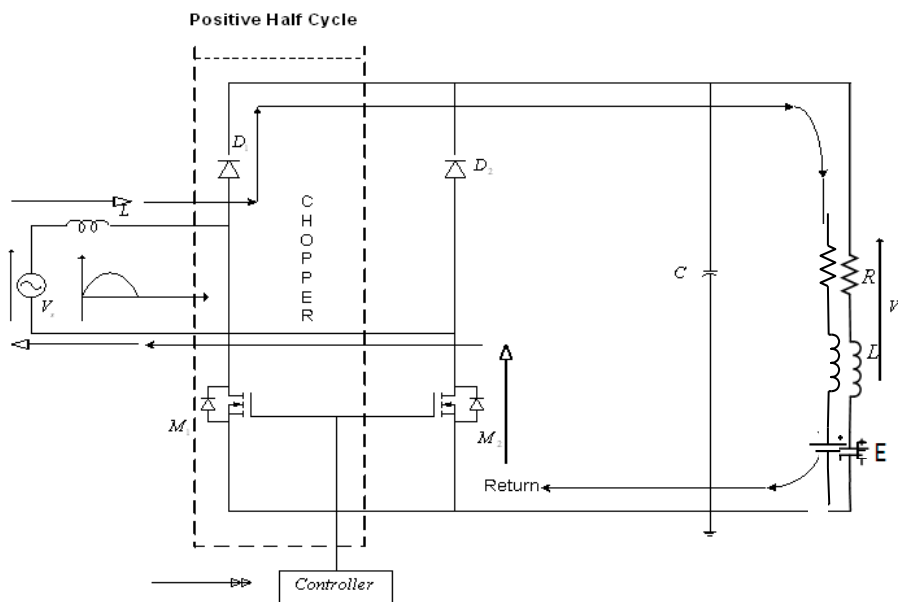


Fig.5.25: Current Flow path for the Positive half cycle.

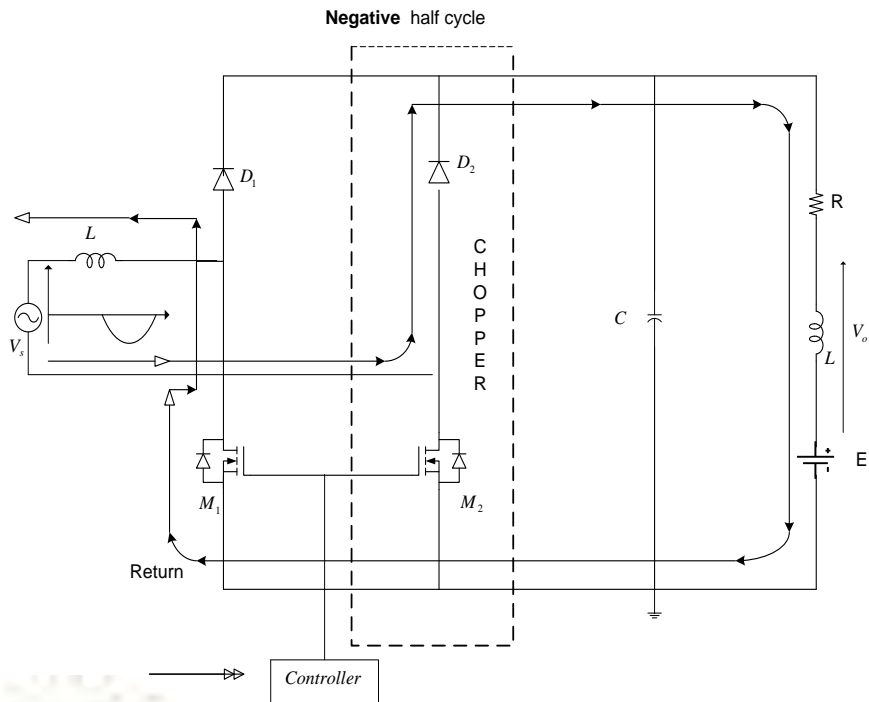


Fig.5.26: Current Flow path for the negative half cycle.

(a) Positive “Half Cycle”.

When the AC input goes positive, the gate of MOSFET M_1 is driven high and current flows through the input, and through the inductor, storing energy. When M_1 turns off, energy in the inductor is released and current flows through D_1 , through the load and returns through the body diode of M_2 back to the input mains as shown in Fig.5.25.

During the off – time, the current flows through the inductor “L” (during this time, the inductor discharges its energy) into the boost diode D_1 and close the circuit through the load.

(b) Negative “Half Cycle”

During the negative half cycle, circuit operation is mirrored as the positive half cycle as shown in Fig.5.26. M_2 turns ON, current flows through the inductor storing energy. When M_2 turns off, energy is released as current flows through D_2 through the load and back to the mains through the body diode of M_1 .

It should be noted that the two power MOSFETs are driven synchronously. It does not matter whether the sections are performing as an active boost or as a path for the current to return. In either case, there is the benefit of lower power dissipation when current flows through the power MOSFETs during the return phase.

Figure 5.28: shows the Circuit Layout for the simultaneous gate firing of the MOSFETs (or Thyristors) of the proposed design

Another way to understand the proposed circuit is to view its modes of operation as illustrated in Fig. 5.27.

Mode 1 in Fig.5.27 (a) occurs when the input ac voltage is positive and the switches are open (off). Current flows through diode D_1 through the capacitor and load and back through the anti-parallel diode of M_2 . Fig.5.27 (b) shows Mode 2, which occurs when the input ac voltage is positive and the switches are closed (on). Input Current flows through switch M_1 and back through the anti – parallel diode of M_2 , thus providing a path for the input current. At the same time, the bulk capacitor discharges and supplies current to the load. Mode 3 in Fig.5.27(c) occurs when the input ac voltage is negative and the switches are open (off). Current flows through diode D_2 , through the capacitor and load and back through the anti-parallel diode of M_1 . Fig.5.27 (d) shows Mode 4, which occurs when the input ac is negative and the switches are closed (on). Input currents flows through switch M_2 and back through the anti – parallel diode of M_1 , thus providing a path for the input current. At the same time, the dc capacitor discharges and supplies current to the load.

5.7.3 Design Considerations of the proposed AC – DC Converter.

Let's suppose that the simplified converter Fig.5.24 is a 2.0kw load, from a 230V_{rms}, 50Hz Single – phase system. The output has a maximum of 400V dc with a switching frequency of 10KHz and it is to be operated in the Continuous Inductor Conduction Mode (CICM).

It is assumed that switching losses and device power loss are negligible.

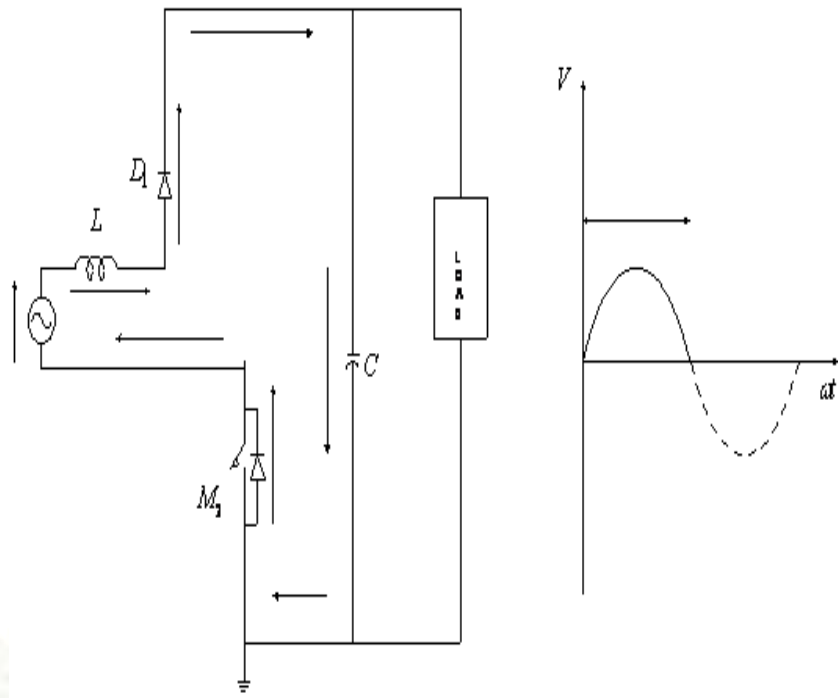
Parameters 'L' and 'C' are determined with the specification that the output ripple voltage shall be within the limits of 5% of the output voltage. The defining equations are derived in Robert et.al (2000).

Since the switching losses are assumed to be zero,

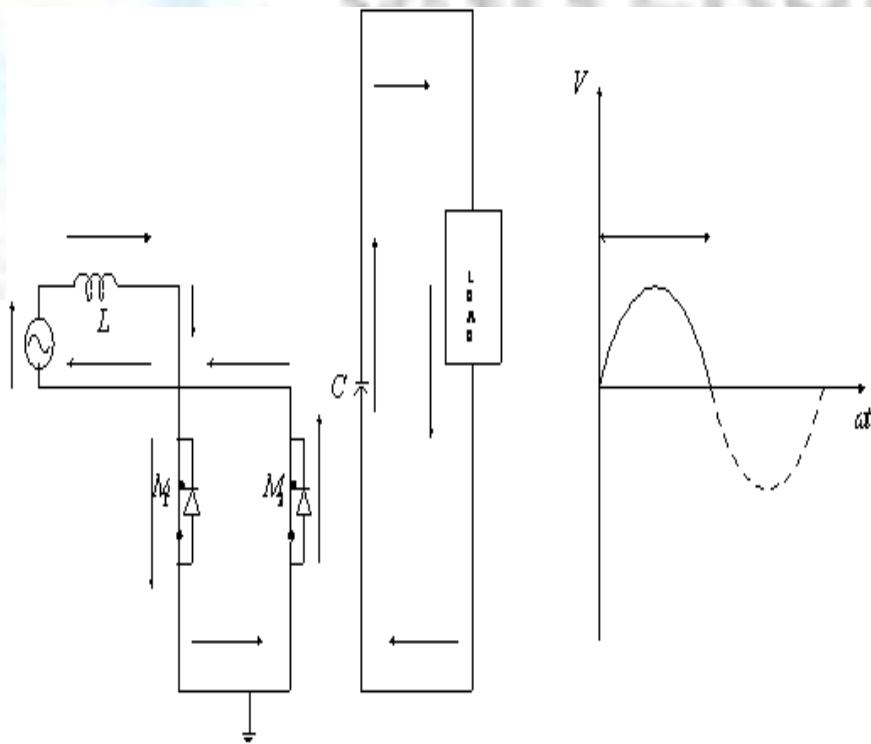
$$P_{in} = P_{out}$$

$$2.0KW = V_{in} I_{in}$$

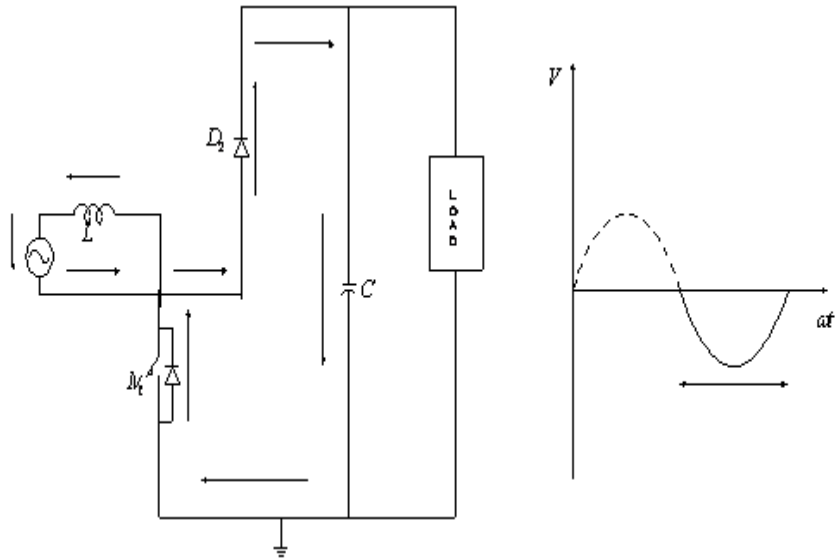
$$I_{in} = \frac{2000}{230} = 8.695A$$



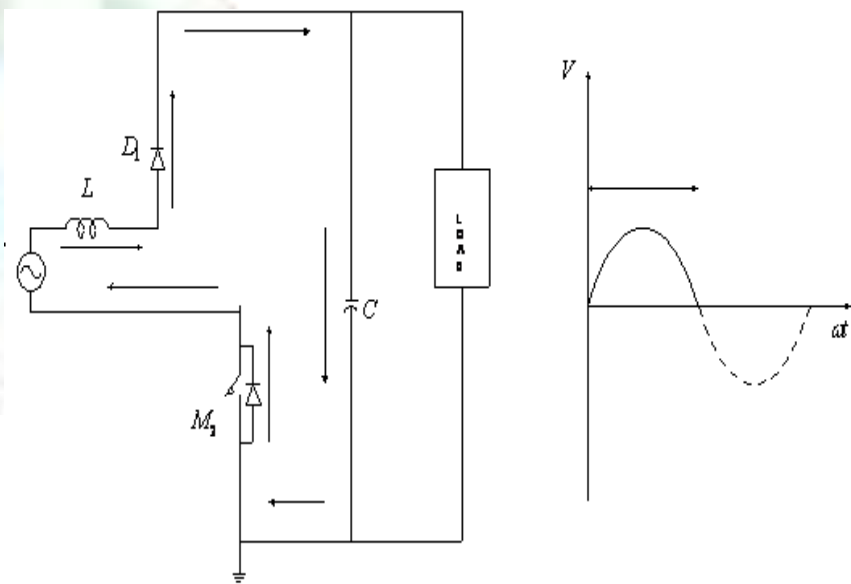
(a)



(b)



(c)



(d)

Fig.5.27: Operation of the Bridgeless converter

- (a) Mode 1
- (b) Mode 2
- (c) Mode 3
- (d) Mode 4

And,

$$I_{out} = I_o = \frac{2000}{400} = 5A$$

Ripple Voltage is assumed to be 5% of output Voltage,

Therefore,

$$\Delta V_c = \frac{5}{100} \times V_o = \frac{5}{100} \times 400 = 20V$$

Also,

$$\Delta V_c = \frac{I_o D}{f_s C}$$

D is the duty cycle; $D = t_{ON}/T$

Where,

$$f_s = 10KHz$$

But for a boost converter,

$$V_o = \frac{V_s}{1-D}$$

Hence,

$$\begin{aligned} D &= 1 - \frac{V_s}{V_o} = 1 - \frac{230}{400} \\ &= 1 - 0.575 \\ &= 0.425 \end{aligned}$$

(The duty circle 'D' is not constant and depends on the supply voltage V_s and the level of output voltage V_o to be achieved)

And,

$$\begin{aligned} C &= \frac{I_o D}{f_s \Delta V} = \frac{5 \times 0.425}{10000 \times 20} \\ &= 10 \times 10^{-6} \\ &= 10\mu F \end{aligned}$$

But a value of $C = 18\mu F$ was chosen as the output capacitor in the experimental work. This is to ensure that the dc output has less ripple content.

It is equally assumed that a 10% value of input current ripple is allowed,

Therefore,

$$\Delta I = \Delta I_L = \frac{10}{100} \times 8.695$$

$$= 0.87A$$

But,

$$\Delta I = \frac{V_s D}{f_s L}$$

Hence,

$$\begin{aligned} L &= \frac{V_s D}{f_s \Delta I} = \frac{230 \times 0.425}{10000 \times 0.8695} \\ &= 112.35 \times 10^{-5} \\ &= 11.23mH \end{aligned}$$

An inductor value of 15mH was used. This is to ensure that the design operates in a CICM. The diode and MOSFET were rated higher than the combined dc voltage and the anticipated ripple value (Sen 1991). The proposed circuit of the new design that was constructed in the laboratory is presented in Fig.5.28. The voltage feed forward PWM switching technique has been adopted.

The feed forward approach is used to generate the gate signals for triggering the Mosfet where the output voltage is (V_o). The error amplifier compares the sampled output voltage (V_{sp}) with a fixed reference voltage, V_{ref} , and generates an error voltage, V_e given by Sen (1991).

$$V_e = V_{ref} - \frac{R_3}{R_4} \left[V_o \left(\frac{R_2}{R_1 + R_2} \right) - V_{ref} \right] \quad (5.23)$$

This error voltage is then fed to the non – inverting input of an open – loop comparator that compares the error voltage with a sawtooth signal at its inverting input. The switching frequency of the sawtooth generator determines the frequency of the converter. The output of the comparator is a PWM SIGNAL. It is high only when the error voltage is higher than the sawtooth signal. This PWM signal is then fed to the base drive circuitry that drives the gates of the two MOSFETS of the proposed converter. The proposed PFC circuit achieved the same Power Factor.

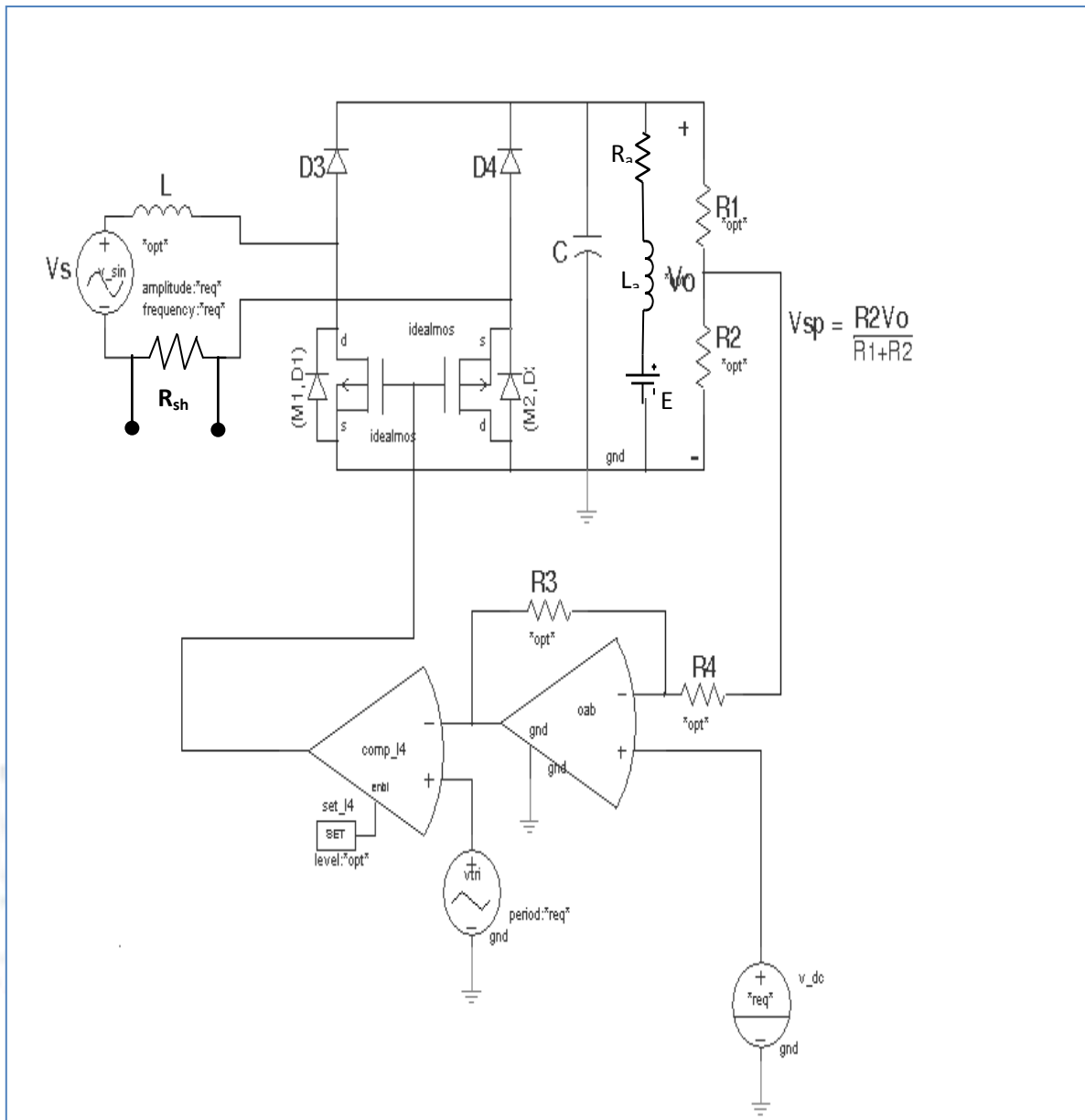


Fig.5.28: Triggering Circuit of the Bridgeless Converter (Voltage feedforward approach) of the proposed AC – DC Converter: Active Boost Control.

CHAPTER SIX

RESULTS AND DISCUSSION

6.1 Waveforms of the Input Voltage, Current and harmonics with PWM PFC

The input current and voltage of the proposed Bridgeless single – phase AC – DC PFC Asymmetric Bridge with PWM Controls modulated at 10KHz and 8KHz are shown in Figs. 6.1 and 6.2. The current and voltage waveforms are almost completely in phase thus giving a near unity power factor. It conforms with the results obtained by Martinez R. et.al (1996) and Lui Bang et.al (2005). Also, all lower order harmonics have been completely reduced as shown in Fig.6.3.

(A) Waveforms of Input Voltage and Current

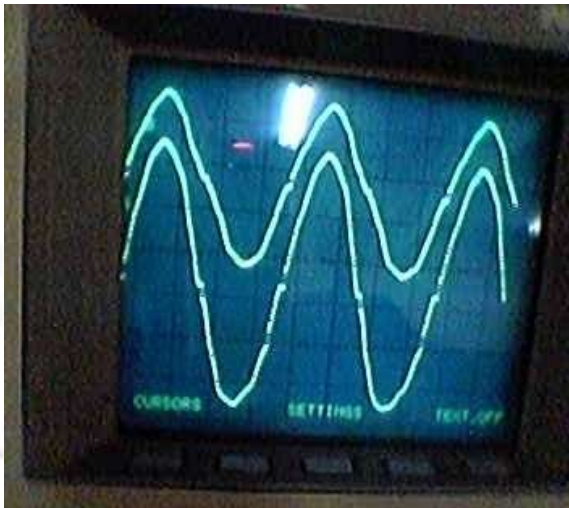


Fig.6.1: Input Current and Voltage waveforms (PF = 0.9998) at 10 KHz

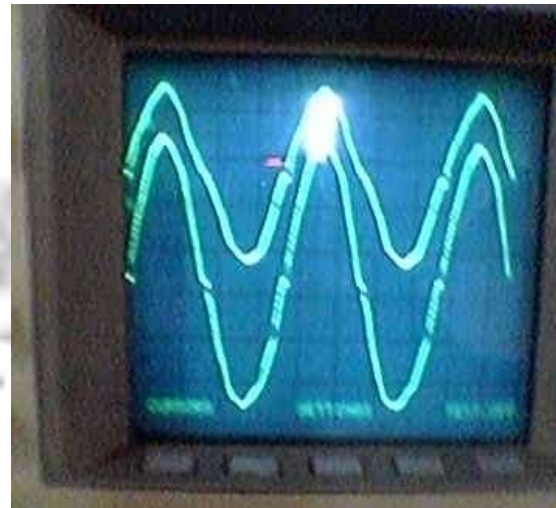


Fig.6.2: Input Current and Voltage waveforms (PF = 0.9996) at 8KHz

Input Current and Voltages: (Upper Curve is CURRENT & lower Curve is VOLTAGE)

(B) Harmonics

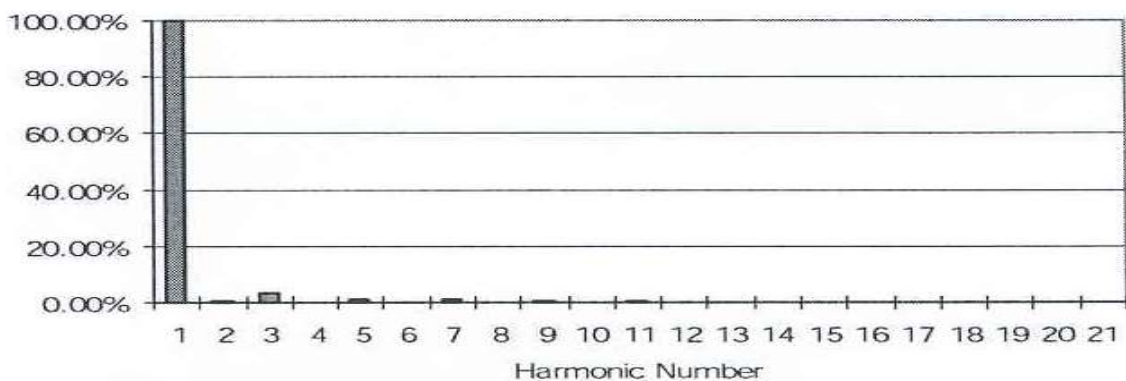


Fig.6.3: Laboratory Results of the PWM Controlled Asymmetric Single – Phase Drive

6.1.1 Comparative Results of the PWM and PAC controls

A comparison of the input current waveforms and harmonics with phase angle (PAC) and PWM controls is presented in Figs.6.4 – 6.5 and Figs.6.6 – 6.7 respectively. The input current waveforms for the PAC shown in Fig.6.4 is distorted due to the presence of harmonics thus, giving a poor power factor whereas, with the PWM, the input current waveform is sinusoidal and in phase with the input voltage leading to an increased power factor. Also, lower order harmonics are present with phase angle controls as shown in Fig.6.6 compared with Fig.6.7 where lower order harmonics are completely eliminated.

(a) Input Current and Voltage Waveforms

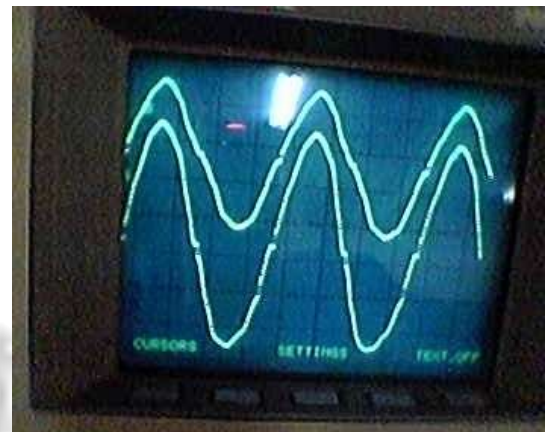
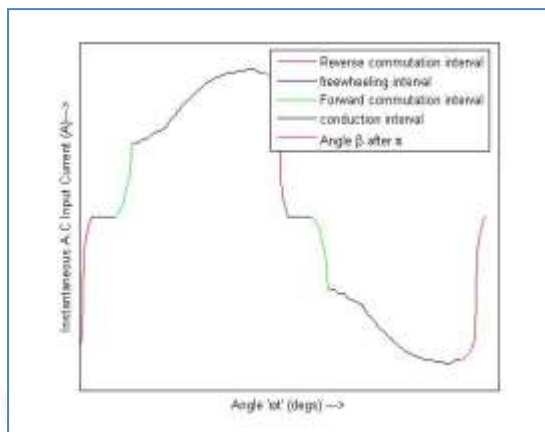


Fig.6.4: Input current waveform of the asymmetrical single phase bridge feeding a DC motor load without PFC control (PF = 0.628)

Fig.6.5: Input current waveform of the asymmetrical single phase bridge feeding a DC motor load with PFC control (PF = 0.9998)

(b) Harmonics

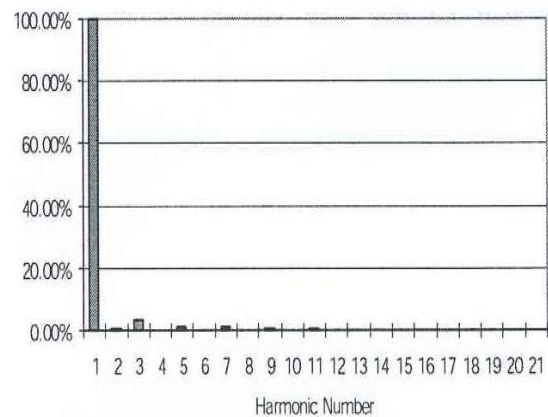
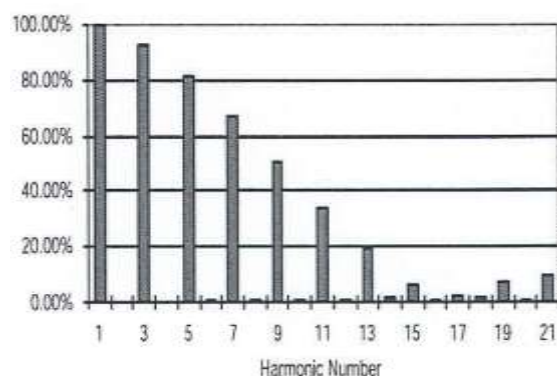


Fig.6.6: Input Harmonic Current for the asymmetrical single phase bridge feeding a DC motor load without PFC control

Fig.6.7: Input Harmonic Current for the asymmetrical single phase bridge feeding a DC motor load with PWM PFC control

6.2 Discussion of Results

The non-linearities that influence the parameters of a D.C motor were modeled at the operating points of the machine to ensure the accuracy of the interval equations. Other non-linearities introduced by the switching action of the semi-conductor devices of the drive are overcome by the piece-wise linear method of analysis. Explicit expressions for current at each interval of operation lead to the piecing together of the non-sinusoidal motor input current and the complete characterisation of the asymmetrical single-phase bridge by solution of transcendental equations. The waveforms of the supply currents of the drive are shown in Figs.3.8 (a-f). It clearly shows that the non-sinusoidal waveform of input current gets more distorted as the firing angle of the thyristors of the drive increases. The behaviour factors of the drive (Displacement factor, harmonic factor, and Power factor) were developed to complete the performance characteristics of the drive. The anticipated increase in power factor deterioration with increased industrialization was further demonstrated from laboratory measurements on a supply system feeding multiple drives and the results displayed in Figs.3.13, 3.14 and 3.15 which clearly indicate a decrease in input power factor as the number of such drives connected to the same source increases. Figure 3.16 shows the variation of Power Factor with numbers of drives. The complete mathematical model of the input current is also applied to obtain the Fourier Spectrum of the motor input Current by the Fourier Integral method. Figures 3.9 and 3.10 reveal that high lower order harmonics are present in input current which can constitute a menace to nearby electronic circuits. They also contribute to the poor input power factor of the bridge supply line. Fig.3.11 suggest that a very high harmonic content is present in the input supply current when the drive is operated between 120 to 160 degrees at a frequency range of 150 – 750Hz. The implication of this is that communication equipment and circuits operating within this range of frequencies will be adversely affected at such significant harmonic levels. Also, signalling in traction systems will be affected too.

Various techniques for poor power factor correction were investigated and the PWM method identified for detailed further study. The PWM control scheme was analysed to obtain expressions for the behaviour factors of the drive. The scheme was then designed and constructed to investigate the drive operation. In Figs. 5.6 – 5.8, a comparison of the behaviour factors of the input current for the Phase Angle Control (PAC) and the Pulse – Width Modulation Control (PWM) of the Asymmetrical Bridge showed improved power factor. Measurements of

the AC input voltage, current, power factor and also the input harmonic current spectrum (Fig.5.21-5.23) were taken. The waveforms of voltage and current when compared are almost in phase implying an achievement of a near unity power factor. Also, the waveform of the input current in Fig.6.4 and Fig.6.5 when compared shows a sinusoidal input current with PWM control. Clearly, Fig.6.4 shows the waveforms of input voltages and current with PWM control technique to be virtually in phase which is in agreement with the results of Martinez R. et.al (1996) and Lui Bang et.al (2005).

The PWM scheme also can be used to eliminate some lower order harmonics by choice of the number of pulses per half cycle. For four pulses, the lowest order harmonic is the 5th as seen in Fig.5.5 (a) and for eight pulses; the lowest order harmonic is the 9th harmonic as shown in Fig.5.5(c). However, the number of pulses per half – cycle must not be too large (Rashid 1993) as it increases the ripple frequency of the motor current. If it is, the switching loss of the thyristor increases and special costly thyristors having low turn – off time are required. Six pulses per half – cycle Fig.5.5(b) appear to be a good choice, in which case harmonic currents below the seventh are eliminated although, higher pulse numbers improve the motor performance and efficiency, (Sen 1991). The PWM control scheme is currently being used in Single – Phase traction systems. Apart from improving the Power Factor and reducing harmonics in the source current, it also reduces the ripple in the motor current and discontinuity of current conduction (Lai and Chen 1991).

CHAPTER SEVEN

CONCLUSION AND RECOMMENDATIONS

7.1 Conclusion

The hypothesis that increased power factor problem would exist in the Nigerian National grid with growth of heavy industries such as the Ajaokuta Steel Company, the Iron and Mining Industries, Aladja Steel and other steel related developmental projects has been established. The non – sinusoidal nature of the ac supply to the asymmetrical single – phase drive was established analytically and experimentally and the waveform distortion shown to worsen as the firing angle of the thyristors of the drive is increased. Also, the power factor gets worse as the number of such drives connected in parallel increases.

It was shown that the conventional PWM Power Factor Correction technique improves the power factor close to unity. However, the proposed bridgeless PFC gives the same improvement in Power Factor. The results of the laboratory experiment in Figs.5.21 and Fig.6.1 show that the input current is a pure sinusoid and in phase with the input voltage and the harmonic spectrum reveals that lower order harmonics had been eliminated. The same result was achieved with the alternate circuit – the bridgeless AC – DC Boost converter which offers a modification of the drive and the control methods. The advantages of the alternate circuit include (Martinez R. et.al 1996):

- The use of fewer semiconductor devices
- Improved characteristics in terms of higher input power factor and sinusoidal shape of input current
- It incorporates an ac side inductor which contributes to the reduction in EMI interference
- Power losses are reduced as a result of the absence of the series diode, therefore leading to higher reliability.

The proposed PFC overcomes the limitations of the conventional active boost PFC for the Single – Phase drives despite its improved power factor. These limitations are:

- The required switching frequency of the boost switch is usually very high which in turn increases the switching losses and lowers efficiency
- Special design of the dc – side inductor is necessary to carry dc current as well as high frequency ripple current.

- Three semi-conductor devices exist in the power flow path and thus contribute to voltage losses and reduced reliability.

7.2 Contributions to Knowledge

1. The research established the poor input power factor problem in industrial drives experimentally and analytically using the Piece – Wise Linear (P.W.L) method of analysis to derive the equations for each interval of operation of the drive. These equations were then put together to obtain the non – sinusoidal waveform of the bridge which is the cause of the poor power factor problem. The research has established the Pulse – Width Modulation (PWM) scheme as an effective method of correcting the poor input Power Factor in drives using simpler and a robust circuit configuration and has improved the input power factor of the Asymmetrical Single – Phase Bridge from 0.628 to 0.998 as displayed by the waveform of Figs. 6.4 and 6.5 respectively.
2. Although some of the PFC circuitry had led to improvement of power factor, they had the limitation of very high switching frequency of the boost switch which in turn increases the switching losses and lowers efficiency and also three semi – conductor devices exist in the power flow path contributing to voltage losses and reduced reliability. The present research proposed an alternative bridge circuit that uses fewer semi – conductor devices to achieve an improved power factor. The approach led to a higher reliability as a result of reduced power loss in circuit devices
3. Hitherto application of industrial drives suffers from lack of information on harmonics resulting from their use. This research has generated a number of drive performance characteristics and monographs that provide information to users of industrial drives, In particular, the communications industry that operate at frequencies that exist in the harmonic spectrum of the drive and the Power Holding Company of Nigeria (PHCN) which suffers the direct consequences of these harmonics will also benefit from this study and will be better informed when developing equipment standards used for their network. Also, the Steel industries that depends on DC and AC motor drives will benefit from the results of this research

7.3 Recommendation for further work

Lack of adequate equipment for measuring the harmonic spectrum of the AC input current made it difficult to compare the predicted harmonic currents with measured currents. Also, piece – wise linear analysis of the proposed AC – DC boost converter and the Diode/MOSFET PWM controlled (Bridgeless) Converter could not be done because of time constraint. Therefore, the areas that could be considered for further work include;

- (a) Measurement of the harmonics in the input current of the drives using a spectrum analyser with a view to comparing predicted harmonics spectrum with measured ones
- (b) A study of the harmonic spectrum of communication signals produced by different networks in the country with a view to identifying the possibility of industrial drives producing significant Electromagnetic Interference – EMI with communication systems
- (c) More detailed analysis of the proposed alternative circuits to the Asymmetrical Single Phase Bridge with a view to achieving their complete characterization and behaviour factors.
- (d) The many models of industrial drives and their control circuits are yet to be packaged in modular form so as to use them to develop experiments for manpower training at undergraduate and post graduate levels.
- (e) Analyses have been carried out for one Drive connected to AC supply to determine the level of harmonics and power factor. It is hereby suggested that a similar analysis be made for two, three and four converters connected in parallel to the same source in order to compare results.

REFERENCES

- Abdel Aziz et al. (2002). LC Compensators for Power Factor Correction of Nonlinear Loads. IEEE Transactions on Power Delivery. 1-6.
- Agarwal, P.D. (1959). Eddy Current Losses in Solid and Laminated iron. Trans. AIEE. Vol.78, Part I, Pages 169 – 181.
- Agu U. (1997). Relative study of the output characteristics of PWM and phase controlled AC-DC converters. Conf. Publication. Electric Power Engineering conf. (EPEC), UNN 4-10
- Andreycak B. (1993-4). Optimizing performance in UC 3854. Power Factor Correction Applications. Unitrode products and Applications Handbook. APEC conf. Proc. 584 – 590
- Aziz J.A and Salam Z. (2004). A New Pulse-Width Modulation (PWM) Scheme for Modular Structured Multilevel Voltage Source Inverter. International Journal of Electronics, Vol. 91, No. 4. 211-226.
- Balogh L, Redl R. (1993). Power – Factor correction with interleaved Boost Converters in continuous – induction mode. APEC conf. Proc., 168 – 174.
- Banerjee S. and Verghese G. (2000). Nonlinear Phenomena in Power Electronics. New York: IEEE Press.
- Basau, S and Bollen M.H.J. (2005). A novel common power factor correction scheme for homes and offices. IEE Trans. Power Delivery, 20: 2257-2263
- Bashi S.M. Mariun N. Noor S.B. and Athab H.S. (2005). Three-phase Single Switch Power Factor Correction Circuit with Harmonic Reduction. Journal of Applied Sciences 5 (1). 80-84
- Basu S, Bollen MHJ. (2005). A novel common power factor correction scheme for homes and offices. IEEE Trans. Power Deliv20, (3), pp. 2257–2263
- Bazinet J, O’Connor J.A.(1994). Analysis and Design of a zero voltage Transition Power Factor Correction Circuit. APEC conf. Proc. 591-597
- Bingsen Wang, Giri Venkafaramanan and Ashish Bendre. (2007). Unity Power Factor Control for Three-Phase Three-Level Rectifiers Without Current Sensors. IEEE Transactions on Industry Applications vol. 43. No. 5. 1341-1348.
- Bowes S.R. (1975). New Sinusoidal Pulse-Width Modulated Inverter. Proceeding of the IEE, 122. 1279-1284.
- Brkovic M, Cuk S. (2001). Input Current Shapper using Cuk converter. INTERLEC conf. Proc, 532-539.

Buso S, Malesani L and Mattavelli P. (1998). Comparison of Current Control Techniques for Active Filter Applications. IEEE Transactions on Industrial Electronics, Vol. 45. No. 5. 722-729.

Canesin C.A, Barbi I. (1996). Analysis and design of constant –frequency peak –current controlled high power factor boost rectifier with slope compensation. Proc. of IEEE Applied Power Electronics Conference, APEC'96, 807-813.

Canesin C.A. (1991). A unity Power Factor Multiple Isolated output switching mode power supply using a single switch. APEC conf. Proc. 430 – 436

Chow M. H. L. Lee Y. S. Lee and Tse C. K. (2000). Single-stage single-switch PFC regulator with unity power factor, fast transient response and low voltage stress. IEEE Trans. Power Electron., vol. 15. No. 1, pp. 156–163.

CSC Cherry Semi – conductor: “Power Conversion IC Data Book”. 1992

Dallego Ennco, Marco Passoni, Gabriele Sassone and Gluseppe Venchi. (2000). Novel Current Transducer in a Single – Phase Active Power Factor System. IEEE Transactions on Power Electronics. Vol. 15, No.3, 234 – 242

Damle, P and Dubey, G.K. (1976). Analysis of a Chopper Fed D.C Series Motor, IEEE Trans., IECEI, Vol. 23. No.1. page 72.

Dewan S.B. (1981). Optimum input and output filters for single-phase rectifier power supply. IEEE Trans. Industry Applications, vol. IA17, No.3, 282-288.

Dixon J.W, Venegas G. and Moran L. (1997). A Series Active Power Filter based on a Sinusoidal Current-Controlled Voltage-Source Inverter. IEEE Transactions on Industrial Electronics, Vol. 44, No. 5. 612-620.

Dixon Jr. L. H. (1990) High Power Factor Preregulator for Off-Line Power Supplies, in Unitrode Switching Regulated Power Supply Design Manual. Murrumbidgee, NH

Djemouai A, Sawan M and Slamani M. (2000). New CMOS Integrated Pulse Width Modulator for Voltage Conversion Application. Proceedings of the 7th IEEE International Conference on Electronics, Circuits and Systems, 116-119.

Dong Dai, Shengnan Li, Xikui Ma, and Chi K. Tse. (2007). Slow-Scale Instability of Single-Stage Power-Factor-Correction Power Supplies. IEEE Transactions on Circuits and Systems. VOL. 54, NO. 8. Pp. 1724 - 1735

Dranga O. Tse C. K, Iu H. H. C and Nagy I (2003). Bifurcation behavior of a power-factor-correction boost converter. Int. J. Bifur. Chaos, vol. 13, no. 10, pp. 3107–3114.

Dubey G.K, Doradla S.R, A.Joshi and Sinha R.M.K. (1986). Thyristorised Power Controllers. John Wiley and sons USA, 1st Edition.

Durry D, Farrer W and Jones B.L. (2000). Performance of thyristor bridge converters employing flywheeling. Proc. IEE, vol.127, 268-276.

Enjeti P.N, Ziogas P.D and Lindsay J.F. (1990). Programmed PWM Techniques to Eliminate Harmonics: A Critical Evaluation. IEEE Transactions on Industry Applications, 26, 302-316.

Enjeti P.N. and Martinez R. (1993). A high performance single – phase AC - Dc rectifier with Input Power Factor Correction. IEEE. Applied power Electronics Conf. (APEC). Proc. Pp. 190-195

Erickson R, M. Madigan, and Singer S. (2000). Design of a simple High – Power – Factor Rectifier Based on the Flyback Converter. APEC. Conf. Proc., 792-801.

Erickson R.W. (1997). Fundamental of Power Electronics. New York, NY, USA, Chapman & Hall.

Farmer W and Andrew D.F. (1978). Fully controlled regenerative bridge with half- controlled characteristics”. Proc. IEE, vol.125. 235-243

Femain A., Sebastin J, Villegas P, Hermando M.M and D.G Lamar. (2005). Dynamic limit of a power factor preregulator. IEEE Trans. Ind. Electron, vol.52, no.1 77-87.

Fujita H and Akagi H. (1998). The Unified Power Flow Conditioner: The Integration of Series- and Shunt-Active Filters”. IEEE Transactions on Power Electronics, Vol. 13, No. 2, 315-322.

Grahame G., Holmes Thomas, Lipo A. (2003). Pulse Wave Modulation for Power Converters: Principles and practice. John Wiley and sons Inc. Ist Edition.

Grigore, V and Kyyra J. (2000). A step-down converter with low input current for power factor correction. Applied Power Electronics Conference and Exposition. APEC 2000. Fifteenth Annual IEEE 1: 188-194.

Hanigovszki N. (2005). EMC Output Filters for Adjustable Speed Drives. Ph.D. Dissertation, Inst. Energy Techn. Aalborg Univ., Aalborg, Denmark.

Helonde J.B and Hiwakar C.S. (2008). Implementation of Direct Current Controlled PWM on Three Phase BLDC Motor Drive using Four-Switch Converter. Technology and Innovation for Sustainable Development Conference, 300-305.

Holmes G.D and Lipo T.A.(2003). Pulse Width Modulation for Power Converters. Principles and Practice, IEEE Press.

Ismail Daut, Rosnazri Ali and Soib Taib (2006). Design of a Single-Phase Rectifier with Improved Power Factor and Low THD using Boost Converter Technique. American Journal of Applied Sciences 3 (7). Pp. 1902-1904

- Itoh J.I and Fujita K. (2000). Novel Unity Power Factor Circuits using Zero-Vector for Single-Phase Input System. IEEE Trans. Power Electronics, Vol. 15. 36-43.
- Itoh R and Deng K. Ishizaka. (1989). Single-Phase Sinusoidal Converter using MOSFETs, IEE Proceedings, Vol. 136, No. 5, 237-242.
- Iu H. H. C. Zhou Y and Tse C. K, (2003). Fast-scale instability in a PFC boost converter under average current mode control. Int. J. Circuit Theory Appl., vol. 31, no. 6, pp. 611–624.
- JJaehong Hahn, Prasad N. Enjeti and Pitel Ira J. (2002). A new three-phase Power Factor Correction (PFC) scheme using two single-phase modules. IEEE Transactions on Industry Applications vol. 38. No. 1. 123-130.
- Kataoka T, Mizumachi K and Miyaira J. (1977). A pulse-width controlled AC-DC converter to Improve Power Factor and Waveforms of AC line current. IEEE Conference Record, ISPC-77, New York.
- Kataoka T, Mizumachi K and Miyaira J (1979). A pulse-width controlled ac-dc converter to improve power factor and waveforms of ac line current. IEEE Trans. On Ind. Appl, vol.15. 670-675.
- Kelley A.W, Hallouda M. A, Moore M.D, and Nance J. L (1991). Near unity power factor single-phase ac-to-dc converter using a phase-controlled rectifier. Proc. of IEEE. Applied Power Electronics Conference, APEC'91, 387-392.
- Kelly A.W, Yadusky W.F. (1989). Rectifier design for minimum line – current harmonics and maximum power factor. Proc of IEEE Applied Power Electronics Conference. APEC'89, 13-22.
- Kelly A.W, Yadusky W.F. (1992). Rectifier design for minimum line – current harmonics and maximum power factor. IEEE Trans. On Power Electronics, vol.7, No.2. 332-341.
- Kil S.-K, Cheng D.K.-W. Lu D.D.-C. (2008). Analysis and design of a single-phase hybrid mode power factor correction converter. IET Power Electron. Vol. 1, No. 1, pp. 72–83
- Kielgas H and Nill R. (1977). Converter Propulsion Systems with 3-Phase Induction Motors for Electric Traction Vehicles. IEEE Conference Record, ISPC-77, New York. 336-344
- Kit Sum K (1998). Improved valley-fill passive power factor correction current shaper approaches IEC specification limits. PCIM Magazine, 42-51.
- Kocher M.J, Steigerwald R.L.(1983). An AC – to – DC Converter with High Quality Input Waveforms. IEEE Trans. On Industry Applications. Vol. 1A – 19. No. 4. 586 – 599.
- Kolar J.W and Drofenik U. (1999). A new switching loss reduced discontinuous PWM scheme for a unidirectional three – phase/switch/level boost – type PWM rectifier. Proc.21st INTELEC, Copenhagen, Denmark, 29-38.

Krishnomoorthy K.A, Dubey G.K and Revankar G. N. (1978). Converter control with selective reduction of line harmonics. Proc. IEE, vol.125, No. 2, 141-145.

Krishnomoorthy K.A, Dubey G.K and Revankar G.N. (1978). General methods for selective reduction of line harmonics. Proc. IEE, vol.125, No. 11, 1269-70.

Krishnomoorthy K.A, Dubey G.K and Revankar G.N. (1978). Sequence control of converters with less triplen harmonics. Jn. Intn. Of Engineers: Electrical Engineering Div. Vol.59, 100-105.

Lai J.S, Chen D.(1993). Design Consideration for Power Factor Correction Boost Converter operating at the Boundary of continuous conduction and discontinuous mode. APEC conf. Proc. 267 – 273.

Laszlo, H, Yungtaek Jung and Milan M. Jovanovic. (2007). Performance Evaluation of Bridgeless PFC Boost Rectifiers. IEE. Pp 165-171

Lazaro A., Barrado A., Sanz M, Salas V and Olias E. (2007). New Power Factor Correction AC-DC converter with reduced storage capacitor voltage. IEEE Trans. Ind. Electron. Vol. 54. No. 1: 384-397.

Liu K.H, Lin Y.L. (1989). Current waveforms Distortions in Power Factor Correction Circuits Employing Discontinuous – Mode Boost Converters. PESC. Conf. Proc., 825 – 829.

Liu Y and Smedley, K. (2003). Control of a Dual Boost power factor corrector for high power applications. IECON 29th Annual Conference of the IEEE. Volume 3, Issue , 2-6 PP. 2929-2932.

LoCascio J, Walban M. T. (1990). Active Power Factor Correction using a Flyback Topology”. PCIM conf. Proc., 10 – 17.

Lu DDC, Cheng DK-W, Lee Y-S (2005). Analysis of a high-power factor AC–DC converter with reduced current and voltage stresses. IEE Proc., Electr. Power Appl. 152, (4), pp. 943–952

Lu DDC, Cheng DK-W, Lee Y-S. (2001). A single-switch power factor corrected converter with reduced repeated power processing’. Proc. IEEE Power Electronics Drive Systems (PEDS). Bali, Indonesia, pp. 26–32

Lu DDC, Cheng DK-W, Lee Y-S. (2003). Analysis and design of a single-stage single switch power factor corrected converter with direct power transfer’, IEICE Trans. Commun. E86-B, (12), pp. 3606–3613

Maksimovic D. (1994). Design of the clamp – current High – power-Factor Boost Rectifier. APEC conf. Proc, 584 – 590

Maksimovic D. (1995). Design of the clamped-current high power factor boost rectifier. IEEE Trans. on Industry Applications, Vol.31, No.5, 986-992.

Malinowski M. Kazmierkowski M. P. (2004). Simple direct power control of three-phase PWM rectifier using space – vector modulation (DPC-SVM). IEEE Trans. Ind. Electron, vol.51, no.2, 539-544.

Marek Gotfryd. (2000). Output Voltage and Power Limits in Boost Power Factor in the Discontinuous Inductor Current Mode”. IEEE Transactions on Power Electronics, vol.15. No.1.

Martin K.H. Cheung, Martin H.L Chow and Chi K. Tse. (2008). Practical design and evaluation of a 1KW PFC Power Supply based on Reduced Redundant power processing principle. IEEE Transaction on Industrial Electronics. Vol. 55. No.2. 665-673.

Martinez R, Enjeti P.N. (1996). A high – performance Single – Phase rectifier with input Power Factor Correction. IEEE Transaction on Power Electronics, Vol.II. No.2, 311-317.

Mazumder S. K. A. Nayfeh H, and Boroyevich D. (2001). Theoretical and experimental investigation of the fast- and slow-scale instabilities of a dc/dc converter, IEEE Trans. Power Electron., vol. 16, no. 2, pp. 201–216.

Mehta P, Mukhopadhyay S and Orhun E (1974). Forced commutated ac-dc converter-controlled dc drives. IEE conference on Power Electronics – Power semi-conductors and their Applications, Conference Publications123. 146.-154

Mellitt, B and Rashis. (1974). Analysis of DC Chopper circuits by computer – based piece – wise linear techniques PROC. IEE, 121(3). pages 173 – 178

Metha P and Mukhopadhyay. (1974). Modes of operation in converter – controlled DC drives. PROC. IEE Vol. 121, no.3. 219-227

Minghua Fu and Qing Chen. (2001). A DSP Based Controller for Power Factor Correction in a Rectifier Circuit. Sixteenth Annual IEEE Applied Power Electronics Conference and Exposition, pp. 144-149.

Mipanic P.N. (1968). The through pass inverter and its application to induction motor speed control”. IEEE Transactions on PAS. Vol. PAS-87, 234-246

Mohammed S. Agamy (2008) Single Stage Power Factor Corrected Three-Level Resonant Converters. Ph.D Thesis. Queen’s University, Kingston, Ontario, Canada

Mohan N, Undeland T.M and Robbins W.P. (1995). Power Electronics: Converters, Applications and Design. New York, NY, USA, John Wiley & Sons. Inc. 132-176

Mukher, K.C. (1961). Certain Approaches to the Electromagnetic field problems pertaining to Dynamo Electric Machines. IEE Monograph, Vol. Part C, Pages 405 -411

- Nagy I. (2001). Nonlinear phenomena in power electronics. *J. Automatika*. Vol. 42. No. 3–4, pp. 117–132.
- Nalbant M.K, Klein J. (1990). Design of a 1kw power factor correction circuit. *PCIM conf. Proc.*, 7 – 24.
- Nisit, D. C and Chattopadhyay. (1978). Modelling an SCR Bridge DC motor drive. *IEEE Transaction. IECI – 25*. pages 187 - 189
- Okoro C. C. (1980). An evaluation of the effects of Ripples on DC machines. Ph.D Thesis. University of Birmingham
- Okoro C.C (1987). Behaviour factors of Asymmetrical single-phase converter. *Nigerian Journal of Engineering and Technology*, vol.10. No.11-7
- Okoro C.C. (1982). Performance Evaluation of a DC motor Fed from an Asymmetrical Single-Phase Bridge. *Proc. IEE*, vol.129. PTB No.5, 289-98.
- Okoro C.C. (1986). Behaviour factors of power supply with the asymmetrical single – phase converter load (unpublished)
- Oleschuk V and Blaabjerg F. (2002). Direct Synchronized PWM Techniques with Linear Control Functions for Adjustable Speed Drives. *Proc. Of the 17th Annual IEEE Applied Power Electronics Conference and Exposition (APEC)*, Vol. 1. 76-82.
- Omar A.M, Rahim N.A. and Mekhilef S. (2004). Three-Phase Synchronous PWM for Flyback Converter with Power-Factor Correction using FPGA ASIC design. *IEEE Transactions on Industrial Electronics*, Vol. 51, No. 1. 96-106.
- Orabi M. and Ninomiya T. (2003). Nonlinear dynamics of power-factor-correction converter. *IEEE Trans. Ind. Electron.*, vol. 50, no. 6, pp.1116–1125.
- Pandey A, Prof. B. Singh and Prof. D.P Kothari. (2004). Comparative Evaluation of Single – Phase Unity Power Factor AC – DC Converter Topologies. *IE (I) Journal – EL PP102 – 109*
- Patel H.K and Dubey G.K. (1983). Evaluation of time ratio control schemes for thyristor controlled drives. *Jp. Intn. Of Engineers. Electrical Engineering Div.*
- Patella B.J. Prodic A, Zirger A, and Maksimovic D. (2003). High-frequency digital PWM Controller IC for DC-DC Converters. *IEEE Transactions on Power Electronics*, Vol. 18, No. 1. 438-446.
- Patil P.M and Kurkute S.L. (2006). Speed Control of Three Phase Induction Motor using Single Phase Supply along with Active Power Factor Correction. *ACSE Journal*, Vol. 6, Issue 3. 23-31.

- Patil P.M. (2002). An Active Power Factor Correction Technique for Single Phase AC to DC Boost Converters. Journal of the Institution of Electronics and Telecommunication Engineers. Vol. 43. No.4.
- Pitel Ira and Sarosh, N.T. (1977). A review of the effect and suppression of power converter harmonic. Industry and Application Society, Annual conf. 119-126
- Qiao C and Smetley K.M. (2003). Three-phase unity power factor star connected switch (VIENNA) rectifier with constant frequency intergration control. IEEE Trans. Ind. Electron, vol.18, no.4 952-957.
- Rashid M.H. (1993). Power Electronics: Circuits, Devices and Application. Prentice - Hall, Inc. 2nd Edition, 175-182.
- Redi R, Erisman B.P. (1994). Reducing distortion in peak – current – controlled Boost power – Factor correctors. APEC conf. Proc. 1994, 576 – 583.
- Redl R, Balogh L. (1992). RMS DC Peak and Harmonic currents in High – frequency Power – Factor correctors with capacitive Energy storage. APEC conf. Proc, 533-540.
- Redl R, Kislovski A.S. (1994). Telecom Power Supplies and power quality. IEEE Power Electronics Specialists Conference, PESC. 1137-1144
- Redl R, Tenti P, Daan J and Van Wyk. (1997). Power electronics: Polluting effects”. IEEE spectrum, vol. 345. 33-39
- Redl R. (1991). Power factor correction: Why and how?. Power Supply Design Course, Nurnberg, Germany, 26-28.
- Redl R. (1994). Power factor correction in a single-stage switching-mode power supplies—An overview. Int. J. Electron., vol. 77. No. 5, pp.555–582.
- Redl R. (1994). Power factor correction in single – phase switching –mode power supplies – an overview”. Int. J. Electronics, vol. 77, No.5. 555-582.
- Redl R. (1996). Power electronics and electromagnetic compatibility. Proc. Of. IEEE Power Electronics Specialist Conference. PESC. 15-21
- Robert Martinez and Enjeti P.N. (2000). A High performance Single- Phase Rectifier with input power factor correction. IEEE Transaction on Power Electronics, Vol. II, No.2.154-163
- Rossetto, L, Spiazzi, G and Trenti, P. (2004). Control Techniques For Power Factor Correction Converters. Applied Power Electronics Conference and Exposition. APEC pp 154-162
- Sebastian, J, Jaureguizar, M and Uceda, J. (1994). Industrial Electronics, Control and Instrumentation. IECON. , 20th International Conference Volume 3, Pp. 1688 - 1693

Sen P.C and Doradia S.R (1976). Symmetrical and Extinction angle control of solid state series motor Drive". IEEE Trans.IECI. -23, 31-38.

Sen P.C. (1991). Thyristorised DC Drives. John Wiley and Sons Inc. 1st Edition. Florida. Krieger Publishing Company.

Silva C. Power Factor Correction with the UC 3854". Application Note; Unitrode Integrated circuit.

Silva C. (2001). Power Factor Correction with the UC 3854". Application Note; Unitrode Integrated circuit.

Simonetti D.S.L, Sebastin J, Dos Reis, and Uceda J. (1992). .Design criteria for Sepic and Cuk converters as Power Factor Pre-regulators in Discontinuous Conduction Mode. IECON conf. Proc., 283-288

Sinha, N.K. (1974). Modelling of D.C motors for Control Applications, Trans. IEEE. IECI, Vol. 21. No. 2. Pages 84 – 88.

Sokai N, Sum K and Hamil D. (1998). A capacitor –fed, voltage step-down, single-phase, non isolated rectifier. Proc. Of IEEE Applied Power Electronics Conference, APEC'98. 208-215.

Spangler J, Hussain B, and Behera A.K (1991). Electronic fluorescent ballast using a power factor correction technique for loads greater than 300watts". Proc. of IEEE Applied Power Electronics Conference, APEC'91. 393-399.

Srinivasan,R and Oruganti, R. (1998). A unity Power Factor Converter Using Half - Bridge Topology. Power Electronics IEEE Transactions. Vol. 13, No.3 PP. 487-500

Stephanie Bibian and Hua Jin. (2001). Digital Control with Improved Performance for Boost Power Factor Correction Circuits. Applied Power Electronics Conference and Exposition, Sixteenth Annual IEEE. 137-143.

Szabados, B. (1972). A realistic mathematical model for D.C motors. Control Engineering. U.S.A, Vol.19, No. 3, pages 49 – 53

Tao, F.F and Lee F.C. (2000). A critical – conduction –mode single – stage power factor correction electronic ballast. Applied Power Electronics Conference and Exposition. APEC 2000. Fifteenth Annual IEEE 1: 603-609.

Trzynadlowski A.M, Wang Z, Nagashima J, Stancu C and Zelechowski M. (2003). Comparative Investigation of PWM Techniques for a New Drive for Electric Vehicles. IEEE Transactions on Industry Applications. Vol. 39, No. 5. 1396-1403.

Tse C. K. and di Bernardo M.(2002). Complex behavior of switching power converters. Proc. IEEE, vol. 90, no. 5, pp. 768–781.

- Tse C. K.(2003). *Complex Behavior of Switching Power Converters*. Boca Raton, FL: CRC.
- Tse CK. (2003). Circuit theory of power factor correction in switching converters. *Int. J. Circuit Theory Appl.*, 31, (2), pp. 157–198
- Venkatarmmaman G. and Wang B (2004). Dynamic modeling and control of a three-phase pulse – width modulated converters using phasors. *Proc. 35th Annual IEEE Power Electron Spec. Conf. Anchen, Germany*. 2822-2828.
- Vorperian V and Ridley R. B. (1990). A simple scheme for unity power factor rectification for high frequency ac buses”. *IEEE Trans. on Power Electronics*, Vol. 5, No. 1. 77-87.
- Wanfeng Zhang, Guang Feng, Yanfei Liu and Bin Wu. (2003). A New Protective control Strategy for Power Factor Correction. *APEC*. 403-409.
- Wanfeng zhang, Guang Feng, Yanfei Liu and Bin Wu. (2003). Analysis and Implementation of a New PFC Digital Control Method. *PESC*. 335-341.
- Whittington H.W., Flynn B.W., and Macpherson D.E. (2002). *Switch mode power Supplies; Design and Construction*. Research studies press Ltd, 1st Edition. 14-22.
- Wong S. C, Tse C. K, Orabi M and Ninomiya T. (2006).The method of double averaging: An approach for modeling power-factor-correction switching converters. *IEEE Trans. Circuits Syst. I, Reg. Papers*, vol. 53, no. 2, pp. 454–462.
- Wu X, Tse C. K, Dranga O, and Lu J. (2006). Fast-scale instability of single stage power-factor-correction power supplies. *IEEE Trans. Circuits Syst. I, Reg. Papers*, vol. 53, no. 1, pp. 204 – 213.
- Wu X, Tse C. K, Wong S. C and Lu J. (2006). Fast-scale bifurcation in single-stage PFC power supplies operating with DCM boost stage and CCM forward stage. *Int. J. Circuit Theory Appl.*, vol. 34, no. 3, pp. 341–355.
- Ying-Tung Hsiao (2001). Design of Filters for Reducing Harmonic Distortion and Correcting Power Factor in Industrial Distribution Systems. *Journal of Science and Engineering*, Vol. 4, No. 3, pp. 193-199
- Youssef N.H.H, Funlech F and Ajhaddad K. (2003).Small signal modeling and control design of a three –phase AC/DC Vienna converter. *Proc. 29th Annual IEEE IECON Roanoke, VA*.
- Zander H. (1973). Self – commutated rectifier to improve line conditions. *Proc. IEE*, vol. 120. No.9, 126-132
- Zheren Lai, Keyue Ma Smedley. (1998). A Family of Continuous Conduction Mode Power Factor Correction Controllers based on the General Pulse-Width Modulator. *IEEE Transactions on Power Electronics*, Vol. 13, No. 3. 501-510.

- Zhou C (1989). Design and Analysis of an Active Power Factor Correction Circuit, M.S. Thesis, Virginia Polytechnic Institute and State University.
- Zhou C, Ridley R.B and Lee F.C. (1990). Design and Analysis of a Hysteretic Boost Power Factor Correction Circuit. PESC conf. Proc. 800 – 807
- Zhou C, Jovanovic M. (1992). Design Trade – offs in continuous current-mode controlled Boost Power- Factor correction circuits. HPFC conf. Proc. Pp. 209 – 220.
- Zhou C, Jovanovic M. (1992). Design Trade – offs in continuous current-mode controlled Boost Power- Factor correction circuit. HPFC conf. Proc, 209 – 220.
- Zhou C. (1998). Design and Analysis of an Active Power Factor Correction Circuit. M.S. Thesis. Virginia Polytechnic Institute and State University
- Zuccato A, Rossetto L. (1997). Understanding and complying with CISPR and IEC 1000 standards on EMC. EPE Association Tutorial. European Power Electronics Conference EPE'97.
- Rossetto, L, Spiazzi, G and Trenti, P. (2004). Control Techniques For Power Factor Correction Converters. Applied Power Electronics Conference and Exposition. APEC pp 154-162
- Pandey A, Prof. B. Singh and Prof. D.P Kothari. (2004). Comparative Evaluation of Single – Phase Unity Power Factor AC – DC Converter Topologies. IE (I) Journal – EL PP102 – 109
- Laszlo, H, Yungtaek Jung and Milan M. Jovanovic. (2007). Performance Evaluation of Bridgeless PFC Boost Rectifiers. IEE. Pp 165-171
- Enjeti P.N. and Martinez R. (1993). A high performance single – phase AC - Dc rectifier with Input Power Factor Correction. IEEE. Applied power Electronics Conf. (APEC). Proc. Pp. 190-195
- Liu Y and Smedley, K. (2003). Control of a Dual Boost power factor corrector for high power applications. IECON 29th Annual Conference of the IEEE. Volume 3, Issue , 2-6 PP. 2929-2932.
- Srinivasan,R and Oruganti, R. (1998). A unity Power Factor Converter Using Half - Bridge Topology. Power Electronics IEEE Transactions. Vol. 13, No.3 PP. 487-500
- Lu, B, Dong, W, Zhao, Q and Lee, F.C. (2003). “Performance evaluation of CoolMOSTM and SiC diode for single – phase power factor correction applications”, APEC. Vol.2.Pp. 651 - 657

APPENDICES

APPENDIX I

Analysis for obtaining AC input current of the drive

(A) Forward commutation interval

This is defined by interval $\alpha < \omega t < \alpha + \mu$

And having initial condition $i = 0$ at $\omega t = 0$

Equation for current during this interval is obtained from the equivalent circuit of Fig.3.5 (a) as;

$$L_s \frac{di}{dt} + R_s i = E_1 \sin(\omega t + \alpha) \quad (1)$$

Where R_s and L_s are the source supply resistance and inductance respectively.

Using integrating factor method of solving differential equations

$$I. F = e^{\int \frac{R_s}{L_s} dt} = e^{\frac{R_s t}{L_s}} = e^{\frac{t}{\tau_1}}$$

$$\text{Where } \tau_1 = \frac{L_s}{R_s}$$

So that,

$$i(t) \cdot e^{\frac{t}{\tau_1}} = \int \frac{E_1}{L_s} \sin(\omega t + \alpha) e^{\frac{t}{\tau_1}} dt + C \quad (2)$$

$$\text{Since } \frac{E_1}{L_s} \int \sin(\omega t + \alpha) e^{\frac{t}{\tau_1}} dt = \frac{E_1}{L_s} \int u dv = \frac{E_1}{L_s} [uv - \int v du]$$

Where,

$$u = \sin(\omega t + \alpha), \text{ and } dv = e^{\frac{t}{\tau_1}}, du = \omega \cos(\omega t + \alpha), v = \tau_1 e^{\frac{t}{\tau_1}}$$

Therefore,

$$\begin{aligned} \int \sin(\omega t + \alpha) e^{\frac{t}{\tau_1}} dt &= \tau_1 \sin(\omega t + \alpha) e^{\frac{t}{\tau_1}} - \int \omega \tau_1 e^{\frac{t}{\tau_1}} \cos(\omega t + \alpha) dt \\ &= \tau_1 \sin(\omega t + \alpha) e^{\frac{t}{\tau_1}} - \omega \tau_1 \int e^{\frac{t}{\tau_1}} \cos(\omega t + \alpha) dt \end{aligned} \quad (3)$$

Again from equation (3),

$$\int \cos(\omega t + \alpha) e^{\frac{t}{\tau_1}} dt = uv - \int v du$$

Where,

$$u = \cos(\omega t + \alpha), \quad du = -\omega \sin(\omega t + \alpha), \quad dv = e^{\frac{t}{\tau_1}}, \quad v = \tau_1 e^{\frac{t}{\tau_1}}$$

Hence,

$$\int \cos(\omega t + \alpha) e^{\frac{t}{\tau_1}} dt = \tau_1 \cos(\omega t + \alpha) e^{\frac{t}{\tau_1}} + \omega \tau_1 \int \sin(\omega t + \alpha) e^{\frac{t}{\tau_1}} dt \quad (4)$$

Combining equations (3) and (4),

$$\begin{aligned} \frac{E_1}{L_s} \int \sin(\omega t + \alpha) e^{\frac{t}{\tau_1}} dt \\ = \frac{E_1}{L_s} \left[\tau_1 \sin(\omega t + \alpha) e^{\frac{t}{\tau_1}} - \omega \tau_1 \left(\tau_1 \cos(\omega t + \alpha) e^{\frac{t}{\tau_1}} + \omega \tau_1 \int \sin(\omega t + \alpha) e^{\frac{t}{\tau_1}} dt \right) dt \right] \end{aligned}$$

Now, if $I = \int \sin(\omega t + \alpha) e^{\frac{t}{\tau_1}} dt$ then,

$$\frac{E_1}{L_s} I = \frac{E_1}{L_s} \left[\tau_1 \sin(\omega t + \alpha) e^{\frac{t}{\tau_1}} - \omega \tau_1^2 \left(\cos(\omega t + \alpha) e^{\frac{t}{\tau_1}} - (\omega \tau_1)^2 I \right) \right]$$

$$\therefore I[1 + (\omega \tau_1)^2] = [\tau_1 \sin(\omega t + \alpha) - \omega \tau_1^2 \cos(\omega t + \alpha)] e^{\frac{t}{\tau_1}}$$

$$I = \frac{\tau_1 e^{\frac{t}{\tau_1}}}{(1 + \omega \tau_1^2)} [\sin(\omega t + \alpha) - \omega \tau_1 \cos(\omega t + \alpha)]$$

$$\text{Since } \tau_1 = \frac{L_s}{R_s}, \quad |z| = \sqrt{(\omega L_s)^2 + R_s^2}$$

$$\therefore 1 + (\omega L_s)^2 = 1 + \frac{(\omega L_s)^2}{R_s^2} = \frac{1}{R_s^2} (R_s^2 + (\omega L_s)^2)$$

Hence,

$$I = \frac{L_s}{R_s} \cdot \frac{e^{\frac{t}{\tau_1}} [\sin(\omega t + \alpha)]}{\frac{1}{R_s^2} (R_s^2 + (\omega L_s)^2)} - \frac{\omega L_s}{R_s^2} \cos(\omega t + \alpha)$$

Simplifying yields,

$$I = \frac{L_s e^{\frac{t}{\tau_1}}}{\sqrt{(\omega L_s)^2 + R_s^2}} \cdot \frac{|R_s \sin(\omega t + \alpha) - \omega L_s \cos(\omega t + \alpha)|}{\sqrt{(\omega L_s)^2 + R_s^2}}$$

In the analysis,

$$\frac{R_s}{\sqrt{(\omega L_s)^2 + R_s^2}} = \cos \theta_1, \frac{\omega L_s}{\sqrt{(\omega L_s)^2 + R_s^2}} = \sin \theta_1, \tan^{-1} \left(\frac{\omega L_s}{R_s} \right) = \theta_1, |z| = \sqrt{(\omega L_s)^2 + R_s^2}$$

$$I = L_s \frac{e^{\frac{t}{\tau_1}}}{|z|} \cdot \sin(\omega t + \alpha - \theta_1) + c$$

$$\therefore i(t) e^{\frac{t}{\tau_1}} = \frac{E_1}{L_s} \cdot L_s \frac{e^{\frac{t}{\tau_1}}}{|z|} \cdot \sin(\omega t + \alpha - \theta_1) + c \quad (5)$$

Applying initial condition, $\omega t = 0, i(t) = 0$

$$\therefore c = \frac{E_1}{L_s} \cdot \frac{L_s}{|z|} \sin(\alpha - \theta_1) + c$$

$$c = -\frac{E_1}{L_s} \cdot \frac{L_s}{|z|} \sin(\alpha - \theta_1) = \frac{E_1}{|z|} \cdot \sin(\theta_1 - \alpha_1)$$

$$\therefore i(t) = \frac{E_1}{|z|} \sin(\omega t + \alpha - \theta_1) + \frac{E_1}{|z|} \cdot \sin(\alpha - \theta_1) e^{-\frac{t}{\tau_1}} \quad (6)$$

If $K_1 = \frac{E_1}{|z|}$, then $i(t)$ becomes,

$$i(t) = K_1 \left[\sin(\omega t + \alpha - \theta_1) + \sin(\theta_1 - \alpha_1) e^{-\frac{t}{\tau_1}} \right] \quad (7)$$

From equation (7), the current at the end of the interval when $\omega t = \mu, i(t) = I_{ao}$, then,

$$I_{ao} = K_1 \left[\sin(\mu + \alpha - \theta_1) + \sin(\theta_1 - \alpha_1) e^{-\left(\frac{\mu}{\omega \tau_1}\right)} \right] \quad (8)$$

(B) Conduction interval ($\alpha + \mu < \omega t < \pi$)

In this interval $\alpha + \mu < \omega t < \pi$, the current flows in the path shown in Fig. 3.5(b) and the equation governing this interval with respect to the equivalent circuit is defined by equation (9).

$$L \frac{di}{dt} + Ri + E = E_1 \sin(\omega t + \alpha + \mu) \quad (9)$$

Where $L = L_s + L_1 + L_a$

And,

$$R = R_s + R_a$$

Initial conditions $i(t) = I_{a0}$ when $\omega t = 0$

Rewriting equation (9), gives

$$\frac{di}{dt} + \frac{E}{L}i = \frac{E_1}{L}\sin(\omega t + \alpha + \mu) - \frac{E}{L} \quad (10)$$

Using integrating factor method of solving differential equations

$$\text{I. F} = e^{\int \frac{R}{L} dt} = e^{\frac{t}{\tau}}$$

Where $\tau = \frac{L}{R}$

$$i(t) \cdot e^{\frac{t}{\tau}} = \int \left(\frac{E_1}{L} \sin(\omega t + \alpha + \mu) - \frac{E}{L} \right) e^{\frac{t}{\tau}} dt + C$$

i.e,

$$i(t) \cdot e^{\frac{t}{\tau}} = \frac{E_1}{L} \int \sin(\omega t + \alpha + \mu) e^{\frac{t}{\tau}} dt - \frac{E}{L} \int e^{\frac{t}{\tau}} dt + C \quad (11)$$

From equation (3) and (4),

$$\int \sin(\omega t + \alpha + \mu) e^{\frac{t}{\tau}} dt = \sin(\omega t + \alpha + \mu) \tau e^{\frac{t}{\tau}} - \int \tau e^{\frac{t}{\tau}} \cdot \omega \cos(\omega t + \alpha + \mu) dt \quad (12)$$

Also,

$$\int \cos(\omega t + \alpha + \mu) e^{\frac{t}{\tau}} dt = \cos(\omega t + \alpha + \mu) \tau e^{\frac{t}{\tau}} + \int \tau e^{\frac{t}{\tau}} \cdot \omega \sin(\omega t + \alpha + \mu) dt \quad (13)$$

Substituting equation (13) into equation (12), gives:

$$\int \sin(\omega t + \alpha + \mu) e^{\frac{t}{\tau}} dt = \tau \sin(\omega t + \alpha + \mu) e^{\frac{t}{\tau}} - \omega \tau \left[\tau e^{\frac{t}{\tau}} \cos(\omega t + \alpha + \mu) + \omega \tau \int \sin(\omega t + \alpha + \mu) e^{\frac{t}{\tau}} dt \right] \quad (14)$$

Let $I = \int \sin(\omega t + \alpha + \mu) e^{\frac{t}{\tau}} dt$,

Then equation (14) simplifies to;

$$\left[1 + \omega^2 \tau^2 \right] I = \tau \sin(\omega t + \alpha + \mu) e^{\frac{t}{\tau}} - \omega \tau^2 \cos(\omega t + \alpha + \mu) e^{\frac{t}{\tau}} \quad (15)$$

$$\therefore I = \frac{\tau \sin(\omega t + \alpha + \mu) e^{\frac{t}{\tau}} - \omega \tau^2 \cos(\omega t + \alpha + \mu) e^{\frac{t}{\tau}}}{(1 + (\omega \tau)^2)} \quad (16)$$

i.e,

$$I = \frac{\tau e^{\frac{t}{\tau}}}{(1 + (\omega \tau)^2)} [\sin(\omega t + \alpha + \mu) - \omega \tau \cos(\omega t + \alpha + \mu)]$$

If $\tau = \frac{L}{R}$, $|z| = \sqrt{R^2 + (\omega L)^2}$, and $\theta_2 = \tan^{-1} \left(\frac{\omega L}{R} \right)$

$$\therefore I = \frac{L}{R} e^{\frac{t}{\tau}} \cdot \frac{1}{|z|^2} \cdot R^2 \left[\sin(\omega t + \alpha + \mu) - \frac{\omega L}{R} \cos(\omega t + \alpha + \mu) \right]$$

$$= L \frac{e^{\frac{t}{\tau}}}{|z|} \cdot \left[\frac{R}{|z|} \sin(\omega t + \alpha + \mu) - \frac{\omega L}{|z|} \cos(\omega t + \alpha + \mu) \right]$$

$$= L \frac{e^{\frac{t}{\tau}}}{|z|} [\cos \theta_2 \sin(\omega t + \alpha + \mu) - \sin \theta_2 \cos(\omega t + \alpha + \mu)]$$

$$= L \frac{e^{\frac{t}{\tau}}}{|z|} \sin(\omega t + \alpha + \mu - \theta_2)$$

$$\therefore i(t) e^{\frac{t}{\tau}} = \frac{E_1}{L} I - \frac{E}{L} \cdot \frac{L}{R} e^{\frac{t}{\tau}} + C \quad (17)$$

Substituting the expression of 'I' into equation (17),

$$i(t) e^{\frac{t}{\tau}} = \frac{E_1}{L} \cdot L \frac{e^{\frac{t}{\tau}}}{|z|} \sin(\omega t + \alpha + \mu - \theta_2) - \frac{E}{L} \cdot \frac{L}{R} e^{\frac{t}{\tau}} + C$$

Hence,

$$i(t) = \frac{E_1}{|z|} e^{\frac{t}{\tau} - \frac{t}{\tau}} \sin(\omega t + \alpha + \mu - \theta_2) - \frac{E_1}{R} e^{\frac{t}{\tau} - \frac{t}{\tau}} + C e^{-\frac{t}{\tau}}$$

$$= \frac{E_1}{|z|} \sin(\omega t + \alpha + \mu - \theta_2) - \frac{E}{R} + C e^{-\frac{t}{\tau}}$$

Applying the initial condition, $\omega t = 0$, $i(t) = I_{ao}$

$$\therefore I_{ao} = \frac{E_1}{|z|} \sin(\omega t + \alpha + \mu - \theta_2) - \frac{E}{R} + C$$

$$\therefore C = I_{ao} - \frac{E_1}{|z|} \sin(\omega t + \alpha + \mu - \theta_2) + \frac{E}{R} \quad (18)$$

Thus,

$$i(t) = \frac{E_1}{|z|} \sin(\omega t + \alpha + \mu - \theta_2) - \frac{E}{R} + \left(I_{a0} - \frac{E_1}{|z|} \sin(\omega t + \alpha + \mu - \theta_2) + \frac{E}{R} \right) e^{-\frac{t}{\tau}} \quad (19)$$

Suppose, $k_2 = \frac{E_1}{|z|}$, $P = \frac{E}{E_1}$, $\tau = \frac{L}{R}$, and $\theta_2 = \tan^{-1} \left(\frac{\omega L}{R} \right)$,

Then, $\frac{E}{R} = \frac{E}{E_1} \cdot \frac{E_1}{R} = P k_2$ and $\frac{E_1}{|z|} = \frac{E_1}{R} = \frac{R}{|z|} = k_2 \cdot \cos \theta_2$

$$\therefore i(t) = k_2 \cos \theta_2 \sin(\omega t + \alpha + \mu - \theta_2) - P k_2 + (I_{a0} - k_2 \cos \theta_2 \sin(\alpha + \mu - \theta_2) + P k_2) e^{-\frac{t}{\tau}}$$

$$\text{i.e, } i(t) = k_2 [\cos \theta_2 \sin(\omega t + \alpha + \mu - \theta_2) - P] + [k_2 (\cos \theta_2 \sin(\theta_2 - \alpha - \mu) + P) + I_{a0}] e^{-\frac{t}{\tau}} \quad (20)$$

(C) Freewheeling interval $0 < \omega t < \alpha$

In this interval, the load is not connected to the supply, current flows in the path shown in Fig.3.5(c).

This interval is define by the equation

$$L_2 \frac{di}{dt} + R_a i = -E \quad (21)$$

Whose initial condition is $i(t) = I_1$ at $\omega t = 0$

Rewriting equation (21) gives;

$$\frac{di}{dt} + \frac{R_a}{L_2} i = -\frac{E}{L_2} \quad (22)$$

Using integrating factor method of solving differential equations

$$\text{I. F} = e^{\int \frac{R_a}{L_2} dt} = e^{\frac{R_a t}{L_2}} = e^{\frac{t}{\tau_2}}$$

Where $\tau_2 = \frac{L_2}{R_a}$

$$I \cdot e^{\frac{t}{\tau_2}} = \int -\frac{E}{L_2} e^{\frac{t}{\tau_2}} dt + C \quad (23)$$

Integrating equation (23);

$$i \cdot e^{\frac{t}{\tau_2}} = -\frac{E}{L_2} \cdot \frac{L_2}{R_a} e^{\frac{t}{\tau_2}} + C \quad (24)$$

$$\text{Therefore, } i(t) = -\frac{E}{R_a} + C e^{-\frac{t}{\tau_2}} \quad (25)$$

Applying initial condition $\omega t = 0; i(t) = I_1$

$$\text{Therefore } I_1 = -\frac{E}{R_a} + C$$

Which gives $C = I_1 + \frac{E}{R_a}$ hence, equation (25) becomes;

$$i(t) = -\frac{E}{R_a} + [I_1 + \frac{E}{R_a}]e^{-\frac{t}{\tau_2}}$$

$$\text{Or, } i(t) = I_1 e^{-\frac{t}{\tau_2}} - \frac{E}{R_a}[1 - e^{-\frac{t}{\tau_2}}] \quad (26)$$

At $\omega t = x$, then $t = \frac{x}{\omega}$

Equation (26) can then be written as;

$$i(x) = I_1 e^{-\frac{x}{\omega\tau_2}} - \frac{E}{R_a}[1 - e^{-\frac{x}{\omega\tau_2}}] \quad (27)$$

When $\omega t = \alpha, i(t) = 0$, then, $t = \frac{\alpha}{\omega}$

Substituting the value of 't' into equation (26);

$$0 = I_1 e^{-\frac{\alpha}{\omega\tau_2}} - \frac{E}{R_a}[1 - e^{-\frac{\alpha}{\omega\tau_2}}] \quad (28)$$

Therefore,

$$I_1 = \frac{\frac{E}{R_a}[1 - e^{-\frac{\alpha}{\omega\tau_2}}]}{e^{-\frac{\alpha}{\omega\tau_2}}} \quad (29)$$

Also, the current at $x = \pi$ during the conduction interval is equally ' I_1 '.

$$\therefore x = \omega t + \alpha + \mu = \pi, \text{ then, } t = \frac{(x - \alpha - \mu)}{\omega}$$

Hence from equation (29);

$$I_1 = k_2[\cos\theta_2 \sin\theta_2 - p] + [k_2(\cos\theta_2 \sin(\theta_2 - \alpha) + p) + I_{a0}]e^{-\frac{(\pi - \alpha - \mu)}{\omega\tau}} \quad (30)$$

Equation (8) can be substituted into equation (30) to give a transcendental equation $f(\mu)$ emanating from a combination of equation (29) and (30) which is solved to obtain the commutation angle, ' μ ' for the gating angle ' α '

Fig.(3.6) Shows the variation of the commutation angle ' μ ' as the firing angle ' α ' is altered.

Angle 'β' after 'π'

The freewheeling diode ' D_2 ' in Fig.3.5(c) becomes forward biased when the instantaneous supply voltage equals the induced voltage in the source inductance. The induced voltage in the source inductance reverses biases ' D_2 ', until the angle ' β ' after ' π ' when this voltage is neutralized by the instantaneous supply voltage. The current in the conducting thyristor begins to decay to zero and in attempt to oppose this, the voltage in the armature circuit inductance forward biases ' D_2 to begin the freewheeling mode Mellitt (1974)

If the angle ' β ' is defined as $\beta = x - \pi$ then the equation for current in the conduction interval-as shown in equation (20) becomes;

$$i(\beta) = k_2[\cos\theta_2\sin(\beta - \theta_2) - P] + [k_2(\cos\theta_2\sin(\theta_2 - \alpha - \mu) + P) + I_{ao}]e^{-\frac{(\pi+\beta-\alpha-\mu)}{\omega\tau}} \quad (31)$$

The freewheeling interval begins when;

$$E_1\sin\beta + L_s\frac{di(\beta)}{d\beta} = 0 \quad (32)$$

From equation 31),

$$\frac{di(\beta)}{d\beta} = -k_2[\cos\theta_2\cos(\beta - \theta_2)] - \frac{1}{\omega\tau_2}[k_2(\cos\theta_2\sin(\theta_2 - \alpha - \mu) + P) + I_{ao}]e^{-\frac{(\pi+\beta-\alpha-\mu)}{\omega\tau}} \quad (33)$$

Now, using equation (33) in (32),

$$E_1\sin\beta - L_s[\cos\theta_2\cos(\beta - \theta_2)] - \frac{1}{\omega\tau_2}[k_2(\cos\theta_2\sin(\theta_2 - \alpha - \mu) + P) + I_{ao}]e^{-\frac{(\pi+\beta-\alpha-\mu)}{\omega\tau}} = 0 \quad (34)$$

If $k = k_2(\cos\theta_2\sin(\theta_2 - \alpha - \mu) + p)$,

$$\text{Then, } E_1\sin\beta - L_s[\cos\theta_2\cos(\beta - \theta_2)] + \frac{(k+I_{ao})}{\omega\tau_2}e^{-\frac{(\pi-\beta-\mu)}{\omega\tau}} = 0 \quad (35)$$

The value of the motor input current at the beginning of the freewheeling is obtained from equation (31) but the value of the angle ' β ' after π corresponding to this current is obtained by solving the transcendental equation (35).

The relationship between ' α ' and ' β ' is shown in Fig. (3.7).

(D) Reverse Commutation or Extinction Interval $\pi + \beta < x < \pi + \beta + x_s$

The reverse commutation of current from a conducting thyristor is opposed by the voltage induced in the source inductance. Defining ωt from $x = \pi$, the current in the reverse commutating thyristor falls to zero from the value at $x = \pi + \beta$, i.e I_β .

The equation of current obtained from the equivalent circuit of Fig.3.5 (d) is

$$L_s \frac{di}{dt} + R_s = -E_1 \sin(\omega t + \beta) \quad (36)$$

Re-arranging,

$$\frac{di}{dt} + \frac{R_s}{L_s} = \frac{-E_1 \sin(\omega t + \beta)}{L_s}$$

$$\text{Natural Component} = Ae^{\frac{-t}{\tau_1}}$$

$$\text{Where, } \tau_1 = \frac{L_s}{R_s}$$

$$\text{Forced Response} = i_f(t) = \frac{-E_1}{z} \sin(\omega t + \beta - \theta_1)$$

$$\text{Where, } \theta_1 = \tan^{-1} \left(\frac{\omega L_s}{R_s} \right), \text{ and } z = \sqrt{R^2 + (\omega L)^2}$$

$$\therefore i(t) = Ae^{\frac{-t}{\tau_1}} - \frac{E_1}{z} \sin(\omega t + \beta - \theta_1) \quad (37)$$

$$\text{Initial condition, } \omega t = 0, i(t) = I_\beta$$

Hence,

$$A = I_\beta - \frac{E_1}{z} \sin(\theta_1 - \beta) \quad (38)$$

Substituting equation (38) in (37);

$$i(t) = -\frac{E_1}{z} \sin(\omega t + \beta - \theta_1) - \left[\frac{E_1}{z} \sin(\theta_1 - \beta) - I_\beta \right] e^{\frac{-t}{\tau_1}} \quad (39)$$

$$= -K_1 \sin(\omega t + \beta - \theta_1) - [K_1 \sin(\theta_1 - \beta) - I_\beta] \quad (40)$$

$$\text{Where, } K_1 = \frac{E_1}{z}$$

The equations of currents for the different intervals put together and plotted for different firing angles are displayed in Fig. 3.8

APPENDIX II:

Analysis of the Harmonics produced by the controller

The harmonic spectrum of the motor input current is obtained from Fourier analysis of the explicit expressions for the armature current over a period of the waveform such that;

$$i(x) = \sum_{n=2}^{\infty} (A_n \cos nx + B_n \sin nx) \quad (1)$$

The coefficients A_n and B_n are obtained as

$$A_n = \frac{1}{T} \int_0^T i(x) \cos nx \, dx \quad (2)$$

$$B_n = \frac{1}{T} \int_0^T i(x) \sin nx \, dx \quad (3)$$

T is the period.

For A_n ($n = 1, 3, 5, \dots, \infty$)

For free-wheeling,

For the free-wheeling interval, $0 < x < \alpha$, the corresponding A_n is expressed as;

$$A_n = \frac{2}{\pi} \int_0^{\pi} i(x) \cos nx \, dx = \frac{2}{\pi} \left\{ \int_0^{\alpha} i(x) \cos nx \, dx + \int_{\alpha}^{\alpha+\mu} i(x) \cos nx \, dx + \int_{\alpha+\mu}^{\pi} i(x) \cos nx \, dx \right\} \quad (4)$$

Equation governing this interval is

$$i(x) = \left(I_1 + \frac{E}{R_a} \right) e^{-x/\omega\tau_2} - \frac{E}{R_a} \quad (5)$$

$$A_{n1} = \frac{2}{\pi} \int_0^{\alpha} \left[\left(I_1 + \frac{E}{R_a} \right) e^{-x/\omega\tau_2} - \frac{E}{R_a} \right] \cos nx \, dx \quad (6)$$

$$A_{n1} = \frac{2}{\pi} \left(I_1 + \frac{E}{R_a} \right) \int_0^{\alpha} e^{-x/\omega\tau_2} \cos nx \, dx - \frac{2}{\pi} \frac{E}{R_a} \int_0^{\alpha} \cos nx \, dx \quad (7)$$

Resolving equation (7) into parts and solving accordingly,

$$\therefore \int_0^{\alpha} \cos nx \, dx = \frac{\sin nx}{n} \quad (8)$$

$$\text{And } \int_0^{\alpha} e^{-x/\omega\tau_2} \cos nx \, dx = I \quad (9)$$

Using integration by parts for equation (9)

$$\int u dv = uv - \int v du$$

Where $u = e^{-x/\omega\tau_2}$ and $du = -\frac{e^{-x/\omega\tau_2}}{\omega\tau_2}$

$$dv = \cos nx dx \text{ and } v = \frac{\sin nx}{n}$$

$$\begin{aligned} I &= \frac{e^{-x/\omega\tau_2} \sin nx}{n} - \int_0^\alpha \frac{e^{-x/\omega\tau_2} \sin nx}{n\omega\tau_2} dx \\ &= \frac{e^{-x/\omega\tau_2} \sin nx}{n} + \frac{1}{n\omega\tau_2} \int_0^\alpha e^{-x/\omega\tau_2} \sin nx dx \end{aligned} \quad (10)$$

Applying integration by parts for equation (10),

Where $u = e^{-x/\omega\tau_2}$ and $du = -\frac{e^{-x/\omega\tau_2}}{\omega\tau_2}$

$$dv = \sin nx dx \text{ and } v = \frac{-\cos nx}{n}$$

$$\begin{aligned} &= -\frac{e^{-x/\omega\tau_2} \cos nx}{n} - \int_0^\alpha \frac{e^{-x/\omega\tau_2} \cos nx}{n\omega\tau_2} dx \\ I &= \frac{e^{-x/\omega\tau_2} \sin nx}{n} + \frac{1}{n\omega\tau_2} \left[-\frac{e^{-x/\omega\tau_2} \cos nx}{n} - \frac{1}{n\omega\tau_2} I \right] \end{aligned} \quad (11)$$

$$\therefore I \left[1 + \frac{1}{(n\omega\tau_2)^2} \right] = \frac{e^{-x/\omega\tau_2} \sin nx}{n} - \frac{e^{-x/\omega\tau_2} \cos nx}{n^2 \omega\tau_2}$$

$$I \left[\frac{1+(n\omega\tau_2)^2}{(n\omega\tau_2)^2} \right] = \frac{e^{-x/\omega\tau_2} \sin nx}{n} - \frac{e^{-x/\omega\tau_2} \cos nx}{n^2 \omega\tau_2}$$

$$I = \left[\frac{n(\omega\tau_2)^2 e^{-x/\omega\tau_2} \sin nx}{1+(n\omega\tau_2)^2} - \frac{\omega\tau_2 e^{-x/\omega\tau_2} \cos nx}{1+(n\omega\tau_2)^2} \right]_0^\alpha \quad (12)$$

Applying equation (12) in equation (9),

$$\therefore I = \int_0^\alpha e^{-x/\omega\tau_2} \cos nx dx = \left[\frac{n(\omega\tau_2)^2 e^{-x/\omega\tau_2} \sin nx}{1+(n\omega\tau_2)^2} - \frac{\omega\tau_2 e^{-x/\omega\tau_2} \cos nx}{1+(n\omega\tau_2)^2} \right]_0^\alpha \quad (13)$$

Hence combining equation (8) and (13) in equation (6),

$$A_{n1} = \frac{2}{\pi} \left(I_1 + \frac{E}{R_a} \right) \left[\frac{n(\omega\tau_2)^2 e^{-x/\omega\tau_2} \sin nx}{1+(n\omega\tau_2)^2} - \frac{\omega\tau_2 e^{-x/\omega\tau_2} \cos nx}{1+(n\omega\tau_2)^2} \right]_0^\alpha - \frac{E \sin n\alpha}{R_a n} \quad (14)$$

$$\therefore A_{n1} = \frac{2}{\pi} \left(I_1 + \frac{E}{R_a} \right) \frac{n(\omega\tau_2)^2 e^{-x/\omega\tau_2} \sin n\alpha - \omega\tau_2 e^{-x/\omega\tau_2} \cos n\alpha + \omega\tau_2}{1+(n\omega\tau_2)^2} - \frac{E \sin n\alpha}{R_a n} \quad (15)$$

For the conduction interval $(\alpha + \mu < x < \pi)$

This interval is defined as $\alpha + \mu < x < \pi$

Equation governing this is

$$i(x) = K_2(\cos \theta_2 \sin(x - \theta_2) - P) + \{K_2(\cos \theta_2 \sin(\theta_2 - x) + P) + I_{ao}\}e^{-(x-\alpha-\mu)/\omega\tau} \quad (16)$$

$$\begin{aligned} \therefore A_{n2} &= \frac{2}{\pi} K_2 \cos \theta_2 \int_{\alpha+\mu}^{\pi} \sin(x - \theta_2) \cos nx dx - \frac{2}{\pi} K_2 P \int_{\alpha+\mu}^{\pi} \cos nx dx + \\ &+ \frac{2}{\pi} \{K_2(\cos \theta_2 \sin(\theta_2 - x) + P) + I_{ao}\} \int_{\alpha+\mu}^{\pi} e^{-(x-\alpha-\mu)/\omega\tau} \cos nx dx \end{aligned} \quad (17)$$

Resolving equation (17) into parts and solving accordingly,

$$\int_{\alpha+\mu}^{\pi} \cos nx dx = -\frac{\sin n(\alpha+\mu)}{n} \quad (18)$$

$$\text{And } \int_{\alpha+\mu}^{\pi} \sin(x - \theta_2) \cos nx dx = I_1 \quad (19)$$

Applying Integration by part where

$$\int u dv = uv - \int v du = I_1$$

$$du = \cos(x - \theta_2) dx \quad v = \frac{\sin nx}{n}$$

$$I_1 = -\frac{\sin(x-\theta_2) \sin nx}{n} - \int \frac{\sin nx \cos(x-\theta_2)}{n} dx \quad (20)$$

Integrating equation (20) by parts, where

$$du = -\sin(x - \theta_2) dx \quad \text{and } v = -\frac{\cos nx}{n}$$

$$\begin{aligned} \int \frac{\sin nx \cos(x-\theta_2)}{n} dx &= -\frac{\cos(x-\theta_2) \cos nx}{n} - \int \frac{\cos nx \sin(x-\theta_2)}{n} dx \\ &= -\frac{\cos(x-\theta_2) \cos nx}{n} - \frac{1}{n} I_1 \end{aligned} \quad (21)$$

$$I_1 = \frac{\sin(x-\theta_2) \sin nx}{n} - \frac{1}{n} \left[-\frac{\cos(x-\theta_2) \cos nx}{n} - \frac{1}{n} I_1 \right]$$

$$I_1 = \frac{\sin(x-\theta_2) \sin nx}{n} + \frac{\cos(x-\theta_2) \cos nx}{n^2} + \frac{1}{n^2} I_1$$

$$\therefore I_1 \left\{ 1 - \frac{1}{n^2} \right\} = \frac{\sin(x-\theta_2) \sin nx}{n} + \frac{\cos(x-\theta_2) \cos nx}{n^2}$$

$$I_1 = \frac{n \sin(x-\theta_2) \sin nx}{n^2-1} + \frac{\cos(x-\theta_2) \cos nx}{n^2-1} \quad (22)$$

Hence,

$$\int_{\alpha+\mu}^{\pi} \sin(x - \theta_2) \cos nx dx = I_1 \left[\frac{n \sin(x - \theta_2) \sin nx}{n^2 - 1} + \frac{\cos(x - \theta_2) \cos nx}{n^2 - 1} \right]_{\alpha+\mu}^{\pi}$$

Substituting the limits,

$$\int_{\alpha+\mu}^{\pi} \sin(x - \theta_2) \cos nx dx = \frac{-\cos \theta_2 \cos n\pi - n \sin(\alpha + u - \theta_2) \sin n(\alpha + u) - \cos(\alpha + u - \theta_2) \cos n(\alpha + u)}{n^2 - 1} \quad (23)$$

$$\text{Also} \quad \int_{\alpha+\mu}^{\pi} e^{-(x-\alpha-u)/\omega\tau} \cos nx dx = I_2 \quad (24)$$

Using integration by part; $\int u dv = uv - \int v du = I_2$

$$\text{Where} \quad du = -\frac{1}{\omega\tau} e^{-(x-\alpha-u)/\omega\tau} dx \quad \text{and} \quad v = \frac{\sin nx}{n}$$

$$I_2 = \frac{e^{-(x-\alpha-\mu)/\omega\tau} \sin nx}{n} + \frac{1}{n\omega\tau} \int e^{-(x-\alpha-\mu)/\omega\tau} \sin nx dx \quad (25)$$

Integrating $\int e^{-(x-\alpha-\mu)/\omega\tau} \sin nx dx$ by parts, where

$$u = e^{-(x-\alpha-u)/\omega\tau} \quad \text{and} \quad dv = \sin nx$$

$$du = \frac{-e^{-(x-\alpha-\mu)/\omega\tau}}{n\omega\tau} \quad \text{and} \quad v = \frac{-\cos nx}{n}$$

$$I_2 = \frac{e^{-(x-\alpha-u)/\omega\tau} \sin nx}{n} + \frac{1}{n\omega\tau} \left[\frac{-\cos nx e^{-(x-\alpha-u)/\omega\tau}}{n} - \frac{1}{n\omega\tau} I_2 \right]$$

$$I_2 = \left[\frac{e^{-(x-\alpha-\mu)/\omega\tau} \sin nx}{n} - \frac{\cos nx e^{-(x-\alpha-\mu)/\omega\tau}}{n^2 \omega\tau} - \frac{1}{(n\omega\tau)^2} I_2 \right]$$

$$I_2 \left[1 + \frac{1}{(n\omega\tau)^2} \right] = \frac{e^{-(x-\alpha-\mu)/\omega\tau} \sin nx}{n} - \frac{\cos nx e^{-(x-\alpha-\mu)/\omega\tau}}{n^2 \omega\tau}$$

$$\therefore I_2 = \frac{(n\omega\tau)^2}{1+(n\omega\tau)^2} \left\{ \frac{e^{-(x-\alpha-\mu)/\omega\tau} \sin nx}{n} - \frac{\cos nx e^{-(x-\alpha-\mu)/\omega\tau}}{n^2 \omega\tau} \right\}$$

$$I_2 = \frac{n(\omega\tau)^2 e^{-(x-\alpha-\mu)/\omega\tau} \sin nx - (\omega\tau)^2 \cos nx e^{-(x-\alpha-\mu)/\omega\tau}}{1+(n\omega\tau)^2} \quad (26)$$

Applying equation (26) in equation (24),

$$\begin{aligned} \int_{\alpha+u}^{\pi} e^{-(x-\alpha-\mu)/\omega\tau} \cos nx dx &= \left[\frac{n(\omega\tau)^2 e^{-(x-\alpha-\mu)/\omega\tau} \sin nx - (\omega\tau)^2 \cos nx e^{-(x-\alpha-\mu)/\omega\tau}}{1+(n\omega\tau)^2} \right]_{\alpha+u}^{\pi} \\ &= \left[\frac{n(\omega\tau)^2 e^{-(\pi-\alpha-\mu)/\omega\tau} \sin n\pi - \omega\tau \cos n\pi e^{-(\pi-\alpha-\mu)/\omega\tau}}{1+(n\omega\tau)^2} - \frac{n(\omega\tau)^2 \sin n(\alpha+\mu) - \omega\tau \cos n(\alpha+\mu)}{1+(n\omega\tau)^2} \right] \end{aligned}$$

$$= \frac{-\omega\tau\cos n\pi e^{-(\pi-\alpha-\mu)/\omega\tau} - n(\omega\tau)^2 \sin n(\alpha+\mu) + \omega\tau \cos n(\alpha+\mu)}{1+(n\omega\tau)^2} \quad (27)$$

Combining equations (18), (23) and (27) in equation (16), gives

$$\begin{aligned} A_{n2} &= \frac{2}{\pi} K_2 \cos \theta_2 \left[\frac{-\cos \theta_2 \cos n\pi - n \sin(\alpha+\mu-\theta_2) \sin n(\alpha+\mu) - \cos(\alpha+\mu-\theta_2) \cos n(\alpha+\mu)}{n^2-1} \right] \\ &\quad - \frac{2}{\pi} K_2 P \left[-\frac{\sin n(\alpha+\mu)}{n} \right] \\ &\quad + \frac{2}{\pi} \{K_2(\cos \theta_2 \sin(\theta_2 - x) + P) + I_{a0}\} \left[\frac{-\omega\tau\cos n\pi e^{-(\pi-\alpha-\mu)/\omega\tau} - n(\omega\tau)^2 \sin n(\alpha+\mu) + \omega\tau \cos n(\alpha+\mu)}{1+(n\omega\tau)^2} \right] \end{aligned} \quad (28)$$

For the forward commutation interval

This interval is defined as $\alpha < x < \alpha + \mu$

$$\text{And the governing equation is } i(t) = K_1 \{ \sin(\omega t + \alpha - \theta_1) + \sin(\theta_1 - \alpha) e^{-t/\tau_1} \} \quad (29)$$

In this case, $x = \omega t + \alpha$

$$i(x) = K_1 \{ \sin(x - \theta_1) + \sin(\theta_1 - \alpha) e^{-(x-\alpha)/\omega\tau_1} \} \quad (30)$$

$$A_{n3} = \int_{\alpha}^{\alpha+\mu} i(x) \cos nxdx \quad (31)$$

Applying equation (30) in equation (31),

$$A_{n3} = \frac{2}{\pi} K_1 \int_{\alpha}^{\alpha+\mu} \{ \sin(x - \theta_1) + \sin(\theta_1 - \alpha) e^{-(x-\alpha)/\omega\tau_1} \} \cos nxdx \quad (32)$$

Resolving equation (32) into parts and solving accordingly,

$$A_{n3} = \frac{2}{\pi} K_1 \int_{\alpha}^{\alpha+\mu} \sin(x - \theta_1) \cos nxdx + \frac{2}{\pi} K_1 \sin(\theta_1 - \alpha) \int_{\alpha}^{\alpha+\mu} e^{-(x-\alpha)/\omega\tau_1} \cos nxdx \quad (33)$$

Applying integration by part

$$dv = \cos nxdx \quad \text{and} \quad u = \sin(x - \theta_1)$$

$$v = \frac{\sin nx}{n} \quad \text{and} \quad du = \cos(x - \theta_1)$$

Therefore,

$$I = \frac{\sin nx \sin(x-\theta_1)}{n} - \frac{1}{n} \int \sin nx \cos(x - \theta_1) dx \quad (34)$$

Applying integration by part for $\int \sin nx \cos(x - \theta_1) dx$

$$\int u dv = uv - \int v du$$

Where $v = \frac{-\cos nx}{n}$ and $dv = \sin nx$

$$u = \cos(x - \theta_1) \text{ and } du = \sin(x - \theta_1)$$

$$\therefore \int \sin nx \cos(x - \theta_1) dx = \frac{-\cos nx \cos(x - \theta_1)}{n} - \frac{1}{n} \int \sin n(x - \theta_1) \cos nx dx \quad (35)$$

Hence,
$$I = \frac{\sin nx \sin(x - \theta_1)}{n} + \frac{-\cos nx \cos(x - \theta_1)}{n^2} + \frac{1}{n^2} I \quad (36)$$

$$I \left[1 - \frac{1}{n^2} \right] = \frac{\sin nx \sin(x - \theta_1)}{n} + \frac{-\cos nx \cos(x - \theta_1)}{n^2}$$

$$\therefore I = \frac{n \sin nx \sin(x - \theta_1) + \cos nx \cos(x - \theta_1)}{n^2 - 1} \quad (37)$$

$$\int_{\alpha}^{\alpha+\mu} \sin(x - \theta_1) \cos nx dx = \left[\frac{n \sin nx \sin(x - \theta_1) + \cos nx \cos(x - \theta_1)}{n^2 - 1} \right]_{\alpha}^{\alpha+\mu}$$

$$\int_{\alpha}^{\alpha+\mu} \sin(x - \theta_1) \cos nx dx = \left[\frac{n \sin n(\alpha+u) \sin(\alpha+u - \theta_1) + \cos n(\alpha+u) \cos(\alpha+u - \theta_1)}{n^2 - 1} \right] - \left[\frac{n \sin n\alpha \sin(\alpha - \theta_1) + \cos n\alpha \cos(\alpha - \theta_1)}{n^2 - 1} \right] \quad (38)$$

Therefore,

$$\int_{\alpha}^{\alpha+\mu} \sin(x - \theta_1) \cos nx dx = \frac{n \sin n(\alpha+u) \sin(\alpha+u - \theta_1) + \cos n(\alpha+u) \cos(\alpha+u - \theta_1) - n \sin n\alpha \sin(\alpha - \theta_1) - \cos n\alpha \cos(\alpha - \theta_1)}{n^2 - 1} \quad (39)$$

Also, $\int_{\alpha}^{\alpha+\mu} e^{-(x-\alpha)/\omega\tau_1} \cos nx dx = I_2$

Applying Integration by parts

$$du = \frac{-e^{-(x-\alpha)/\omega\tau_1}}{n\omega\tau_1} \text{ and } v = \frac{\sin nx}{n}$$

$$I_2 = \frac{e^{-(x-\alpha)/\omega\tau_1} \sin nx}{n} + \int_{\alpha}^{\alpha+u} \frac{e^{-(x-\alpha)/\omega\tau_1} \sin nx}{n\omega\tau_1} dx \quad (40)$$

Integrating $\int_{\alpha}^{\alpha+\mu} \frac{e^{-(x-\alpha)/\omega\tau_1} \sin nx}{n\omega\tau_1} dx$ by parts,

Where $du = \frac{-e^{-(x-\alpha)/\omega\tau_1}}{n\omega\tau_1}$ $v = \frac{-\cos nx}{n}$

$$\therefore \int_{\alpha}^{\alpha+\mu} \frac{e^{-(x-\alpha)/\omega\tau_1} \sin nx}{n\omega\tau_1} dx = - \frac{e^{-(x-\alpha)/\omega\tau_1} \cos nx}{n} - \left[\frac{1}{n\omega\tau_1} \right] \int_{\alpha}^{\alpha+\mu} \frac{e^{-(x-\alpha)/\omega\tau_1} \cos nx}{n\omega\tau_1} dx \quad (41)$$

Applying equation (40) in equation (39), therefore

$$I_2 = \frac{e^{-(x-\alpha)/\omega\tau_1} \sin nx}{n} + \frac{1}{n\omega\tau_1} \left[\frac{e^{-(x-\alpha)/\omega\tau_1} \cos nx}{n} - \frac{1}{n\omega\tau_1} I_2 \right]$$

$$I_2 \left[1 + \frac{1}{(n\omega\tau_1)^2} \right] = \frac{e^{-(x-\alpha)/\omega\tau_1} \sin nx}{n} - \frac{e^{-(x-\alpha)/\omega\tau_1} \cos nx}{n^2\omega\tau_1}$$

$$I_2 = \frac{(n\omega\tau_1)^2}{1+(n\omega\tau_1)^2} \left\{ \frac{e^{-(x-\alpha)/\omega\tau_1} \sin nx}{n} - \frac{e^{-(x-\alpha)/\omega\tau_1} \cos nx}{n^2\omega\tau_1} \right\}$$

Therefore,

$$\begin{aligned} I_2 &= \int_{\alpha}^{\alpha+\mu} e^{-(x-\alpha)/\omega\tau_1} \cos nx dx = \left[\frac{n(\omega\tau_1)^2 e^{-(x-\alpha)/\omega\tau_1} \sin nx - \omega\tau_1 e^{-(x-\alpha)/\omega\tau_1} \cos nx}{1+(n\omega\tau_1)^2} \right]_{\alpha}^{\alpha+\mu} \\ &= \frac{n(\omega\tau_1)^2 e^{-u/\omega\tau_1} \sin n(\alpha+u) - \omega\tau_1 e^{-u/\omega\tau_1} \cos n(\alpha+u) - n(\omega\tau_1)^2 \sin n\alpha + \omega\tau_1 \cos n\alpha}{1+(n\omega\tau_1)^2} \end{aligned} \quad (42)$$

Therefore, combining equations (33) and (42) in equation (32) gives

$$\begin{aligned} A_{n3} &= \frac{2}{\pi} K_1 \left\{ \frac{n \sin n(\alpha+u) \sin(\alpha+u-\theta_1) + \cos n(\alpha+u) \cos(\alpha+u-\theta_1) - n \sin n\alpha \sin(\alpha-\theta_1) - \cos n\alpha \cos(\alpha-\theta_1)}{n^2-1} \right\} + \\ &\frac{2}{\pi} K_1 \sin(\theta_1 - \alpha) \left\{ \frac{n(\omega\tau_1)^2 e^{-u/\omega\tau_1} \sin n(\alpha+u) - \omega\tau_1 e^{-u/\omega\tau_1} \cos n(\alpha+u) - n(\omega\tau_1)^2 \sin n\alpha + \omega\tau_1 \cos n\alpha}{1+(n\omega\tau_1)^2} \right\} \end{aligned} \quad (43)$$

Since $A_n = A_{n1} + A_{n2} + A_{n3}$

Therefore combining equations (15), (28) and (32) for the A_n 's,

$$\begin{aligned} A_n &= \\ &\frac{2}{\pi} \left(I_1 + \frac{E}{R_a} \right) \frac{n(\omega\tau_2)^2 e^{-x/\omega\tau_2} \sin n\alpha - \omega\tau_2 e^{-x/\omega\tau_2} \cos n\alpha + \omega\tau_2}{1+(n\omega\tau_2)^2} - \frac{E}{R_a} \frac{\sin n\alpha}{n} + \\ &\frac{2}{\pi} K_2 \cos\theta_2 \left[\frac{-\cos\theta_2 \cos n\pi - n \sin(\alpha+\mu-\theta_2) \sin n(\alpha+\mu) - \cos(\alpha+\mu-\theta_2) \cos n(\alpha+\mu)}{n^2-1} \right] - \frac{2}{\pi} K_2 P \left[-\frac{\sin n(\alpha+\mu)}{n} \right] \\ &+ \frac{2}{\pi} \{ K_2 (\cos\theta_2 \sin(\theta_2 - x) + P) + I_{a0} \} \left[\frac{-\omega\tau \cos n\pi e^{-(\pi-\alpha-\mu)/\omega\tau} - n(\omega\tau)^2 \sin n(\alpha+\mu) + \omega\tau \cos n(\alpha+\mu)}{1+(n\omega\tau)^2} \right] \\ &+ \frac{2}{\pi} K_1 \sin(\theta_1 - \alpha) \left\{ \frac{n(\omega\tau_1)^2 e^{-\mu/\omega\tau_1} \sin n(\alpha+\mu) - \omega\tau_1 e^{-\mu/\omega\tau_1} \cos n(\alpha+\mu) - n(\omega\tau_1)^2 \sin n\alpha + \omega\tau_1 \cos n\alpha}{1+(n\omega\tau_1)^2} \right\} \\ &+ \frac{2}{\pi} K_1 \left\{ \frac{n \sin n(\alpha+\mu) \sin(\alpha+\mu-\theta_1) + \cos n(\alpha+\mu) \cos(\alpha+\mu-\theta_1) - n \sin n\alpha \sin(\alpha-\theta_1) - \cos n\alpha \cos(\alpha-\theta_1)}{n^2-1} \right\} \end{aligned} \quad (44)$$

$$A_n = \frac{1}{\pi} \left[\begin{aligned} & \frac{k_3}{n+1} [\cos((n+1)(\alpha+u) - \theta_2) - (-1)^{n+1} \cos \theta_2] \\ & - \frac{k_3}{n-1} [\cos((n-1)(\alpha+u) + \theta_2) - (-1)^{n-1} \cos \theta_2] \\ & + 2 \left(\frac{A_6 \sin n(\alpha+u) - A_5 \sin n\alpha}{n} \right) \\ & + \frac{2k_6 \omega \tau}{1 + (n\omega\tau)^2} \left[\cos n(\alpha+u) - n\omega\tau \sin n(\alpha+u) - (-1)^n e^{-\left(\frac{\pi-\alpha-u}{\omega\tau}\right)} \right] \\ & + \frac{2(I_1 + A_3) \omega \tau_2}{1 + (n\omega\tau_2)^2} \left(1 + e^{-\frac{\alpha}{\omega\tau_2}} (n\omega\tau_2 \sin n\alpha - \cos n\alpha) \right) \\ & + \frac{k_1}{n+1} (\cos((n+1)\alpha - \theta_1) - \cos((n+1)(\alpha+u) - \theta_1)) \\ & - \frac{k_1}{n-1} (\cos((n-1)\alpha + \theta_1) - \cos((n-1)(\alpha+u) + \theta_1)) \\ & + \frac{2k_1 \sin(\theta_1 - \alpha) \omega \tau_1}{1 + (n\omega\tau_1)^2} \left(e^{-\frac{u}{\omega\tau_1}} (n\omega\tau_1 \sin n(\alpha+u) - \cos n(\alpha+u)) + \cos n\alpha \right) \end{aligned} \right] \quad (45)$$

For B_n

Free-wheeling interval

$$B_{n1} = \frac{2}{\pi} \int_0^\alpha i(x) \sin nxdx \quad (46)$$

$$\therefore B_{n1} = \frac{2}{\pi} \int_0^\alpha \left[\left(I_1 + \frac{E}{R_a} \right) e^{-x/\omega\tau_2} - \frac{E}{R_a} \right] \sin nxdx$$

$$B_{n1} = \frac{2}{\pi} \left(I_1 + \frac{E}{R_a} \right) \int_0^\alpha e^{-x/\omega\tau_2} \sin nxdx - \frac{2}{\pi} \frac{E}{R_a} \int_0^\alpha \sin nxdx \quad (47)$$

Resolving equation (47) into parts and solving accordingly,

$$\therefore \int_0^\alpha \sin nxdx = \left[\frac{-\cos nx}{n} \right]_0^\alpha \quad (48)$$

$$= \frac{-\cos n\alpha}{n} + \frac{1}{n}$$

$$= \frac{1 - \cos n\alpha}{n} \quad (49)$$

$$\text{And } \int_0^\alpha e^{-x/\omega\tau_2} \sin nxdx = I_1 \quad (50)$$

Applying integration by part for the equation (50)

$$\int u dv = uv - \int v du$$

Where $u = e^{-x/\omega\tau_2}$ and $du = -\frac{e^{-x/\omega\tau_2}}{\omega\tau_2}$

$$dv = \sin nx dx \quad v = \frac{-\cos nx}{n}$$

$$\begin{aligned} I_1 &= \frac{-e^{-x/\omega\tau_2} \cos nx}{n} - \int_0^\alpha \frac{e^{-x/\omega\tau_2} \cos nx}{n\omega\tau_2} dx \\ &= \frac{-e^{-x/\omega\tau_2} \cos nx}{n} - \frac{1}{n\omega\tau_2} \int_0^\alpha e^{-x/\omega\tau_2} \cos nx dx \end{aligned} \quad (51)$$

Applying integration by part for $\int_0^\alpha e^{-x/\omega\tau_2} \cos nx dx$ again,

$$\int u dv = uv - \int v du$$

Where $u = e^{-x/\omega\tau_2}$ and $du = -\frac{e^{-x/\omega\tau_2}}{\omega\tau_2}$

$$dv = \cos nx dx \quad v = \frac{\sin nx}{n}$$

$$\int_0^\alpha e^{-x/\omega\tau_2} \cos nx dx = \frac{e^{-x/\omega\tau_2} \sin nx}{n} + \int_0^\alpha \frac{e^{-x/\omega\tau_2} \cos nx}{n\omega\tau_2} dx \quad (52)$$

Applying equation (52) in equation (51)

$$I_1 = \frac{-e^{-x/\omega\tau_2} \sin nx}{n} + \frac{1}{n\omega\tau_2} \left[-\frac{e^{-x/\omega\tau_2} \cos nx}{n} - \frac{1}{n\omega\tau_2} I_1 \right]$$

$$\therefore I_1 \left[1 + \frac{1}{(n\omega\tau_2)^2} \right] = \frac{-e^{-x/\omega\tau_2} \cos nx}{n} - \frac{e^{-x/\omega\tau_2} \sin nx}{n^2 \omega\tau_2}$$

$$I_1 = \frac{(n\omega\tau_2)^2}{1+(n\omega\tau_2)^2} \left[\frac{-e^{-x/\omega\tau_2} \cos nx}{n} - \frac{e^{-x/\omega\tau_2} \sin nx}{n^2 \omega\tau_2} \right]$$

$$\therefore I_1 = \frac{-n(\omega\tau_2)^2 e^{-x/\omega\tau_2} \cos nx}{1+(n\omega\tau_2)^2} - \frac{\omega\tau_2 e^{-x/\omega\tau_2} \sin nx}{1+(n\omega\tau_2)^2} \quad (53)$$

$$\therefore I_1 = \int_0^\alpha e^{-x/\omega\tau_2} \sin nx dx = \left[\frac{-n(\omega\tau_2)^2 e^{-x/\omega\tau_2} \cos nx}{1+(n\omega\tau_2)^2} - \frac{\omega\tau_2 e^{-x/\omega\tau_2} \sin nx}{1+(n\omega\tau_2)^2} \right]_0^\alpha \quad (54)$$

$$= \frac{-n(\omega\tau_2)^2 e^{-\alpha/\omega\tau_2} \cos n\alpha}{1+(n\omega\tau_2)^2} - \frac{\omega\tau_2 e^{-\alpha/\omega\tau_2} \sin n\alpha}{1+(n\omega\tau_2)^2} + \frac{n(\omega\tau_2)^2}{1+(n\omega\tau_2)^2}$$

$$= \frac{-n(\omega\tau_2)^2 e^{-\alpha/\omega\tau_2} \cos n\alpha - \omega\tau_2 e^{-\alpha/\omega\tau_2} \sin n\alpha + n(\omega\tau_2)^2}{1+(n\omega\tau_2)^2} \quad (55)$$

Combining equations (49) and (55) in equation (47),

$$\therefore B_{n1} = \frac{2}{\pi} \left(I_1 + \frac{E}{R_a} \right) \left[\frac{-n(\omega\tau_2)^2 e^{-\alpha/\omega\tau_2} \cos n\alpha - \omega\tau_2 e^{-\alpha/\omega\tau_2} \sin n\alpha + n(\omega\tau_2)^2}{1 + (n\omega\tau_2)^2} \right] - \frac{2}{\pi} \frac{E}{R_a} \left(\frac{1 - \cos n\alpha}{n} \right) \quad (56)$$

For conduction interval

This interval is defined as; $\alpha + u < x < \pi$

And the governing equation is

$$i(x) = K_2(\cos \theta_2 \sin(x - \theta_2) - P) + \{K_2(\cos \theta_2 \sin(\theta_2 - x) + P) + I_{ao}\} e^{-(x-\alpha-u)/\omega\tau} \quad (57)$$

$$\text{But } B_{n2} = \frac{2}{\pi} \int_{\alpha+u}^{\pi} i(x) \sin nxdx$$

Therefore,

$$\begin{aligned} B_{n2} &= \frac{2}{\pi} K_2 \cos \theta_2 \int_{\alpha+u}^{\pi} \sin(x - \theta_2) nxdx - \frac{2}{\pi} K_2 P \int_{\alpha+u}^{\pi} \cos nxdx \\ &\quad + \frac{2}{\pi} \{ \{K_2(\cos \theta_2 \sin(\theta_2 - x) + P) + I_{ao}\} \int_{\alpha+u}^{\pi} e^{-(x-\alpha-u)/\omega\tau} \cos nxdx \end{aligned} \quad (58)$$

Breaking the equation into parts and applying different methods of analysis,

$$I_1 = \int_{\alpha+u}^{\pi} \sin(x - \theta_2) \sin nxdx \quad (59)$$

Applying integration by part to equation (59),

$$\int u dv = uv - \int v du = I_1$$

$$du = \cos(x - \theta_2) dx \quad v = \frac{-\cos nx}{n}$$

$$I_1 = -\frac{\sin(x-\theta_2) \cos nx}{n} + \int \frac{\cos nx \cos(x-\theta_2)}{n} dx \quad (60)$$

Integrating $\int \frac{\cos nx \cos(x-\theta_2)}{n} dx$ by parts

$$du = -\sin(x - \theta_2) dx \quad \text{and} \quad v = \frac{\sin nx}{n}$$

$$\int \frac{\cos nx \cos(x-\theta_2)}{n} dx = \frac{\cos(x-\theta_2) \sin nx}{n} + \int \frac{\sin nx \sin(x-\theta_2)}{n} dx \quad (61)$$

$$I_1 = -\frac{\sin(x-\theta_2) \cos nx}{n} + \frac{1}{n} \left[\frac{\cos(x-\theta_2) \sin nx}{n} + \frac{1}{n} I_1 \right]$$

$$I_1 \left(1 - \frac{1}{n^2} \right) = \frac{-\sin(x-\theta_2) \cos nx}{n} + \frac{\cos(x-\theta_2) \sin nx}{n^2}$$

$$I_1 = \frac{n^2}{n^2-1} \left\{ \frac{-\sin(x-\theta_2) \cos nx}{n} + \frac{\cos(x-\theta_2) \sin nx}{n^2} \right\} \quad (62)$$

Therefore,

$$I_1 = \int_{\alpha+\mu}^{\pi} \sin(x - \theta_2) \sin nx dx = \frac{n^2}{n^2-1} \left[\frac{-\sin(x-\theta_2) \cos nx}{n} + \frac{\cos(x-\theta_2) \sin nx}{n^2} \right]_{\alpha+\mu}^{\pi} \quad (63)$$

$$= \frac{-n \sin(\pi-\theta_2) \cos n\pi + \cos(\pi-\theta_2) \sin n\pi}{n^2-1} - \frac{-n \sin(\alpha+u-\theta_2) \cos n(\alpha+u) + \cos(\alpha+u-\theta_2) \sin n(\alpha+u)}{n^2-1}$$

$$= \frac{n \sin \theta_2 \cos n\pi + n \sin(\alpha+u-\theta_2) \cos n(\alpha+u) - \cos(\alpha+u-\theta_2) \sin n(\alpha+u)}{n^2-1} \quad (64)$$

$$\text{Also, } \int_{\alpha+\mu}^{\pi} \sin nx dx = \left[-\frac{\cos nx}{n} \right]_{\alpha+\mu}^{\pi}$$

$$= \frac{-\cos n\pi + \cos n(\alpha+\mu)}{n}$$

$$= \frac{\cos n(\alpha+\mu) - \cos n\pi}{n} \quad (65)$$

$$\text{And } \int_{\alpha+\mu}^{\pi} e^{-(x-\alpha-u)/\omega\tau} \sin nx dx = I_2 \quad (66)$$

Using integration by parts

$$\int u dv = uv - \int v du$$

$$\text{Where } u = e^{-(x-\alpha-\mu)/\omega\tau} \text{ and } du = -\frac{e^{-(x-\alpha-\mu)/\omega\tau}}{\omega\tau}$$

$$dv = \sin nx dx \text{ and } v = \frac{-\cos nx}{n}$$

$$I_1 = \frac{-e^{-(x-\alpha-\mu)/\omega\tau} \cos nx}{n} - \int_{\alpha+\mu}^{\pi} \frac{e^{-(x-\alpha-\mu)/\omega\tau} \cos nx}{n\omega\tau} dx \quad (67)$$

$$= \frac{-e^{-(x-\alpha-\mu)/\omega\tau} \cos nx}{n} - \frac{1}{n\omega\tau} \int_{\alpha+\mu}^{\pi} e^{-(x-\alpha-\mu)/\omega\tau} \cos nx dx \quad (68)$$

Applying integration by part again,

$$\int u dv = uv - \int v du$$

$$\text{Where } u = e^{-(x-\alpha-\mu)/\omega\tau} \text{ and } du = -\frac{e^{-(x-\alpha-\mu)/\omega\tau}}{\omega\tau}$$

$$dv = \cos nx dx \text{ and } v = \frac{\sin nx}{n}$$

$$= \frac{e^{-(x-\alpha-\mu)/\omega\tau} \sin nx}{n} + \int_0^{\alpha} \frac{e^{-(x-\alpha-\mu)/\omega\tau} \cos nx}{n\omega\tau} dx$$

$$\begin{aligned}
\therefore I_1 &= \frac{-e^{-(x-\alpha-\mu)/\omega\tau} \sin nx}{n} + \frac{1}{n\omega\tau} \left[-\frac{e^{-(x-\alpha-\mu)/\omega\tau} \cos nx}{n} - \frac{1}{n\omega\tau} I_1 \right] \\
\therefore I_1 \left[1 + \frac{1}{(n\omega\tau)^2} \right] &= \frac{-e^{-(x-\alpha-\mu)/\omega\tau} \cos nx}{n} - \frac{e^{-(x-\alpha-\mu)/\omega\tau} \sin nx}{n^2\omega\tau} \\
I_1 &= \frac{(n\omega\tau)^2}{1+(n\omega\tau)^2} \left[\frac{-e^{-(x-\alpha-\mu)/\omega\tau} \cos nx}{n} - \frac{e^{-(x-\alpha-\mu)/\omega\tau} \sin nx}{n^2\omega\tau} \right] \\
I_1 &= \frac{-n(\omega\tau)^2 e^{-(x-\alpha-\mu)/\omega\tau} \cos nx}{1+(n\omega\tau)^2} - \frac{\omega\tau e^{-(x-\alpha-\mu)/\omega\tau} \sin nx}{1+(n\omega\tau)^2} \tag{69}
\end{aligned}$$

Hence,

$$\begin{aligned}
\int_{\alpha+u}^{\pi} e^{-(x-\alpha-\mu)/\omega\tau} \sin nx dx &= \left[\frac{-n(\omega\tau)^2 e^{-(x-\alpha-\mu)/\omega\tau} \cos nx}{1+(n\omega\tau)^2} - \frac{\omega\tau e^{-(x-\alpha-\mu)/\omega\tau} \sin nx}{1+(n\omega\tau)^2} \right]_{\alpha+u}^{\pi} \\
&= \frac{[-n(\omega\tau)^2 e^{-(x-\alpha-\mu)/\omega\tau} \cos n\pi]}{1+(n\omega\tau)^2} - \frac{[\omega\tau e^{-(x-\alpha-\mu)/\omega\tau} \sin n\pi]}{1+(n\omega\tau)^2} - \frac{[-n(\omega\tau)^2 \cos n(\alpha+\mu)] - [\omega\tau \sin n(\alpha+\mu)]}{1+(n\omega\tau)^2} \\
&= \frac{n(\omega\tau)^2 e^{-(x-\alpha-\mu)/\omega\tau} \cos n\pi + n(\omega\tau)^2 \cos n(\alpha+\mu) - \omega\tau \sin n(\alpha+\mu)}{1+(n\omega\tau)^2} \tag{70}
\end{aligned}$$

Combining equations (64), (65) and (70) in equations (58), gives

$$\begin{aligned}
\therefore B_{n2} &= \frac{2}{\pi} K_2 \cos \theta_2 \left[\frac{n \sin \theta_2 \cos n\pi + n \sin(\alpha+\mu-\theta_2) \cos n(\alpha+\mu) - \cos(\alpha+\mu-\theta_2) \sin n(\alpha+\mu)}{n^2-1} \right] \\
&\quad - \frac{2}{\pi} K_2 P \left[\frac{\cos n(\alpha+\mu) - \cos n\pi}{n} \right] \\
&\quad + \frac{2}{\pi} \{ K_2 (\cos \theta_2 \sin(\theta_2 - x) + P + I_{a0}) \left[\frac{n(\omega\tau)^2 e^{-(x-\alpha-\mu)/\omega\tau} \cos n\pi + n(\omega\tau)^2 \cos n(\alpha+\mu) - \omega\tau \sin n(\alpha+\mu)}{1+(n\omega\tau)^2} \right] \} \tag{71}
\end{aligned}$$

For the forward commutation interval

This interval is defined as; $\alpha < x < \alpha + \mu$

$$\text{And the governing equation is } i(t) = K_1 \{ \sin(\omega t + \alpha - \theta_1) + \sin(\theta_1 - \alpha) e^{-t/\tau_1} \} \tag{72}$$

In this case, $x = \omega t + \alpha$

$$i(x) = K_1 \{ \sin(x - \theta_1) + \sin(\theta_1 - \alpha) e^{-(x-\alpha)/\omega\tau_1} \}$$

$$B_{n3} = \frac{2}{\pi} K_1 \int_{\alpha}^{\alpha+\mu} i(x) \sin nx dx$$

$$B_{n3} = \frac{2}{\pi} K_1 \int_{\alpha}^{\alpha+\mu} \{ \sin(x - \theta_1) + \sin(\theta_1 - \alpha) e^{-(x-\alpha)/\omega\tau_1} \} \sin nx dx$$

$$B_{n3} = \frac{2}{\pi} K_1 \int_{\alpha}^{\alpha+\mu} \sin(x - \theta_1) \sin nxdx + \frac{2}{\pi} K_1 \sin(\theta_1 - \alpha) \int_{\alpha}^{\alpha+\mu} e^{-(x-\alpha)/\omega\tau_1} \sin nxdx \quad (73)$$

Breaking the equation into parts and applying different methods of analysis,

$$\int_{\alpha}^{\alpha+\mu} \sin(x - \theta_1) \sin nxdx = I \quad (74)$$

Integrating by part $dv = \cos nxdx$ and $u = \sin(x - \theta_1)$

$$v = \frac{\sin nx}{n} \text{ and } du = \cos(x - \theta_1)$$

$$I = \frac{-\cos nx \sin(x-\theta_1)}{n} + \frac{1}{n} \int \cos nx \cos(x - \theta_1) dx \quad (75)$$

Applying integration by part for $\int \cos nx \cos(x - \theta_1) dx$

$$\int u dv = uv - \int v du$$

$$v = \frac{\sin nx}{n} \text{ and } dv = \cos nx$$

$$u = \cos(x - \theta_1) \text{ and } du = -\sin(x - \theta_1)$$

$$\therefore \int \cos nx \cos(x - \theta_1) dx = \frac{\sin nx \cos(x-\theta_1)}{n} + \frac{1}{n} \int \sin n(x - \theta_1) \sin nxdx$$

$$I = \frac{-\cos nx \sin(x-\theta_1)}{n} + \frac{-\sin nx \cos(x-\theta_1)}{n^2} + \frac{1}{n^2} I$$

$$I \left[1 - \frac{1}{n^2} \right] = \frac{-\cos nx \sin(x-\theta_1)}{n} + \frac{-\sin nx \cos(x-\theta_1)}{n^2}$$

$$\therefore I = \frac{-n \cos nx \sin(x-\theta_1) + \sin nx \cos(x-\theta_1)}{n^2 - 1} \quad (76)$$

$$\int_{\alpha}^{\alpha+\mu} \sin(x - \theta_1) \sin nxdx = \left[\frac{-n \cos nx \sin(x-\theta_1) + \sin nx \cos(x-\theta_1)}{n^2 - 1} \right]_{\alpha}^{\alpha+\mu} \quad (77)$$

$$\int_{\alpha}^{\alpha+\mu} \sin(x - \theta_1) \sin nxdx$$

$$= \left[\frac{-n \cos n(\alpha + \mu) \sin(\alpha + \mu - \theta_1) + \sin n(\alpha + \mu) \cos(\alpha + \mu - \theta_1)}{n^2 - 1} \right] - \left[\frac{-n \cos n\alpha \sin(\alpha - \theta_1) + \sin n\alpha \cos(\alpha - \theta_1)}{n^2 - 1} \right] \quad (78)$$

$$\int_{\alpha}^{\alpha+\mu} \sin(x - \theta_1) \sin nxdx = \frac{-n \sin n(\alpha + \mu) \sin(\alpha + \mu - \theta_1) + \sin n(\alpha + \mu) \cos(\alpha + \mu - \theta_1) + n \cos n\alpha \sin(\alpha - \theta_1) - \sin n\alpha \cos(\alpha - \theta_1)}{n^2 - 1} \quad (79)$$

$$\text{Then } \int_{\alpha}^{\alpha+\mu} e^{-(x-\alpha)/\omega\tau_1} \sin nx dx = I_2 \quad (80)$$

Applying integration by parts, where

$$du = \frac{-e^{-(x-\alpha)/\omega\tau_1}}{\omega\tau_1} \quad \text{and} \quad v = \frac{-\cos nx}{n}$$

$$I_2 = \frac{-e^{-(x-\alpha)/\omega\tau_1} \cos nx}{n} - \int_{\alpha}^{\alpha+\mu} \frac{e^{-(x-\alpha)/\omega\tau_1} \cos nx}{n\omega\tau_1} dx \quad (81)$$

Applying integration by parts for $\int_{\alpha}^{\alpha+\mu} e^{-(x-\alpha)/\omega\tau_1} \cos nx dx$

$$du = \frac{-e^{-(x-\alpha)/\omega\tau_1}}{n\omega\tau_1} \quad \text{and} \quad v = \frac{\sin nx}{n}$$

$$\therefore \int_{\alpha}^{\alpha+\mu} \frac{e^{-(x-\alpha)/\omega\tau_1} \sin nx}{n\omega\tau_1} dx = -\frac{e^{-(x-\alpha)/\omega\tau_1} \cos nx}{n} - \int_{\alpha}^{\alpha+\mu} \frac{e^{-(x-\alpha)/\omega\tau_1} \cos nx}{n\omega\tau_1} dx$$

$$I_2 = \frac{-e^{-(x-\alpha)/\omega\tau_1} \cos nx}{n} - \frac{1}{n\omega\tau_1} \left[\frac{e^{-(x-\alpha)/\omega\tau_1} \sin nx}{n} + \frac{1}{n\omega\tau_1} I_2 \right]$$

$$I_2 \left[1 + \frac{1}{(n\omega\tau_1)^2} \right] = \frac{-e^{-(x-\alpha)/\omega\tau_1} \cos nx}{n} - \frac{e^{-(x-\alpha)/\omega\tau_1} \sin nx}{n^2 \omega\tau_1}$$

$$I_2 = \frac{(n\omega\tau_1)^2}{1+(n\omega\tau_1)^2} \left\{ \frac{-e^{-(x-\alpha)/\omega\tau_1} \cos nx}{n} - \frac{e^{-(x-\alpha)/\omega\tau_1} \sin nx}{n^2 \omega\tau_1} \right\} \quad (82)$$

$$\begin{aligned} I_2 &= \int_{\alpha}^{\alpha+\mu} e^{-(x-\alpha)/\omega\tau_1} \sin nx dx = \left[\frac{-n(\omega\tau_1)^2 e^{-(x-\alpha)/\omega\tau_1} \cos nx - \omega\tau_1 e^{-(x-\alpha)/\omega\tau_1} \sin nx}{1+(n\omega\tau_1)^2} \right]_{\alpha}^{\alpha+\mu} \\ &= \frac{n(\omega\tau_1)^2 e^{-u/\omega\tau_1} \cos n(\alpha+\mu) - \omega\tau_1 e^{-u/\omega\tau_1} \sin n(\alpha+\mu) + n(\omega\tau_1)^2 \cos n\alpha + \omega\tau_1 \sin n\alpha}{1+(n\omega\tau_1)^2} \end{aligned} \quad (83)$$

Therefore, combining equations (79) and (83) in equations (73)

$$\begin{aligned} B_{n3} &= \frac{2}{\pi} K_1 \left\{ \frac{-n \cos n(\alpha+\mu) \sin(\alpha+\mu-\theta_1) + \sin n(\alpha+\mu) \cos(\alpha+\mu-\theta_1) - n \cos n\alpha \sin(\alpha-\theta_1) - \sin n\alpha \cos(\alpha-\theta_1)}{n^2-1} \right\} + \\ &\frac{2}{\pi} K_1 \sin(\theta_1 - \alpha) \left\{ \frac{-n(\omega\tau_1)^2 e^{-u/\omega\tau_1} \cos n(\alpha+\mu) - \omega\tau_1 e^{-u/\omega\tau_1} \sin n(\alpha+\mu) + n(\omega\tau_1)^2 \cos n\alpha + \omega\tau_1 \sin n\alpha}{1+(n\omega\tau_1)^2} \right\} \end{aligned} \quad (84)$$

$$\text{Since, } B_n = B_{n1} + B_{n2} + B_{n3} \quad (85)$$

Therefore,

$$\begin{aligned}
B_n = & \frac{2}{\pi} \left\{ \left(I_1 + \frac{E}{R_a} \right) \left[\frac{-n(\omega\tau_2)^2 e^{-\alpha/\omega\tau_2} \cos n\alpha - \omega\tau_2 e^{-\alpha/\omega\tau_2} \sin n\alpha + n(\omega\tau_2)^2}{1 + (n\omega\tau_2)^2} \right] - \frac{2}{\pi} \frac{E}{R_a} \left(\frac{1 - \cos n\alpha}{n} \right) + \right. \\
& K_2 \cos \theta_2 \left[\frac{n \sin \theta_2 \cos n\pi + n \sin(\alpha + \mu - \theta_2) \cos n(\alpha + \mu) - \cos(\alpha + \mu - \theta_2) \sin n(\alpha + \mu)}{n^2 - 1} \right] \left. \right\} \\
& - \frac{2}{\pi} \left\{ K_2 P \left[\frac{\cos n(\alpha + \mu) - \cos n\pi}{n} \right] \right\} \\
& + \frac{2}{\pi} \{ K_2 (\cos \theta_2 \sin(\theta_2 - \alpha) + P) + \\
& I_{a0} \} \left[\frac{n(\omega\tau_2)^2 e^{-(x-\alpha-\mu)/\omega\tau_2} \cos n\alpha + n(\omega\tau_2)^2 \cos n(\alpha + \mu) - \omega\tau_2 \sin n(\alpha + \mu)}{1 + (n\omega\tau_2)^2} \right] \\
& + K_1 \left\{ \frac{-n \cos n(\alpha + \mu) \sin(\alpha + \mu - \theta_1) + \sin n(\alpha + \mu) \cos(\alpha + \mu - \theta_1) - n \cos n\alpha \sin(\alpha - \theta_1) - \sin n\alpha \cos(\alpha - \theta_1)}{n^2 - 1} \right\} + \\
& K_1 \sin(\theta_1 - \alpha) \left\{ \frac{n(\omega\tau_1)^2 \cos n\alpha + \omega\tau_1 \sin n\alpha - n(\omega\tau_1)^2 e^{-u/\omega\tau_1} \cos n(\alpha + \mu) - \omega\tau_1 e^{-u/\omega\tau_1} \sin n(\alpha + \mu)}{1 + (n\omega\tau_1)^2} \right\}
\end{aligned} \tag{86}$$

$$\begin{aligned}
B_n = & \frac{1}{\pi} \left[\begin{aligned}
& \frac{k_3}{n+1} \left[\sin((n+1)(\alpha+u) - \theta_2) + (-1)^{n+1} \sin \theta_2 \right] \\
& - \frac{k_3}{n-1} \left[\sin((n-1)(\alpha+u) + \theta_2) - (-1)^{n-1} \sin \theta_2 \right] \\
& + \frac{2}{n} \left(A_6 \left((-1)^n - \cos n(\alpha+u) \right) - A_5 (1 - \cos n\alpha) \right) \\
& + \frac{2k_6 \omega\tau}{1 + (n\omega\tau)^2} \left[n\omega\tau \cos n(\alpha+u) - n\omega\tau (-1)^n e^{-\left(\frac{\pi - \alpha - u}{\omega\tau}\right)} + \sin n(\alpha+u) \right] \\
& + \frac{2(I_1 + A_5)\omega\tau_2}{1 + (n\omega\tau_2)^2} \left(n\omega\tau_2 - e^{-\frac{\alpha}{\omega\tau_2}} (n\omega\tau_2 \cos n\alpha + \sin n\alpha) \right) \\
& + \frac{k_1}{n-1} \left(\sin((n-1)(\alpha+u) + \theta_1) - \sin((n-1)\alpha + \theta_1) \right) \\
& - \frac{k_1}{n+1} \left(\sin((n+1)(\alpha+u) - \theta_1) - \sin((n+1)\alpha - \theta_1) \right) \\
& + \frac{2k_1 \sin(\theta_1 - \alpha)\omega\tau_1}{1 + (n\omega\tau_1)^2} \left(\begin{aligned}
& \frac{n\omega\tau_1 \cos n\alpha + \sin n\alpha}{-e^{-u/\omega\tau_1} (n\omega\tau_1 \cos n(\alpha+u) + \sin n(\alpha+u))}
\end{aligned} \right)
\end{aligned} \right]
\end{aligned} \tag{87}$$

$$i(x) = \sum_{n=2}^{\infty} (A_n \cos nx + B_n \sin nx)$$

$$\begin{aligned}
& B_n \\
&= \frac{2}{\pi} \left\{ \left(I_1 + \frac{E}{R_a} \right) \left[\frac{-n(\omega\tau_2)^2 e^{-\alpha/\omega\tau_2} \cos n\alpha - \omega\tau_2 e^{-\alpha/\omega\tau_2} \sin n\alpha + n(\omega\tau_2)^2}{1 + (n\omega\tau_2)^2} \right] \right. \\
&\quad - \frac{2}{\pi} \frac{E}{R_a} \left(\frac{1 - \cos n\alpha}{n} \right) \\
&\quad \left. + K_2 \cos\theta_2 \left[\frac{n \sin\theta_2 + n \sin(\alpha + u - \theta_2) \cos n(\alpha + u) - \cos(\alpha + u - \theta_2) \sin n(\alpha + u)}{n^2 - 1} \right] \right\} \\
&- \frac{2}{\pi} \left\{ K_2 P \left[\frac{\cos n(\alpha + u) - 1}{n} \right] \right\} \\
&+ \frac{2}{\pi} \{ K_2 (\cos\theta_2 \sin(\theta_2 - x) + P) + \\
&I_{ao} \} \left[\frac{n(\omega\tau_2)^2 e^{-(\pi - \alpha - u)/\omega\tau_2} \cos n\alpha - \omega\tau_2 e^{-\alpha/\omega\tau_2} \sin n\alpha + \omega\tau_2 \sin n(\alpha + u)}{1 + (n\omega\tau_2)^2} \right] \\
&+ \frac{2}{\pi} K_1 \left\{ \frac{-n \cos n(\alpha + u) \sin(\alpha + u - \theta_1) + \sin n(\alpha + u) \cos(\alpha + u - \theta_1) - n \cos n\alpha \sin(\alpha - \theta_1) - \sin n\alpha \cos(\alpha - \theta_1)}{n^2 - 1} \right\} + \\
&\frac{2}{\pi} K_1 \sin(\theta_1 - \alpha) \left\{ \frac{n(\omega\tau_1)^2 \cos n\alpha + \omega\tau_1 \sin n\alpha - n(\omega\tau_1)^2 e^{-u/\omega\tau_1} \cos n(\alpha + u) - \omega\tau_1 e^{-u/\omega\tau_1} \sin n(\alpha + u)}{1 + (n\omega\tau_1)^2} \right\} \quad (88)
\end{aligned}$$

$$A_n = A_{n1} + A_{n2} + A_{n3} \quad (89)$$

$$\begin{aligned}
&= \frac{2}{\pi} \left(I_1 + \frac{E}{R_a} \right) \frac{n(\omega\tau_2)^2 e^{-x/\omega\tau_2} \sin n\alpha - \omega\tau_2 e^{-x/\omega\tau_2} \cos n\alpha + \omega\tau_2}{1 + (n\omega\tau_2)^2} - \frac{E}{R_a} \frac{\sin n\alpha}{n} \\
&+ \frac{2}{\pi} K_2 \cos\theta_2 \left[\frac{-\cos\theta_2 - n \sin(\alpha + u - \theta_2) \sin n(\alpha + u) - \cos(\alpha + u - \theta_2) \cos n(\alpha + u)}{n^2 - 1} \right] \\
&- \frac{2}{\pi} K_2 P \left[-\frac{\sin n(\alpha + u)}{n} \right] \\
&+ \frac{2}{\pi} \{ K_2 (\cos\theta_2 \sin(\theta_2 - x) + P) \\
&\quad + I_{ao} \} \left[\frac{-\omega\tau \cos n\pi e^{-(\pi - \alpha - u)/\omega\tau} - n(\omega\tau)^2 \sin n(\alpha + u) + \omega\tau \cos n(\alpha + u)}{1 + (n\omega\tau)^2} \right] \\
&+ \frac{2}{\pi} K_1 \sin(\theta_1 \\
&- \alpha) \left\{ \frac{n(\omega\tau_1)^2 e^{-u/\omega\tau_1} \sin n(\alpha + u) - \omega\tau_1 e^{-u/\omega\tau_1} \cos n(\alpha + u) - n(\omega\tau_1)^2 \sin n\alpha + \omega\tau_1 \cos n\alpha}{1 + (n\omega\tau_1)^2} \right\} \\
&+ \frac{2}{\pi} K_1 \left\{ \frac{n \sin n(\alpha + u) \sin(\alpha + u - \theta_1) + \cos n(\alpha + u) \cos(\alpha + u - \theta_1) - n \sin n\alpha \sin(\alpha - \theta_1) - \cos n\alpha \cos(\alpha - \theta_1)}{n^2 - 1} \right\} \quad (90)
\end{aligned}$$

APPENDIX III

Generalised Analysis for the Phase Angle Control (PAC).

Consider the waveform of Fig. 4.1 for the phase angle control (PAC) of converter.

The average output voltage is,

$$V_{dc} = \frac{1}{\pi} \int_0^{\pi} V_m \sin \omega t d(\omega t) \quad (1)$$

$$= \frac{1}{\pi} \left[\int_{\alpha}^{\pi} V_m \sin \omega t d(\omega t) \right]$$

$$= \frac{V_m}{\pi} \left[-\cos \omega t \right]_{\alpha}^{\pi}$$

$$= \frac{V_m}{\pi} \left[\cos \alpha - \cos \pi \right]$$

$$= \frac{V_m}{\pi} (1 + \cos \alpha) \quad (2)$$

V_{dc} can be varied from $\frac{2V_m}{\pi}$ to 0 as α varies from 0 to π .

The maximum voltage is,

$$V_{d \max} = \frac{2V_m}{\pi}$$

Hence the normalized voltage is,

$$V_n = \frac{V_{dc}}{V_{d \max}} = \frac{\frac{V_m}{\pi} (1 + \cos \alpha)}{\frac{2V_m}{\pi}}$$

$$= \frac{1}{2} (1 + \cos \alpha) \text{ pu.} \quad (3)$$

The rms value of the input current is given by,

$$I_s = \left[\frac{1}{\pi} \int_{\alpha}^{\pi} i_s^2(t) d(\omega t) \right]^{\frac{1}{2}} \quad (4)$$

$$= \left[\frac{1}{\pi} \int_{\alpha}^{\pi} I_a^2(t) d(\omega t) \right]^{\frac{1}{2}}$$

$$= \left[\frac{I_a^2}{\pi} \left| \omega t \right|_{\alpha}^{\pi} \right]^{\frac{1}{2}}$$

$$= \frac{I_a}{\sqrt{\pi}} [\pi - \alpha]^{\frac{1}{2}}$$

$$= I_a \left[1 - \frac{\alpha}{\pi} \right]^{\frac{1}{2}} \quad (5)$$

The instantaneous input current is,

$$i_s(t) = I_{dc} + \sum_{n=1,2,3,\dots}^{\infty} a_n \text{Cos}n\omega t + b_n \text{Sinn}\omega t \quad (6)$$

where,

$$I_{dc} = \frac{1}{2\pi} \int_0^{2\pi} i_s(t) d(\omega t) = \frac{1}{2\pi} \int_{\alpha}^{2\pi} I_a(t) d(\omega t)$$

$$= \frac{1}{2\pi} \left[\int_{\alpha}^{\pi} I_a(t) d(\omega t) - \int_{\pi+\alpha}^{2\pi} I_a(t) d(\omega t) \right]$$

$$= \frac{I_a}{2\pi} \left[\left| \omega t \right|_{\alpha}^{\pi} - \left| \omega t \right|_{\pi+\alpha}^{2\pi} \right]$$

$$= \frac{I_a}{2\pi} [\pi - \alpha - 2\pi + (\pi + \alpha)] = 0 \quad (7)$$

$$a_n = \frac{1}{\pi} \int_0^{2\pi} i_s(t) \text{Cosn } \omega t d(\omega t) \quad (8)$$

$$= \frac{1}{\pi} \left[\int_{\alpha}^{\pi} I_a(t) \text{Cosn } \omega t d(\omega t) - \int_{\pi+\alpha}^{2\pi} I_a(t) \text{Cosn } \omega t d(\omega t) \right]$$

$$= \frac{I_a}{n\pi} \left[\text{Sinn } \omega t \Big|_{\alpha}^{\pi} - \text{Sinn } \omega t \Big|_{\pi+\alpha}^{2\pi} \right]$$

$$= \frac{I_a}{n\pi} [\text{Sinn } \pi - \text{Sinn } \alpha - \text{Sinn } 2\pi + \text{Sinn}(\pi + \alpha)]$$

$$= \frac{I_a}{n\pi} [\text{Sinn } \pi - \text{Sinn } \alpha - \text{Sinn } 2\pi + \text{Sinn } \pi \text{Cosn } \alpha + \text{Cosn } \pi \text{Sinn } \alpha]$$

$$= \frac{-2I_a}{n\pi} \text{Sinn } \alpha \quad \text{For } n=1, 3, 5, \dots \quad (n = \text{odd}) \quad (9)$$

$$= 0 \quad \text{For } n=2, 4, 6, \dots \quad (n = \text{even}) \quad (10)$$

and,

$$b_n = \frac{1}{\pi} \int_0^{2\pi} i_s(t) \text{Sinn } \omega t \quad (11)$$

$$= \frac{1}{\pi} \left[\int_{\alpha}^{\pi} I_a(t) \text{Sinn } \omega t d(\omega t) - \int_{\pi+\alpha}^{2\pi} I_a(t) \text{Sinn } \omega t d(\omega t) \right]$$

$$= \frac{I_a}{n\pi} \left[-\text{Cosn } \omega t \Big|_{\alpha}^{\pi} - \left(-\text{Cosn } \omega t \Big|_{\pi+\alpha}^{2\pi} \right) \right]$$

$$= \frac{I_a}{n\pi} [\text{Cosn } \alpha - \text{Cosn } \pi - (\text{Cosn}(\pi + \alpha) - \text{Cosn } 2\pi)]$$

$$= \frac{I_a}{n\pi} [\text{Cosn } \alpha - \text{Cosn } \pi + \text{Cosn } 2\pi - \text{Cosn } \pi \text{Cosn } \alpha + \text{Sinn } \pi \text{Sinn } \alpha]$$

$$= \frac{2I_a}{n\pi} [1 + \text{Cos}n\alpha] \quad \text{For } n = 1, 3, 5, \dots \dots \text{ (n = odd)} \quad (12)$$

$$= 0 \quad \text{For } n = 2, 4, 6, \dots \dots \text{ (n = even)} \quad (13)$$

Since $I_{dc} = 0$, equation (6) can be written as,

$$i_s(t) = \sum_{n=1,3,5,\dots}^{\infty} \sqrt{2}I_{s_n} \text{Sinn}(\omega t + \phi_{s_n}) \quad (14)$$

where,

$$I_{s_n} = \frac{1}{\sqrt{2}} (a_n^2 + b_n^2)^{\frac{1}{2}} \quad (15)$$

Substituting,

$$\begin{aligned} &= \frac{2I_a}{\sqrt{2n\pi}} \left[\text{Sin}^2 n\alpha + (1 + \text{Cos}n\alpha)^2 \right]^{\frac{1}{2}} \\ &= \frac{\sqrt{2}I_a}{n\pi} \left[\text{Sin}^2 n\alpha + 1 + 2\text{Cos}n\alpha + \text{Cos}^2 n\alpha \right]^{\frac{1}{2}} \\ &= \frac{\sqrt{2}I_a}{n\pi} \left[2(1 + \text{Cos}n\alpha) \right]^{\frac{1}{2}} \\ &= \frac{\sqrt{2}I_a}{n\pi} \left[2 * 2\text{Cos}^2 \frac{n\alpha}{2} \right]^{\frac{1}{2}} \\ &= \frac{2\sqrt{2}I_a}{n\pi} \text{Cos} \frac{n\alpha}{2} \end{aligned} \quad (16)$$

and,

$$\phi_{s_n} = \tan^{-1} \frac{a_n}{b_n} \quad (17)$$

$$\begin{aligned}
&= \tan^{-1} \frac{-2I_a \text{Sinn} \alpha}{n\pi} \\
&= \tan^{-1} \frac{\frac{2I_a}{n\pi} (1 + \text{Cosn} \alpha)}{\frac{2I_a \text{Sinn} \alpha}{n\pi}} \\
&= \tan^{-1} \frac{-\text{Sinn} \alpha}{(1 + \text{Cosn} \alpha)} \tag{18}
\end{aligned}$$

But,

$$\text{Sinn} \alpha = 2 \text{Sin} \frac{n\alpha}{2} \text{Cos} \frac{n\alpha}{2} \tag{19}$$

$$(1 + \text{Cosn} \alpha) = 2 \text{Cos}^2 \frac{n\alpha}{2} \tag{20}$$

Therefore equation (18) becomes,

$$\begin{aligned}
\phi_n &= \tan^{-1} \frac{-2 \text{Sin} \frac{n\alpha}{2} \text{Cos} \frac{n\alpha}{2}}{2 \text{Cos}^2 \frac{n\alpha}{2}} \\
&= \tan^{-1} \left(\tan \frac{-n\alpha}{2} \right) \\
&= \frac{-n\alpha}{2} \tag{21}
\end{aligned}$$

But $\phi_n = \phi_{s_n}$

Hence,

Displacement factor (DF) is,

$$\begin{aligned}
DF &= \text{Cos} \phi_{s_1} \\
&= \text{Cos} \left(\frac{-\alpha}{2} \right) \tag{22}
\end{aligned}$$

$$= \cos \frac{\alpha}{2} \quad (23)$$

Harmonic factor (HF) is,

$$HF = \left[\left(\frac{I_s}{I_{s_1}} \right)^2 - 1 \right]^{\frac{1}{2}} \quad (24)$$

$$= \left[\frac{\frac{I_a^2}{\pi} (\pi - \alpha)}{\frac{8I_a}{\pi^2} \cos^2 \frac{\alpha}{2}} - 1 \right]^{\frac{1}{2}}$$

$$= \left[\frac{\pi(\pi - \alpha)}{8 \cos^2 \frac{\alpha}{2}} - 1 \right]^{\frac{1}{2}}$$

$$= \left[\frac{\pi(\pi - \alpha)}{8 \frac{(1 + \cos \alpha)}{2}} - 1 \right]^{\frac{1}{2}}$$

$$= \left[\frac{\pi(\pi - \alpha)}{4(1 + \cos \alpha)} - 1 \right]^{\frac{1}{2}} \quad (25)$$

Power factor (PF) is,

$$PF = \frac{I_{s_1}}{I_s} \cos \phi_1 \quad (26)$$

$$\begin{aligned}
&= \frac{\frac{2\sqrt{2}}{\pi} \cos \frac{\alpha}{2}}{\frac{I_a}{\sqrt{\pi}} (\pi - \alpha)^{\frac{1}{2}}} \cos \frac{\alpha}{2} \\
&= \frac{2\sqrt{2} \cos^2 \frac{\alpha}{2}}{[\pi(\pi - \alpha)]^{\frac{1}{2}}} \\
&= \frac{\sqrt{2}(1 + \cos \alpha)}{[\pi(\pi - \alpha)]^{\frac{1}{2}}} \tag{27}
\end{aligned}$$



UNIVERSITY
OF LAGOS

APPENDIX IV

Generalised Analysis for the Symmetrical Angle Control (SAC).

Consider the waveform of Fig. 4.2 for the phase angle control (PAC) of converter

The average output voltage is:

$$V_{dc} = \frac{1}{\pi} \int_{\alpha}^{\pi-\alpha} V_m \sin \omega t d(\omega t) \quad (1)$$

$$= \frac{V_m}{\pi} \left[-\cos \omega t \right]_{\alpha}^{\pi-\alpha}$$

$$= \frac{V_m}{\pi} [\cos \alpha - \cos(\pi - \alpha)]$$

$$= \frac{V_m}{\pi} [\cos \alpha - (\cos \pi \cos \alpha - \sin \pi \sin \alpha)]$$

$$= \frac{V_m}{\pi} [\cos \alpha + \cos \alpha]$$

$$= \frac{2V_m}{\pi} \cos \alpha \quad (2)$$

and V_{dc} can be varied from $\frac{2V_m}{\pi}$ to 0 (zero) by varying α from 0 to $\frac{\pi}{2}$.

\therefore The maximum average output voltage is,

$$V_{dm} = \frac{2V_m}{\pi}$$

The normalized output voltage is given by,

$$V_n = \frac{V_{dc}}{V_{dm}} = \frac{\frac{2V_m \cos \alpha}{\pi}}{\frac{2V_m}{\pi}}$$

$$= \cos \alpha \text{ pu} \quad (3)$$

The rms output voltage is given by:

$$V_{rms} = \left[\frac{1}{\pi} \int_{\alpha}^{\pi-\alpha} V_m^2 \sin^2 \omega t d(\omega t) \right]^{\frac{1}{2}} \quad (4)$$

$$= \frac{V_m}{\sqrt{\pi}} \left[\int_{\alpha}^{\pi-\alpha} \left(\frac{1 - \cos 2\omega t}{2} \right) d(\omega t) \right]^{\frac{1}{2}}$$

$$= \frac{V_m}{\sqrt{\pi}} \left[\left[\left(\frac{\omega t}{2} - \frac{\sin 2\omega t}{4} \right) \right]_{\alpha}^{\pi-\alpha} \right]$$

$$= \frac{V_m}{\sqrt{\pi}} \left[\left\{ \frac{2(\pi - \alpha) - 2\alpha}{4} \right\} - \left\{ \frac{\sin 2(\pi - \alpha) - \sin 2\alpha}{4} \right\} \right]^{\frac{1}{2}}$$

$$= \frac{V_m}{\sqrt{\pi}} \left[\left\{ \frac{2\pi - 4\alpha - (\sin 2\pi \cos 2\alpha - \cos 2\pi \sin 2\alpha) + \sin 2\alpha}{4} \right\} \right]^{\frac{1}{2}}$$

$$= \frac{V_m}{\sqrt{\pi}} \left[\frac{2\pi - 4\alpha + \sin 2\alpha + \sin 2\alpha}{4} \right]^{\frac{1}{2}}$$

$$= \frac{V_m}{\sqrt{\pi}} \left[\frac{2\pi - 4\alpha + 2\sin 2\alpha}{4} \right]^{\frac{1}{2}}$$

$$= \frac{V_m}{\sqrt{2\pi}} [\pi - 2\alpha + \sin 2\alpha]^{\frac{1}{2}} \quad (5)$$

The instantaneous input current is;

$$i_s(t) = I_{dc} + \sum_{n=1,2,3,\dots}^{\infty} (a_n \cos n \omega t + b_n \sin n \omega t) \quad (6)$$

where,

$$\begin{aligned}
a_0 = I_{dc} &= \frac{1}{2\pi} \left[\int_{\alpha}^{\pi-\alpha} I_a d(\omega t) - \int_{\pi+\alpha}^{2\pi-\alpha} I_a d(\omega t) \right] \\
&= \frac{I_a}{2\pi} \left[\left. \omega t \right|_{\alpha}^{\pi-\alpha} - \left. \omega t \right|_{\pi+\alpha}^{2\pi-\alpha} \right] \\
&= \frac{I_a}{2\pi} \left[\pi - \alpha - \alpha - (2\pi - \alpha - (\pi + \alpha)) \right] \\
&= 0
\end{aligned}$$

and
$$a_n = \frac{1}{\pi} \int_0^{2\pi} i_s(t) \text{Cos} n \omega t d(\omega t)$$

$$\begin{aligned}
&= \frac{1}{\pi} \left[\int_{\alpha}^{\pi-\alpha} I_a \text{Cos} n \omega t d(\omega t) - \int_{\pi+\alpha}^{2\pi-\alpha} I_a \text{Cos} n \omega t d(\omega t) \right] \\
&= \frac{I_a}{\pi} \left[\left. \frac{\text{Sinn} \omega t}{n} \right|_{\alpha}^{\pi-\alpha} - \left. \frac{\text{Sinn} \omega t}{n} \right|_{\pi+\alpha}^{2\pi-\alpha} \right] =
\end{aligned}$$

$$\frac{I_a}{n\pi} \left[\{ \text{Sinn}(\pi - \alpha) - \text{Sinn} \alpha \} - \{ \text{Sinn}(2\pi - \alpha) - \text{Sinn}(\pi + \alpha) \} \right]$$

$$= \frac{I_a}{n\pi} \left[\left\{ \text{Sinn} \pi \text{Cos} n \alpha - \text{Cos} n \pi \text{Sinn} \alpha - \text{Sinn} \alpha - \text{Sinn} 2\pi \text{Cos} n \alpha + \text{Cos} n 2\pi \text{Sinn} \alpha \right\} \right. \\ \left. + \text{Sinn} \pi \text{Cos} n \alpha + \text{Cos} n \pi \text{Sinn} \alpha \right]$$

$$= 0 \text{ for all values of } n \tag{7}$$

$$\therefore a_n = 0 \tag{8}$$

$$b_n = \frac{1}{\pi} \int_0^{2\pi} i_s(t) \text{Sinn} \omega t d(\omega t) \tag{9}$$

$$= \frac{1}{\pi} \left[\int_{\alpha}^{\pi-\alpha} I_a \text{Sinn} \omega t d(\omega t) - \int_{\pi+\alpha}^{2\pi-\alpha} I_a \text{Sinn} \omega t d(\omega t) \right]$$

$$\begin{aligned}
&= \frac{I_a}{n\pi} \left[-\text{Cosn } \omega t \Big|_{\alpha}^{\pi-\alpha} - \left| -\text{Cosn } \omega t \right|_{\pi+\alpha}^{2\pi-\alpha} \right] \\
&= \frac{I_a}{n\pi} \left[\{-\text{Cosn}(\pi - \alpha) + \text{Cosn } \alpha\} + \text{Cosn}(2\pi - \alpha) - \text{Cosn}(\pi + \alpha) \right] \\
&= \frac{I_a}{n\pi} \left[\left\{ \begin{aligned} &-\text{Cosn } \pi \text{Cosn } \alpha - \text{Sinn } \pi \text{Sinn } \alpha + \text{Cosn } \alpha + \text{Cosn } 2\pi \text{Cosn } \alpha + \text{Sinn } 2\pi \text{Sinn } \alpha \\ &-\text{Cosn } \pi \text{Cosn } \alpha + \text{Sinn } \pi \text{Sinn } \alpha \end{aligned} \right\} \right] \\
&= \frac{I_a}{n\pi} \left[\text{Cosn } \alpha - 2\text{Cosn } \pi \text{Cosn } \alpha + \text{Cosn } 2\pi \text{Cosn } \alpha \right] \\
&= \frac{4I_a}{n\pi} \text{Cosn } \alpha \quad \text{For } n = 1, 3, 5, \dots (n = \text{odd}) \tag{10}
\end{aligned}$$

$$= 0 \quad \text{For } n = 2, 4, 6, \dots (n = \text{even}) \tag{11}$$

Since $I_{dc} = 0$

Again, equation (6) can be written as;

$$i_s(t) = \sum_{n=1,3,5,\dots}^{\infty} \sqrt{2} I_n \text{Sin}(n\omega t + \phi_n) \tag{12}$$

where,

$$\phi_n = \tan^{-1} \frac{a_n}{b_n} = 0 \tag{13}$$

Displacement factor DF is,

$$\begin{aligned}
DF &= \text{Cos } \phi_1 \\
&= \text{Cos } 0^\circ \\
&= 1 \tag{14}
\end{aligned}$$

The rms value of the harmonic input current is:

$$I_{s_n} = \frac{1}{\sqrt{2}} [a_n^2 + b_n^2]^{\frac{1}{2}} \quad (15)$$

$$= \frac{1}{\sqrt{2}} * \frac{4}{n\pi} I_a \text{Cos} n \alpha$$

$$= \frac{2\sqrt{2}}{n\pi} I_a \text{Cos} n \alpha \quad (16)$$

∴ The rms value of the fundamental current is:

$$I_{s_1} = \frac{2\sqrt{2}}{\pi} I_a \text{Cos} \alpha \quad (17)$$

The rms input current is:

$$I_s = \left[\frac{1}{\pi} \int_{\alpha}^{\pi-\alpha} I_a^2 d(\omega t) \right]^{\frac{1}{2}} \quad (18)$$

$$= \frac{I_a}{\sqrt{\pi}} \left[\omega t \Big|_{\alpha}^{\pi-\alpha} \right]^{\frac{1}{2}}$$

$$= \frac{I_a}{\sqrt{\pi}} |\pi - \alpha - \alpha|^{\frac{1}{2}}$$

$$= \frac{I_a}{\sqrt{\pi}} [\pi - 2\alpha]^{\frac{1}{2}}$$

$$= I_a \left(1 - \frac{2\alpha}{\pi} \right)^{\frac{1}{2}} \quad (19)$$

Hence, the harmonic factor can be written in the form;

$$HF = \left[\left(\frac{I_s}{I_{s_1}} \right)^2 - 1 \right]^{\frac{1}{2}} \quad (20)$$

Substituting,

$$\begin{aligned}
 &= \left| \frac{(\pi - 2\alpha)}{\frac{\pi}{8\cos^2\alpha} - 1} \right|^{\frac{1}{2}} \\
 &= \left[\frac{(\pi - 2\alpha)}{\pi} * \frac{\pi^2}{8\cos^2\alpha} - 1 \right]^{\frac{1}{2}} \\
 &= \left[\frac{\pi(\pi - 2\alpha)}{8\cos^2\alpha} - 1 \right]^{\frac{1}{2}} \tag{21}
 \end{aligned}$$

∴ Input Power factor PF from equation (3-31) is,

$$PF = \frac{I_{s_1}}{I_s} \cos \phi_1 \tag{22}$$

$$\begin{aligned}
 &= \frac{\left(\frac{2\sqrt{2}I_a \cos \alpha}{\pi} \right)}{\frac{I_a (\pi - 2\alpha)^{\frac{1}{2}}}{\sqrt{\pi}}} \\
 &= \frac{2\sqrt{2}\cos \alpha}{\pi} * \frac{\sqrt{\pi}}{(\pi - 2\alpha)^{\frac{1}{2}}} \\
 &= \frac{2\sqrt{2}\cos \alpha}{\sqrt{\pi}(\pi - 2\alpha)^{\frac{1}{2}}} \\
 &= \frac{2\sqrt{2}\cos \alpha}{[\pi(\pi - 2\alpha)]^{\frac{1}{2}}} \tag{23}
 \end{aligned}$$

APPENDIX V

Generalised Analysis for the Sequence with Forced Commutation Control.

Consider the waveform of Fig. 4.1 for the Sequence with Forced Commutation

This technique is used for high- voltage applications where two or more converters are connected in series to share the voltage and to improve the power factor. In the circuits shown below, the

turns ratio is $\frac{N_p}{N_s} = 2$ and if α_1 and α_2 are the delay angles of Converter 1 and Converter 2

respectively, the maximum output voltage is obtained by setting $\alpha_1 = \alpha_2 = 0$

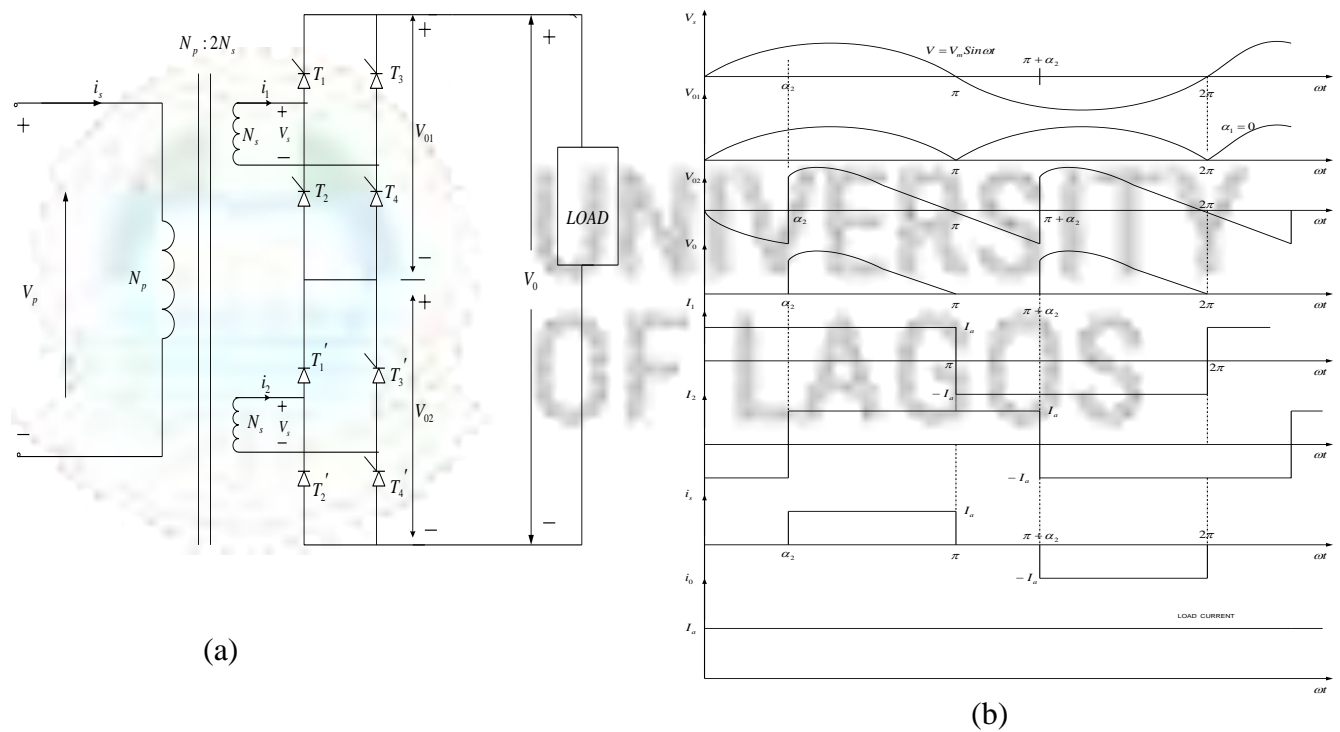


Fig.4.1: Sequential Control with Forced Commutation.

(a) Circuits

(b) Waveform of Current and Voltage

The operation is such that one converter is operated to obtain an output voltage from 0 to $\frac{V_{dm}}{2}$ and the other converter is bypassed through its freewheeling diode. To obtain output voltage from $\frac{V_{dm}}{2}$ to V_{dm} , one converter is fully turned on (at delay angle, $\alpha_1 = 0$) and the delay angle of the other converter α_2 is varied. The waveform shows the output voltage, input currents to the converter and the input current from the supply when both the converters are operating with a highly inductive load.

From the generalised analysis for (PAC), the average output voltages of two semi-converters are:

$$V_{dc1} = \frac{V_m}{\pi} (1 + \cos \alpha_1)$$

$$V_{dc2} = \frac{V_m}{\pi} (1 + \cos \alpha_2)$$

The resultant output voltage of converters is:

$$\begin{aligned} V_{dc} &= V_{dc1} + V_{dc2} \\ &= \frac{V_m}{\pi} (2 + \cos \alpha_1 + \cos \alpha_2) \end{aligned}$$

The maximum average output voltage for $\alpha_1 = \alpha_2 = 0$ is

$$V_{dm} = \frac{4V_m}{\pi}$$

If converter 1 is operating:

$$0 \leq \alpha_1 \leq \pi,$$

then,

$$V_{dc} = V_{dc1} + V_{dc2}$$

$$= \frac{V_m}{\pi} (1 + \cos \alpha_1) \quad (1)$$

and the normalized average output voltage is;

$$V_n = \frac{V_{dc}}{V_{dm}} = 0.25(1 + \cos \alpha_1) \quad (2)$$

If both converters are operating:

$$\alpha_1 = 0 \quad \text{and} \quad 0 \leq \alpha_2 \leq \pi$$

then,

$$\begin{aligned} V_{dc} &= V_{dc1} + V_{dc2} \\ &= \frac{V_m}{\pi} (3 + \cos \alpha_2) \end{aligned} \quad (3)$$

and the normalized average output voltage is;

$$V_n = \frac{V_{dc}}{V_{dm}} = 0.25(3 + \cos \alpha_2) \quad (4)$$

Analysis.

For $0.5 < V_{dc} < 1.0 \text{ pu}$

$$V_{dc} = \frac{1}{\pi} \int_0^{\pi} V_m \sin \omega t d(\omega t) \quad (5)$$

$$= \frac{1}{\pi} \left[\int_0^{\alpha} \frac{V_m}{2} \sin \omega t d(\omega t) + \int_{\alpha}^{\pi-\alpha} V_m \sin \omega t d(\omega t) + \int_{\pi-\alpha}^{\pi} \frac{V_m}{2} \sin \omega t d(\omega t) \right]$$

$$= \frac{V_m}{\pi} \left[\frac{1}{2} |-\cos \omega t|_0^{\alpha} + |-\cos \omega t|_{\alpha}^{\pi-\alpha} + \frac{1}{2} |-\cos \omega t|_{\pi-\alpha}^{\pi} \right]$$

$$\begin{aligned}
&= \frac{V_m}{\pi} \left[\frac{1 - \cos \alpha}{2} + \cos \alpha - \cos(\pi - \alpha) + \frac{\cos(\pi - \alpha) - \cos \pi}{2} \right] \\
&= \frac{V_m}{\pi} \left[\frac{1}{2} + \frac{\cos \alpha}{2} - \cos(\pi - \alpha) + \frac{\cos(\pi - \alpha)}{2} + \frac{1}{2} \right] \\
&= \frac{V_m}{\pi} \left[1 + \frac{\cos \alpha}{2} - \frac{1}{2} (\cos \pi \cos \alpha + \sin \pi \sin \alpha) \right] \\
&= \frac{V_m}{\pi} \left[1 + \frac{\cos \alpha}{2} + \frac{\cos \alpha}{2} \right] \\
&= \frac{V_m}{\pi} (1 + \cos \alpha) \tag{6}
\end{aligned}$$

V_{dc} can be varied from $\frac{2V_m}{\pi}$ to 0 as α varies from 0 to π

The maximum voltage is V_{dm}

$$\therefore V_{dm} = \frac{2V_m}{\pi} \tag{7}$$

Hence the normalized voltage is $V_n = \frac{V_{dc}}{V_{max}}$

$$\begin{aligned}
&= \frac{\frac{V_m}{\pi} (1 + \cos \alpha)}{\frac{2V_m}{\pi}} \\
&= \frac{1}{2} (1 + \cos \alpha) pu \tag{8}
\end{aligned}$$

The rms value of the input current is given by,

$$I_s = \left[\frac{1}{\pi} \int_{\alpha}^{\pi} i_s^2(t) dt \right]^{\frac{1}{2}} \tag{9}$$

$$\begin{aligned}
&= \frac{1}{\sqrt{\pi}} \left[\int_0^{\alpha} \frac{I_a^2}{4} (t) dt + \int_{\alpha}^{\pi-\alpha} I_a^2 (t) dt + \int_{\pi-\alpha}^{\pi} \frac{I_a}{2} (t) dt \right]^{\frac{1}{2}} \\
&= \frac{I_a}{\sqrt{\pi}} \left[\left| \frac{\omega t}{4} \right|_0^{\alpha} + \left| \omega t \right|_{\alpha}^{\pi-\alpha} + \left| \frac{\omega t}{4} \right|_{\pi-\alpha}^{\pi} \right]^{\frac{1}{2}} \\
&= \frac{I_a}{\sqrt{\pi}} \left[\frac{\alpha}{4} + (\pi - \alpha) - \alpha + \frac{\pi - (\pi - \alpha)}{4} \right]^{\frac{1}{2}} \\
&= \frac{I_a}{\sqrt{\pi}} \left[\frac{\alpha}{4} + \pi - 2\alpha + \frac{\pi - \pi + \alpha}{4} \right]^{\frac{1}{2}} \\
&= \frac{I_a}{\sqrt{\pi}} \left[\frac{-3\alpha}{2} + \pi \right]^{\frac{1}{2}} \\
&= \frac{I_a}{\sqrt{\pi}} \left[\pi - \frac{3\alpha}{2} \right]^{\frac{1}{2}} \\
&= I_a \left[1 - \frac{3\alpha}{2\pi} \right]^{\frac{1}{2}} \tag{10}
\end{aligned}$$

The instantaneous input current is given as,

$$i_s(t) = I_{dc} + \sum_{i=1,2,3,\dots}^{\infty} a_n \text{Cos}n \omega t + b_n \text{Sinn} \omega t \tag{11}$$

Due to symmetry,

$$I_{dc} = 0 \tag{12}$$

$$b_n = \frac{1}{\pi} \int_0^{2\pi} i_s(t) \text{Sinn} \omega t d(\omega t) \tag{13}$$

$$\begin{aligned}
&= \frac{2}{\pi} \int_0^\alpha \frac{I_a}{2} \text{Sinn} \omega t d(\omega t) + \int_\alpha^{\pi-\alpha} I_a \text{Sinn} \omega t d(\omega t) + \int_{\pi-\alpha}^\pi \frac{I_a}{2} \text{Sinn} \omega t d(\omega t) \\
&= \frac{2I_a}{n\pi} \left[\left| \frac{-\text{Cosn} \omega t}{2} \right|_0^\alpha + \left| -\text{Cosn} \omega t \right|_\alpha^{\pi-\alpha} + \left| \frac{-\text{Cosn} \omega t}{2} \right|_{\pi-\alpha}^\pi \right] \\
&= \frac{2I_a}{n\pi} \left[\frac{1 - \text{Cosn} \alpha}{2} + \text{Cosn} \alpha - \text{Cosn}(\pi - \alpha) + \frac{\text{Cosn}(\pi - \alpha) - \text{Cosn} \pi}{2} \right] \\
&= \frac{2I_a}{n\pi} \left[\frac{1 - \text{Cosn} \alpha}{2} + \text{Cosn} \alpha - \frac{\text{Cosn}(\pi - \alpha)}{2} - \frac{\text{Cosn} \pi}{2} \right] \\
&= \frac{2I_a}{n\pi} \left[\frac{1}{2} + \frac{\text{Cosn} \alpha}{2} - \frac{\text{Cosn} \pi \text{Cosn} \alpha + \text{Sinn} \pi \text{Sinn} \alpha}{2} - \frac{\text{Cosn} \pi}{2} \right] \\
&= \frac{2I_a}{n\pi} [1 + \text{Cosn} \alpha] \quad \text{For } n=1, 3, 5, \dots \quad (n = \text{Odd}) \quad (14) \\
&= 0 \quad \text{For } n=2, 4, 6, \dots \quad (n = \text{even}) \quad (15)
\end{aligned}$$

Similarly,

$$a_n = \frac{1}{\pi} \int_0^{2\pi} i_s(t) \text{Cosn} \omega t d(\omega t) \quad (16)$$

$$\begin{aligned}
&= \frac{1}{\pi} \left[\int_0^\alpha \frac{I_a}{2} \text{Cosn} \omega t d(\omega t) + \int_\alpha^{\pi-\alpha} I_a \text{Cosn} \omega t d(\omega t) + \int_{\pi-\alpha}^\pi \frac{I_a}{2} \text{Cosn} \omega t d(\omega t) - \right. \\
&\quad \left. \int_\pi^{\pi+\alpha} \frac{I_a}{2} \text{Cosn} \omega t d(\omega t) - \int_{\pi+\alpha}^{2\pi-\alpha} I_a \text{Cosn} \omega t d(\omega t) - \int_{2\pi-\alpha}^{2\pi} \frac{I_a}{2} \text{Cosn} \omega t d(\omega t) \right] \\
&= \frac{I_a}{n\pi} \left[\left| \frac{\text{Sinn} \omega t}{2} \right|_0^\alpha + \left| \text{Sinn} \omega t \right|_\alpha^{\pi-\alpha} + \left| \frac{\text{Sinn} \omega t}{2} \right|_{\pi-\alpha}^\pi - \left| \frac{\text{Sinn} \omega t}{2} \right|_\pi^{\pi+\alpha} - \right. \\
&\quad \left. \left| \text{Sinn} \omega t \right|_{\pi+\alpha}^{2\pi-\alpha} - \left| \frac{\text{Sinn} \omega t}{2} \right|_{2\pi-\alpha}^{2\pi} \right]
\end{aligned}$$

$$\begin{aligned}
&= \frac{I_a}{n\pi} \left[\frac{\text{Sinn}\alpha}{2} - 0 + \text{Sinn}(\pi - \alpha) - \text{Sinn}\alpha + \frac{\text{Sinn}\pi - \text{Sinn}(\pi - \alpha)}{2} - \frac{\text{Sinn}(\pi + \alpha)}{2} + \frac{\text{Sinn}\pi}{2} - \right. \\
&\quad \left. \text{Sinn}(2\pi - \alpha) + \text{Sinn}(\pi + \alpha) - \frac{\text{Sinn}2\pi}{2} + \frac{\text{Sinn}(2\pi - \alpha)}{2} \right] \\
&= \frac{I_a}{n\pi} \left[\frac{\text{Sinn}\alpha}{2} - \text{Sinn}\alpha + \text{Sinn}(\pi - \alpha) + \frac{\text{Sinn}\pi}{2} - \frac{\text{Sinn}(\pi - \alpha)}{2} - \frac{\text{Sinn}(\pi + \alpha)}{2} - \text{Sinn}(2\pi - \alpha) + \right. \\
&\quad \left. \text{Sinn}(\pi + \alpha) + \frac{\text{Sinn}(2\pi - \alpha)}{2} \right] \\
&= \frac{I_a}{n\pi} \left[\frac{\text{Sinn}\alpha}{2} - \text{Sinn}\alpha + \frac{\text{Sinn}(\pi - \alpha)}{2} + \frac{\text{Sinn}\pi}{2} + \frac{\text{Sinn}(\pi + \alpha)}{2} - \frac{\text{Sinn}(2\pi - \alpha)}{2} \right] \\
&= \frac{I_a}{n\pi} \left[\frac{-\text{Sinn}\alpha}{2} + \frac{(\text{Sinn}\pi\text{Cosn}\alpha - \text{Cosn}\pi\text{Sinn}\alpha)}{2} + \frac{\text{Sinn}\pi}{2} + \frac{\text{Sinn}\pi\text{Cosn}\alpha + \text{Cosn}\pi\text{Sinn}\alpha}{2} - \right. \\
&\quad \left. \frac{\text{Sinn}2\pi\text{Cosn}\alpha + \text{Cosn}2\pi\text{Sinn}\alpha}{2} \right] \\
&= \frac{I_a}{2n\pi} [-\text{Sinn}\alpha - \text{Cosn}\pi\text{Sinn}\alpha + \text{Cosn}\pi\text{Sinn}\alpha + \text{Cosn}2\pi\text{Sinn}\alpha] \\
&= 0 \quad \text{For all values of } n \tag{17}
\end{aligned}$$

The harmonic value of the harmonic content is,

$$I_{sn} = \frac{1}{\sqrt{2}} (a^2 + b^2)^{\frac{1}{2}} \tag{18}$$

$$\begin{aligned}
&= \frac{0 + \frac{2I_a}{n\pi} (1 + \text{Cosn}\alpha)}{\sqrt{2}} \\
&= \frac{\sqrt{2}I_a (1 + \text{Cosn}\alpha)}{n\pi} \tag{19}
\end{aligned}$$

Equation (11) can be re-written as,

$$i_s(t) = \sum_{n=1,2,3,\dots}^{\infty} \sqrt{2} I_n \text{Sinn}(\omega t + \phi_n) \quad (20)$$

where,

$$\phi_n = \tan^{-1} \frac{a_n}{b_n} \quad (21)$$

$$= 0 \quad \text{since, } a_n = 0 \quad (22)$$

Displacement factor (DF) is,

$$DF = \text{Cos} \phi_1 \quad (23)$$

$$= \text{Cos} 0^\circ$$

$$= 1 \quad (24)$$

Harmonic factor (HF) is,

$$HF = \left[\left(\frac{I_s}{I_{s1}} \right)^2 - 1 \right]^{\frac{1}{2}} \quad (25)$$

Substituting values for I_s and I_{s1} ,

$$= \left[\left[\frac{\left(\frac{2\pi - 3\alpha}{2\pi} \right)^{\frac{1}{2}}}{\frac{\sqrt{2}}{\pi} (1 + \text{Cos} \alpha)} \right]^2 - 1 \right]^{\frac{1}{2}}$$

$$= \left[\frac{2\pi - 3\alpha}{2\pi} * \frac{\pi^2}{2(1 + \text{Cos} \alpha)^2} - 1 \right]^{\frac{1}{2}}$$

$$= \left[\frac{\pi(2\pi - 3\alpha)}{4(1 + \cos \alpha)^2} - 1 \right]^{\frac{1}{2}}$$

$$= \left[\frac{\pi \left(\pi - \frac{3\alpha}{2} \right)}{2(1 + \cos \alpha)^2} - 1 \right]^{\frac{1}{2}} \quad (26)$$

Power factor (PF) is,

$$PF = \frac{I_{s1}}{I_s} \cos \phi_1 \quad (27)$$

$$= \frac{\sqrt{2}(1 + \cos \alpha)}{\pi \left(1 - \frac{3\alpha}{2\pi} \right)^{\frac{1}{2}}} \quad (28)$$

A similar analysis can be carried out for the interval; $0 < V_a < 0.5$ pu to obtain,

$$V_n = \frac{\cos \alpha}{2} \text{ pu} \quad (29)$$

$$DF = 1 \quad (30)$$

$$HF = \left[\frac{\pi(\pi - 2\alpha)}{8\cos^2 \alpha} - 1 \right]^{\frac{1}{2}} \quad (31)$$

$$PF = \frac{2\sqrt{2}\cos \alpha}{\pi \left(1 - \frac{2\alpha}{\pi} \right)^{\frac{1}{2}}} \quad (32)$$

APPENDIX VI

Generalised Analysis for the Pulse Width Modulation Control.

Consider the waveform of Fig. 4.5 for the Sequence with Forced Commutation

The output voltage and the performance parameter of the converter can be determined in two steps: [67, 70, 90-94].

- (i) By considering only one pair of pulses such that if one pulse starts at $\omega t = \alpha_1$ and ends at $\omega t = \alpha_1 + \delta_1$, the other pulse starts at $\omega t = \pi + \alpha_1$ and ends at $\omega t = (\pi + \alpha_1 + \delta_1)$ and
- (ii) By combining the effects of all points. If m^{th} pulse starts at $\omega t = \alpha_m$ and its width is δ_m , the average output voltage due to 'p' number of pulse is found from:

$$\sum_{m=1}^p \left[\frac{2}{2\pi} \int_{\alpha_m}^{\alpha_m + \delta_m} V_m \sin \omega t d(\omega t) \right] \quad (1)$$

$$= \frac{V_m}{\pi} \sum_{m=1}^p [-\cos \omega t]_{\alpha_m}^{\alpha_m + \delta_m}$$

$$= \frac{V_m}{\pi} \sum_{m=1}^p [\cos \alpha_m - \cos(\alpha_m + \delta_m)] \quad (2)$$

Let $\beta_m = (\alpha_m + \delta_m)$

Then the maximum dc voltage is $\frac{2V_m}{\pi}$ obtained by varying α_m and β_m from 0 to π

The normalized dc output voltage V_n ,

$$V_n = \frac{V_{dc}}{V_{d \max}} \quad (3)$$

$$= \frac{\frac{V_m}{\pi} \sum_{m=1}^p [\cos \alpha_m - \beta_m]}{\frac{2V_m}{\pi}}$$

$$= \frac{1}{2} \sum_{m=1}^p [\cos \alpha_m - \cos \beta_m] \quad (4)$$

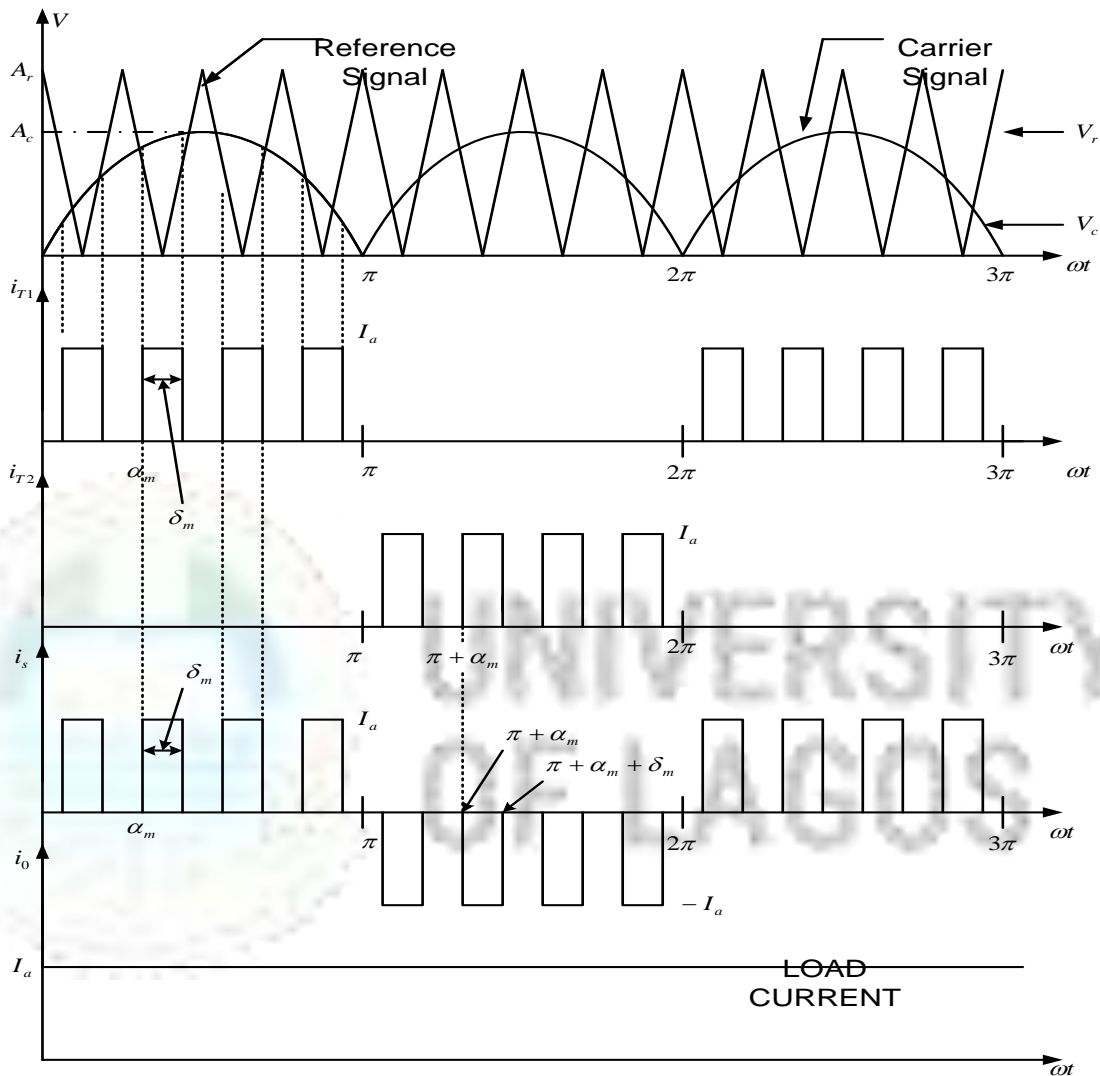


Fig.5.4: Waveforms of Currents and Voltages for Sinusoidal PWM

If the load current with an average of I_a is continuous and has negligible ripples, the instantaneous current can be expressed as:

$$i_s(t) = I_{dc} + \sum_{n=1,2,3,\dots}^{\alpha} (a_n \cos n \omega t + b_n \sin n \omega t) \quad (5)$$

And due to symmetry of the input current waveform, there will be no even harmonics and I_{dc} will be zero and the coefficients of equation (5) are:

$$a_n = \frac{1}{\pi} \int_0^{2\pi} i_s(t) \text{Cosn } \omega t d(\omega t) \quad (6)$$

$$= \sum_{m=1}^p \left[\frac{1}{\pi} \int_{\alpha_m}^{\alpha_m + \delta_m} I_a \text{Cosn } \omega t d(\omega t) - \int_{\pi + \alpha_m}^{\pi + \alpha_m + \delta_m} I_a \text{Cosn } \omega t d(\omega t) \right]$$

$$= \frac{I_a}{n\pi} \sum_{m=1}^p \left[\text{Sinn } \omega t \Big|_{\alpha_m}^{\alpha_m + \delta_m} - \text{Sinn } \omega t \Big|_{\pi + \alpha_m}^{\pi + \alpha_m + \delta_m} \right]$$

$$= \frac{I_a}{n\pi} \sum_{m=1}^p \left[\text{Sinn}(\alpha_m + \delta_m) - \text{Sinn} \alpha_m - \text{Sinn}(\pi + \alpha_m + \delta_m) - \text{Sinn}(\pi + \alpha_m) \right]$$

$$= \frac{I_a}{n\pi} \sum_{m=1}^p \left[\begin{aligned} & \left(\text{Sinn} \alpha_m \text{Cosn } \delta_m + \text{Cosn } \alpha_m \text{Sinn} \delta_m - \text{Sinn} \alpha_m \right) - \left(\text{Sinn} \pi \text{Cosn}(\alpha_m + \delta_m) \right) \\ & \left(\text{Sinn} \pi \text{Cosn } \alpha_m - \text{Cosn } \pi \text{Sinn} \alpha_m \right) - \left(\text{Sinn} \pi \text{Cosn}(\alpha_m + \delta_m) \right) \\ & \left(\text{Sinn} \pi \text{Cosn}(\alpha_m + \delta_m) + \text{Cosn } \pi \text{Sinn}(\alpha_m + \delta_m) \right) \end{aligned} \right] \\ = 0 \quad \text{for } n = 2, 4, 6 \dots \quad (7)$$

Similarly,

$$b_n = \frac{1}{\pi} \int_0^{2\pi} i_s(t) \text{Sinn } \omega t \quad (8)$$

$$= \sum_{m=1}^p \left[\frac{1}{\pi} \int_{\alpha_m}^{\alpha_m + \delta_m} I_a \text{Sinn } \omega t d(\omega t) - \frac{1}{\pi} \int_{\pi + \alpha_m}^{\pi + \alpha_m + \delta_m} I_a \text{Sinn } \omega t d(\omega t) \right]$$

$$= \frac{I_a}{n\pi} \sum_{m=1}^p \left[-\text{Cosn } \omega t \Big|_{\alpha_m}^{\alpha_m + \delta_m} - \left(-\text{Cosn } \omega t \Big|_{\pi + \alpha_m}^{\pi + \alpha_m + \delta_m} \right) \right]$$

$$= \frac{I_a}{\pi n} \sum_{m=1}^p \left[\text{Cosn } \alpha_m - \text{Cosn}(\alpha_m + \delta_m) + \text{Cosn}(\pi + \alpha_m + \delta_m) - \text{Cosn}(\pi + \alpha_m) \right]$$

$$= \frac{I_a}{\pi n} \sum_{m=1}^p \left[\begin{aligned} & \left(\text{Cosn } \alpha_m - \text{Cosn}(\alpha_m + \delta_m) + \text{Cosn } \pi \text{Cosn}(\alpha_m + \delta_m) - \text{Sinn } \pi \text{Sinn}(\alpha_m + \delta_m) \right) \\ & \left(\text{Cosn } \pi \text{Cosn } \alpha_m + \text{Sinn } \pi \text{Sinn} \alpha_m \right) \end{aligned} \right]$$

$$= 0 \quad \text{For } n = 0, 2, 4, \dots \text{ (n=even)} \quad (9)$$

$$= \frac{I_a}{\pi n} \sum_{m=1}^p [\text{Cosn } \alpha_m - \text{Cosn}(\alpha_m + \delta_m) - \text{Cosn}(\alpha_m + \delta_m) + \text{Cosn } \alpha_m]$$

$$= \frac{I_a}{\pi n} \sum_{m=1}^p [2\text{Cosn } \alpha_m - 2\text{Cosn}(\alpha_m + \delta_m)]$$

$$= \frac{2I_a}{\pi n} \sum_{m=1}^p [\text{Cosn } \alpha_m - \text{Cosn}(\alpha_m + \delta_m)] \quad \text{For } n = 1, 3, 5, \dots \quad (10)$$

Hence equation (5) can see re-written as:

$$i_s(t) = \sum_{n=1,3,5}^{\infty} \sqrt{2} I_a \text{Sin}(n\omega t + \phi_n) \quad (11)$$

where,

$$\phi_n = \tan^{-1} \frac{a_n}{b_n} = 0 \quad (12)$$

Since, $a_n = 0$

$$\text{and } I_{s_n} = \frac{1}{\sqrt{2}} [a_n + b_n]^{\frac{1}{2}} = \frac{b_n}{\sqrt{2}} \quad (13)$$

= rms value of the nth harmonic component of the input current.

Substituting equation (7) and (10) in (13),

$$I_{s_1} = \frac{\frac{2I_a}{\pi n} \sum_{m=1}^p [\text{Cosn } \alpha_m - \text{Cosn}(\alpha_m + \delta_m)]}{\sqrt{2}} \quad (14)$$

$$I_{s_1} = \frac{\sqrt{2} I_a}{\pi} \sum_{m=1}^p [\text{Cos } \alpha_m - \text{Cos}(\alpha_m + \delta_m)] \quad (15)$$

The rms value of the input current is,

$$\begin{aligned}
 I_s &= \left[\frac{1}{\pi} \int_0^{\pi} i_s^2(t) dt \right]^{\frac{1}{2}} \\
 &= \frac{1}{\sqrt{\pi}} \left[\int_{\alpha_m}^{\alpha_m + \delta_m} I_a^2(t) dt \right]^{\frac{1}{2}} \\
 &= \frac{I_a}{\sqrt{\pi}} \left[t \Big|_{\alpha_m}^{\alpha_m + \delta_m} \right]^{\frac{1}{2}} \\
 &= \frac{1}{\sqrt{\pi}} [(\alpha_m + \delta_m) - \alpha_m]^{\frac{1}{2}}
 \end{aligned}
 \tag{16}$$

For all pulses,

$$I_s = \frac{I_a}{\sqrt{\pi}} \left[\sum_{m=1}^p [(\alpha_m + \delta_m) - \alpha_m] \right]^{\frac{1}{2}}
 \tag{17}$$

Displacement factor DF is,

$$DF = \cos \phi_1
 \tag{18}$$

From equation (4),

$$\phi_1 = 0$$

Hence,

$$\begin{aligned}
 DF &= \cos 0^\circ \\
 &= 1
 \end{aligned}
 \tag{19}$$

Harmonic factor HF is,

$$HF = \left[\left(\frac{I_s}{I_{s1}} \right)^2 - 1 \right]^{\frac{1}{2}} \quad (20)$$

$$= \left[\frac{\frac{I_a^2}{\pi} \sum_{m=1}^p ((\alpha_m + \delta_m) - \alpha_m)}{\frac{2I_a^2}{\pi^2} \left[\sum_{m=1}^p \cos \alpha_m - \cos(\alpha_m + \delta_m) \right]^2} - 1 \right]^{\frac{1}{2}}$$

$$= \left[\frac{\pi \sum_{m=1}^p [(\alpha_m + \delta_m) - \alpha_m]}{2 \sum_{m=1}^p [\cos \alpha_m - \cos(\alpha_m + \delta_m)]^2} - 1 \right]^{\frac{1}{2}} \quad (21)$$

The input power factor PF is,

$$PF = \frac{I_{s1}}{I_s} \cos \phi_1 \quad (22)$$

substituting equations (15), (17) and (19), in (22)

$$= \frac{\sqrt{2} I_a \sum_{m=1}^p [\cos \alpha_m - \cos(\alpha_m + \delta_m)]}{\frac{I_a}{\sqrt{\pi}} \sum_{m=1}^p [(\alpha_m + \delta_m) - \alpha_m]^{\frac{1}{2}}} * 1$$

$$= \frac{\sqrt{2} \sum_{m=1}^p [\cos \alpha_m - \cos(\alpha_m + \delta_m)]}{\sqrt{\pi} \sum_{m=1}^p [(\alpha_m + \delta_m) - \alpha_m]^{\frac{1}{2}}}$$

$$= \sqrt{\frac{2}{\pi}} \frac{\sum_{m=1}^p [\cos \alpha_m - \cos(\alpha_m + \delta_m)]}{\sum_{m=1}^p [(\alpha_m + \delta_m) - \alpha_m]^{\frac{1}{2}}} \quad (23)$$

APPENDIX VII

Matlab programming of the expressions of PF, HF and DF for the various technique summarized in table 6.1

Matlab Computer programming for Power Factor

```
alpha=0.01:0.1:pi;
```

```
a=cos(alpha);
```

```
b=1+a;
```

```
c=sqrt(2)*b;
```

```
d=alpha./pi;
```

```
e=1-d;
```

```
f=sqrt(e);
```

```
g=pi*f;
```

```
pf=c./g;
```

```
vout=b./2;
```

```
plot(vout,pf,'c:*')
```

```
xlabel('Output Voltage (Va) in pu')
```

```
ylabel('Power Factor (PF)')
```

```
> hold on
```

```
>> alpha=0.01:0.1:pi;
```

```
a=cos(alpha);
```

```
b=3+a;
```

```
c=3*alpha;
```

```
d=c./2;
```

```
e=2*pi-d;
```

```
f=pi*e;
```

```
g=sqrt(f);
```

```
pf=b./g;
```

```
vout=b./4;
```

```
>> plot(vout,pf,'m:s')
```

```
>> hold on
```

```
>> h=1+a;
```

```
i=sqrt(2)*h;
```

```
j=alpha./pi;
```

```
k=1-j;
```

```
l=sqrt(k);
```

```
m=pi*l;
```

```
pf=i./m;
```

```
vout=h./4;
```

```
>> plot(vout,pf,'m:s')
```

UNIVERSITY
OF LAGOS

```

>> xlabel('Output Voltage (Va)')
>> ylabel('Power Factor (PF)')
>> hold on
>> alpha=0.01:0.1:pi;
a=1-cos(alpha);
b=sqrt(2)*a;
c=pi*alpha;
d=sqrt(c);
pf=b./d;
vout=a./2;
>> plot(vout,pf,'y:d')
>> xlabel('Output Voltage (Va)')
>> ylabel('Power Factor (PF)')
>> alpha=0.01:0.1:pi;
a=sqrt(2)*2;
b=a*cos(alpha);
c=2*alpha;
d=pi-c;
e=pi*d;
f=sqrt(e);
pf=b./f;
vout=cos(alpha);
>> plot(vout,pf,'r:+')
Warning: Imaginary parts of complex X and/or Y arguments ignored.
>> xlabel('Output Voltage (Va) in (pu)')
>> ylabel('Power Factor (PF)')
>> hold on
>> alpha=0.01:0.1:pi./2;
h=sqrt(2)*cos(alpha);
m=2*h;
o=2*alpha;
p=o./pi;
q=1-p;
r=sqrt(q);
s=pi*r;
pf=m./s;
t=cos(alpha);
vout=t./2;
>> plot(vout,pf,'g:<')
>> hold on

```

```

>> alpha=0.01:0.1:pi./2;
a=1+cos(alpha);
b=sqrt(2)*a;
c=3*alpha;
d=c./2;
e=pi-d;
f=pi*e;
g=sqrt(f);
pf=b./g;
vout=a./2;
>> plot(vout,pf,'g:<')
>> hold on
>> alpha=0.01:0.1:pi;
deta=pi;
a=cos(alpha)-cos(alpha+deta);
b=sqrt(deta);
c=sqrt(2/pi);
d=a./b;
pf=c*d;
vout=a./2;
pplot(vout,pf,'k:^')
xlabel('Output Voltage (Va) in pu')
>> ylabel('Power Factor (PF)')

```

2 Computer Programming for Harmonic Factor (HF)

```

alpha=0.01:0.1:pi;
a=pi-alpha;
b=pi*a;
c=1+cos(alpha);
d=4*c;
e=b./c;
f=e-1;
hf=sqrt(f);
vout=c./2;
>> plot(vout,hf,'c:*')
>> xlabel('Output Voltage (Va) in pu')
>> ylabel('Harmonic Factor (HF)')
>> hold on

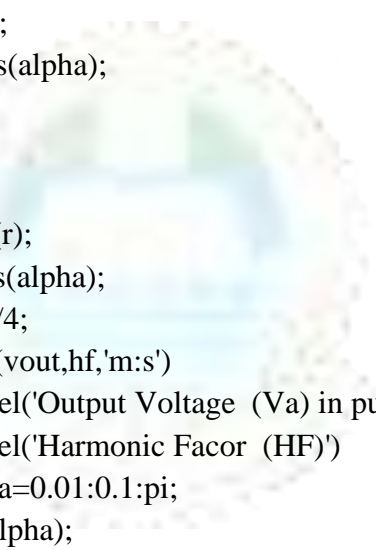
```

UNIVERSITY
OF LAGOS

```

>> alpha=0.01:0.1:pi;
a=pi-alpha;
b=pi*a;
c=1+cos(alpha);
d=4*c;
e=b./d;
f=e-1;
hf=sqrt(f);
vout=c./4;
>> plot(vout,hf,'m:s')
>> hold on
>> g=3*alpha;
j=g./4;
m=pi-j;
n=pi*m;
o=3*cos(alpha);
p=5+o;
q=n./p;
r=q-1;
hf=sqrt(r);
s=3+cos(alpha);
vout=s./4;
>> plot(vout,hf,'m:s')
>> xlabel('Output Voltage (Va) in pu')
>> ylabel('Harmonic Factor (HF)')
>> alpha=0.01:0.1:pi;
a=cos(alpha);
b=1-a;
c=4*b;
d=pi*alpha;
e=d./c;
f=e-1;
hf=sqrt(f);
vout=b./2;
>> plot(vout,hf,'y:d')
>> xlabel('Output Voltage (Va) in pu')
>> ylabel('Harmonic Factor (HF)')
>> hold on
>> alpha=0.01:0.1:pi;
a=2*alpha;

```



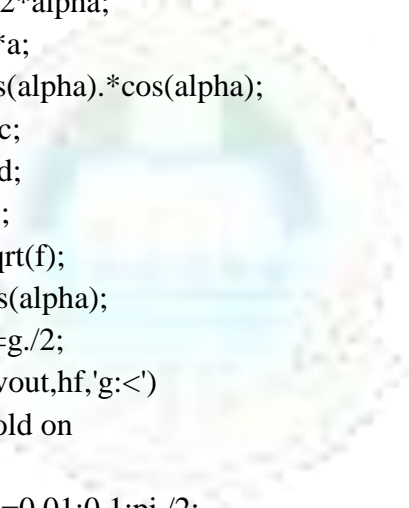
UNIVERSITY
OF LAGOS

```

b=pi-a;
c=pi*b;
d=cos(a);
e=1+d;
f=4*e;
g=c./f;
i=g-1;
hf=sqrt(i);
vout=cos(alpha);
>> plot(vout,hf,'r:+')
Warning: Imaginary parts of complex X and/or Y arguments ignored.
>> xlabel('Output Voltage (Va) in pu')
>> ylabel('Harmonic Facor (HF)')
>> alpha=0.01:0.1:pi./2;
a=pi-2*alpha;
b=pi*a;
c=cos(alpha).*cos(alpha);
d=8*c;
e=b./d;
f=e-1;
hf=sqrt(f);
g=cos(alpha);
vout=g./2;
plot(vout,hf,'g:<')
>> hold on

alpha=0.01:0.1:pi./2;
i=3*alpha;
j=i./2;
k=pi-j;
l=pi*k;
m=1+cos(alpha);
n=m.*m;
o=2*n;
p=l./o;
q=p-1;
hf=sqrt(q);
vout=m./2;
>> plot(vout,hf,'g:<')
>> hold on

```



UNIVERSITY
OF LAGOS

```

>> alpha=0.01:0.1:pi;
deta=pi;
a=cos(alpha)-cos(alpha+deta);
b=sqrt(deta);
vout=a./2;
e=pi*b;
f=2*a;
g=e./f;
h=g-1;
hf=sqrt(h);
>> plot(vout,hf,'k:^')
Warning: Imaginary parts of complex X and/or Y arguments ignored.
>> xlabel('Output Voltage (Va) in pu')
>> ylabel('Harmonic Factor (HF)')

```

Computer Programming for Displacement Factor

```

alpha=0.01:0.1:pi;
c=cos(alpha);
vout=c./2;
for t=1:1:32;
df(t)=1;
end;
>> plot(vout,df,'g:<')
>> hold on
>> a=1+c;
>> vout=a./2;
>> for t=1:1:32;
df(t)=1;
end;
>> plot(vout,df,'g:<')
>> xlabel('Output Voltage (Va) in pu')
>> ylabel('Displacement Factor (DF)')
>> hold on
>> alpha=0.01:0.1:pi;
a=alpha./2;
df=cos(a);
b=1+cos(alpha);
vout=b./2;
>> plot(vout,df,'c:*')
>> hold on

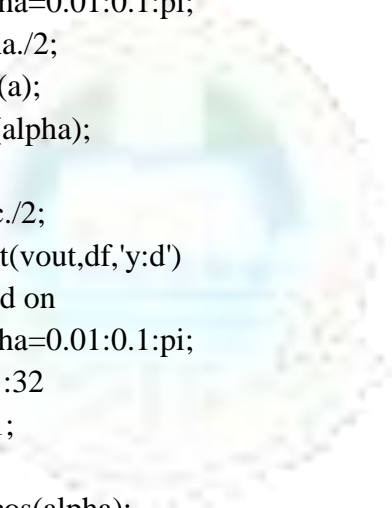
```

UNIVERSITY
OF LAGOS

```

>> alpha=0.01:0.1:pi;
a=alpha./2;
df=cos(a);
b=1+cos(alpha);
c=b./4;
vout=c;
>> plot(vout,df,'m:s')
>> hold on
>> d=3+cos(alpha);
vout=d./4;
h=10+6*cos(alpha);
i=sqrt(h);
df=d./i;
>> plot(vout,df,'m:s')
>> alpha=0.01:0.1:pi;
a=alpha./2;
df=sin(a);
b=cos(alpha);
c=1-b;
vout=c./2;
>> plot(vout,df,'y:d')
>> hold on
>> alpha=0.01:0.1:pi;
for t=1:32
df(t)=1;
end;
vout=cos(alpha);
>> plot(vout,df,'r:+')
>> hold on
>> alpha=0.01:0.1:pi;
t=1:1:32;
df(t)=1;
alpha=0.01:0.1:pi;
deta=pi;
for t=1:1:32;
df(t)=1;
end;
a=cos(alpha)-cos((alpha)+deta);
vout=a./2;
>> plot(vout,df,'k:^')

```



UNIVERSITY
OF LAGOS

APPENDIX VIII

Published Paper I

This was a paper presented and published from my research work in the proceedings of International Conference and Exhibition on Power Systems held at the University of Lagos, Akoka, Lagos, Nigeria, 23 – 25 July, 2007 Pages 191 - 197

THE INPUT POWER FACTOR PROBLEM FOR INDUSTRIAL DRIVES

Prof. C.C.Okoro and O.D. Osunde

Department of Electrical and Electronics Engineering

University of Lagos, Lagos, Nigeria.

Email: ccokoro@hotmail.com and osundave2@yahoo.com.

ABSTRACT: This paper presents the input power factor problem of an Industrial drive connected to a DC motor load and operated either in the continuous or discontinuous mode. An indepth mathematical analysis of the drive system, its behaviour factors (Harmonic factor, Displacement factor, Power factor etc) and techniques for poor power factor reduction is also discussed.

Keywords: Drives, Power Factor, Harmonic Factor, Displacement Factor.

1. INTRODUCTION

With the re – awakening of the long abandoned Ajaokuta Steel Rolling mills, Aluminum Smelting plant at Ikot – Abasi, Aladja Steel rolling mills, a large number of converters are expected to be in use. Also, the development of many kilometers of rails from Aladja, following the immediate take off of the Ajaokuta Steel Mills and associated industrialization in the steel sector is expected to increase the harmonic currents produced by drives in Power Holding Company of Nigeria (PHCN) network and hence will bring the associated problems to the fore [2].

Industrial drives connected to an electricity distribution network; introduce non – sinusoidal waveforms at the ac input side as a result of the switching action of the devices. It also produces a non – sinusoidal line current due to the non – linear input characteristics. With the steadily increasing use of such drives, line current harmonics have become a significant problem. Their adverse effects on the power system are well recognized [1-3].

Okoro [2], in his study reveals that the presence of harmonics in the supply waveforms has a wide – ranging effects on the supply system. These include:

- Degradation of system voltage waveforms and of equipment performance and effective life.
- Overheating in transformers and induction motors, shunt capacitors, power cables, electrical machines and switchgear leading to premature ageing.
- Increased transmission losses, protective system mal – operation, communication system interference and above all

- Poor input power factor

These reports were influenced by the identified interest in the many factors that affect the magnitude of the ripple fed to the controlled machine and their impact on the overall performance of the drives. To clearly present this problem, the single – phase asymmetrical bridge converter has been chosen as a peculiar drive for the analysis because it has a wide range of application and presents the worst form of harmonics [1-4]. Fourier series has been employed to gain understanding of the basic operation and behaviour of a typical Single – Phase Asymmetrical Bridge Converter Controller.

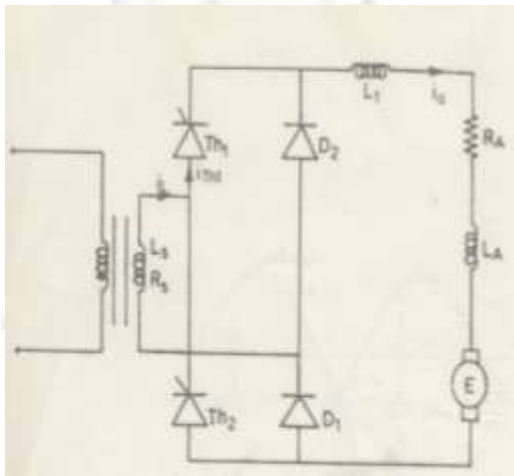


Figure 1: The Asymmetrical Bridge Converter.

2. ANALYSIS OF THE ASYMMETRICAL SINGLE – PHASE BRIDGE.

2.1 Discontinuous Armature Current

The basic circuit of the asymmetrical single – Phase Bridge shown in Figure (1) has been studied and analyzed in previous work [1, 2, 6, 7]. The current and voltage waveforms are shown in Figure (2). Explicit expression of the input current can be obtained by

analyzing the half – cycle equivalent circuits in Figure (3) for the different intervals assuming that the terminal condition of one interval are the initial conditions for the next interval.

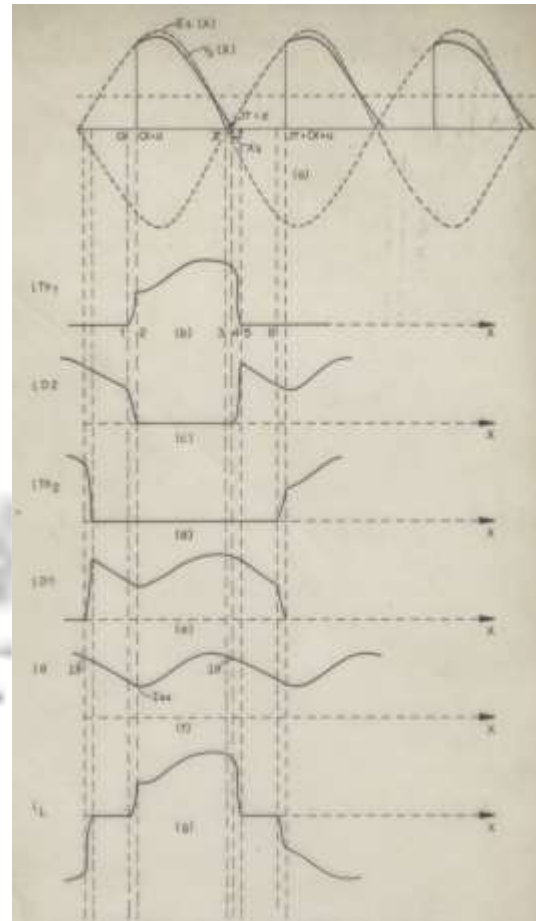


Figure 2: Waveforms of the bridge converter;

(a) Voltage waveforms

(b) – (g) Current waveforms

Operating Intervals:

1 – 2 Forward Commutation of TH_1

2 – 3 Conduction of TH_1

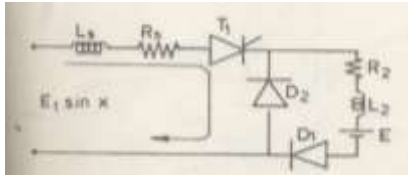
3 – 4 Angle β after π for to become forward biased

4 – 5 Extinction interval

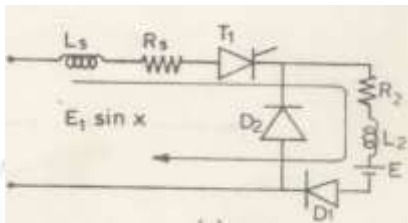
5 – 6 Freewheeling interval

(c) Freewheeling interval $0 < x < \alpha$

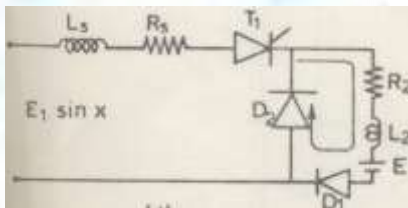
(d) Reverse Commutation or Extinction interval $\pi + \beta < x < \pi + \beta + x_s$



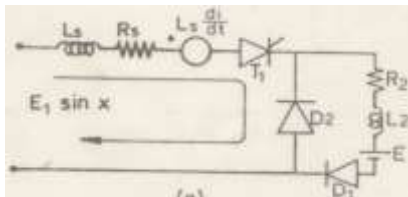
(a)



(b)



(c)



(d)

Figure 3: Half circle equivalent circuit showing path of current during different intervals

(a) Forward Commutation interval $\alpha < x < \alpha + u$

(b) Conduction interval $\alpha + u < x < \pi$

The simplifying equations are based on the following assumptions [8-12].

- That the thyristors are ideal switches
- That a steady state condition has been established to justify repetitive representation of the cycles.
- Non – linearity in operation of the machine is included in the parameters of the system equations.
- That the motor is separately excited.

In the forward commutation interval, $\alpha < x < \alpha + u$, fig. 3(b), before the current in a thyristor gated at delay angle ' α ' reaches the value of current in the armature, the equation for the circuit of fig. 3(b) in which the forward commutating current flows is:

$$R_s i + L_s \frac{di}{dt} = E_1 \sin(\omega t + \alpha) \quad (1)$$

With initial condition $i = 0$ at $\omega t = 0$, the current in this interval is given by:

$$i(t) = K_1 \left\{ \sin(\omega t + \alpha - \theta_1) + \sin(\theta_1 - \alpha) \exp\left(\frac{-t}{\tau_1}\right) \right\} \quad (2)$$

Where, $k_1 = \frac{E_1}{Z_1}$, $Z_1 = R_s + j\omega L_s$, $\tau_1 = \frac{L_s}{R_s}$

$$\theta_1 = \tan^{-1} \frac{\omega L_s}{R_s}$$

Current at the end of the interval when $\omega t = u$ is:

$$I_{ao} = K_1 \left\{ \sin(\omega t + \alpha - \theta_1) + \sin(\theta_1 - \alpha) \exp\left(\frac{-u}{\omega\tau_1}\right) \right\} \quad (3)$$

In the interval $\alpha + u \leq x < \pi$, the current flows in the path shown in Fig. 3(b) and is given by the equation,

$$L \frac{di}{dt} + Ri + E = E_1 \sin(\omega t + \alpha + u) \quad (4)$$

Where, $L = L_s + L_1 + L_a$, $R = R_s + R_a$

With the initial condition $i = I_{ao}$ at $\omega t = 0$, the current in the interval is:

$$i(x) = K_2 [\cos\theta_2 \sin(x - \theta_2) - P] + \{K_2 [\cos\theta_2 \sin(\theta_2 - \alpha - u) + P] + I_{ao}\} * \exp\left(-\left(\frac{x - \alpha - u}{\omega t}\right)\right) \quad (5)$$

Where, $K_2 = \frac{E_1}{R}$, $P = \frac{E}{E_1}$, $\theta_2 = \tan^{-1} \frac{\omega L}{R}$

$$\tau = \frac{L}{R}$$

and, $x = \omega t + \alpha + u$

In the interval $0 < x < \alpha$, the load is not connected to the supply, current flows in the path shown in fig. 3(c) and is given by;

$$L_2 \frac{di}{dt} + iR_a = -E \quad (6)$$

Where, $L_2 = L_1 + L_a$

With initial current I_1 at $x = 0$, the current in the free-wheeling interval is;

$$i(x) = I_1 \exp\left(\frac{-x}{\omega\tau_2}\right) - \left(\frac{E}{R_a}\right) \left(1 - \exp\left(\frac{-x}{\omega\tau_2}\right)\right) \quad (7)$$

Where, $\tau_2 = \frac{L_2}{R_a}$

At $x = \alpha + u$, the current is I_{ao} , which is given by the equation;

$$I_{ao} = I_1 \exp\left(\frac{-(\alpha + u)}{\omega\tau_2}\right) - \left(\frac{E}{R_a}\right) \left(1 - \exp\left(\frac{-(\alpha + u)}{\omega\tau_2}\right)\right) \quad (8)$$

Combining equations (3) and (8), gives the current at $x = 0$ as;

$$I_1 = \left[\frac{E}{R_a} \left\{ K_1 \left\{ \sin(u + \alpha - \theta_1) + \sin(\theta_1 - \alpha) \exp\left(\frac{-u}{\omega\tau_1}\right) \right\} + \right\} * \exp\left(\frac{(\alpha + u)}{\omega\tau_2}\right) - \frac{E}{R_a} \right] \quad (9)$$

The current at $x = \pi$, during the conduction interval is also equal to I_1 , giving

$$I_1 = K_2 [\cos\theta_2 \sin\theta_2 - P] + \left\{ K_2 \left[\frac{\cos\theta_2 \sin(\theta_2 - \alpha - u) + P}{I_{ao}} \right] + \right\} * \exp\left(\frac{-(\pi - \alpha - u)}{\omega\tau}\right) \quad (10)$$

Combining equations (9) and (10), gives a transcendental equation $f(u)$ which can be solved to obtain the commutation angle ' u ' for the gating angle ' α '.

The free - wheeling diode D_2 in Fig. 3(c) becomes forward biased when the instantaneous supply voltage equals the source inductance. The induced voltage reverse biases D_2 , until the angle after ' π ' when this voltage is neutralized by the instantaneous supply voltage. The current in the conducting thyristor begins to decay to zero and in an attempt to oppose this, the

voltage in the armature circuit inductance forward biases ‘ D_2 ’ to begin the freewheeling mode.

The reverse commutation of current from a conducting thyristor is opposed by the voltage induced in the source inductance. Defining ‘ ωt ’ from $x = \pi$, the current in a reverse commutating thyristor falls to zero from the value at $x = \pi + \beta$ i.e I_β .

So, in the interval $\pi + \beta < x < \pi + \beta + \lambda$, the conducting thyristor switches off and the expression for current during this interval is obtained from the describing equation of current from Fig.3 (d);

$$L_s \frac{di}{dt} + R_s i = -E_1 \sin(\omega t + \beta) \quad (11)$$

With the initial condition $i = I_\beta$, the current during the extinction process is;

$$i(t) = -K_1 [\sin(\omega t + \beta - \theta_1)] - [K_1 \sin(\theta_1 - \beta) - I_\beta] * \exp\left(\frac{-t}{\tau_1}\right) \quad (12)$$

These equations for the current at the various intervals summed together, gives the current drawn from the supply by the motor load as shown in Fig. 2.

Work is still been done , to predict the harmonics and the relationships of the behaviour factors (power factor, harmonic factor, displacement factor, peak factor, distortion factor, etc).

2.2 Continuous Armature Current

The waveform of currents of the drive when operating in a continuous armature current

mode is as shown in Figure (4). The assumptions [5-6] are:

- That the load is inductive
- That the load current is continuous.

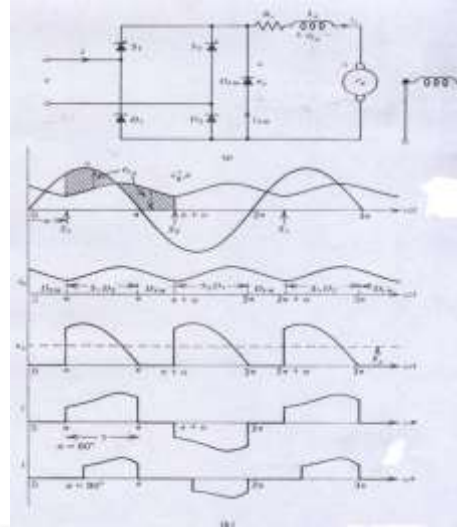


Figure (4): Speed control of a separately excited dc motor by a single phase Asymmetric bridge converter.

(a) Power circuit

(b) Voltage and current waveforms for continuous motor current

The instantaneous input current to an asymmetrical single – Phase Bridge can be expressed in Fourier series:

$$i_s(t) = I_{dc} + \sum_{n=1,2,\dots}^{\infty} (a_n \cos n\omega t + b_n \sin n\omega t) \quad (13)$$

Where

$$I_{dc} = \frac{1}{2\pi} \int_0^{2\pi} i_s(t) d(\omega t) \\ = \frac{1}{2\pi} \left[\int_{\alpha}^{\pi} i_a(t) d(\omega t) - \int_{\pi+\alpha}^{2\pi} i_a(t) d(\omega t) \right]$$

Simplifying yields,

$$I_{dc} = 0 \quad (14)$$

$$\begin{aligned} a_n &= \frac{1}{\pi} \int_{\alpha}^{2\pi} i_s(t) \cos n\omega t d(\omega t) \\ &= \frac{1}{\pi} \left[\int_{\alpha}^{\pi} I_a(t) \cos n\omega t d(\omega t) - \int_{\pi+\alpha}^{2\pi} I_a(t) \cos n\omega t d(\omega t) \right] \\ &= \frac{-2I_a}{n\pi} \sin n\alpha \quad \text{For } n = 1, 3, 5, \dots \text{ odd} \end{aligned}$$

Also,

$$b_n = \frac{1}{\pi} \int_{\alpha}^{2\pi} i_s(t) \sin n\omega t d(\omega t) \quad (15)$$

$$= \frac{2I_a}{n\pi} (1 + \cos n\alpha) \quad \text{for } n = 1, 3, 5, \dots \quad (16)$$

Equation (13) can be written as

$$i_s(t) = \sum_{n=1,3,5,\dots}^{\infty} \sqrt{2} I_{sn} \text{Sinn}(n\omega t + \phi_n) \quad (17)$$

where,

$$I_{sn} = \frac{1}{\sqrt{2}} (a_n^2 + b_n^2)^{\frac{1}{2}} \quad (18)$$

This is the nth harmonic current of the input.

Substituting for a_n and b_n ,

$$= \frac{2\sqrt{2}I_a}{n\pi} \cos \frac{n\alpha}{2} \quad (19)$$

$$\text{And, } \phi_n = \frac{-n\alpha}{2} \quad (20)$$

Hence equation (17) becomes;

$$i_s(t) = \frac{4I_a}{n\pi} \sum_{n=1,3,5,\dots}^{\infty} \left[\cos \frac{n\alpha}{2} \sin \left(n\omega t - \frac{n\alpha}{2} \right) \right] \quad (21)$$

The fundamental current is obtained by setting $n = 1$

From equation (19)

$$I_{s_1} = \frac{2\sqrt{2}}{\pi} I_a \cos \frac{\alpha}{2} \quad (\text{i.e. } n = 1) \quad (22)$$

Determination of I_s :

$$\begin{aligned} I_s &= \left[\frac{2}{2\pi} \int_{\alpha}^{\pi} I_a^2 d(\omega t) \right]^{\frac{1}{2}} \\ &= \left[\frac{I_a^2}{\pi} |\omega t| \right]_{\alpha}^{\pi} \\ &= I_a \left[1 - \frac{\alpha}{\pi} \right]^{\frac{1}{2}} \quad (23) \end{aligned}$$

Power factor [6, 7] is defined as;

$$\text{PF} = \frac{I_{s_1}}{I_s} \cos \phi_{s_1}$$

Where,

$$\phi_{s_1} = -\frac{\alpha}{2} \quad \text{From equation (20)}$$

and,

$$\begin{aligned} \text{PF} &= \frac{I_{s_1}}{I_s} \cos \frac{\alpha}{2} = \left[\frac{\frac{2\sqrt{2}}{\pi} I_a \cos \frac{\alpha}{2}}{I_a \left(1 - \frac{\alpha}{\pi} \right)^{\frac{1}{2}}} \right] \cos \frac{\alpha}{2} \\ &= \frac{\sqrt{2} [1 + \cos \alpha]}{[\pi(\pi - \alpha)]^{\frac{1}{2}}} \quad (24) \end{aligned}$$

Equation (24) shows the relationship between Power Factor and the thyristor firing angle. An increase in the firing angle reduces the power factor

The expression for harmonic factor [6,7] is;

$$HF = \left[\frac{I_{s_1}^2 - I_s^2}{I_{s_1}^2} \right]^{\frac{1}{2}} = \left[\left(\frac{I_s}{I_{s_1}} \right)^2 - 1 \right]^{\frac{1}{2}}$$

Substituting for I_s and I_{s_1}

$$HF = \left[\frac{\pi(\pi - \alpha)}{4(1 + \cos \alpha)} - 1 \right]^{\frac{1}{2}} \quad (25)$$

If ϕ_{s_1} is the angle between the fundamental component of the input current and AC input voltage, then the displacement factor DF is:

$$DF = \cos \phi_{s_1} = \cos \frac{-n\alpha}{2}$$

$$\cos \phi_{s_1} = \cos \left(\frac{-\alpha}{2} \right) \quad (26)$$

3. RESULTS

The expressions derived in equation (21) for the instantaneous input current are plotted in Figure (5) for various firing angle of the thyristors of the drive. Their corresponding harmonics are displayed in Figure (6). Evidently, the PF, HF and the DF varies with the delay or firing angle and their plots are shown in Figures (7)

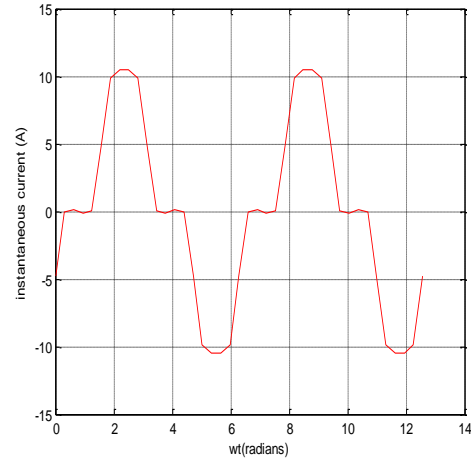


Figure (5): Waveform of input current for a delay angle of ' α ' = 60 degrees

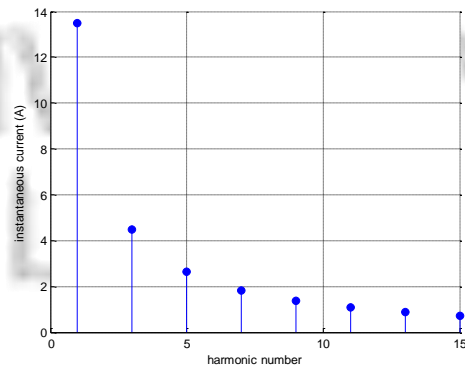
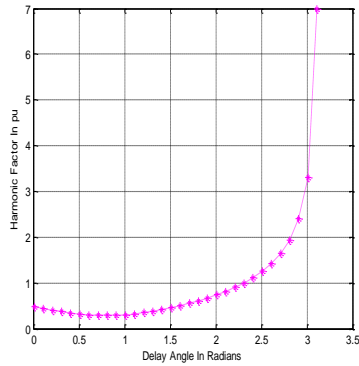
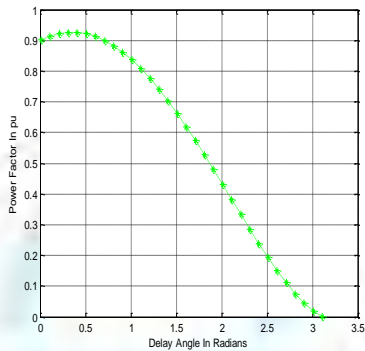


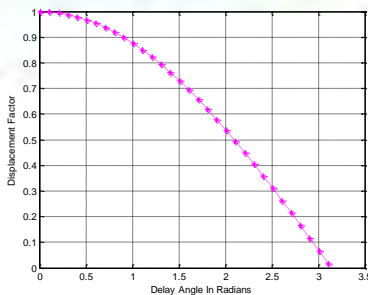
Figure (6): Harmonics of the single – phase asymmetric bridge converter



(a)



(b)



(c)

Figure (7): Behaviour factors of the bridge

- (a) Harmonic factor
- (b) Power factor
- (c) Displacement factor

It should be noted that the power factor worsen as the number of such drives connected to the supply system increase The theory for this situation is being developed.

4. Conclusion

The realization of the full potential of steel plants already built in the country would increase the level of non – linear loads connected to the National Grid. Unless there is an understanding of the effects of these loads and adequate implementation of harmonic suppression and reduction techniques, more problems are bound to arise. This paper has contributed to locally available information on harmonic sources and their effect on the supply line. Increased local interests in the phenomenon of equipment and system failure as a result of harmonic induced resonances are hereby encouraged. An important point to note is that the power factor of the supply system worsens as the firing or delay angle of the thyristors of the drive increases.

5. References

1. Okoro, C .C, (1982), “Performance Evaluation of a D.C. Motor Fed from an Asymmetrical Single – Phase Bridge, 1982, Proc. IEE, Vol. 129, PTB. No.5, pages 289 – 298
2. Okoro, C.C, (1987), “Behaviour Factors of the Asymmetrical Single – Phase Converter”, Nigerian Journal of Engineering and Technology, Vol. 10, No.1, April 1987, pages 1-17.
3. Okoro, C.C. (1985), “Commutation in D.C. Machines with Input Ripple”, International Conference on

- Electrical Machines, IEE, Savoy Place, London. Sept. 1985, Conf. PUB, 254, pages 295 – 298
4. Okoro, C .C. (1993), “A Qualitative Investigation of Flux Pulsations in a D.C Machine with Input Current Ripple”, International Conference on Electrical Machines and Drives, University of Oxford, 8 – 10th Nov. 1993. Page 146 - 154
 5. P.C Sen (1981) “Thyristor DC Drives. John Wiley and Sons Ltd. NY, 1981.
 6. Muhammed R. Rashid: (1993), “Power Electronics: Devices and Application”. Prentice-Hall Inc. 2nd Edition 1993.
 7. P.Mehta, S. Mukhopadhyay, (1974), “Modes of operation in Converter – Controlled D.C drives’. Proc. IEE, Vol. 121, No. 3, March, 1974. Pages 468-474.
 8. Agu, U (1997), “Relative study of the output characteristics of PWM and Phase controlled AC – DC converters”, Conf. Publication, Electric Power Engineering Conference (EPEC), UNN, 4-5th. Dec. 1997. Pages 132 – 140.
 9. Fuhao, T and Miyalvi, S: (1974), “Ac – DC Converter with improved power Factor and Current Waveform on AC side, Electrical Engineering in Japan, Vol. 94, No. 4, 1974. Pages 89-96.
 10. Zander H: (1973), “Self Commutated Rectifier to improve Line Conditions”, Proc. IEE, Vol. 120, No. 9, Sept. 1973
 11. Ira Pitel and Sarosh, N. T.: (1977), A review of the effects and suppression of Power Converter Harmonics”. Industry and Application Society, Annual Conference, 1997, pages 119-120.
 12. Dewan, S. B. et al: (1970). “Input Filter Design with Static Power Converters”, IEE Industry and General Applications, Vol. IGA – 6, No. 4, July/Aug.1970. Pages 326 – 335.

APPENDIX IX

Published Paper II

This was a paper presented and published from my research work in the proceedings of International Conference on Emerging trends, research directions and training requirements of 21st century Electrical and Electronics Engineering held at the University of Lagos, Akoka, Lagos, Nigeria, 22 – 24 July, 2009 Pages 52 - 56

BRIDGELESS ASYMMETRICAL SINGLE – PHASE AC – DC BOOST CONVERTER FOR POWER FACTOR CORRECTION

O.D. Osunde

Department of Electrical and Electronics Engineering
University of Lagos, Lagos, Nigeria.

Email: osundave2@yahoo.com

ABSTRACT: A simplified approach of a Pulse Width Modulated Single Phase AC – DC converter for power factor correction is investigated as a more efficient and cheaper alternative to the conventional asymmetrical Boost converter for Power Factor Correction. The Bridgeless asymmetrical AC – DC Boost converter employs fewer semi – conductor devices thereby reducing power losses and increased reliability. It has a higher efficiency compared to the conventional boost PFC that suffers from high conduction loss. It is however limited to low and medium power applications.

Keywords: Bridgeless Boost converter, Power Factor Correction (PFC), PWM

I.INTRODUCTION

Single switch PFC is the most widely used topology for the PFC applications because of its simplicity and smaller EMI filter size. Due to the high conduction losses and switching losses, this circuit has a low efficiency at low input line voltage. With the development of super junction MOSFET,

switching losses of the PFC circuit is dramatically improved [1]. Meanwhile, the circuit still suffers from forward voltage drop of the rectifier bridge caused by high conduction losses, especially at low input line. To reduce the rectifier bridge conduction losses, different topologies have been developed. Among these topologies, the bridgeless boost which does not require circuit switch, is quite simple and has a high performance [2][3]. The bridgeless PFC generates less conduction losses compared with the conventional PFC. Although the circuit structure is simple, the location of the boost inductor on the AC side makes it difficult to sense the AC line voltage and inductor current. In this paper, the bridgeless asymmetrical boost that was designed and constructed is reported. Also, measurements of the input current and voltage waveforms together with the input power factor are presented. A comparative cost analysis of the conventional asymmetric is also made.

II The Bridgeless and the Conventional Boost Converter

The bridgeless PFC boost rectifiers of Fig.2, also called the dual boost PFC rectifiers, compared to the conventional PFC boost rectifier of Fig.1, generally, improve the efficiency of the front-end PFC stage by

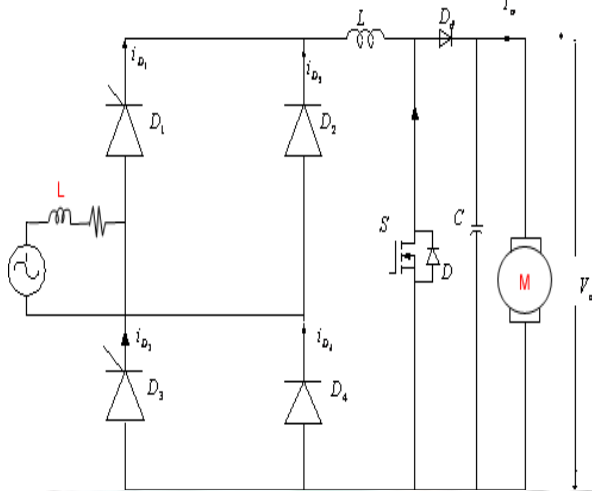
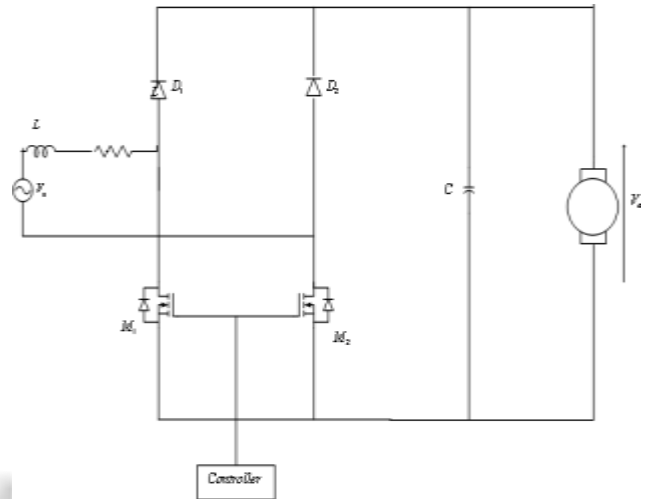


Fig.1: Asymmetrical Single Phase AC –DC Boost- type Converter with input power factor correction

This is easily done by replacing the thyristors of the asymmetrical single - phase bridge converter in Fig.1 by a power MOSFET with a diode connected between the drain and the source of the MOS switch as shown in Fig.2. A thyristor could be used as the switching device too although the MOSFET is a fast switching device. The series diode D_d in the conventional boost circuitry of Fig.1 has been eliminated. Also, the dc – side inductor is no longer necessary and instead an ac – side inductor is required. The advantages of this circuit are :

- Improved characteristics in terms of input power factor and sinusoidal shape of the input current.

eliminating one diode forward-voltage drop in the line-current path. The bridgeless configuration presented in this paper, avoids the need for the drive input bridge, yet maintains the classic boost arrangement.



Fig, 2:Bridgeless Asymmetrical Single – Phase AC –DC PFC configuration

- Only two semi-conductor device drops exist in the power flow path at any given instant.
- The boost inductor ‘L’ on the ac side contributes to the reduction in EMI interference

III Circuit Analysis.

The analysis can be discussed in two ways [4-5], one of such ways is presented here. First, to analyze the operation, the circuit of Fig.2 can be viewed as two sections: section one operates as the boost stage (positive half cycle) and the second operates as the return path for AC signal during the negative half cycle [6-7].

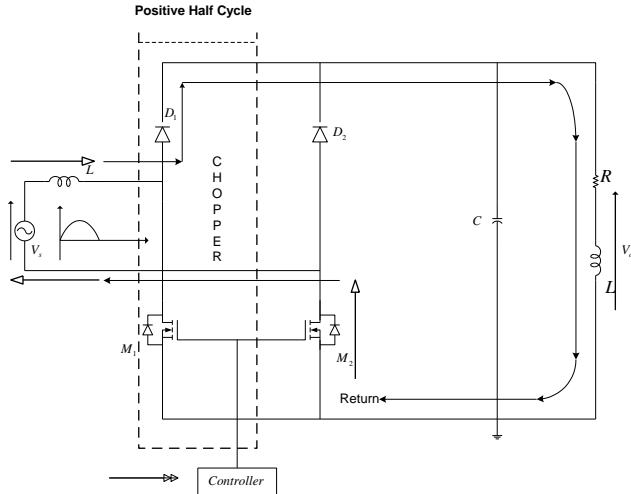


Fig.3: Bridgeless PFC Configuration for the positive half cycle

(a) Positive “Half Cycle”.

When the AC input goes positive, the gate of MOSFET M_1 is driven high and current flows through the input, and through the inductor, storing energy. When M_1 turns off, energy in the inductor is released and current flows through D_1 , through the load and returns through the body diode of M_2 back to the input mains Fig.3.

During the off – time, the current flows through the inductor ‘L’ (during this time, the inductor discharges its energy) into the boost diode D_1 and close the circuit through the load.

(b) Negative “Half Cycle”

During the negative half cycle, circuit operation is mirrored as the positive half cycle as shown in Fig.4, M_2 turns ON, current flows through the inductor storing energy. When M_2 turns off, energy is released as current flows through D_2 through the load and back to the mains through the body diode of M_1 .

It should be noted that the two power MOSFETs are driven synchronously. It does not matter whether the sections are performing as an active boost or as a path for the current to return. In either case, there is the benefit of lower power dissipation

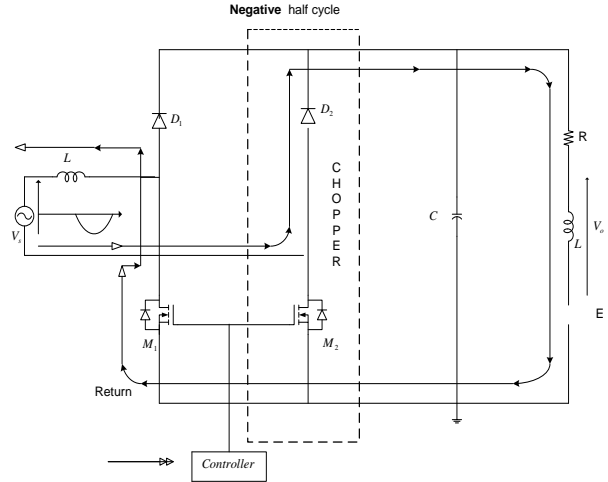


Fig.4: Bridgeless PFC Configuration for the negative half cycle

when current flows through the power MOSFETs during the return phase.

Fig.5 shows the Circuit Layout for the simultaneous gate firing of the MOSFETs (or Thyristors) of the bridgeless circuit by PWM controls

IV Design Considerations

The circuit of Fig.2 is to supply a 2.0kw load, from a 230V_{rms}, 50Hz Single – phase source. The output has a maximum of 400V dc with a switching frequency of 10KHz. It is operated in the Continuous Inductor Conduction Mode (CICM) [4].

It is assumed that switching losses and device power loss are negligible.

Parameters ‘L’ and ‘C’ are determined with the specification that the output ripple voltage shall be within the limits of 5% of the output voltage. The defining equations are derived in [6].

Since the switching losses are assumed to be zero,

$$P_{in} = P_{out}$$

$$2.0KW = V_{in} I_{in}$$

$$I_{in} = \frac{2000}{230} = 8.695A$$

And,

$$I_{out} = I_o = \frac{2000}{400} = 5A$$

Ripple Voltage is assumed to be 5% of output Voltage,

Therefore,

$$\Delta V_c = \frac{5}{100} \times V_o = \frac{5}{100} \times 400 = 20V$$

Also,

$$\Delta V_c = \frac{I_o D}{f_s C}$$

D is the duty cycle; $D = t_{ON}/T$

Where,

$$f_s = 10KHz$$

But for a boost converter,

$$V_o = \frac{V_s}{1-D}$$

Hence,

$$\begin{aligned} D &= 1 - \frac{V_s}{V_o} = 1 - \frac{230}{400} \\ &= 1 - 0.575 \\ &= 0.425 \end{aligned}$$

And,

$$\begin{aligned} C &= \frac{I_o D}{f_s \Delta V} = \frac{5 \times 0.425}{10000 \times 20} \\ &= 10 \times 10^{-6} \\ &= 10\mu F \end{aligned}$$

But a value of $C = 18\mu F$ was chosen as the output capacitor for the experimental work. This is to ensure that the dc output has less ripple content.

It is equally assumed that a 10% value of input current ripple is allowed,

Therefore,

$$\begin{aligned} \Delta I &= \Delta I_L = \frac{10}{100} \times 8.695 \\ &= 0.87A \end{aligned}$$

But,

$$\Delta I = \frac{V_s D}{f_s L}$$

Hence,

$$\begin{aligned} L &= \frac{V_s D}{f_s \Delta I} = \frac{230 \times 0.425}{10000 \times 0.8695} \\ &= 112.35 \times 10^{-5} \\ &= 11.23mH \end{aligned}$$

An inductor value of 15mH was used. This is to ensure that the design operates in a CICM. The diode and MOSFET were rated higher than the combined dc voltage and the anticipated ripple value [8]. The experimental circuit is presented in Fig.6

V Simplified PWM controls

The feed forward approach is used to generate the MOSFET gate signals where the output voltage is sampled (V_{sp}). The error amplifier compares the sampled output voltage (V_{sp}) with a fixed reference voltage, V_{ref} , and generates an error voltage, V_e given by [8].

$$V_e = V_{ref} - \frac{R_3}{R_4} \left[V_o \left(\frac{R_2}{R_1 + R_2} \right) - V_{ref} \right]$$

This error voltage is then fed to the non – inverting input of an open – loop comparator that compares the error voltage with a sawtooth signal at its inverting input. The switching frequency of the sawtooth generator determines the frequency of the converter. The output of the comparator is a PWM SIGNAL. It is high only when the error voltage is higher than the sawtooth signal. This PMW signal is then fed to the base drive circuitry that drives the gates of the two MOSFETS of the proposed converter. The bridgeless PFC circuit achieves the same improvement in power factor as the conventional boost PFC except that it overcomes its limitations.

VI. Laboratory Model

Figure 5 shows the laboratory model of the bridgeless asymmetrical boost converter.

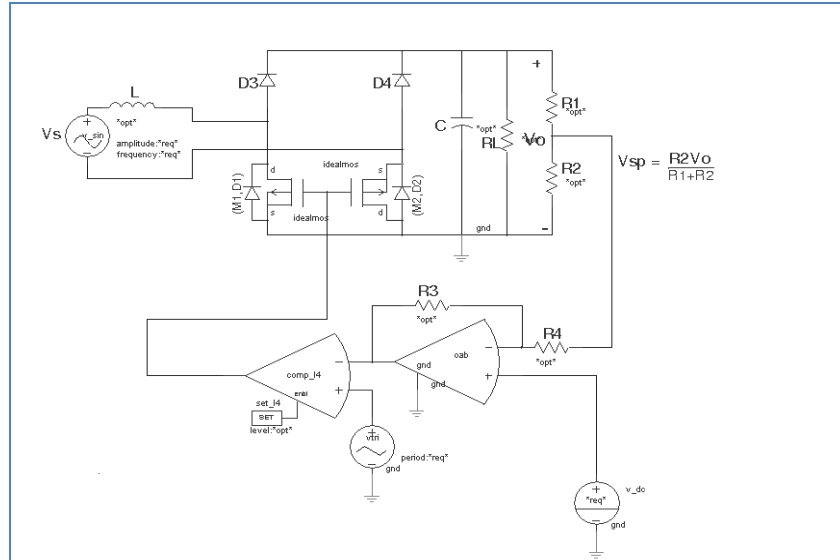


Fig.5: A laboratory model of the Bridgeless converter



Fig. 6: Experimental test rig of the Bridgeless Asymmetrical AC – DC Boost Converter

VII. Results

Experimental results are presented in Figs.7 to 9. Clearly, the input current is in phase with the voltage and the harmonics spectrum shows that lower order harmonics has been significantly reduced while higher order

harmonics can be filtered out if present. The bridgeless asymmetrical boost converter circuit gives the same improvement in power factor as the conventional boost converter, but it is cheaper to build.

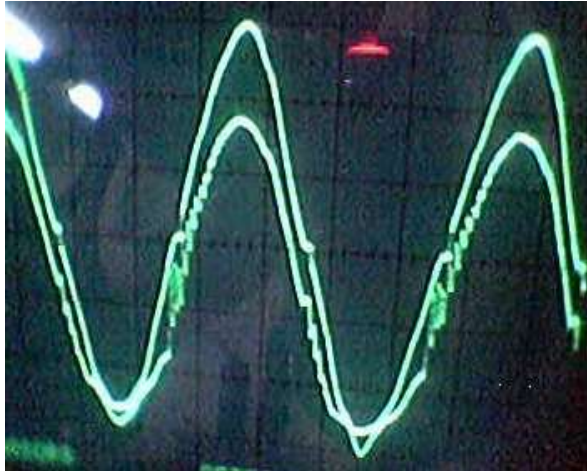


Fig.7:Waveform of current and voltage for the Bridgeless Asymmetrical Boost Converter



Fig.8:Waveform of current and Voltage for the conventional Asymmetrical Boost Converter

In Figs. 6-7, the upper waveform represents the current whilst the lower waveform represents the voltage. The harmonics

spectrum is essentially the same and it is presented in Fig. 8

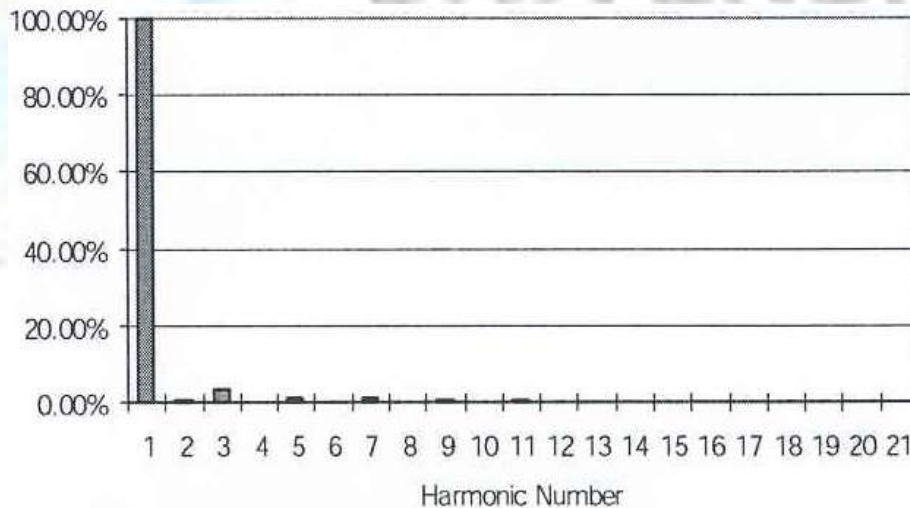


Fig.9: Harmonic Spectrum

VIII. Discussions and Conclusion

In an effort to improve the performance of the front end PFC, the Bridgeless AC – DC converter was considered in other to maximize the power supply efficiency, and minimized its component count. In terms of

cost, the bridgeless boost converter is by far cheaper than the conventional asymmetrical boost AC - DC converter. While Two thousand (N2, 000.00) is requires to build the bridgeless converter, It takes Twelve thousand, six hundred naira (N12, 600.00) to construct the conventional boost converter.

The circuit arrangement of the bridgeless PFC boost converter compared with the conventional PFC boost converter, shows that a diode has been eliminated from the line-current path, so that the line current simultaneously flows through only two semiconductors resulting in reduced conduction losses and a higher efficiency. However, the bridgeless PFC boost converter has significantly larger noise than the conventional PFC boost rectifier [9-11]

IX REFERENCES

- [1] Lu, B, Dong, W, Zhao, Q, Lee, F.C.; "Performance evaluation of CoolMOSTM and SiC diode for single – phase power factor correction applications", APEC '03.Pages:651 - 657 vol.2
- [2] Liu J.; Chen W.; Zhang J.; Xu, D.; Lee, F.C.; "Evaluation of power losses in different CCM mode single-phaseboost PFC converters via a simulation tool", IAS 2001, Pages:2455 - 2459 vol.4
- [3] Srinivasan, R.; Oruganti, R.; "A unity power factor converter using half-bridge boost topology", IEEE Transactions on Power Electronics, Volume: 13 Issue: 3, May 1998, Pages:487 – 500
- [4] Trzynadlowski A.M, Wang Z, Nagashima J, Stancu C and Zelechowski M. "Comparative Investigation of PWM Techniques for a New Drive for Electric Vehicles". IEEE Transactions on Industry Applications. Vol. 39, No. 5. 2003. 1396-1403.
- [5] Enjeti P.N, Ziogas P.D and Lindsay J.F. "Programmed PWM Techniques to Eliminate Harmonics: A Critical Evaluation". IEEE Transactions on Industry Applications, 26, 1990. Pp 302-316.
- [6] Robert Martinez and Enjeti P.N. "A High performance Single- Phase Rectifier with input power factor correction" IEEE Transaction on Power Electronics, Vol. II, No.2. 2000. Pp 154-163
- [7] Laszlo, H, Yungtaek Jung and Milan M. Jovanovic. "Performance Evaluation of Bridgeless PFC Boost Rectifiers". IEE. 2007. Pp 165-171
- [8] Osunde,O.D "Input Power Factor Problem and correction for Industrial Drives". A thesis presented to the School of Post Graduate Studies of the University of Lagos, Lagos, Nigeria (2009).
- [6] Okoro C.C "Behaviour factors of Asymmetrical single-phase converter". Nigerian Journal of Engineering and Technology, vol.10. 1987. No.11-7
- [7] Okoro C.C. "Performance Evaluation of a DC motor Fed from an Asymmetrical Single-Phase Bridge". Proc. IEE, 1982. vol.129. PTB No.5, 289-98.
- [8] Sen P.C. "Thyristorised DC Drives". John Wiley and Sons Inc. 1991. 1st Edition. Florida. Krieger Publishing Company.
- [9] Liu Y and Smedley, K. "Control of a Dual Boost power factor corrector for high power applications". IECON 29th Annual Conference of the IEEE.Volume 3, Issue , 2-6. 2003. PP. 2929-2932.

- [10] Liu Y and Smedley, K. "Control of a Dual Boost power factor corrector for high power applications". IECON 29th Annual Conference of the IEEE. Volume 3, Issue , 2-6. 2003. PP. 2929-2932
- [11] Robert Martinez and Enjeti P.N. "A High performance Single- Phase Rectifier with input power factor correction". IEEE Transaction on Power Electronics, Vol. II, No.2. 2000. Pp 154-163
- [12] Laszlo, H, Yungtaek Jung and Milan M. Jovanovic. "Performance Evaluation of Bridgeless PFC Boost Rectifiers". IEE. 2007. Pp 165-171



UNIVERSITY
OF LAGOS

APPENDIX X

Unpublished Papers

1. Correction of Input Power Factor Problem in Industrial Drives
2. Impact of Harmonics in Communications Systems and Circuits
3. Bridgeless Asymmetrical Single – Phase AC – DC Converter for Power Factor Correction



UNIVERSITY
OF LAGOS